8-27-2012

Sensitivity study of turbulent flow simulations over a rotating disk

Michael Snider

Michael Aaron Snider
Candidate

Mechanical Engineering
Department

This thesis is approved, and it is acceptable in quality and form for publication:

Approved by the Thesis Committee:

Svetlana Poroseva , Chairperson

C. Randall Truman

Peter Vorobieff

SENSITIVITY STUDY OF TURBULENT FLOW SIMULATIONS OVER A ROTATING DISK

by

MICHAEL AARON SNIDER

B.S., MECHANICAL ENGINEERING
UNIVERSITY OF NEW MEXICO, 2009

THESIS

Submitted in Partial Fulfillment of the
Requirements for the Degree of

Master of Science
Mechanical Engineering

The University of New Mexico
Albuquerque, New Mexico

July, 2012

Acknowledgments

The author would like to acknowledge the UNM Center for Advanced Research Computing for providing systems and consulting support and the parallel computational resources used in this work. The author would also like to thank Prof. J.K. Eaton (Stanford University) for helping with the experimental data and to CD-adapco for providing Star-CCM+[8] to the University of New Mexico for academic purposes.

SENSITIVITY STUDY OF TURBULENT FLOW SIMULATIONS OVER A ROTATING DISK

by

Michael Aaron Snider

B.S., Mechanical Engineering, University of New Mexico, 2009
M.S., Mechanical Engineering, University of New Mexico, 2012

Abstract

With increasing demand for renewable energy, there is a need for accurate and reliable simulations of a flow around a wind turbine. To be of use as an engineering design and planning tool, such simulations should be conducted in a timely manner. This can be achieved if a flow is modeled with Reynolds-Averaged Navier-Stokes turbulence models. To reduce uncertainties associated with numerical simulations from the simulation results, one has to ensure the convergence of results with respect to various simulation parameters. In this paper, the effect of the size of computational domain, boundary proximity, grid stretching, and initial grid wall spacing is analyzed. Simulations are conducted with several turbulence models using structured meshes. Due to the complex geometry of wind turbines, a flow over an infinite rotating disk is considered in the current paper as a first step. Such flow represents a rotating wind turbine with an infinite number of blades.

Table of Contents

List of Tables

List of Figures

Standard *k*-*ε* turbulence model sensitivity study

Step 1

Step 2

Step 3

Step 4

Step 5

Standard *k-ω* turbulence model sensitivity study

Step 1

Step 2

Step 3

Step 4

Step 5

SST turbulence model sensitivity study

Step 1

Step 5

High-Reynolds Number Spalart-Allmaras turbulence model sensitivity study

Step 1

Step 2

Step 3

Step 4

Step 5

Reynolds Stress Transport Model sensitivity study

Step 1

Step 2

Step 3

Step 4

Step 5

Turbulence Model Comparison

Wall Treatment

Nomenclature

C_f = skin friction coefficient

q^2 = twice the turbulent kinetic energy

r = radial position on infinite disk measured from axis of rotation

Re = Reynolds number, $\omega r^2/\nu$

$Re_{\delta 2}$ = momentum thickness Reynolds number, $\omega r\delta_2/\nu$

u_r = laminar flow radial velocity component

u_z = laminar flow axial velocity component

u_θ = laminar flow tangential velocity component

u = instantaneous tangential velocity in rotating reference frame

u' = tangential velocity fluctuation in rotating reference frame

v = instantaneous axial velocity

v' = axial velocity fluctuation

w = instantaneous radial velocity

w' = radial velocity fluctuation

y = physical distance normal to rotating disk's surface (axial direction)

y^+ = non-dimensional distance normal to rotating disk's surface, $y\mu_\tau/\nu$

U = mean tangential velocity in rotating reference frame

U^+ = mean velocity in tangential direction in wall units, U/μ_τ

U_∞ = Local disk surface speed, ωr

$|U|$ = mean velocity vector magnitude

W = mean radial velocity

δ_2 = momentum thickness

ρ = fluid density

μ_τ = friction velocity in tangential direction, $U_\infty\sqrt{(C_f/2)}$

τ = shear stress vector magnitude

ω = angular velocity (rad/s)

ν = kinematic viscosity

I. Introduction

With the increased demand for clean energy and reduced carbon emission, there has been substantial growth in the wind energy industry in the past decade. This trend is expected to continue. IBIS World reports that the wind energy industry is expected to experience the second highest rate of revenue growth from 2010 to 2016 compared to other national industry sectors.[1] Wind energy production is estimated to generate 1.92% of the world's electricity by the end of 2011 and 9.1% of the electricity demand by 2020.[2]

To achieve these goals, it is important to better understand and predict the behavior of a flow around a wind turbine as this is a key for designing efficient wind turbines and planning wind farms. A valuable insight into the flow dynamics and fluid–structure interaction can be obtained through numerical simulations. However, the scale of the problem and the flow complexity limit the choice of computational tools available for conducting accurate simulations. Indeed, requirements for the computational grid resolution and the range of Reynolds numbers of interest make both Direct Numerical Simulations and Large Eddy Simulations computationally unfeasible. Flow simulations with the Reynolds-Averaged Navier-Stokes (RANS) turbulence models, on the other hand, seem to be a reasonable choice. They can be conducted in a wide range of Reynolds numbers without any limitation, simulations are computationally inexpensive, and numerical codes are easily accessible as commercial or publicly available software.

A problem with any numerical simulations including RANS simulations is how to ensure that their results correctly reproduce features of interest of a real flow. This is of particular importance for a flow around a wind turbine as experimental and observational data are scarce. A necessary step is to conduct a sensitivity analysis of simulation results with respect to the choice of a turbulence model and model parameters, the size of a computational domain, grid resolution, boundary and initial conditions, and the accuracy of implemented numerical schemes among other factors.

In industry, a typical practice is to rely on commercial software for conducting simulations. It means that only a limited number of simulation parameters can vary. The current study seeks to analyze the convergence of simulation results with respect to the size of computational domain, boundary proximity, grid stretching, and initial grid wall spacing. These parameters were chosen to be varied following the recommendations for CFD calculations in NASA's OVERFLOW 2.1

user manual[17]. A turbulent flow is modeled with a few standard RANS models: a one-equation Spalart-Allmaras model[3], two-equation k - ε and $k - \omega$ models[4,5], SST[6] and RST[7] models. These are options available to vary in Star-CCM+[8] software, which is a commonly used CFD package in industry. The computational domain and grids are generated in ICEM[9] and then imported into Star-CCM+[8].

Due to the geometric complexity of wind turbines, as a first step, simulations of a flow over a rotating disk have been conducted. Indeed, with the number of blades on a wind turbine approaching infinity, the turbine's geometry transforms to a solid disk. Also assumed is that the disk has an infinite radius. This flow is an excellent test case, because the analytical solution for laminar flows and extensive experimental and LES databases for turbulent flows are available.

The first person that derived a solution for the laminar flow field of a stationary fluid subjected to an infinite disk's rotation was Theodore von Karman[10]. He reformulated the Navier-Stokes equations in terms of a non-dimensional height and derived an approximate solution from the integral form of the boundary layer equation. Cochran[11] improved upon the von Karman's work and numerically obtained an accurate representation of the exact solution in this flow. White[12], expanding on the Cochran's solution, lengthened the solution's domain infinitely above the disk's surface.

Wu and Squires[13] conducted LES simulations of a flow over a rotating disk which was compared to the experimental work of Little and Eaton[14]. In Little and Eaton[14], the experimental set was a rotating disk of one-meter diameter in an otherwise static air volume. The only motion of the fluid was due to the disk's rotation. Measurements were taken at a variety of angular velocities and radial positions in the flow field. Kobayashi, Kohama and Takamadate[15] studied the boundary layer transition in this flow geometry from laminar to turbulent. An experiment was conducted to find the Reynolds number at which the onset of instability and the onset of turbulence occurred in the boundary layer. Particular attention in their work was given to formation of spiral vortices in the transition regime.

In our study, laminar and turbulent flows over an infinite rotating disk are simulated. Laminar flow solutions are compared with the Cochran's solution. Turbulent flow simulations are compared with the data of Little and Eaton[14]. Sensitivity analysis is conducted for both laminar and turbulent flows. This work will be used as a stepping stone to the creation of computational domains that will be suitable for accurate and reliable wind turbine simulations.

II. Simulation Parameters

A. Computational Domain

An initial domain size of 1x5x5 meters in axial, radial and tangential directions, respectively, was chosen as the control volume to simulate a flow over a rotating infinite disk in Star-CCM+[8]. This is the smallest size of computational domain for all laminar flow simulations. Larger sizes did not result in any improvement of the accuracy of simulation results in a laminar flow.

Initial turbulent flow simulations were computed on this domain size. The computational domain size is varied in all three dimensions in this sensitivity study. Specifically, the radial and tangential dimensions were shortened while the axial dimension remained constant; then the axial dimension was reduced, while the radial and tangential dimensions were held constant.

B. Grid

The structured grid resolution in the initial computational domain was set to be 16x50x50 nodes in the axial, radial, and tangential directions, respectively, for laminar flow simulations at Re = 1000 at a radius of 1 m. For turbulent flow simulation at $Re = 10^6$ at a radius of 0.421 m the grid refinement will be varied drastically throughout this study. The grid resolution changes for each simulation as a function of the computational domain size, initial grid wall spacing, and grid stretching.

Initial grid wall spacing is a distance from the disk surface in the axial direction at which the first cell's centroid is placed. It is determined in non-dimensional y^+ units (Eq. 1). Simulations with initial grid wall spacing y^+ = 5, 10, 20, 30, 40, 50, 75, 100 and 200 were conducted, where

$$y^+ = \frac{y\mu_\tau}{\nu} \tag{1}$$

$$\mu_\tau = U_\infty\sqrt{(C_f/2)} \tag{2}$$

$$C_f = \frac{\tau_w}{\rho(U_\infty^2/2)} \tag{3}$$

$$\tau_w = \rho\sqrt{\overline{u'v'}^2 + \overline{v'w'}^2} \quad (4)$$

In (1)-(4), μ_τ is the friction velocity in the rotating reference frame, C_f is the skin friction coefficient and τ_w is the shear stress at the disk's surface. Grid stretching is defined as the ratio of a cell's axial length to the axial length of the adjacent cell closer to the disk's surface. Simulations were conducted with a grid stretching ratio of 1.1, 1.2, 1.3, 1.5 and 2.0.

C. Boundary Conditions

The disk's surface is represented by a wall with a no-slip condition with an assigned value of the angular velocity about the rotation axis, +Y-axis as seen in Fig.1. A velocity inlet is chosen as a boundary condition for a flow entering the computational domain. The remaining side boundaries are pressure outlets with a prescribed gage pressure of zero. This allows fluid to leave the computational domain through these boundaries without returning back into the domain. The fluid velocity at the inlet is set as an input parameter in Star-CCM+[8].

The initial domain (1x5x5 meters) is displayed with the coordinate system in Fig. 1. The location of the line probe at r = 0.421 meters, which is the location the fluid flow data is measured, is highlighted. The wall acting as the disk's surface is highlighted in Fig. 2, the pressure outlet boundaries are highlighted in Fig. 3 and the velocity inlet boundary is highlighted in Fig. 4.

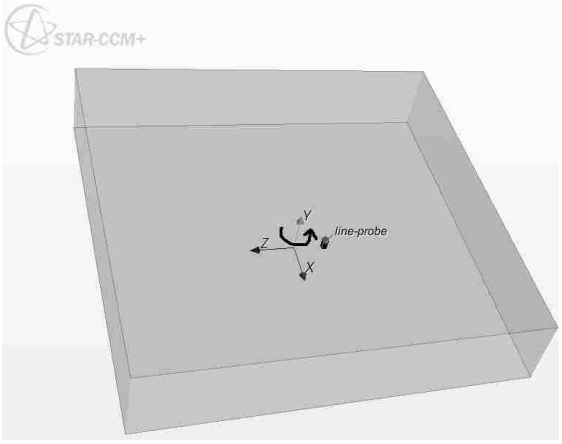

Figure 1. 1x5x5 meter Computational domain. *Computational domain with line probe, located at r=0.421 meters, highlighted. And rotation direction (+Y-axis) displayed.*

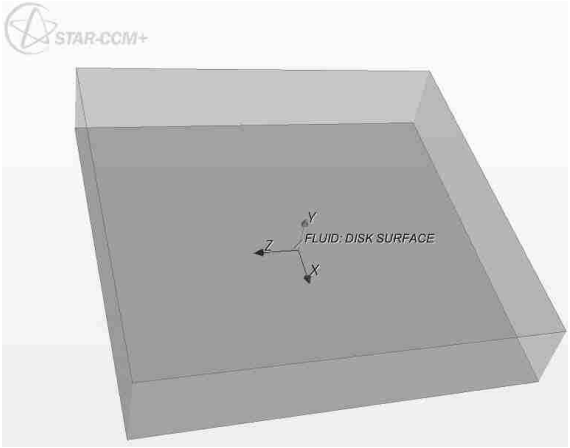

Figure 2. Computational domain with disk surface highlighted.

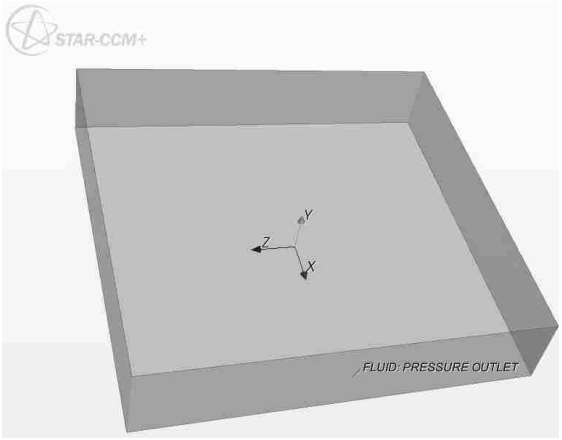

Figure 3. Computational domain with pressure outlets highlighted.

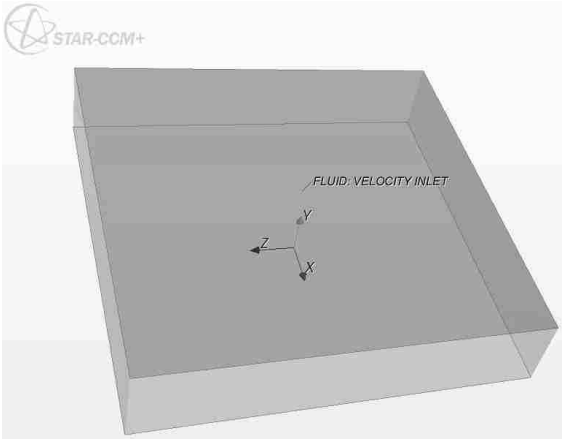

Figure 4. Computational domain with velocity inlet highlighted.

III. Numerical Method

Star-CCM+[8] uses a first and second-order upwind calculation for its convection term. The choice of using one model over another can significantly affect the stability and accuracy of the numerical scheme. For this work, the second-order upwind scheme is used. Although more accurate, it is more computationally demanding and in some simulations the solution convergence properties can be poor due to reduced numerical dissipation.

IV. Turbulence Models

The five turbulence models that will be used in this study are:

- Standard k - ε [4]
- Standard $k - \omega$ [5]
- SST [6]
- High-Reynolds Number Spalart-Allmaras [8]
- Reynolds Stress Transport (RST) [7]

A. Standard k - ε Model

The k - ε turbulence model is a two-equation model in which transport equations are solved for the turbulent kinetic energy and its dissipation rate. Many forms of the k - ε model have been in use for several decades, and it has become the most widely used model for industrial applications.

This type of turbulence model requires additional flow modeling near walls. In the current study the High y^+ Wall Treatment was chosen from the options available in Star-CCM+[8] as the wall function for this model (more discussion on the wall treatment options available in Star-CCM+[8] is provided in Section IV.F). This option is equivalent to the traditional wall function approach, where the relation $U^+ = y^+$ is enforced in the near wall region. In Star-CCM+[8] the High y^+ Wall Treatment is classified as a standard wall law, which is slope-discontinuous between the laminar and turbulent profiles.

In this work, the standard values of the model coefficients are used, as shown in Table 1.

Table 1. Standard k - ε Coefficients Used in Star-CCM+[8]

$C_{\varepsilon 1}$	$C_{\varepsilon 2}$	C_{μ}	C_M	σ_{ε}	σ_k
1.44	1.92	0.09	2.0	1.3	1.0

B. Standard k - ω Model

The k - ω model is also a two-equation model in which the transport equations are solved for the turbulent kinetic energy and the specific dissipation rate, that is, the dissipation rate per unit turbulent kinetic energy. This model is also paired with the High y^+ Wall Treatment mentioned

in the previous model. The k - ω model is used with the standard values of the model coefficients (Table 2).

Table 2. Standard k - ω Coefficients Used in Star-CCM+[8]

α	β	β^*	σ_k	σ_ω
0.52	0.072	0.09	0.5	0.5

C. SST Model

The SST (shear-stress transport) model is a two-equation model that blends together the transport equations of the standard k - ε model and the k - ω model. This model is also combined with the High y^+ Wall Treatment model. The model coefficients used in the SST model simulations are shown in Table 3.

Table 3. Standard SST Coefficients Used in Star-CCM+[8]

a_1	β_1	β_2	β^*	κ	σ_{k1}	σ_{k2}	$\sigma_{\omega 1}$	$\sigma_{\omega 2}$
0.31	0.075	0.0828	0.09	0.41	0.85	1.0	0.5	0.856

D. High-Reynolds Number Spalart-Allmaras Model

The High-Reynolds Number Spalart-Allmaras turbulence model solves a single transport equation for the turbulent viscosity. This model is a modification of the standard Spalart-Allmaras[3] turbulence model developed by the authors of Star-CCM+[8]. In the model, the viscous damping within the buffer layer and viscous sublayer is not included. This model utilizes the High y^+ Wall Treatment model.

In this work, the model is used with the coefficients given in Table 4.

Table 4. High-Reynolds Number Spalart-Allmaras Coefficients Used in Star-CCM+[8]

C_{b1}	C_{b2}	C_{prod}	C_{w2}	C_{w3}	κ	σ
0.1335	0.622	2.0	0.3	2.0	0.41	0.667

E. Reynolds Stress Transport Model

Star-CCM+[8] has a choice of three different Reynolds stress transport turbulence models. In the current study, the Linear Pressure Strain model[7] has been used. The RST model also utilizes the High y^+ Wall Treatment model. The turbulent dissipation rate is modeled as in the k - ε turbulence model, but with different coefficients as seen in Table 5. The turbulent diffusion term is used in isotropic form[16].

Table 5. RSTM Linear Pressure Strain Dissipation Rate Coefficients Used in Star-CCM+[8]

$C_{\varepsilon 1}$	$C_{\varepsilon 2}$
1.44	1.92

F. Wall Modeling

Alongside choosing a turbulence model the user can select how to solve the near wall physics. There are three wall function modeling options in Star-CCM+[8].

- High y^+ Wall Treatment
- Low y^+ Wall Treatment
- All y^+ Wall Treatment

1. High y^+ Wall Treatment:

This wall function model requires that the initial cell's centroid lie within the logarithmic region of flow. Inaccuracies arise when this approach is used in combination with a grid that is too refined near the wall. This wall function segregates the viscous dominated laminar region from the turbulence region and applies the wall law $U^+ = y^+$ in the laminar region and the log law in the turbulent region. Star-CCM+[8] recommends that the wall cell's centroid location be greater than $y^+ = 30$, warning that significant error can occur if the centroid is placed closer than $y^+ = 12$. This wall function is only recommended for high Reynolds number simulations. Hence the "High" in this wall function's title.

In order to obtain a level of consistency between simulations conducted with different models, choosing a wall function that is available for all five turbulence models was a requirement for

this sensitivity study. The High y^+ Wall Treatment was the only wall function that was available for all turbulence models and, therefore, is used in all the simulations in this study. Star-CCM+[8] warns of the inaccuracy danger of using any model other than the All-y^+ model, but due to the simple geometry of a rotating infinite disk where the Reynolds number is known along the radius, the High y^+ Wall Treatment was chosen instead in the current study.

2. Low y^+ Wall Treatment:

This wall treatment approach requires that the grid be highly refined near wall, because no assumption on the flow behavior near a wall is made. To fully resolve the viscous sub-layer, Star-CCM+[8] recommends that the initial cell's centroid lie within $y^+ = 1$ of the wall. Attempting simulations of high Reynolds number flows with this approach would be too computationally expensive, therefore, it is only recommended for simulations of low Reynolds number flows. Hence the "Low" in this wall function's title.

3. All y^+ Wall Treatment:

This wall function model is a blend between the previous two approaches. It calculates wall distances of cell centroids and applies the suitable wall function. Star-CCM+[8] recommends to use this option for all Reynolds number flows whenever it is offered. Hence the "All" in this wall function's title. This approach is not available for all turbulence models. Thus, it has not been selected for the current study.

V. Results

The case of a laminar flow over an infinite rotating disk was studied at a Reynolds number of 1000. The results obtained were compared with the Cochran's solution[11] to validate Star-CCM+[8] solutions and to determine the size of the computational domain for the initial turbulent flow simulations. Turbulent flow simulations were conducted at $Re = 10^6$.

Computations have been conducted using high-performance computing systems available through the Center for Advanced Research Computing at the University of New Mexico. Specifically, the 36-node Nano Linux cluster (2 Intel Xeon 5140 (2.33 GHz) processors per node, 2 cores per processor, 8GB RAM/node, 1300 GFlops) has been used for simulations that were run on up to 8 nodes of the system. A desktop computer was also used for less computationally demanding simulations (Windows 7, 64-bit, Intel Core i7-2600, 3.40GHz, 8GB RAM).

A. Laminar Flow

The size of the computational domain was varied in a laminar flow simulation, but the grid cell size was kept the same. That is, as the computational domain became smaller, the number of cells within the domain decreased. The grids in these laminar simulations have an initial grid wall spacing of y^+=1 (0.01 meters) and a grid stretching of 1.2 in the axial direction. In the radial and tangential direction, there is a uniform cell length of 0.1 meters. The physical dimension above the disk in which the data were sampled was extended to approximately 0.3 meters.

Results of laminar flow simulations for two different sizes of the computational domain are shown in Figs. 1 and 2. Close agreement is demonstrated between the simulation results and the Cochran's solution in both cases. The data was sampled at a radius of 1 *m* on an infinite disk for the Reynolds number of 1000. The data has been smoothed by linearly interpolating the node values.

The laminar flow solution showed no sensitivity in respect to the size of the computational domain, therefore, the smallest domain was chosen for conducting the initial turbulent flow simulations.

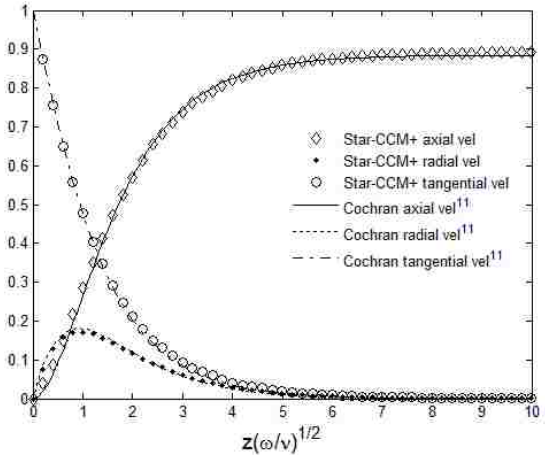

Figure 5. *Re* = 1000 laminar solution for 1x5x5 meter domain, 16x50x50 nodes. *Velocity profiles over the rotating disk.*
— - — o, $u_\theta/\omega r$; - - - •, $u_r/\omega r$; —◊, $-u_z/(v\omega)^{1/2}$.

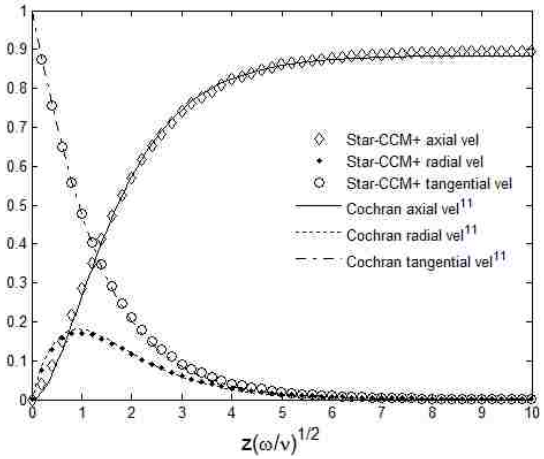

Figure 6. *Re* = 1000 laminar solution for 30x20x20 meter domain, 35x200x200 nodes. *Velocity profiles over the rotating disk.*
— - — o, $u_\theta/\omega r$; - - - •, $u_r/\omega r$; —◊, $-u_z/(v\omega)^{1/2}$.

B. Turbulent Flow

The results of the sensitivity study are presented separately for each turbulence model in their respective sections. Then, results for different models are compared to one another in the comparison section. Every turbulence model underwent the same process to find the least computationally expensive grid that did not greatly impact the accuracy of the Star-CCM+[8] solution. The sensitivity study procedure for each turbulence model consists of the following steps:

Step 1: The initial cell's centroid was located at y^+ values of 5, 10, 20, 30, 40, 50, 75, 100 and 200. The highest y^+ value at which an acceptable solution was generated was held constant for all other grid property sensitivity studies.

Step 2: The grid refinements in the radial and tangential directions were varied between the following nodal resolutions: 508x508, 254x254, 127x127, 64x64 and 32x32. The coarsest grid resolution in these two directions that was able to maintain an accurate solution was chosen to be held constant for the future sensitivity studies.

Step 3: The grid's stretch ratio in the axial direction, normal to disk's surface, was varied as: 1.1, 1.2, 1.3, 1.5 and 2.0. The largest stretch ratio that resulted in accurate results was set as a constant for future sensitivity simulations.

Step 4: The grid domain size in the radial and tangential directions was varied while the axial dimension remained constant. In this sensitivity study, the computational domain sizes of interest were 1 x 1 meters, 2 x 2 meters, 5 x 5 meters and 10 x 10 meters in the radial and tangential directions. The smallest computational domain size that did not affect the solution's accuracy was set as a constant for the last study.

Step 5: The computational domain size in the axial direction was altered for this study. The previous simulations used a domain with the velocity inlet located 1 meter above the disk's surface with a prescribed inlet velocity of 1 *m/s*. At this step, the computational domain size was varied to include axial lengths of 0.1, 0.25, 0.5, 1.0, 2.5 and 5.0 meters. This parameter of the

grid is not as easily modified as others without having an impact on the flow. The velocity inlet is the only boundary where the flow velocity must be prescribed. The velocity profile varies throughout the domain and prescribing the same velocity at the inlet for all the simulations in this sensitivity study would result in a poor comparison. To remedy this as much as possible the largest domain's simulation was run with a prescribed inlet velocity of 1 *m/s* and the axial velocity was measured from data points at 0.1, 0.25, 0.5, 1.0 and 2.5 meters above the disk's surface at a radius of 0.421 meters. To best replicate the flow between simulations this radial position was chosen to measure the axial velocity because it is the radial position at which the data is sampled. These measured velocities were then used as the prescribed inlet velocities for each simulation respectively. Again, the smallest computational domain size that does not result in a poor solution was sought after.

1. Standard *k*-ε model

The standard *k*-ε model was chosen to be the initial turbulence model for the sensitivity studies due to its sensitivity to cell aspect ratios, defined in this paper as the ratio of a cell's length in the radial direction to its length in the axial direction (radial length : axial length). All the grids in this study are identical in the radial and tangential direction, thus a single aspect ratio adequately defines the relative dimensions of a cell.

Care had to be taken to keep the near wall cell's aspect ratio from getting too large. The simulations presented in this section all maintained a maximum aspect ratio of less than 300:1. Simulations with maximum aspect ratios of 1000:1 were attempted but would fail to converge, causing the residuals at each iteration to increase rather than decrease.

Step 1:

The grids used for the y^+ sensitivity study had the following properties:

Computational domain size of 1x5x5 meters (axial x radial x tangential)

Stretch ratio of 1.2 in the axial direction

Uniform radial and tangential resolution of 508x508 nodes

Grids with the following initial cell's centroid y^+ values were included in this sensitivity study.

y^+ = 5 (42 x 508 x 508 nodes)

y^+ = 10 (39 x 508 x 508 nodes)

y^+ = 20 (36 x 508 x 508 nodes)

y^+ = 30 (33 x 508 x 508 nodes)

y^+ = 40 (32 x 508 x 508 nodes)

y^+ = 50 (31 x 508 x 508 nodes)

y^+ = 75 (28 x 508 x 508 nodes)

y^+ = 100 (27 x 508 x 508 nodes)

y^+ = 200 (23 x 508 x 508 nodes)

Since the High y^+ Wall Treatment was used, it was not necessary to go below y^+ = 5 as the simulation results will show. The turbulent mean flow vector magnitude in the rotating reference

frame is shown in Fig. 7. The distance above the disk's surface is normalized by the momentum thickness boundary layer, δ_2:

$$\delta_2 = \int_0^{\infty} \frac{U}{U_\infty}\left(1 - \frac{U}{U_\infty}\right) dy \tag{5}$$

This was chosen as the normalizing variable for the experimental data[14] rather than the boundary layer thickness, δ_{99}. In order to obtain the boundary layer thickness experimentally, the distance above the spinning disk's surface, at which the flow has 1% the velocity of the spinning disk's surface speed (ωr), must be measured. It would have been unrealistic to have enough physical measurement points far from the disk's surface to accurately measure this. Measuring the momentum thickness only requires detailed measurements near the disk's surface which is more practical in physical experiments.

All of the simulation results agree very well except near the disk's surface. This disagreement is due to the refinement differences near the wall. Straight lines are seen in the simulation profiles of the grids with high y^+ values. These straight lines are the linear interpolation across the cell that is a result of the data smoothing procedure utilized in Star-CCM+[8]. The data smoothing across the cell is done for all y^+ values but is only seen in the high y^+ simulations due to the length of these cells.

Figure 8 is a bar graph of errors. The vertical axis is the percent error and the horixontal axis displayes a bar for each simulation. Errors are obtained by numerically integrating the area between the simulation data and the Little and Eaton[14] measured data with a midpoint rectangular integration scheme

$$error = |g(x_1) - f(x_1)|\left(\frac{|x_2 - x_1|}{2}\right) + |g(x_n) - f(x_n)|\left(\frac{|x_n - x_{n-1}|}{2}\right) + \sum_{i=2}^{n-1} |g(x_i) - f(x_i)|\left(\left|\frac{|x_{i+1} - x_i|}{2} - \frac{|x_i - x_{i-1}|}{2}\right|\right) \tag{6}$$

This calculated area is then normalized by the area under the experimental data[14]:

$$\sum g(x) = g(x_1)\left(\frac{|x_2 - x_1|}{2}\right) + g(x_n)\left(\frac{|x_n - x_{n-1}|}{2}\right) + \sum_{i=2}^{n-1} g(x_i)\left(\left|\frac{|x_{i+1} - x_i|}{2} - \frac{|x_i - x_{i-1}|}{2}\right|\right) \quad (7)$$

to obtain a relative error percentage:

$$average\ \%\ error = \frac{error}{\sum g(x)} \quad (8)$$

In (6)-(8), x is the horizontal axis variable, x_i is the discrete value of the experimental data's[14] horizontal axis variable, $g(x)$ is the experimental data[14] vertical axis value, $f(x)$ is the Star-CCM+[8] vertical axis value and n is the number of experimental data[14] points.

In Figure 9 the crossflow profile is plotted. This plot illustrates the correlation between the radial and tangential velocities. It does not rely on the distance from the disk's surface, but there is a trend that near-wall data is on the left portion of the graph due to decreased velocities. It is clear that there are disagreements in the different simulation results that extend past the near wall region. The simulations with y^+ = 20, 30, 40, and 50 agree almost exactly past the small near-wall discrepancies. However, unlike Fig. 7, the results of the simulations do not converge to a single trend away from the disk's surface. The inaccuracies in the crossflow calculation resulting from the initial cell's centroid proximity to the wall carry throughout the computational domain.

Figure 10 is the error graph of the crossflow profiles with respect to the experimental data[14]. This plot is a tool to visualize crossflow profiles obtained from simulations and experimental data[14]. It should not be used to determine what simulations produced the most accurate results. In some cases, it was observed that the inaccuracies associated with a poor grid resolution moved the simulation's results closer to the experimental data[14].

Figure 11 is the polar plot of the mean velocity profiles. The horizontal axis is the ratio of tangential flow velocity in the rotating reference frame to the tangential velocity of the spinning disk, ωr. The value of this ratio goes to zero at the disk's surface where the no-slip boundary condition is applied. The simulations with y^+ = 20, 30, 40, and 50 seem to agree with one another in the area far from the wall. The y^+ = 5 and 10 simulations overshoot the experimental

data[14] while the simulations with y^+ = 75, 100 and 200 undershoot the experimental data[14]. This plot demonstrates the inadequacy of the High y^+ Wall Treatment near the disk's surface. The y^+ = 200 simulation's initial cell is so large that the data smoothing over the cell accounts for the data in the approximate range $0 \leq U/U_\infty \leq 0.8$. This is why the high y^+ simulation profiles fall off the experimental data[14] trend so abruptly. This same data fall off is visible down to the resolution of y^+ = 10. The experimental data[14] were limited to a minimum value of $U/U_\infty \approx 0.5$ because they could not physically place probes closer to the surface of the disk.

The error graph (Fig. 12) demonstrates that the errors of the simulation profiles obtained with y^+ = 20, 30, 40 and 50 are very close. This confirms our observation that these simulations are in agreement with one another for most of the plot.

Figure 13 is a semi-logarithmic plot of U^+ to y^+. The definition of U^+ is given in Eq. 9.

$$U^+ = \frac{U}{\mu_\tau} \tag{9}$$

This figure has two analytical solutions imposed onto it along with the experimental data[14]. The near wall curve is the law of the wall, where viscous effects dominate the velocity profile and $U^+ = y^+$. This solution is only valid in the range $y^+ \leq 5$. The log law (Eq. 10):

$$U^+ = 2.44 ln y^+ + 5.0 \tag{10}$$

is plotted for the range $y^+ \geq 30$.

The graph again shows the data smoothing of Star-CCM+[8] over the initial cell's length. This data smoothing appears as a curved line due to the logarithmic horizontal axis. It is seen that the High y^+ Wall Treatment is applied throughout the length of the initial cell. This is seen by the slope discontinuity at the boundary of the initial cell. It should be noted that the graph does not include the initial data point at the disk's surface (y^+ = 0) because of the semi-logarithmic scale of the plot. The Star-CCM+[8] simulation profiles starts at the first data point above the disk's surface which is approximately y^+ = 10.

All of the simulation profiles are similar far from the disk's surface and follow the log law and experimental data[14] very closely with the exception of the y^+ = 5 simulation, which shows

disagreement with the experimental data[14] throughout the computational domain. Also, the simulation profile obtained with y^+ = 10 deviates from the other profiles far from the disk's surface and is in better agreement with the experimental data[14]. This is reflected by the error graph in Fig. 14. Figure 14 also shows that the errors of simulation profiles obtained with y^+ = 20, 30, 40 and 50 again are very close. They differ from one another only near the disk's surface.

Figure 15 shows the momentum thickness Reynolds number for each simulation compared to $Re = 10^6$ in the Little and Eaton[14] experiment. The Reynolds number and momentum thickness Reynolds number are defined as

$$Re = \frac{\omega r^2}{\nu}, \tag{11}$$

$$Re_{\delta_2} = \frac{\omega r \delta_2}{\nu}. \tag{12}$$

Figure 16 shows the error of each simulation. Most inaccurate are the results of the simulations with y^+ = 5, 10, 100 and 200. The data of simulations with y^+ = 20, 30, 40 and 50 form a close group, with the result of the simulations with y^+ = 75 only slightly deviating from this group.

Figure 17 plots the value q^2

$$q^2 = \overline{u'^2} + \overline{v'^2} + \overline{w'^2}, \tag{13}$$

which is twice the turbulent kinetic energy normalized by the tangential friction velocity μ_τ^2. The data smoothing in simulations with high y^+ values is visible near the disk's surface. Again, the results of simulations with y^+ = 20, 30, 40 and 50 are in close agreement with each other. Other results deviate from this group. The turbulent kinetic energy data obtained from these simulations does not go to zero at the disk's surface; this is an inaccuracy that arises from using the High y^+ Wall Treatment and is seen throughout this entire study.

Figure 18 shows the average errors of each simulation with respect to the experimental data[14].

Based on the results of the y^+-sensitivity study of the standard k-ε turbulence model with the High y^+ Wall Treatment, the grids with y^+ = 20, 30, 40 and 50 all resulted in data that agreed

with one another very well. The only significant difference between these simulations was observed near the wall.

Star-CCM+[8] recommends to use y^+ = 30 for simulations with the High y^+ Wall Treatment. The overall close agreement of the results of the simulation with y^+ = 30 with experimental data[14] observed in the current study confirms this recommendation for the flow under consideration. Therefore, it was chosen as the y^+ value for the grids on the next sensitivity study of this turbulence model.

Computational expenses of Step 1 in the sensitivity study were rather large because of the fine grids. The computational time of the y^+ = 30 grid's simulation was 5 hours 28 minutes. These computations were done on 4 nodes of the Nano Linux cluster, with 1500 iterations. It will be shown at the end of Step 5 how much computational time can be saved by using an efficient grid.

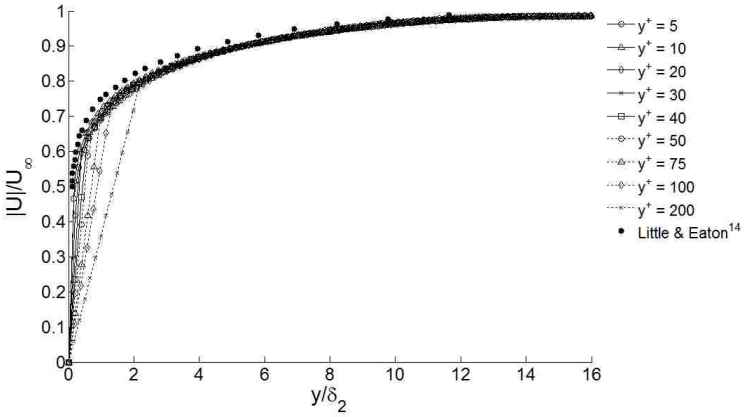

Figure 7. Turbulent mean flow vector magnitude in the rotating reference frame. *Comparison plot of the standard k-ε turbulence model for grids with varying y^+ wall cell centroid values.*

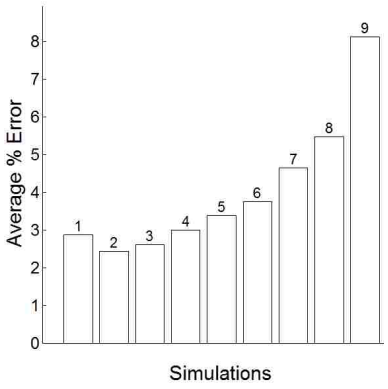

Figure 8. Error of turbulent mean flow vector magnitude. *1: y^+=5, 2: y^+=10, 3: y^+=20, 4: y^+=30, 5: y^+=40, 6: y^+=50, 7: y^+=75, 8: y^+=100, 9: y^+=200*

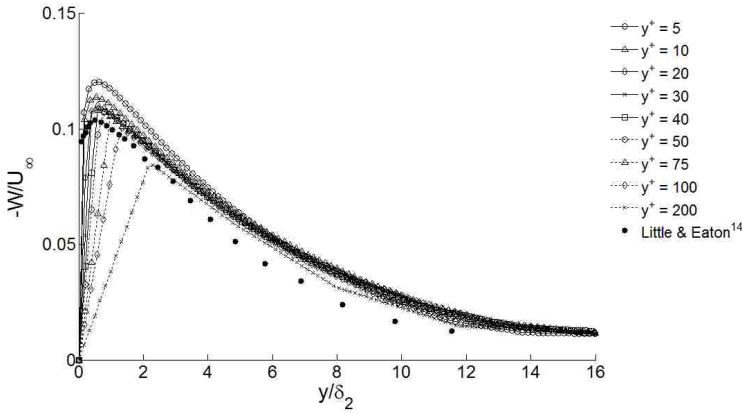

Figure 9. Crossflow profile. *Comparison plot of the standard k-ε turbulence model for grids with varying y^+ wall cell centroid values.*

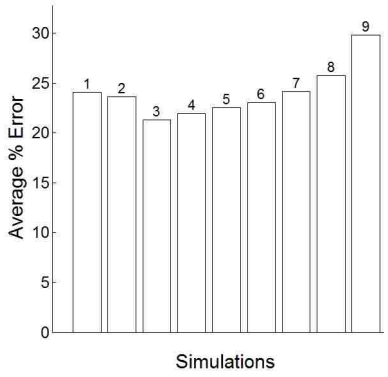

Figure 10. Error of crossflow profile. *1: y^+=5, 2: y^+=10, 3: y^+=20, 4: y^+=30, 5: y^+=40, 6: y^+=50, 7: y^+=75, 8: y^+=100, 9: y^+=200*

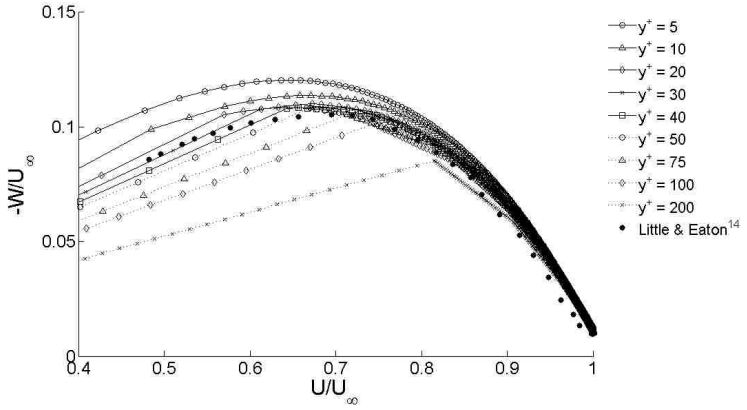

Figure 11. Polar plot of mean velocity profiles. *Comparison plot of the standard k-ε turbulence model for grids with varying y^+ wall cell centroid values.*

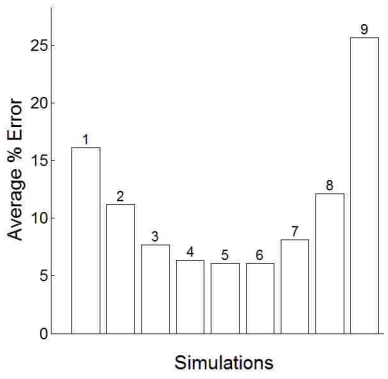

Figure 12. Error of polar mean velocity profiles. *1: y^+=5, 2: y^+=10, 3: y^+=20, 4: y^+=30, 5: y^+=40, 6: y^+=50, 7: y^+=75, 8: y^+=100, 9: y^+=200*

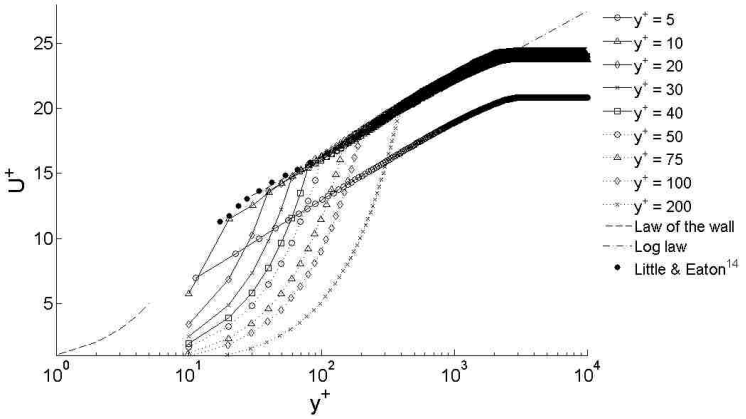

Figure 13. Tangential velocity in rotating reference frame. *Comparison plot of the standard k-ε turbulence model for grids with varying y^+ wall cell centroid values.*

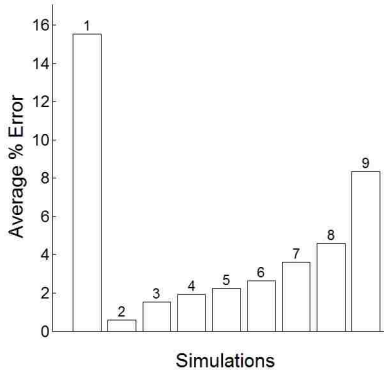

Figure 14. Error of tangential velocity. *1: y^+=5, 2: y^+=10, 3: y^+=20, 4: y^+=30, 5: y^+=40, 6: y^+=50, 7: y^+=75, 8: y^+=100, 9: y^+=200*

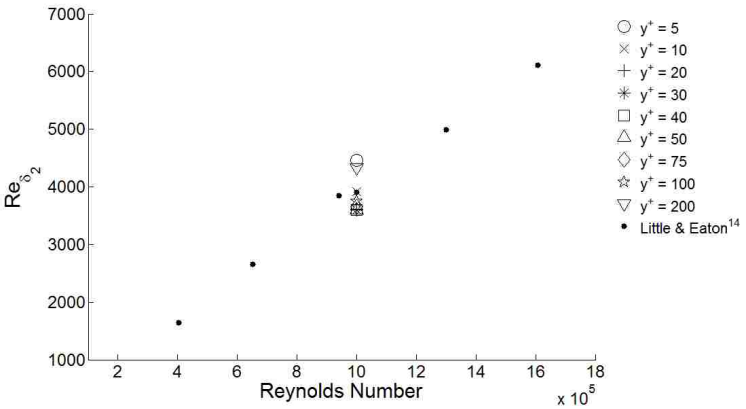

Figure 15. Comparison of momentum thickness Reynolds number. *Comparison plot of the standard k-ε turbulence model for grids with varying y^+ wall cell centroid values.*

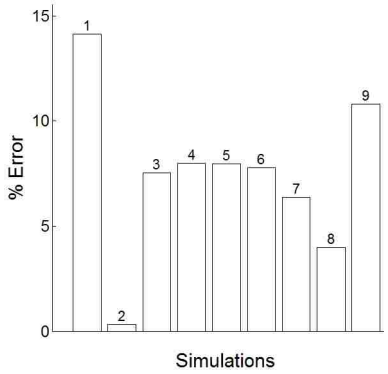

Figure 16. Error of momentum thickness Reynolds number. *1: y^+=5, 2: y^+=10, 3: y^+=20, 4: y^+=30, 5: y^+=40, 6: y^+=50, 7: y^+=75, 8: y^+=100, 9: y^+=200*

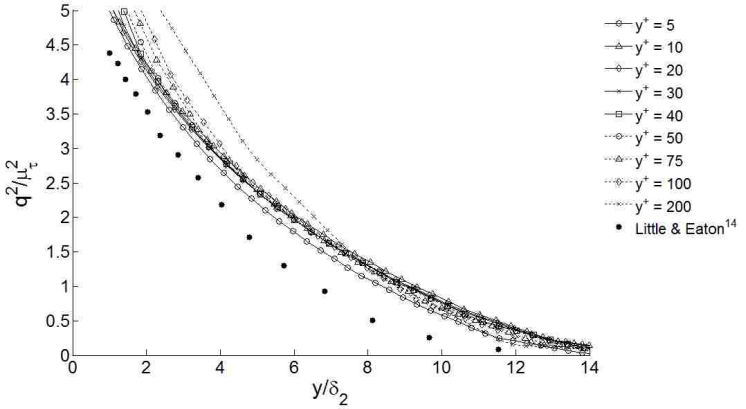

Figure 17. Twice the turbulence kinetic energy. *Comparison plot of the standard k-ε turbulence model for grids with varying y^+ wall cell centroid values.*

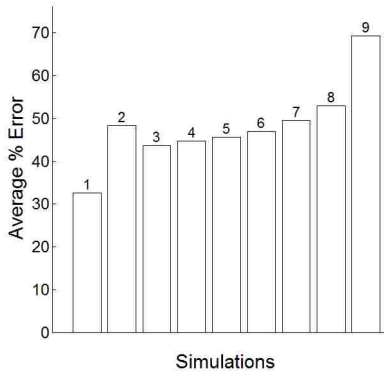

Figure 18. Error of twice the turbulence kinetic energy. *1: y^+=5, 2: y^+=10, 3: y^+=20, 4: y^+=30, 5: y^+=40, 6: y^+=50, 7: y^+=75, 8: y^+=100, 9: y^+=200*

Step 2:

The grids used for the radial and tangential grid resolution sensitivity study had the following properties:

Wall cell's centroid located at $y^+ = 30$

Computational domain size of 1x5x5 meters (axial x radial x tangential)

Stretch ratio of 1.2 in the axial direction

The following grid nodal resolutions were used (axial x radial x tangential):

33 x 508 x 508 (uniform radial and tangential grid spacing of $\approx 0.01\ m$)

33 x 254 x 254 (uniform radial and tangential grid spacing of $\approx 0.02\ m$)

33 x 127 x 127 (uniform radial and tangential grid spacing of $\approx 0.04\ m$)

33 x 64 x 64 (uniform radial and tangential grid spacing of $\approx 0.08\ m$)

33 x 32 x 32 (uniform radial and tangential grid spacing of $\approx 0.16\ m$)

A grid spacing of approximately 0.01 meters in the radial and tangential direction was chosen in Step 1 so that the initial wall cell, in the $y^+ = 5$ grid, would have an aspect ratio of 100:1. This grid resolution was chosen to avoid simulation errors in Star-CCM+[8] that occurred from the cell aspect ratios at the disk's surface being too large. The grid in Step 1 is very fine, which results in a simulation that is computationally expensive. In an effort to determine the standard k-ε turbulence model's sensitivity to grid refinement in the radial and tangential direction, the grid was coarsened. The grid's radial and tangential grid spacing is doubled in each coarser grid. This results in each grid having four times fewer cells in the domain than the previous grid, which drastically reduces the computational time for each simulation. The simulation with the coarsest grid that can reproduce the simulation profiles of the finer grids is sought after.

The turbulent mean flow vector magnitude in the rotating reference frame is shown in Fig. 19. The distance above the disk's surface is normalized by the momentum thickness boundary layer δ_2. Figure 19 shows close agreement between all grid simulation data. Figure 20 shows the average error. All of the simulation errors are similar.

The crossflow profile (Figs. 21 and 22) and the profile of the tangential velocity in the rotating reference frame (Figs. 25 and 26) show more sensitivity to the grid resolution. The

simulation profiles obtained on the coarsest grid, 33x32x32 nodes, deviate from other profiles in both cases.

The polar plot of mean velocity profiles is not sensitive to variations in the grid resolution in radial and tangential directions (Figs. 23 and 24).

Figures 27 and 28 show the momentum thickness Reynolds number and the error for each grid. Interestingly, the solution produced with the grid 33x32x32 is the closest to the experimental data[14].

The turbulent kinetic energy (Figs. 29 and 30) is also sensitive to the grid resolution. Similar to the crossflow and the tangential velocity, the turbulent kinetic energy profile obtained on the coarsest grid 33x32x32 deviates from other solutions.

Based on these results, the standard k-ε turbulence model with the High y^+ Wall Treatment can be conducted on a grid as coarse as 33x64x64 nodes without a loss in the results' accuracy. This equates to an initial wall cell aspect ratio of 66:1.

The grid of $y^+ = 30$ and radial and tangential resolution of 64x64 nodes will be held constant as the sensitivity of the cell stretch ratio in the axial direction is studied in Step 3.

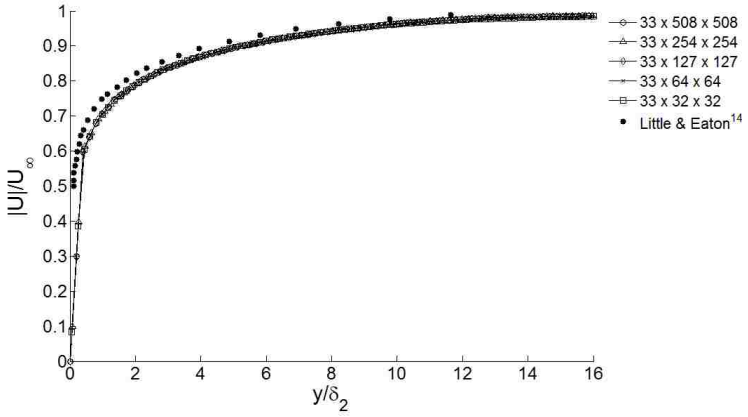

Figure 19. Turbulent mean flow vector magnitude in the rotating reference frame. *Comparison plot of the standard k-ε turbulence model for grids with varying grid resolutions in the radial and tangential directions.*

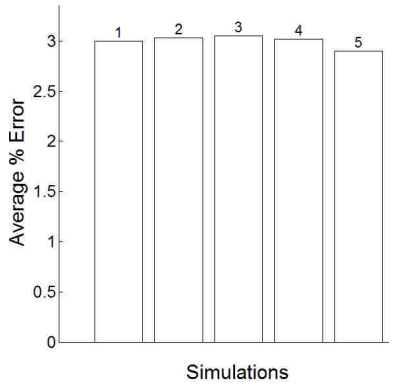

Figure 20. Error of turbulent mean flow vector magnitude. *1: 33x508x508, 2: 33x254x254, 3: 33x127x127, 4: 33x64x64, 5: 33x32x32*

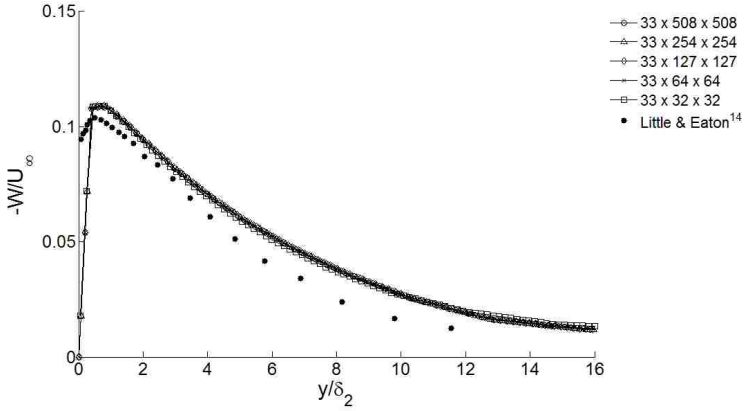

Figure 21. Crossflow profile. *Comparison plot of the standard k-ε turbulence model for grids with varying grid resolutions in the radial and tangential directions.*

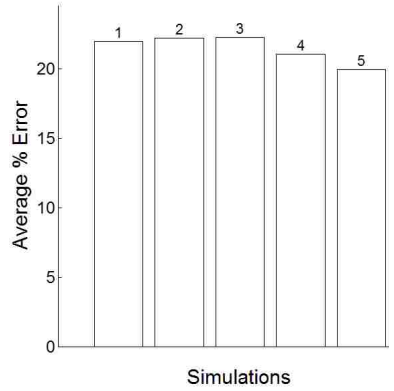

Figure 22. Error of crossflow profile. *1: 33x508x508, 2: 33x254x254, 3: 33x127x127, 4: 33x64x64, 5: 33x32x32*

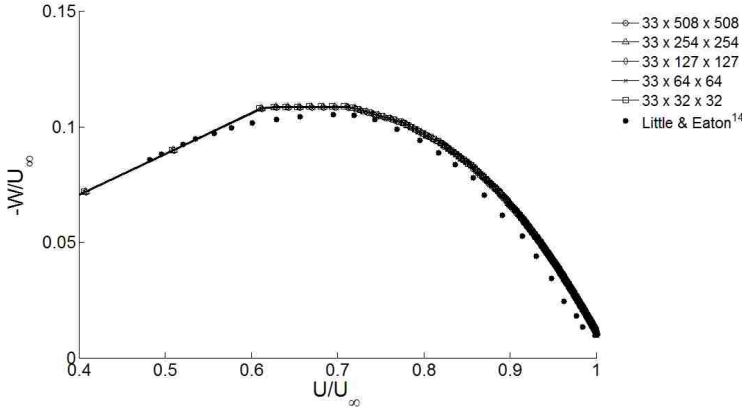

Figure 23. Polar plot of mean velocity profiles. *Comparison plot of the standard k-ε turbulence model for grids with varying grid resolutions in the radial and tangential directions.*

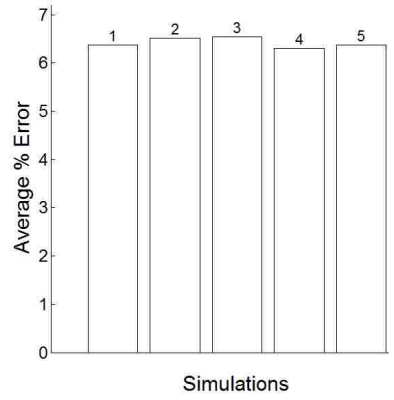

Figure 24. Error of polar mean velocity profiles. *1: 33x508x508, 2: 33x254x254, 3: 33x127x127, 4: 33x64x64, 5: 33x32x32*

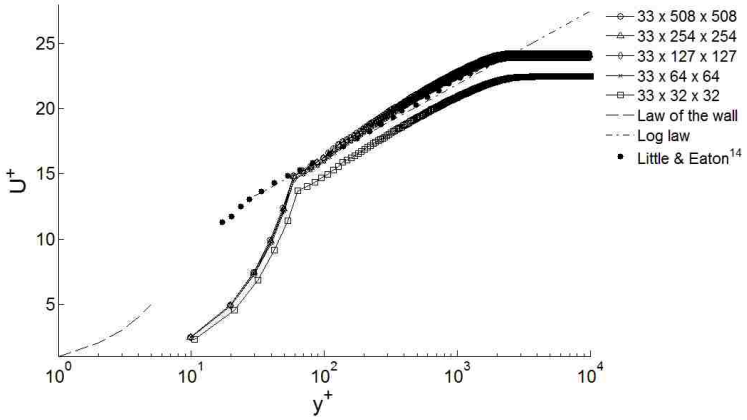

Figure 25. Tangential velocity in rotating reference frame. *Comparison plot of the standard k-ε turbulence model for grids with varying grid resolutions in the radial and tangential directions.*

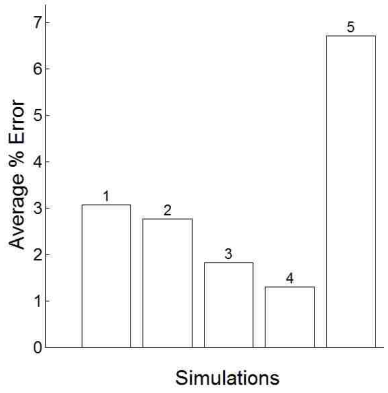

Figure 26. Error of tangential velocity. *1: 33x508x508, 2: 33x254x254, 3: 33x127x127, 4: 33x64x64, 5: 33x32x32*

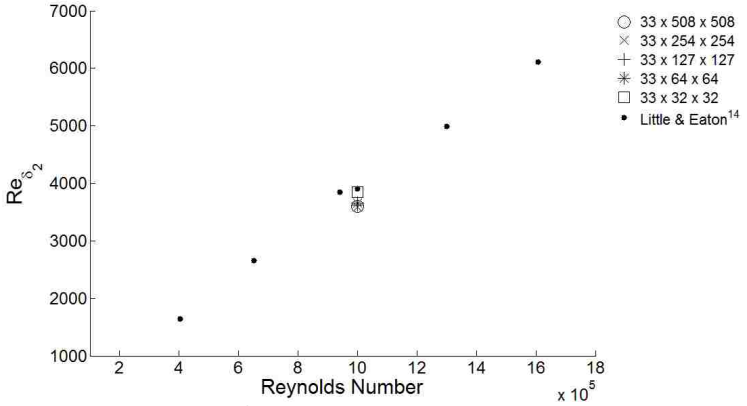

Figure 27. Comparison of momentum thickness Reynolds number. *Comparison plot of the standard k-ε turbulence model for grids with varying grid resolutions in the radial and tangential directions.*

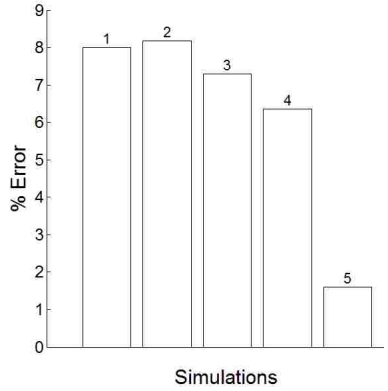

Figure 28. Error of momentum thickness Reynolds number. *1: 33x508x508, 2: 33x254x254, 3: 33x127x127, 4: 33x64x64, 5: 33x32x32*

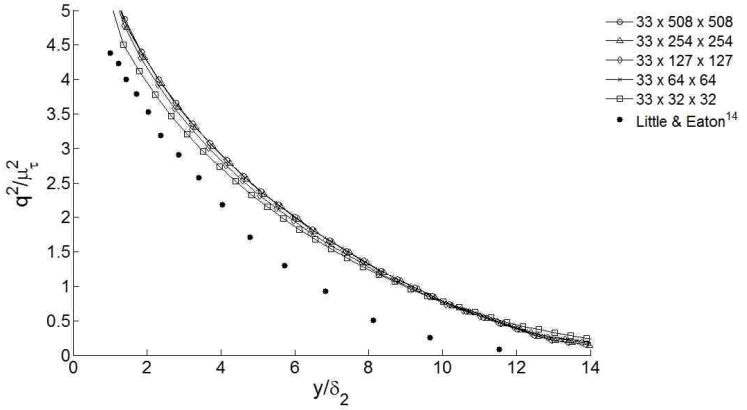

Figure 29. Twice the turbulence kinetic energy. *Comparison plot of the standard k-ε turbulence model for grids with varying grid resolutions in the radial and tangential directions.*

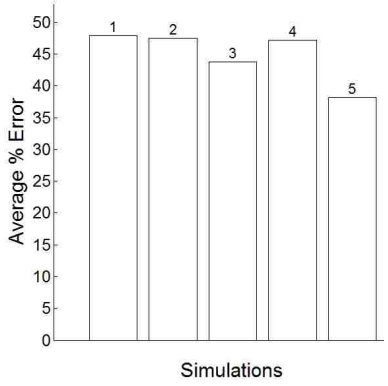

Figure 30. Error of twice the turbulence kinetic energy. *1: 33x508x508, 2: 33x254x254, 3: 33x127x127, 4: 33x64x64, 5: 33x32x32*

Step 3:

The grids used in the axial direction stretch ratio sensitivity study had the following properties:

Wall cell's centroid located at $y^+ = 30$

Computational domain size of 1x5x5 meters (axial x radial x tangential)

Radial and tangential grid resolution of 64x64 nodes (uniform grid spacing of $\approx 0.08\ m$)

In Steps 1 and 2 the grids had a stretch ratio of 1.2. In this study the stretch ratio was changed in each simulation, thus each grid has a different number of nodes in the axial direction. The following stretch ratios were used in this sensitivity study:

1.1 (55 x 64 x 64 nodes)

1.2 (33 x 64 x 64 nodes)

1.3 (25 x 64 x 64 nodes)

1.5 (18 x 64 x 64 nodes)

2.0 (12 x 64 x 64 nodes)

The goal of this sensitivity study is to find the grid with the largest stretch ratio whose simulation profile does not differ significantly from the simulation profiles obtained from smaller stretch ratios.

The turbulent mean flow vector magnitude profiles (Fig. 31 and 32) of all the simulations are in close agreement with one another. Slight variance in the stretch ratio of the 2.0 grid's simulation is visible.

The crossflow profile (Fig. 33 and 34) shows a large variance in the 2.0 stretch ratio simulation, also some slightly smaller discrepancies in the 1.5 stretch ratio simulation are visible.

In the polar plot of mean velocity profiles (Fig. 35 and 36) the only simulation with poor results is the 2.0 stretch ratio grid's simulation.

The momentum thickness Reynolds number (Fig. 39 and 40) is larger in the simulations with grids that have stretch ratios of 1.5 and 2.0 than in the simulations with grids with stretch ratios of 1.1, 1.2 and 1.3.

The turbulent kinetic energy plot (Fig. 41) shows the large discrepancies in the simulation profile with the grid with a stretch ratio 2.0. The turbulent kinetic energy profile of the 1.5

stretch ratio grid's simulation slightly differs from the more refined grids simulation profiles, which is more easily seen in the error graph (Fig. 42).

Based on the results of this sensitivity study it is seen that the simulation profiles of the grids with stretch ratios of 1.1, 1.2 and 1.3 are nearly identical. The subsequent sensitivity studies of the standard k-ε turbulence model with the High y^+ Wall Treatment will be conducted with grids that have a stretch ratio of 1.3 in the axial direction.

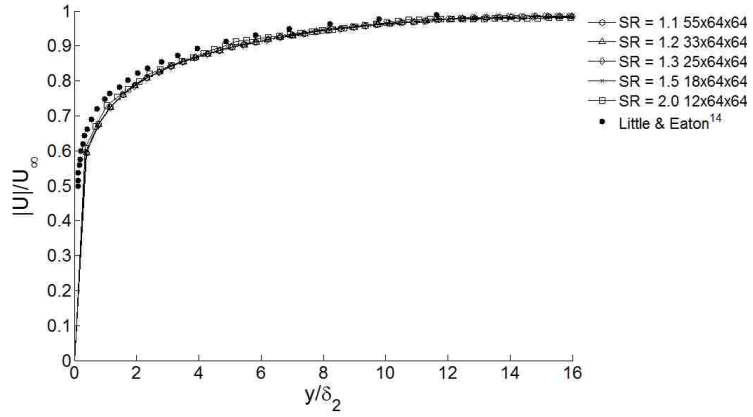

Figure 31. Turbulent mean flow vector magnitude in the rotating reference frame. *Comparison plot of the standard k-ε turbulence model for grids with varying cell stretch ratios in the axial direction.*

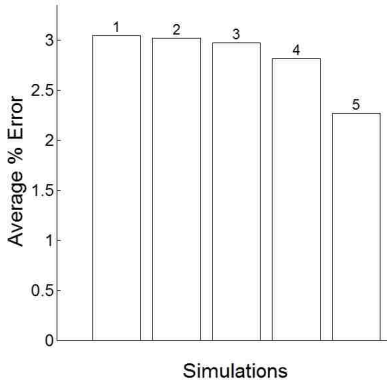

Figure 32. Error of turbulent mean flow vector magnitude. *1: SR=1.1, 2: SR=1.2, 3: SR=1.3, 4: SR=1.5, 5: SR=2.0*

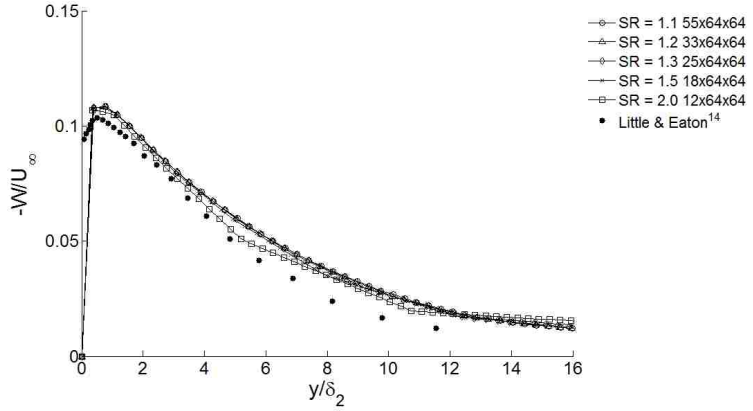

Figure 33. Crossflow profile. *Comparison plot of the standard k-ε turbulence model for grids with varying cell stretch ratios in the axial direction.*

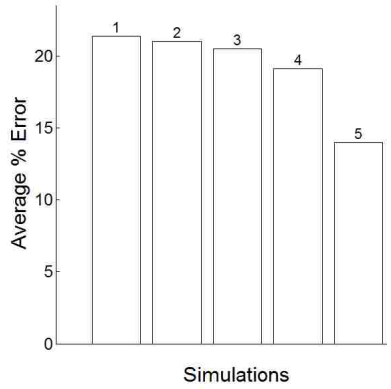

Figure 34. Error of crossflow profile. *1: SR=1.1, 2: SR=1.2, 3: SR=1.3, 4: SR=1.5, 5: SR=2.0*

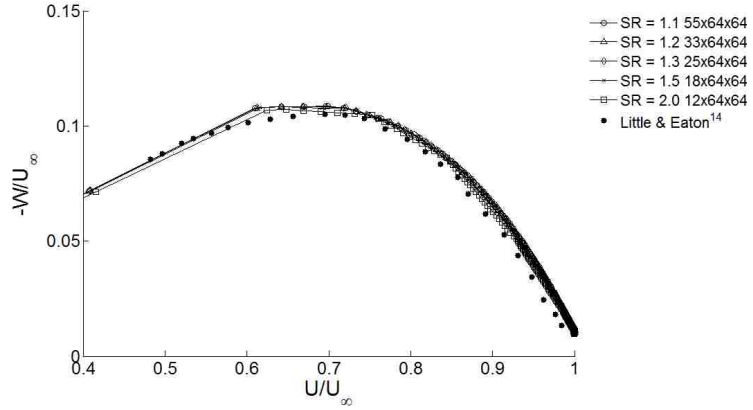

Figure 35. Polar plot of mean velocity profiles. *Comparison plot of the standard k-ε turbulence model for grids with varying cell stretch ratios in the axial direction.*

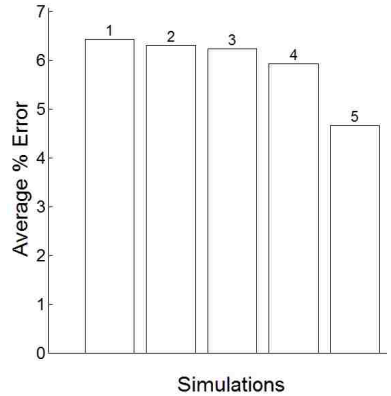

Figure 36. Error of polar mean velocity profiles. *1: SR=1.1, 2: SR=1.2, 3: SR=1.3, 4: SR=1.5, 5: SR=2.0*

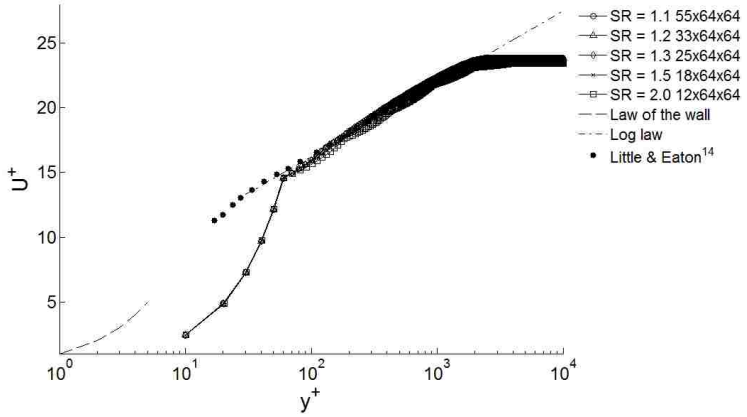

Figure 37. Tangential velocity in rotating reference frame. *Comparison plot of the standard k-ε turbulence model for grids with varying cell stretch ratios in the axial direction.*

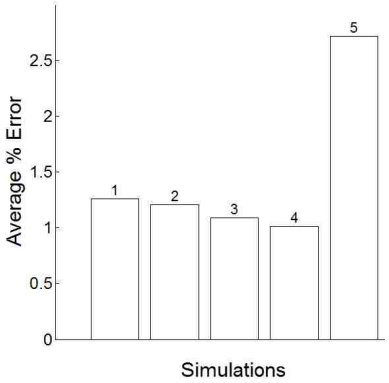

Figure 38. Error of tangential velocity. *1: SR=1.1, 2: SR=1.2, 3: SR=1.3, 4: SR=1.5, 5: SR=2.0*

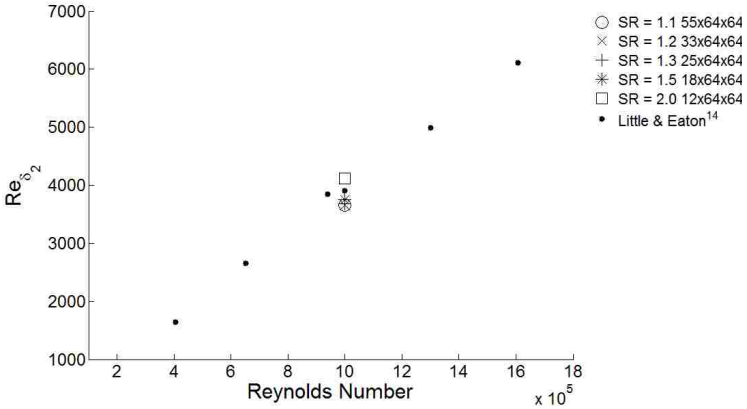

Figure 39. Comparison of momentum thickness Reynolds number. *Comparison plot of the standard k-ε turbulence model for grids with varying cell stretch ratios in the axial direction.*

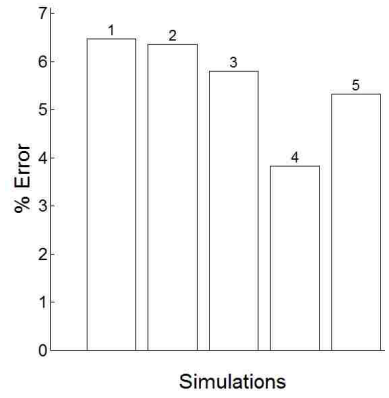

Figure 40. Error of momentum thickness Reynolds number. *1: SR=1.1, 2: SR=1.2, 3: SR=1.3, 4: SR=1.5, 5: SR=2.0*

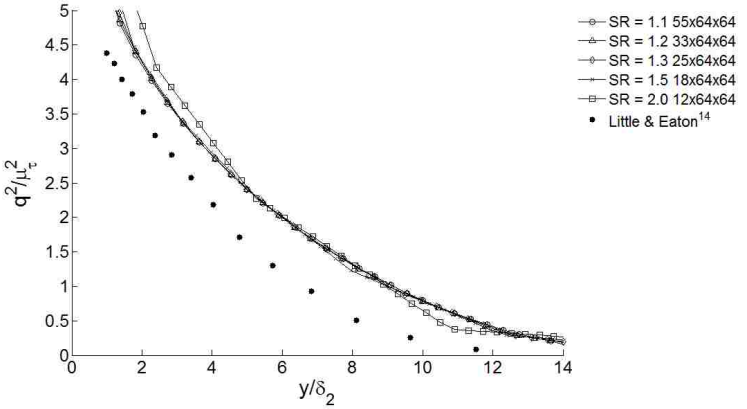

Figure 41. Twice the turbulence kinetic energy. *Comparison plot of the standard k-ε turbulence model for grids with varying cell stretch ratios in the axial direction.*

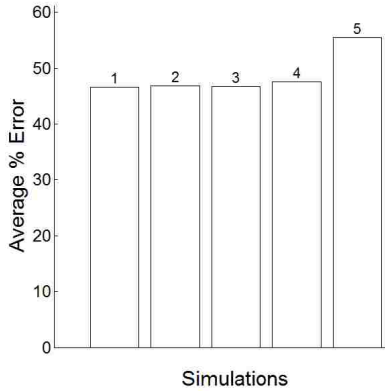

Figure 42. Error of twice the turbulence kinetic energy. *1: SR=1.1, 2: SR=1.2, 3: SR=1.3, 4: SR=1.5, 5: SR=2.0*

Step 4:

The grids used for the radial and tangential wall proximity sensitivity study had the following properties:

Wall cell's centroid located at $y^+ = 30$

Uniform radial and tangential grid spacing of $\approx 0.08\ m$

Stretch ratio of 1.3 in the axial direction

Computational domain size of 1 meter in the axial direction

This sensitivity study will adjust the position of the pressure outlet boundaries. In the previous simulations the computational domain size was 1x5x5 meters in the axial, radial and tangential directions respectively. The line probe at which data is being sampled is at a radius of 0.421 meters from the axis of rotation and extends above the disk's surface 0.1 meters. In Steps 1, 2 and 3 the distance between the line probe and the nearest pressure outlet was 2.079 meters. In this sensitivity study the computational domain was varied in the radial and tangential directions. The domain sizes in this study are:

1 x 10 x 10 meters, 25 x 128 x 128 nodes (axial, radial, tangential)

1 x 5 x 5 meters, 25 x 64 x 64 nodes

1 x 2 x 2 meters, 25 x 26 x 26 nodes

1 x 1 x 1 meters, 25 x 13 x 13 nodes

The goal of this sensitivity study is to find the smallest computational domain whose simulation profile does not vary significantly from the simulation profiles of the larger domains. The smallest computational domain puts the pressure outlets as close as 0.5 meters from the axis of rotation, which is only 0.079 meters from the data sampling locations. The largest domain puts the nearest pressure outlet 4.579 meters away from the data sampling locations.

Figures 43 and 44 show that there is negligible difference between all the profiles of the turbulent mean flow vector magnitude in the rotating reference frame. Only the smallest domain's simulation profile slightly deviates from others far from the disk's surface.

The crossflow profile (Figs. 45 and 46) and the polar plot of the mean velocity profile (Figs. 47 and 48) illustrate sensitivity to the pressure outlets' location. The 1x1x1 meter computational domain simulation profile is unable to replicate the simulation profiles of the other domain sizes.

The tangential velocity in the rotating reference frame (Figs. 49 and 50) is nearly unaffected by the proximity of the pressure outlet. All of the simulation profiles are in close agreement.

In Figure 51 the momentum thickness Reynolds number is shown. The 1x1x1 meter domain simulation's momentum thickness Reynolds number is slightly less than the other simulation's momentum thickness Reynolds number.

Figures 53 and 54 show that the turbulent kinetic energy profile obtained in the 1x1x1 meter domain slightly vary from the simulation profiles obtained in larger domains.

The data of this sensitivity study indicates that the domain size of 1x2x2 meters can be chosen without errors induced onto Star-CCM+'s[8] solution for the standard k-ε turbulence model with the High y^+ Wall Treatment.

The last sensitivity study of this turbulence model uses the radial and tangential domain size of 2x2 meters while the axial domain size is varied.

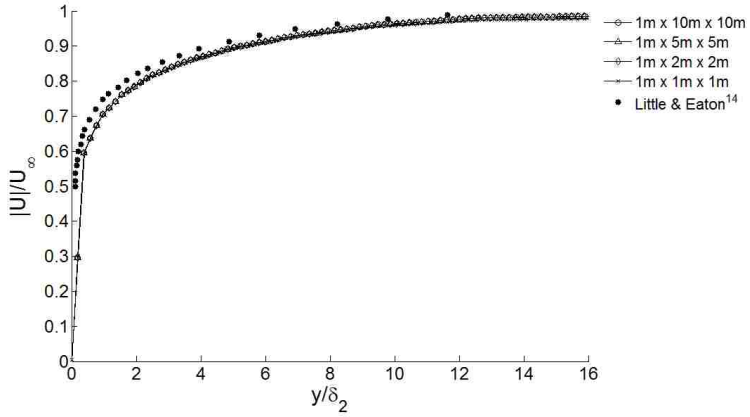

Figure 43. Turbulent mean flow vector magnitude in the rotating reference frame. *Comparison plot of the standard k-ε turbulence model for grids with varying computational domain sizes in the radial and tangential directions.*

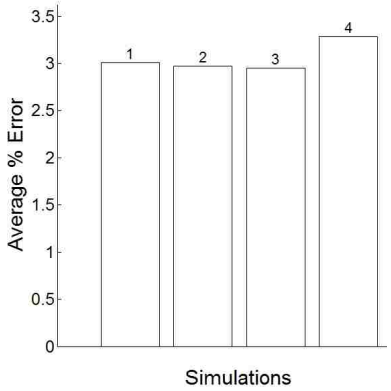

Figure 44. Error of turbulent mean flow vector magnitude. *1: 1x10x10m, 2: 1x5x5m, 3: 1x2x2m, 4: 1x1x1m*

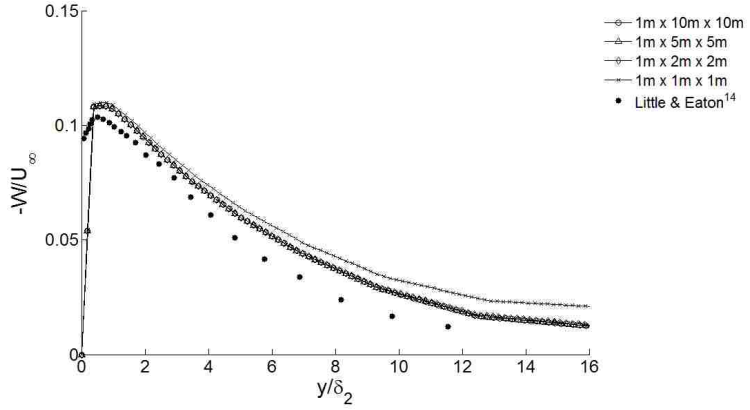

Figure 45. Crossflow profile. *Comparison plot of the standard k-ε turbulence model for grids with varying computational domain sizes in the radial and tangential directions.*

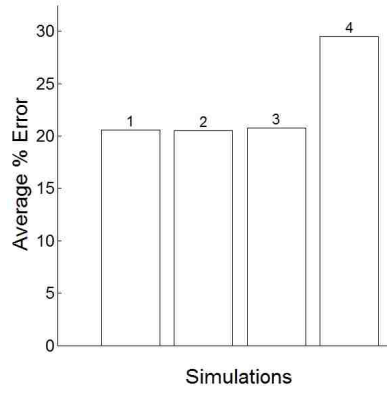

Figure 46. Error of crossflow profile. *1: 1x10x10m, 2: 1x5x5m, 3: 1x2x2m, 4: 1x1x1m*

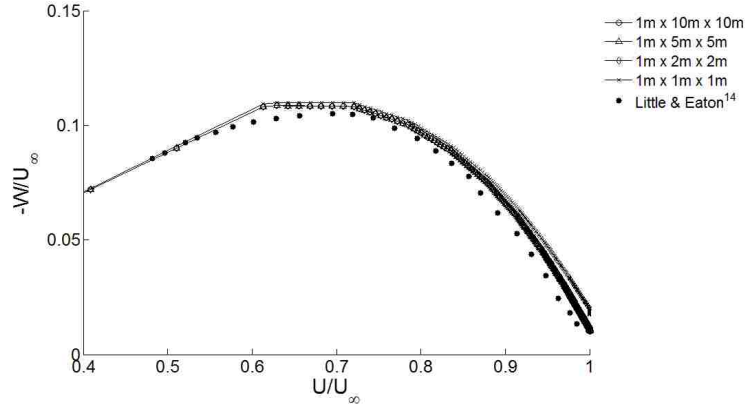

Figure 47. Polar plot of mean velocity profiles. *Comparison plot of the standard k-ε turbulence model for grids with varying computational domain sizes in the radial and tangential directions.*

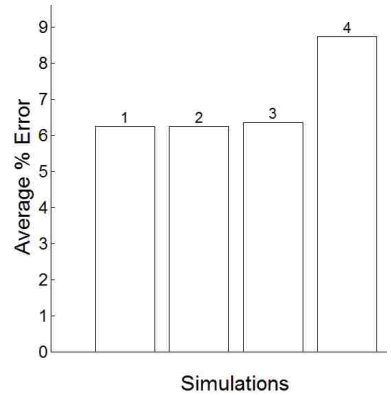

Figure 48. Error of polar mean velocity profiles. *1: 1x10x10m, 2: 1x5x5m, 3: 1x2x2m, 4: 1x1x1m*

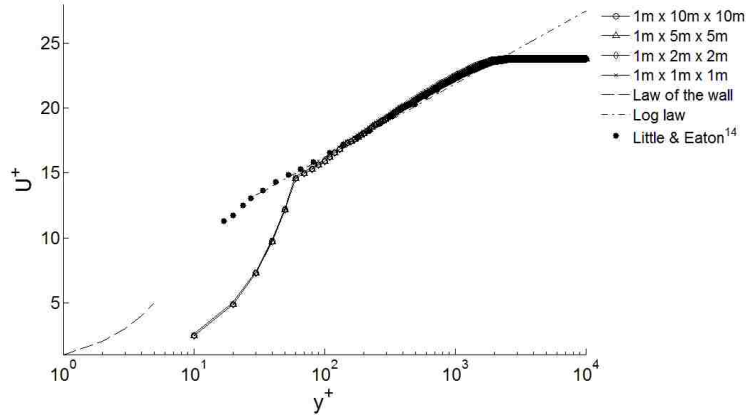

Figure 49. Tangential velocity in rotating reference frame. *Comparison plot of the standard k-ε turbulence model for grids with varying computational domain sizes in the radial and tangential directions.*

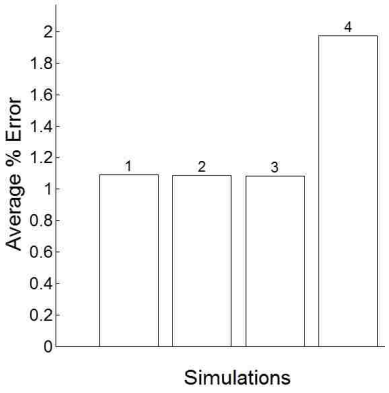

Figure 50. Error of tangential velocity. *1: 1x10x10m, 2: 1x5x5m, 3: 1x2x2m, 4: 1x1x1m*

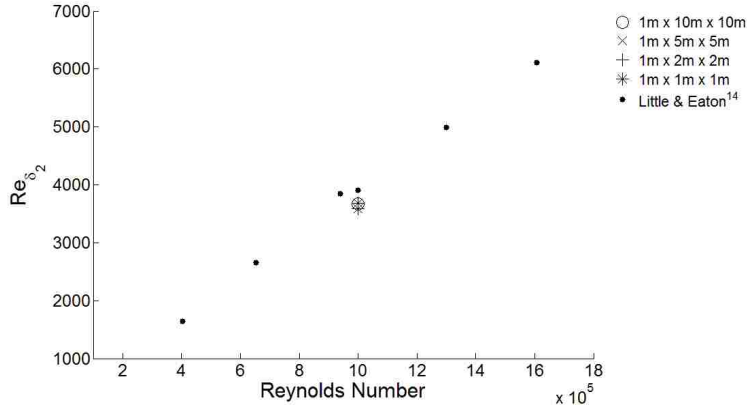

Figure 51. Comparison of momentum thickness Reynolds number. *Comparison plot of the standard k-ε turbulence model for grids with varying computational domain sizes in the radial and tangential directions.*

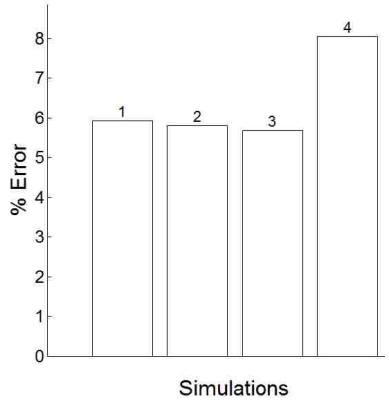

Figure 52. Error of momentum thickness Reynolds number. *1: 1x10x10m, 2: 1x5x5m, 3: 1x2x2m, 4: 1x1x1m*

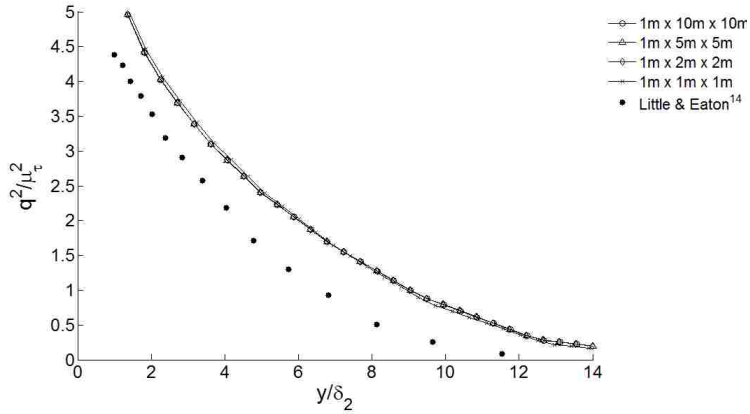

Figure 53. Twice the turbulence kinetic energy. *Comparison plot of the standard k-ε turbulence model for grids with varying computational domain sizes in the radial and tangential directions.*

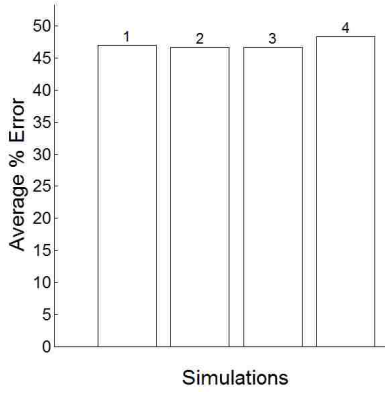

Figure 54. Error of twice the turbulence kinetic energy. *1: 1x10x10m, 2: 1x5x5m, 3: 1x2x2m, 4: 1x1x1m*

Step 5:

The grids used in the axial wall proximity sensitivity study had the following properties:

Wall cell's centroid located at $y^+ = 30$

Computational domain size in the radial and tangential direction of 2x2 meters

Radial and tangential grid resolution of 26x26 nodes (uniform grid spacing of = 0.08 *m*)

Stretch ratio of 1.3 in the axial direction

This sensitivity study will adjust the position of the velocity inlet boundary above the disk's surface. Steps 1-4 positioned the velocity inlet 1 meter above the disk's surface and prescribed an inlet velocity of 1 *m/s*. Adjusting the position of the velocity inlet boundary is not as simple as adjusting the position of the pressure outlet boundaries because the velocity inlet is the only boundary where the flow velocity must be prescribed. Since the flow velocity profile varies throughout the computational domain, the inlet velocity must be set to different values as the velocity inlet's location is altered. The inlet velocity of 1 *m/s* was prescribed on the largest domain of 5x2x2 meters (axial, radial, tangential) and the axial velocity was sampled at locations 2.5, 1.0, 0.5, 0.25 and 0.1 meters above the disk's surface at $r = 0.421$ *m*. The measured axial velocities were prescribed at the velocity inlet for each respective simulation. The domain sizes and inlet velocity prescribed for the simulations in this sensitivity study are as follows:

5 x 2 x 2 meters (axial, radial, tangential), velocity prescribed at inlet = 1 *m/s*

2.5 x 2 x 2 meters, velocity prescribed at inlet = 0.994 *m/s*

1 x 2 x 2 meters, velocity prescribed at inlet = 0.876 *m/s*

0.5 x 2 x 2 meters, velocity prescribed at inlet = 0.672 *m/s*

0.25 x 2 x 2 meters, velocity prescribed at inlet = 0.477 *m/s*

0.1 x 2 x 2 meters, velocity prescribed at inlet = 0.324 *m/s*

The mean flow vector magnitude (Figs. 55 and 56), the profile of tangential velocity in the rotating reference frame (Figs. 61 and 62) and the turbulent kinetic energy profile (Figs. 65 and 66) all show a lack of sensitivity to the velocity inlet's position, as all of the simulation profiles are in close agreement.

The crossflow profile (Fig. 57), the polar plot of mean velocity profiles (Fig. 59) and the momentum thickness Reynolds number (Fig. 63) all show a high sensitivity to the velocity inlet's position. The 5 and 2.5 meter axial domain simulation profiles are in close agreement, while all the other simulation profiles differ from one another. This is clearly seen in the error graphs (Figs. 58, 60 and 62), where the two largest domain simulation results have nearly identical error values while the average error increases as the simulations' domain size decreases.

The computational domain size of 2.5x2x2 meters is the smallest domain size whose simulation results do not stray from simulation results obtained from the largest computational domain. Thus it was chosen, from a practical point of view, as the most suitable grid for this simulation using the standard k-ε turbulence model with the High y^+ Wall Treatment.

The computation time for the simulation using this grid was 3 minutes and 24 seconds, computed on the desktop computer, out to 1500 iterations. Comparing this time to the 5 hours and 28 minutes it took to compute the simulation on the Nano Linux cluster, for the initial y^+ = 30 grid in Step 1, illustrates the benefit of having an efficiently sized grid.

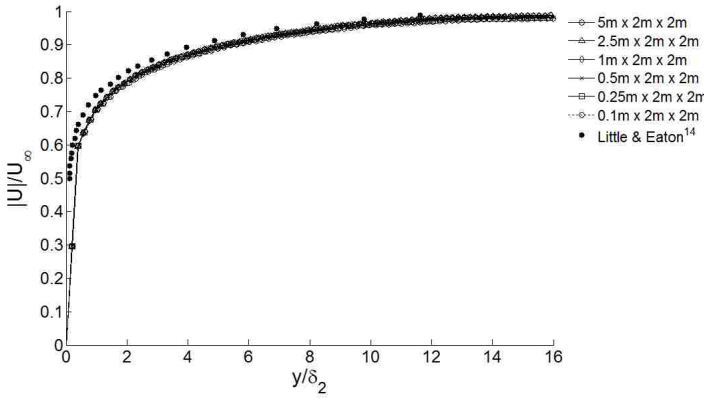

Figure 55. Turbulent mean flow vector magnitude in the rotating reference frame. *Comparison plot of the standard k-ε turbulence model for grids with varying computational domain sizes in the axial direction.*

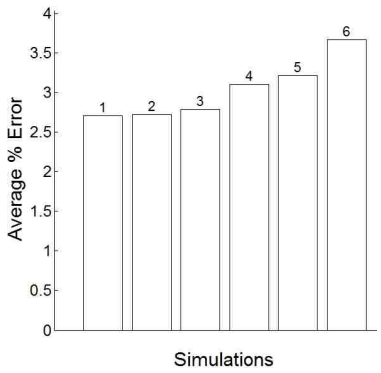

Figure 56. Error of turbulent mean flow vector magnitude. *1: 5x2x2m, 2: 2.5x2x2m, 3: 1x2x2m, 4: 0.5x2x2m, 5: 0.25x2x2m, 6: 0.1x2x2m*

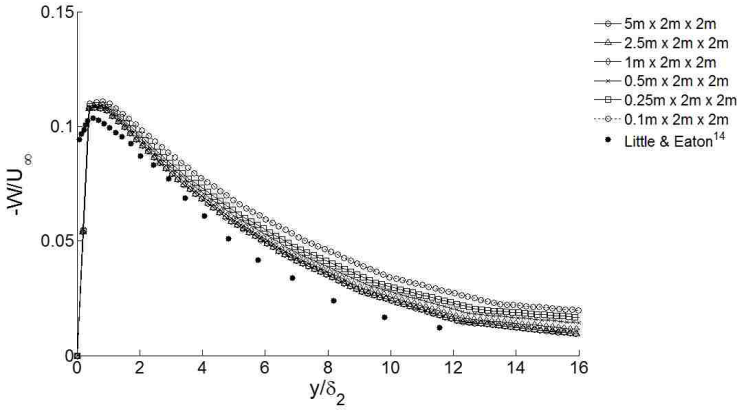

Figure 57. Crossflow profile. *Comparison plot of the standard k-ε turbulence model for grids with varying computational domain sizes in the axial direction.*

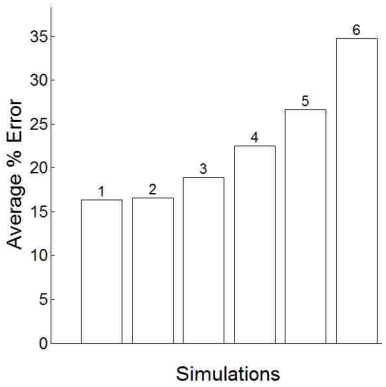

Figure 58. Error of crossflow profile. *1: 5x2x2m, 2: 2.5x2x2m, 3: 1x2x2m, 4: 0.5x2x2m, 5: 0.25x2x2m, 6: 0.1x2x2m*

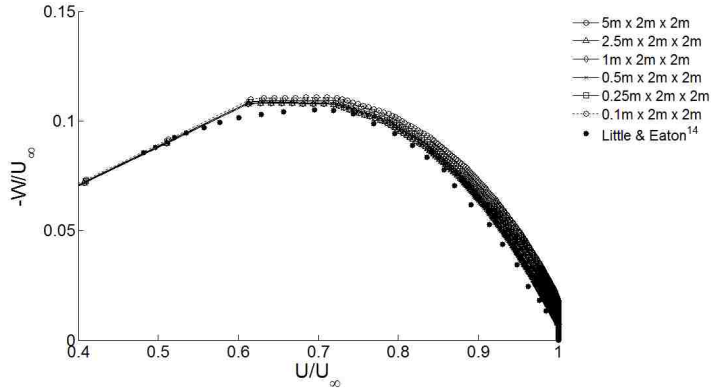

Figure 59. Polar plot of mean velocity profiles. *Comparison plot of the standard k-ε turbulence model for grids with varying computational domain sizes in the axial direction.*

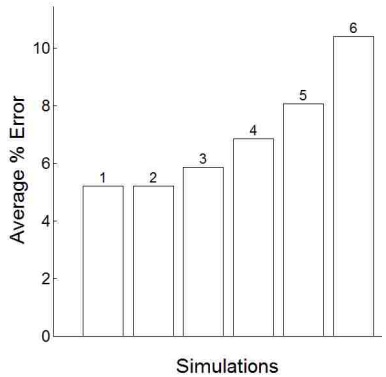

Figure 60. Error of polar mean velocity profiles. *1: 5x2x2m, 2: 2.5x2x2m, 3: 1x2x2m, 4: 0.5x2x2m, 5: 0.25x2x2m, 6: 0.1x2x2m*

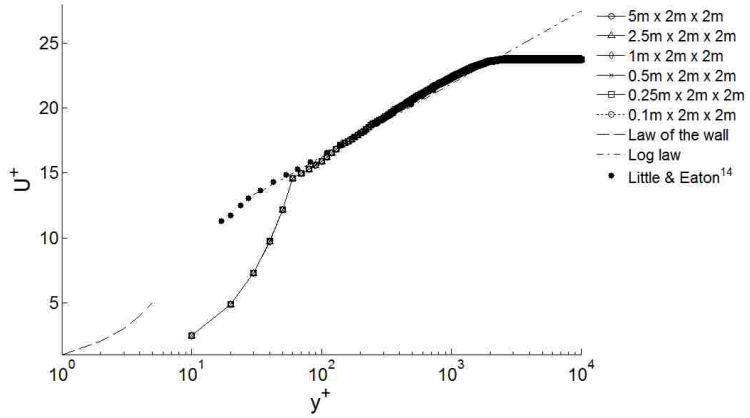

Figure 61. Tangential velocity in rotating reference frame. *Comparison plot of the standard k-ε turbulence model for grids with varying computational domain sizes in the axial direction.*

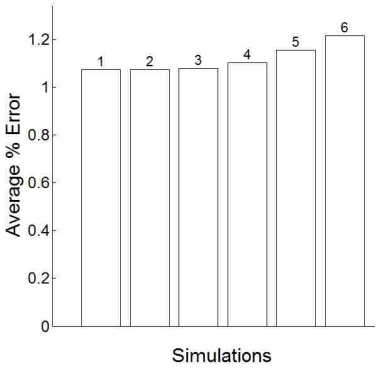

Figure 62. Error of tangential velocity. *1: 5x2x2m, 2: 2.5x2x2m, 3: 1x2x2m, 4: 0.5x2x2m, 5: 0.25x2x2m, 6: 0.1x2x2m*

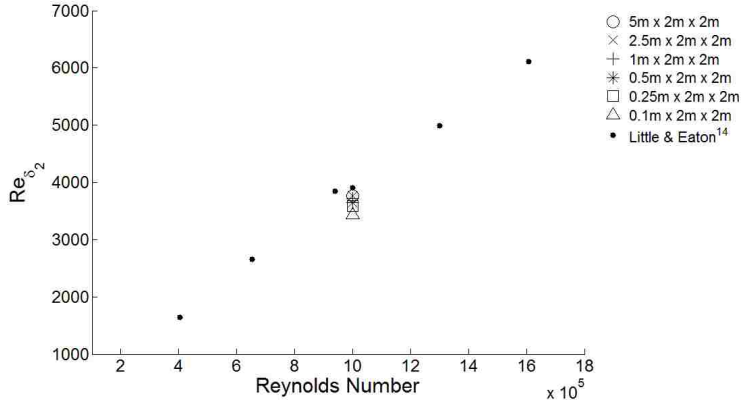

Figure 63. Comparison of momentum thickness Reynolds number. *Comparison plot of the standard k-ε turbulence model for grids with varying computational domain sizes in the axial direction.*

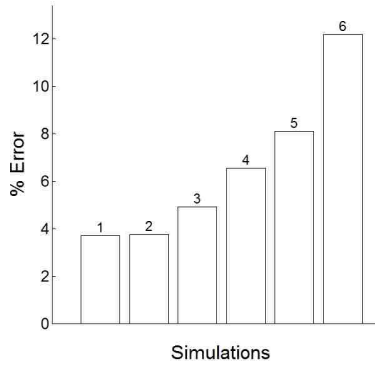

Figure 64. Error of momentum thickness Reynolds number. *1: 5x2x2m, 2: 2.5x2x2m, 3: 1x2x2m, 4: 0.5x2x2m, 5: 0.25x2x2m, 6: 0.1x2x2m*

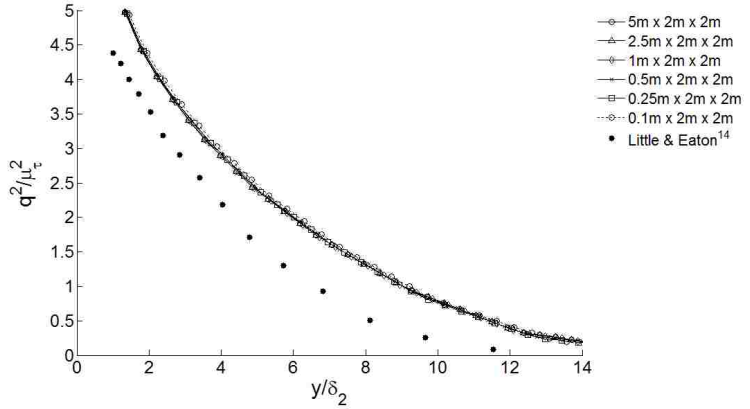

Figure 65. Twice the turbulence kinetic energy. *Comparison plot of the standard k-ε turbulence model for grids with varying computational domain sizes in the axial direction.*

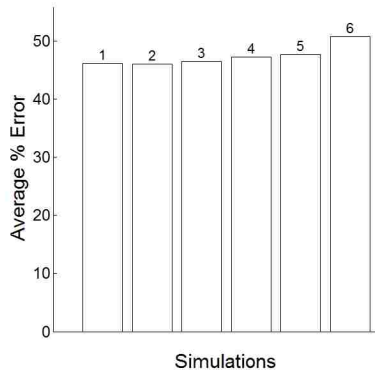

Figure 66. Error of twice the turbulence kinetic energy. *1: 5x2x2m, 2: 2.5x2x2m, 3: 1x2x2m, 4: 0.5x2x2m, 5: 0.25x2x2m, 6: 0.1x2x2m*

2. Standard *k*-ω model

Step 1:

The grids used for the y^+ sensitivity study had the following properties:

Computational domain size of 1x5x5 meters (axial x radial x tangential)

Stretch ratio of 1.2 in the axial direction

Uniform radial and tangential resolution of 508x508 nodes

Grids with the following initial cell's centroid y^+ values were included in this sensitivity study:

y^+ = 5 (42 x 508 x 508 nodes)

y^+ = 10 (39 x 508 x 508 nodes)

y^+ = 20 (36 x 508 x 508 nodes)

y^+ = 30 (33 x 508 x 508 nodes)

y^+ = 40 (32 x 508 x 508 nodes)

y^+ = 50 (31 x 508 x 508 nodes)

y^+ = 75 (28 x 508 x 508 nodes)

y^+ = 100 (27 x 508 x 508 nodes)

y^+ = 200 (23 x 508 x 508 nodes)

Since the High y^+ Wall Treatment was used, it was not necessary to go below y^+ = 5 as the simulation results will show. The turbulent mean flow vector magnitude in the rotating reference frame is shown in Fig. 67. The distance above the disk's surface is normalized by the momentum thickness boundary layer, δ_2. All of the simulation results agree very well except near the disk's surface. This disagreement is due to the refinement differences near the wall. Straight lines are seen in the simulation profiles of the grids with high y^+ values. These straight lines are the linear interpolation across the cell that is a result of the data smoothing procedure utilized in Star-CCM+[8]. The data smoothing across the cell is done for all y^+ values but is only seen in the high y^+ simulations due to the length of these cells. Figure 68 shows the errors of the simulation results. The larger error of the simulations with high y^+ values is mostly due to the data near the disk's surface.

The crossflow profile (Figs. 69 and 70) demonstrates a high sensitivity to different y^+ values near the disk's surface. The y^+ = 20, 30, 40, 50, 75 and 100 simulation profiles agree very well past the near wall discrepancies. The simulations with y^+ = 5 and 10 produce results that overshoot the amount of crossflow near the disk's surface while the simulation with a y^+ = 200 value has a profile that undershoots the amount of crossflow near the disk surface.

Figure 71 is the polar plot of mean velocity profiles. The data obtained from the y^+ = 20, 30, 40, and 50 simulations agree with one another in the area far from the wall. This plot demonstrates the inadequacy of the High y^+ Wall Treatment near the disk's surface for this model as well. The y^+ = 200 simulation's initial cell is so large that the data smoothing over the cell accounts for the data in the approximate range $0 \leq U/U_\infty \leq 0.8$. This is why the high y^+ simulation profiles fall off the experimental data[14] trend so abruptly. This same data fall off is visible down to the resolution of y^+ = 10.

Figure 73 is a semi-logarithmic plot of U^+ vs. y^+. All of the simulation profiles are very similar far from the disk's surface and follow the log law and experimental data[14] very closely with the exception of the y^+ = 5 simulation, which shows disagreement with the experimental data[14] throughout the computational domain. Also, the simulation profile obtained with y^+ = 10 deviates from the other profiles far from the disk's surface and is in better agreement with the experimental data[14]. This is reflected by the error graph in Fig. 74. Figure 74 also shows that the errors of the simulation profiles obtained with y^+ = 20, 30, 40 and 50 again are very similar.

Figure 75 shows the momentum thickness Reynolds number for each simulation compared to the Little and Eaton[14] experiment conducted at $Re = 10^6$. Figure 76 shows the error of each simulation. The data of simulations with y^+ = 5 and 200 have the greatest disagreement with the y^+ = 20, 30, 40 and 50 grid simulation results.

Figure 77 demonstrates that the results of simulations with y^+ = 20, 30, 40 and 50 are in close agreement with each other. Other results vary from this group. The data smoothing in the simulations with high y^+ values is visible near the disk's surface. Figure 78 shows the average errors of each simulation with respect to the experimental data[14].

Based on the results of the y^+-sensitivity study of the standard k-ω turbulence model with the High y^+ Wall Treatment, we can infer that the grids with y^+ = 20, 30, 40 and 50 all resulted in data that agreed with one another very well. The only significant difference between these simulations was observed near the wall.

Based on our observations and the Star-CCM+[8] recommendations, y^+ = 30 was chosen as the y^+ value for the grids in the next sensitivity study of this turbulence model.

Computational expenses of these simulations were also very large because of the fine grids. The computational time of the y^+ = 30 grid's simulation was 5 hours 32 minutes. This computation was done on 4 nodes of the Nano Linux cluster, with 1500 iterations.

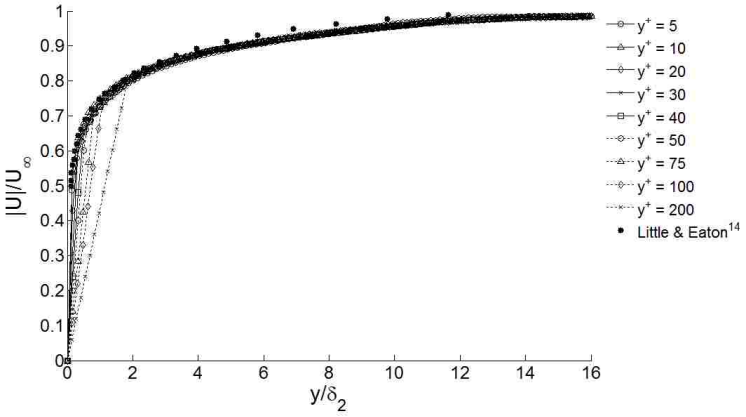

Figure 67. Turbulent mean flow vector magnitude in the rotating reference frame. *Comparison plot of the standard k-ω turbulence model for grids with varying y^+ wall cell centroid values.*

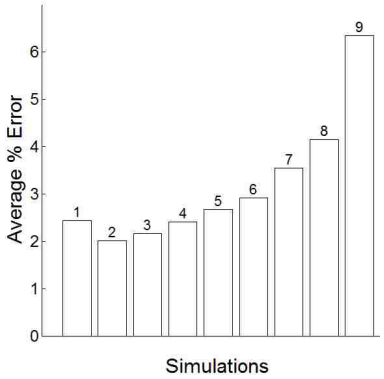

Figure 68. Error of turbulent mean flow vector magnitude. *1: y^+=5, 2: y^+=10, 3: y^+=20, 4: y^+=30, 5: y^+=40, 6: y^+=50, 7: y^+=75, 8: y^+=100, 9: y^+=200*

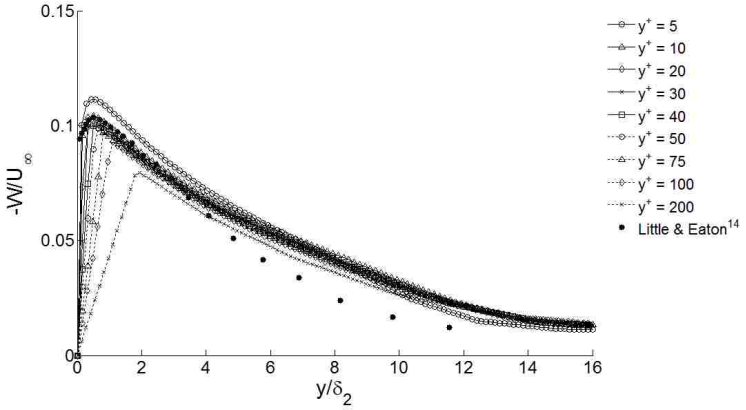

Figure 69. Crossflow profile. *Comparison plot of the standard k-ω turbulence model for grids with varying y^+ wall cell centroid values.*

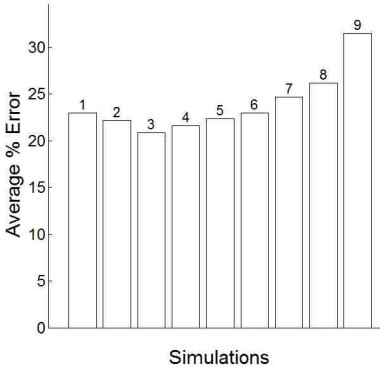

Figure 70. Error of crossflow profile. *1: y^+=5, 2: y^+=10, 3: y^+=20, 4: y^+=30, 5: y^+=40, 6: y^+=50, 7: y^+=75, 8: y^+=100, 9: y^+=200*

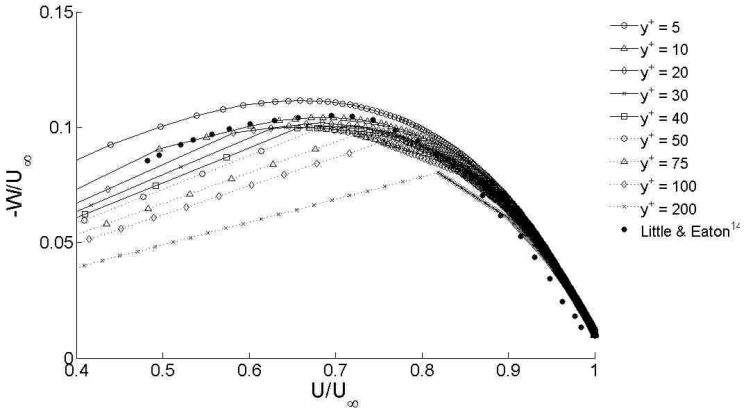

Figure 71. Polar plot of mean velocity profiles. *Comparison plot of the standard k-ω turbulence model for grids with varying y^+ wall cell centroid values.*

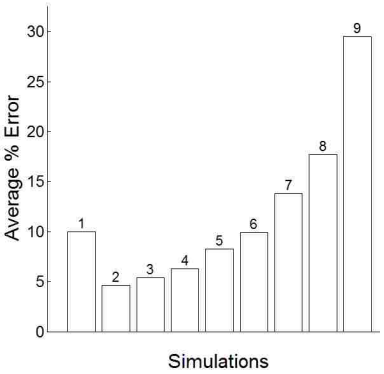

Figure 72. Error of polar mean velocity profiles. *1: y^+=5, 2: y^+=10, 3: y^+=20, 4: y^+=30, 5: y^+=40, 6: y^+=50, 7: y^+=75, 8: y^+=100, 9: y^+=200*

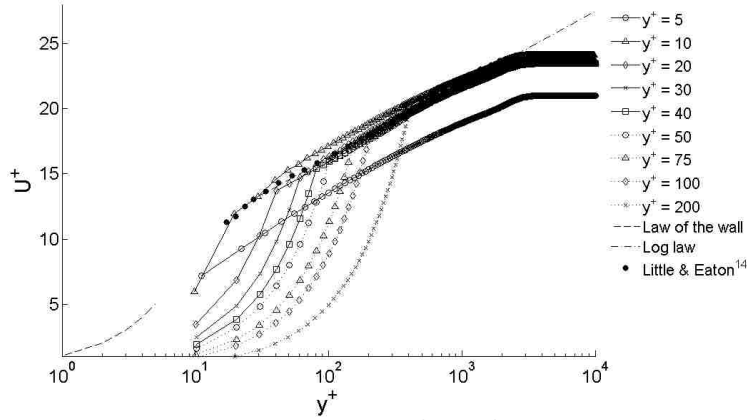

Figure 73. Tangential velocity in rotating reference frame. *Comparison plot of the standard k-ω turbulence model for grids with varying y^+ wall cell centroid values.*

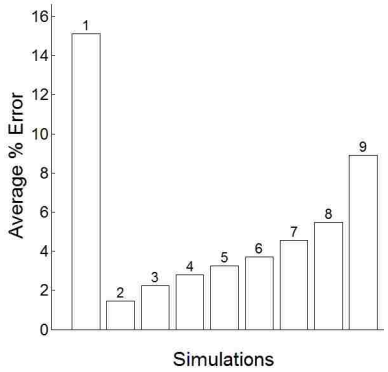

Figure 74. Error of tangential velocity. *1: y^+=5, 2: y^+=10, 3: y^+=20, 4: y^+=30, 5: y^+=40, 6: y^+=50, 7: y^+=75, 8: y^+=100, 9: y^+=200*

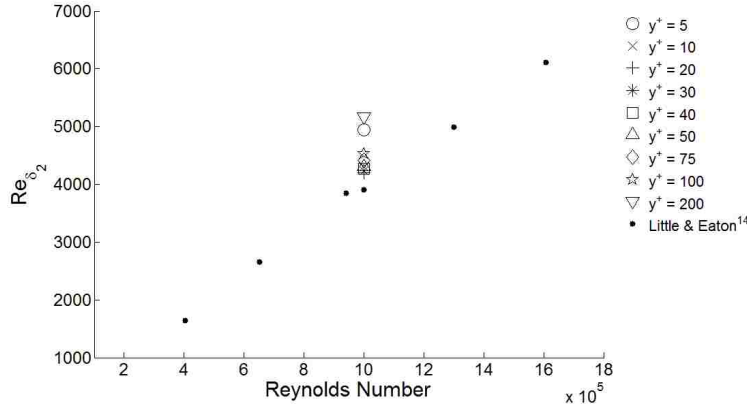

Figure 75. Comparison of momentum thickness Reynolds number. *Comparison plot of the standard k-ω turbulence model for grids with varying y^+ wall cell centroid values.*

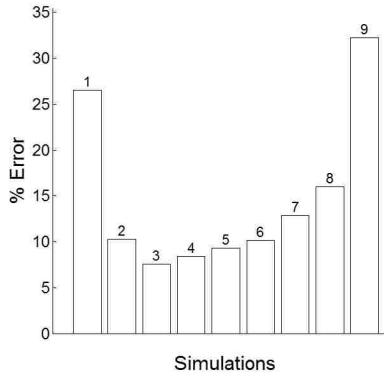

Figure 76. Error of momentum thickness Reynolds number. *1: y^+=5, 2: y^+=10, 3: y^+=20, 4: y^+=30, 5: y^+=40, 6: y^+=50, 7: y^+=75, 8: y^+=100, 9: y^+=200*

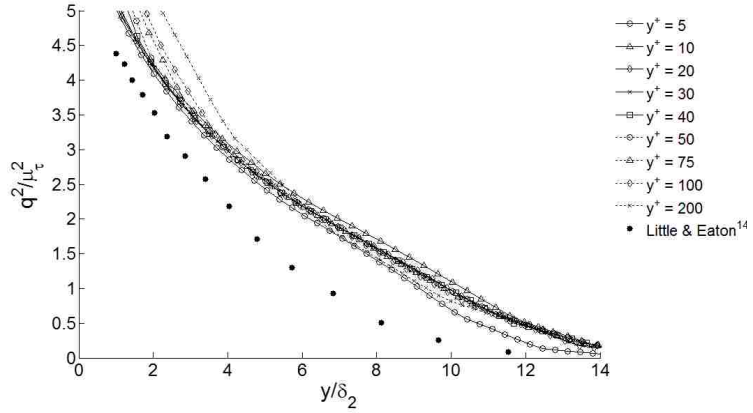

Figure 77. Twice the turbulence kinetic energy. *Comparison plot of the standard k-ω turbulence model for grids with varying y^+ wall cell centroid values.*

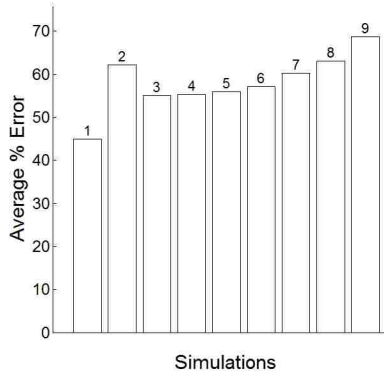

Figure 78. Error of twice the turbulence kinetic energy. *1: y^+=5, 2: y^+=10, 3: y^+=20, 4: y^+=30, 5: y^+=40, 6: y^+=50, 7: y^+=75, 8: y^+=100, 9: y^+=200*

Step 2:

The grids used for the radial and tangential grid resolution sensitivity study had the following properties:

Wall cell's centroid located at $y^+ = 30$

Computational domain size of 1x5x5 meters (axial x radial x tangential)

Stretch ratio of 1.2 in the axial direction

The following grid nodal resolutions were used in this sensitivity study (axial x radial x tangential):

33 x 508 x 508 (uniform radial and tangential grid spacing of $\approx 0.01\ m$)

33 x 254 x 254 (uniform radial and tangential grid spacing of $\approx 0.02\ m$)

33 x 127 x 127 (uniform radial and tangential grid spacing of $\approx 0.04\ m$)

33 x 64 x 64 (uniform radial and tangential grid spacing of $\approx 0.08\ m$)

33 x 32 x 32 (uniform radial and tangential grid spacing of $\approx 0.16\ m$)

The grid in Step 1 is very fine, which results in a simulation that is computationally expensive. In an effort to determine the standard k-ω turbulence model's sensitivity to grid refinement in the radial and tangential direction the grid was coarsened. The grid's radial and tangential grid spacing is doubled in each coarser grid. This results in each grid having four times fewer cells in the domain than the previous grid, which drastically reduces the computational time for each simulation. The simulation with the coarsest grid that can reproduce the simulation profiles of the finer grids is sought after.

The turbulent mean flow vector magnitude in the rotating reference frame is shown in Fig. 79. The distance above the disk's surface is normalized by the momentum thickness boundary layer, δ_2. Figure 79 shows close agreement among all grid simulation data.

The crossflow profile (Figs. 81 and 82), the polar plot of mean velocity profiles (Figs. 83 and 84) and the turbulent kinetic energy (Figs. 89 and 90) all display a slight sensitivity to the grid resolution. The simulation profile of the 33x32x32 node grid differs only slightly from the other simulation profiles.

The profile of the tangential velocity (Figs. 85 and 86) and the momentum thickness Reynolds number (Figs. 87 and 88) show a large sensitivity to the grid resolution. The simulation profiles of the 33x32x32 grid differ from the other simulation profiles.

Based on these results, the standard k-ω turbulence model with the High y^+ Wall Treatment can be conducted on a grid as coarse as 33x64x64 nodes without a loss in the result's accuracy. This equates to an initial wall cell aspect ratio of 66:1.

The grid of $y^+ = 30$ and radial and tangential resolution of 64x64 nodes will be held constant as the sensitivity of the cell stretch ratio in the axial direction is studied in Step 3.

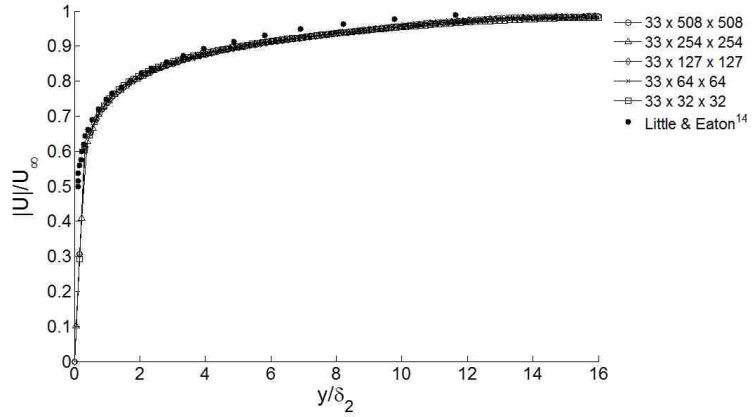

Figure 79. Turbulent mean flow vector magnitude in the rotating reference frame. *Comparison plot of the standard k-ω turbulence model for grids with varying grid resolutions in the radial and tangential directions.*

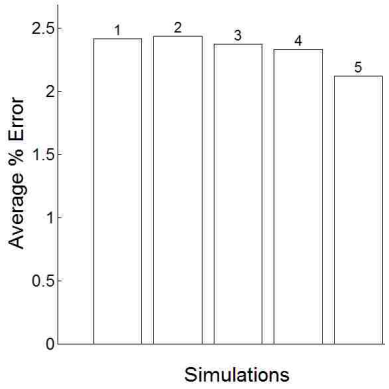

Figure 80. Error of turbulent mean flow vector magnitude. *1: 33x508x508, 2: 33x254x254, 3: 33x127x127, 4: 33x64x64. 5: 33x32x32*

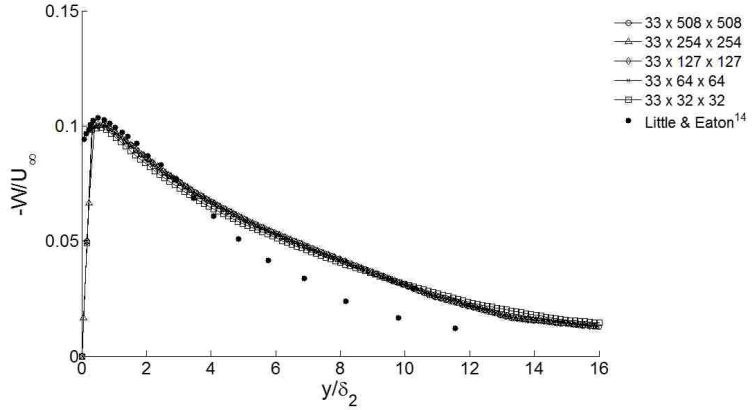

Figure 81. Crossflow profile. *Comparison plot of the standard k-ω turbulence model for grids with varying grid resolutions in the radial and tangential directions.*

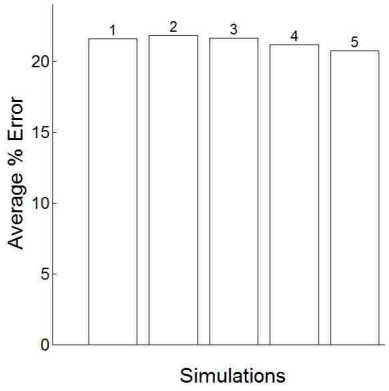

Figure 82. Error of crossflow profile. *1: 33x508x508, 2: 33x254x254, 3: 33x127x127, 4: 33x64x64, 5: 33x32x32*

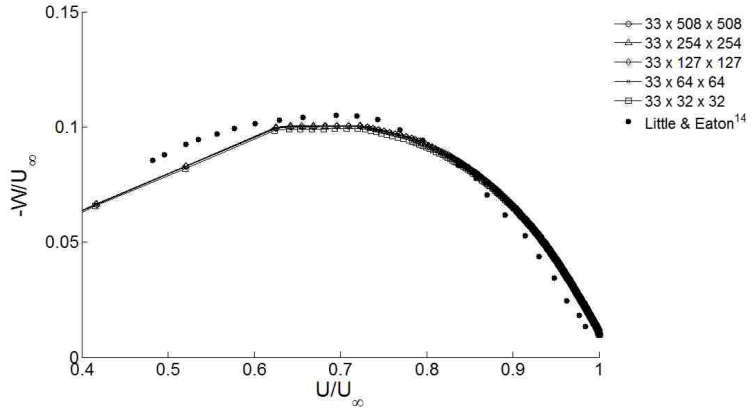

Figure 83. Polar plot of mean velocity profiles. *Comparison plot of the standard k-ω turbulence model for grids with varying grid resolutions in the radial and tangential directions.*

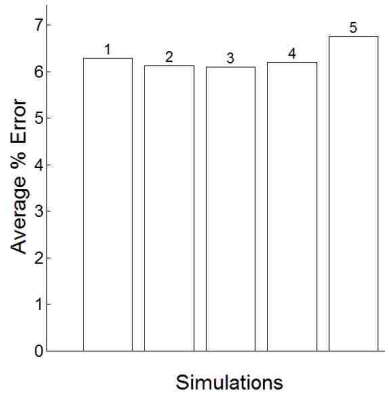

Figure 84. Error of polar mean velocity profiles. *1: 33x508x508, 2: 33x254x254, 3: 33x127x127, 4: 33x64x64, 5: 33x32x32*

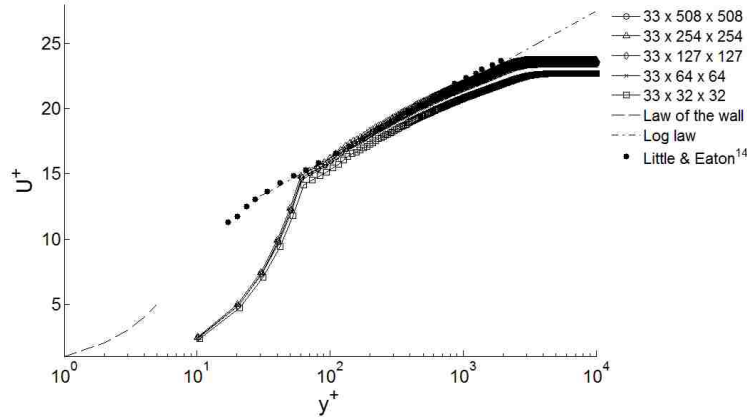

Figure 85. Tangential velocity in rotating reference frame. *Comparison plot of the standard k-ω turbulence model for grids with varying grid resolutions in the radial and tangential directions.*

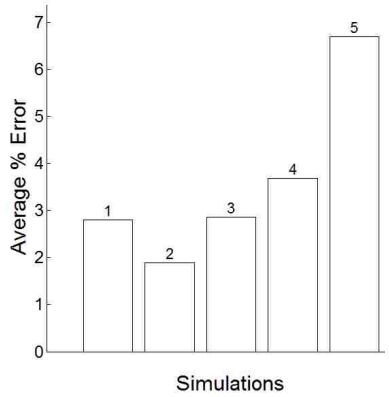

Figure 86. Error of tangential velocity. *1: 33x508x508, 2: 33x254x254, 3: 33x127x127, 4: 33x64x64, 5: 33x32x32*

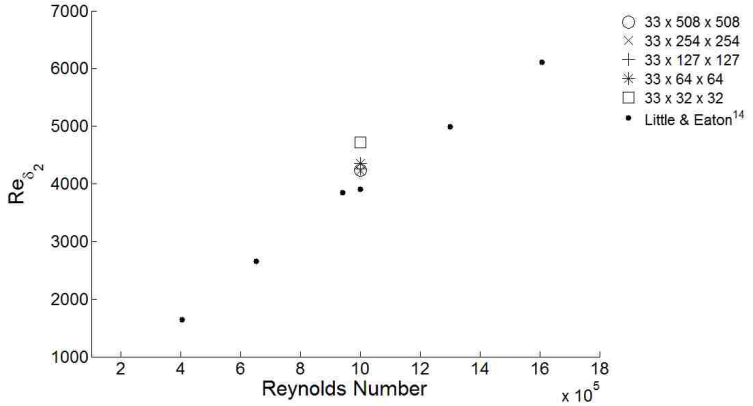

Figure 87. Comparison of momentum thickness Reynolds number. *Comparison plot of the standard k-ω turbulence model for grids with varying grid resolutions in the radial and tangential directions.*

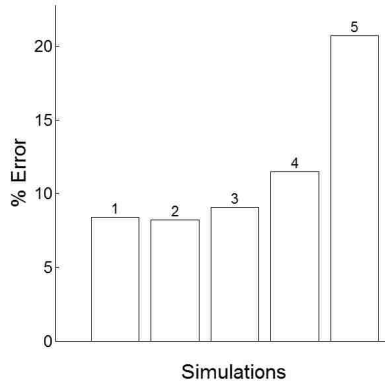

Figure 88. Error of momentum thickness Reynolds number. *1: 33x508x508, 2: 33x254x254, 3: 33x127x127, 4: 33x64x64, 5: 33x32x32*

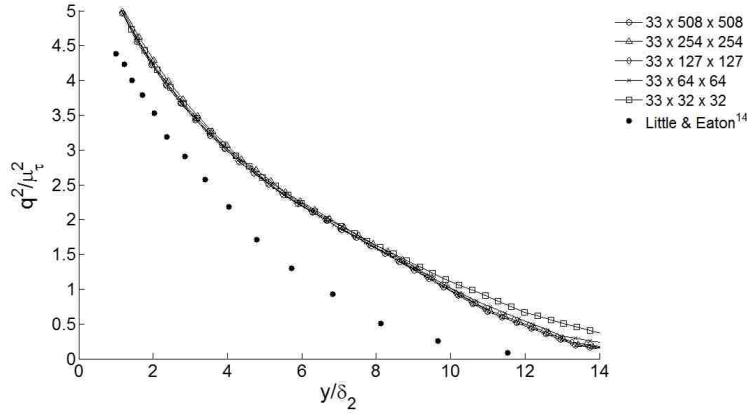

Figure 89. Twice the turbulence kinetic energy. *Comparison plot of the standard k-ω turbulence model for grids with varying grid resolutions in the radial and tangential directions.*

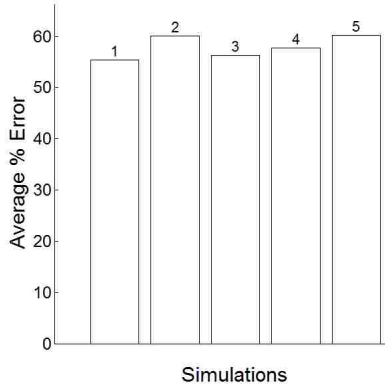

Figure 90. Error of twice the turbulence kinetic energy. *1: 33x508x508, 2: 33x254x254, 3: 33x127x127, 4: 33x64x64, 5: 33x32x32*

Step 3:

The grids used in the axial direction stretch ratio sensitivity study had the following properties:

Wall cell's centroid located at $y^+ = 30$

Computational domain size of 1x5x5 meters (axial x radial x tangential)

Radial and tangential grid resolution of 64x64 nodes (uniform grid spacing of $\approx 0.08\ m$)

In Steps 1 and 2 the grids had a stretch ratio of 1.2. In this study the stretch ratio was changed in each simulation, thus each grid has a different number of nodes in the axial direction. The following stretch ratios were used in this sensitivity study:

1.1 (55 x 64 x 64 nodes)

1.2 (33 x 64 x 64 nodes)

1.3 (25 x 64 x 64 nodes)

1.5 (18 x 64 x 64 nodes)

2.0 (12 x 64 x 64 nodes)

The goal of this sensitivity study is to find the grid with the largest stretch ratio whose simulation profile does not differ significantly from the simulation profiles obtained from smaller stretch ratios.

The turbulent mean flow vector magnitude (Figs. 91 and 92) shows close agreement between all the simulations, with slight variance among all the stretch ratios' simulation profiles.

The crossflow profile (Figs. 93 and 94) of each simulation is noticeably different. The largest discrepancies are observed in the 2.0 stretch ratio's simulation profile. The error graph (Fig. 94) helps to illustrate the lack of agreement among the simulations. Similar observations can be made for the turbulent kinetic energy profile (Figs. 101 and 102).

In the polar plot of mean velocity profiles (Figs. 95 and 96) and the tangential velocity plot (Figs. 97 and 98), the 2.0 stretch ratio's simulation profile differs from the other simulation profiles.

The momentum thickness Reynolds number shows disagreement among all of the simulation results as seen in Figs. 99 and 100.

Based on the results of the sensitivity study we can infer that the simulations of the standard k-ω turbulence model with the High y^+ Wall Treatment are more sensitive to stretch ratio differences than the simulations with the standard k-ε turbulence model with the High y^+ Wall Treatment. The simulation profiles obtained with the 1.1 stretch ratio were not replicated by higher stretch ratio simulation profiles. Therefore, the future sensitivity studies of the standard k-ω turbulence model with the High y^+ Wall Treatment will be simulated on grids that have an axial stretch ratio of 1.1.

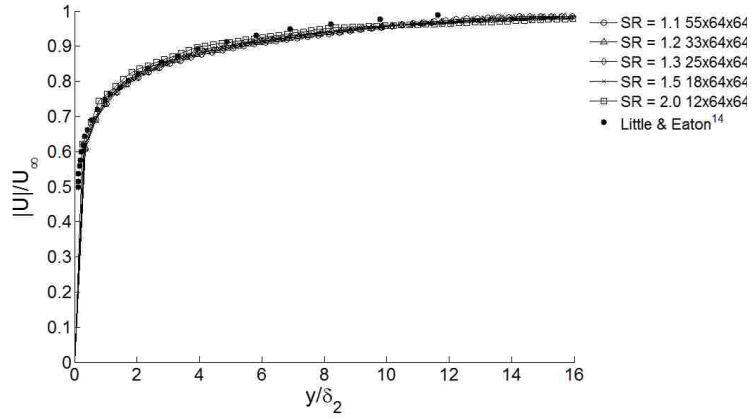

Figure 91. Turbulent mean flow vector magnitude in the rotating reference frame. *Comparison plot of the standard k-ω turbulence model for grids with varying cell stretch ratios in the axial direction.*

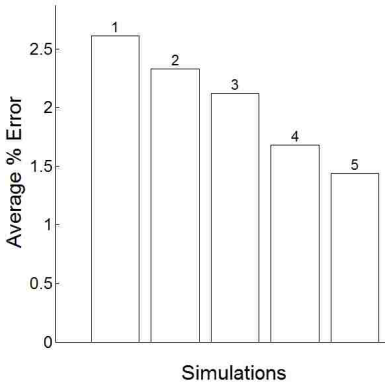

Figure 92. Error of turbulent mean flow vector magnitude. *1: SR=1.1, 2: SR=1.2, 3: SR=1.3, 4: SR=1.5, 5: SR=2.0*

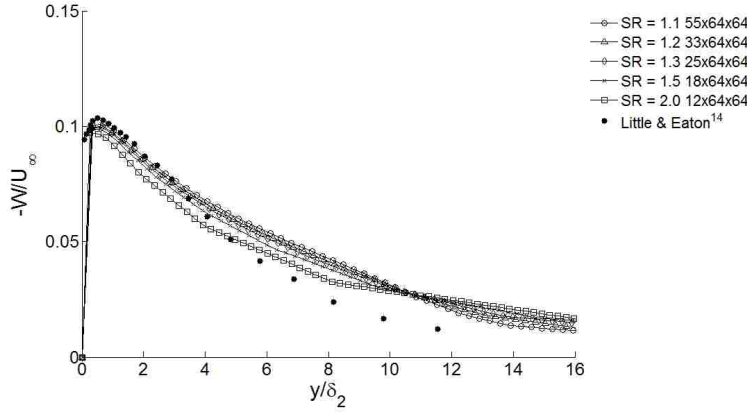

Figure 93. Crossflow profile. *Comparison plot of the standard k-ω turbulence model for grids with varying cell stretch ratios in the axial direction.*

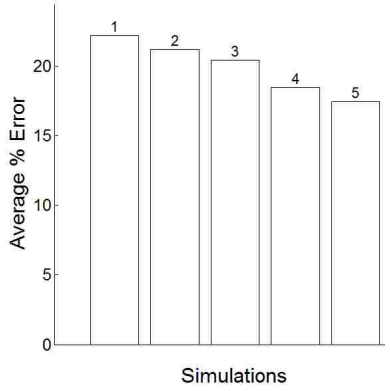

Figure 94. Error of crossflow profile. *1: SR=1.1, 2: SR=1.2, 3: SR=1.3, 4: SR=1.5, 5: SR=2.0*

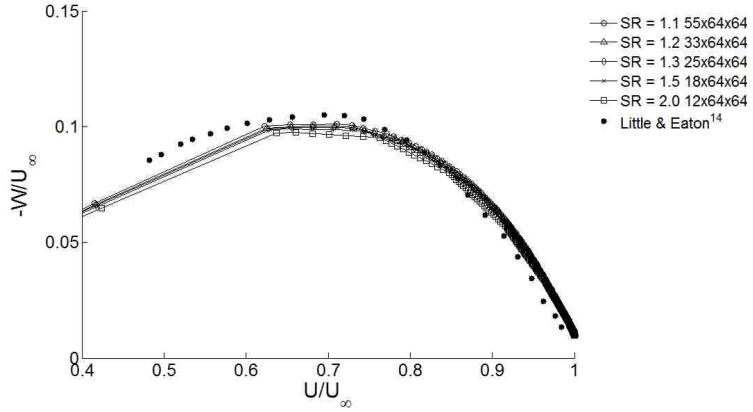

Figure 95. Polar plot of mean velocity profiles. *Comparison plot of the standard k-ω turbulence model for grids with varying cell stretch ratios in the axial direction.*

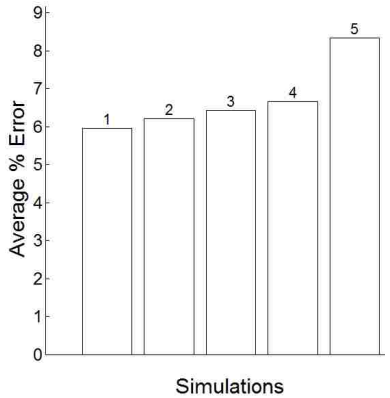

Figure 96. Error of polar mean velocity profiles. *1: SR=1.1, 2: SR=1.2, 3: SR=1.3, 4: SR=1.5, 5: SR=2.0*

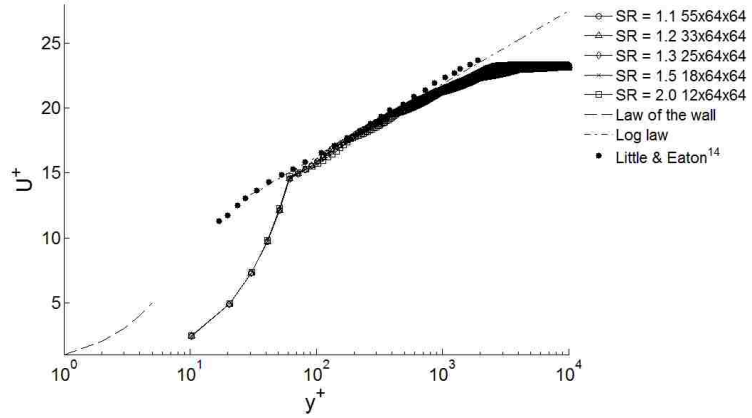

Figure 97. Tangential velocity in rotating reference frame. *Comparison plot of the standard k-ω turbulence model for grids with varying cell stretch ratios in the axial direction.*

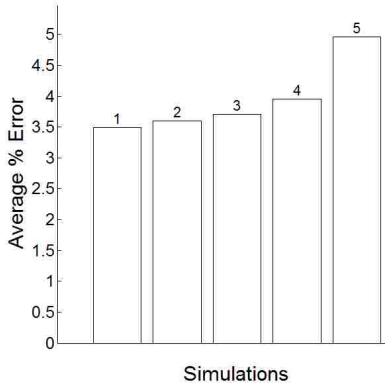

Figure 98. Error of tangential velocity. *1: SR=1.1, 2: SR=1.2, 3: SR=1.3, 4: SR=1.5, 5: SR=2.0*

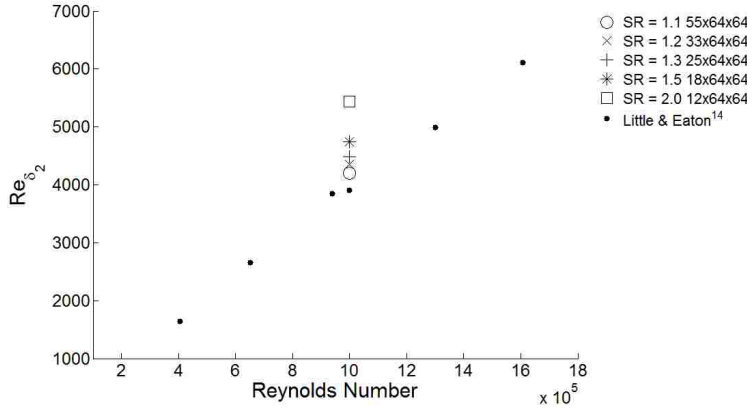

Figure 99. Comparison of momentum thickness Reynolds number. *Comparison plot of the standard k-ω turbulence model for grids with varying cell stretch ratios in the axial direction.*

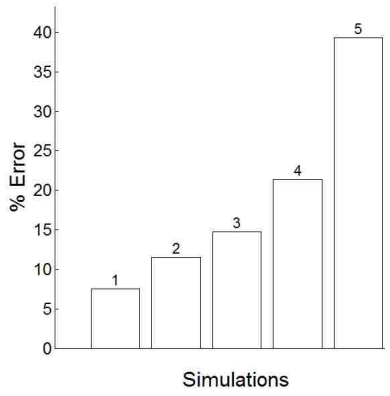

Figure 100. Error of momentum thickness Reynolds number. *1: SR=1.1, 2: SR=1.2, 3: SR=1.3, 4: SR=1.5, 5: SR=2.0*

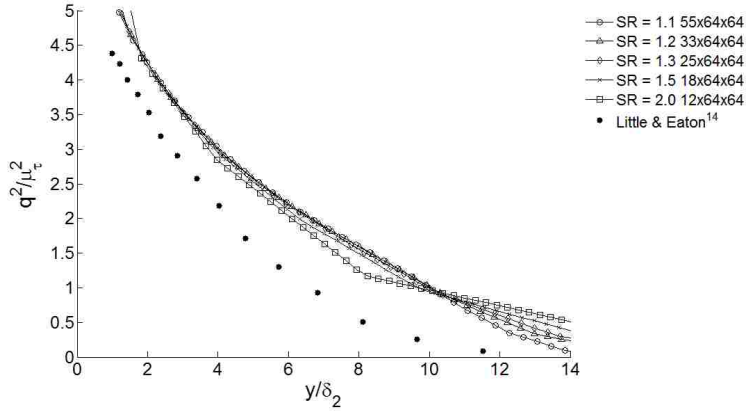

Figure 101. Twice the turbulence kinetic energy. *Comparison plot of the standard k-ω turbulence model for grids with varying cell stretch ratios in the axial direction.*

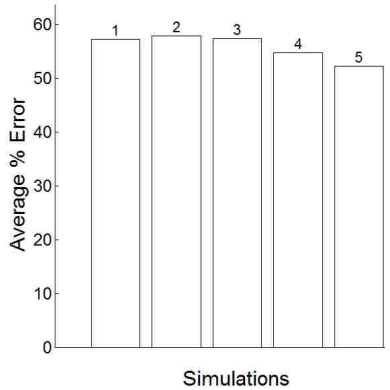

Figure 102. Error of twice the turbulence kinetic energy. *1: SR=1.1, 2: SR=1.2, 3: SR=1.3, 4: SR=1.5, 5: SR=2.0*

Step 4:

The grids used for the radial and tangential wall proximity sensitivity study had the following properties:

Wall cell's centroid located at $y^+ = 30$

Uniform radial and tangential grid spacing of $\approx 0.08\ m$

Stretch ratio of 1.1 in the axial direction

Computational domain size of 1 meter in the axial direction

This sensitivity study will adjust the position of the pressure outlet boundaries. In the previous simulations the computational domain size was 1x5x5 meters in the axial, radial and tangential directions respectively. The line probe at which data is being sampled is at a radius of 0.421 meters from the axis of rotation and extends above the disk's surface 0.1 meters. In Steps 1, 2 and 3 the distance between the line probe and the nearest pressure outlet was 2.079 meters. In this sensitivity study the computational domain was varied in the radial and tangential directions. The domain sizes in this study are:

1 x 10 x 10 meters, 55 x 128 x 128 nodes (axial, radial, tangential)

1 x 5 x 5 meters, 55 x 64 x 64 nodes

1 x 2 x 2 meters, 55 x 26 x 26 nodes

1 x 1 x 1 meters, 55 x 13 x 13 nodes

The goal of this sensitivity study is to find the smallest computational domain whose simulation profile does not vary significantly from the simulation profiles of the larger domains. The smallest computational domain puts the pressure outlets as close as 0.5 meters from the axis of rotation, which is only 0.079 meters from the data sampling locations. The largest domain puts the nearest pressure outlet 4.579 meters away from the data sampling locations.

The turbulent mean flow (Figs. 103 and 104) and the tangential velocity in the rotating reference frame (Figs. 109 and 110) show close agreement among all the simulation profiles.

The crossflow profile (Figs. 105 and 106), the polar plot of mean velocity profiles (Figs. 107 and 108) and the turbulent kinetic energy (Figs. 113 and 114) illustrate the disagreement between 1x1x1 meter domains simulation profile and the other simulation profiles.

In Fig. 111 the momentum thickness Reynolds number is shown. There seems to be no obvious relation between wall proximity and this momentum thickness Reynolds number because the simulation data do not follow a trend. The 1x1x1 and 1x10x10 meter domains' simulation results are in close agreement with one another and are close to the experimental data[14], while the 1x2x2 and 1x5x5 meter domains' simulation results have very similar momentum thickness Reynolds numbers but are further from the experimental data[14].

The data of this sensitivity study, with the exception of the momentum thickness Reynolds number, clearly indicate that the grid size can be as small as 1x2x2 meters without significant errors induced onto Star-CCM+'s[8] solution for this turbulence model. The last sensitivity study will use the radial and tangential domain size of 2x2 meters.

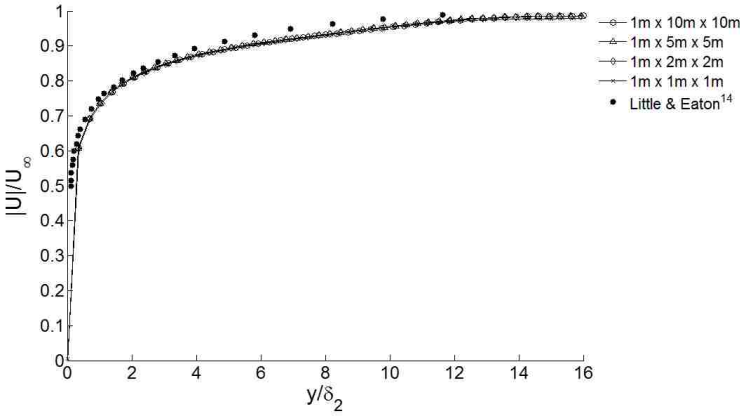

Figure 103. Turbulent mean flow vector magnitude in the rotating reference frame. *Comparison plot of the standard k-ω turbulence model for grids with varying computational domain sizes in the radial and tangential directions.*

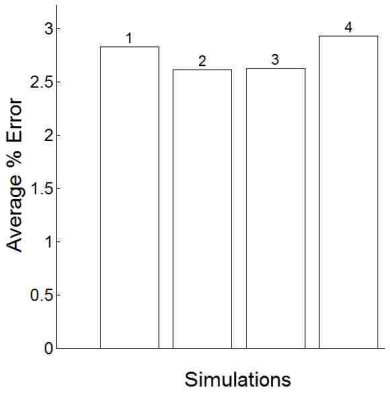

Figure 104. Error of turbulent mean flow vector magnitude. *1: 1x10x10m, 2: 1x5x5m, 3: 1x2x2m, 4: 1x1x1m*

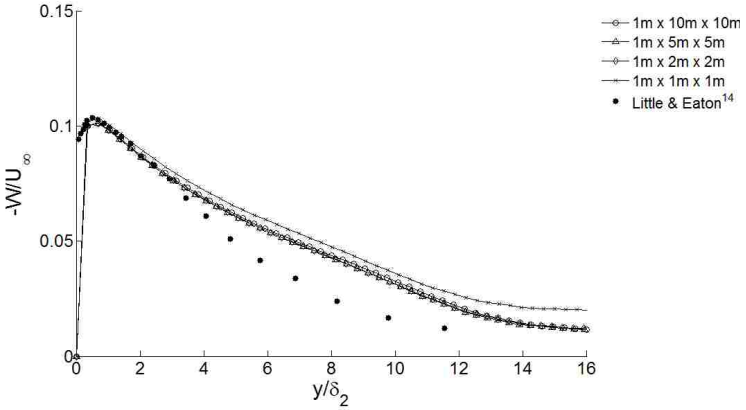

Figure 105. Crossflow profile. *Comparison plot of the standard k-ω turbulence model for grids with varying computational domain sizes in the radial and tangential directions.*

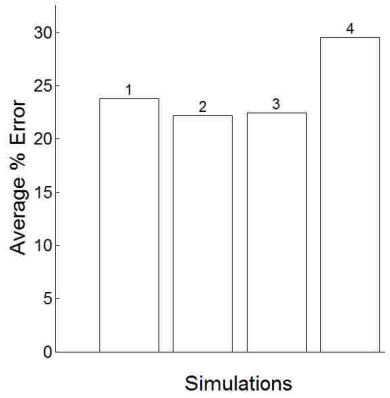

Figure 106. Error of crossflow profile. *1: 1x10x10m, 2: 1x5x5m, 3: 1x2x2m, 4: 1x1x1m*

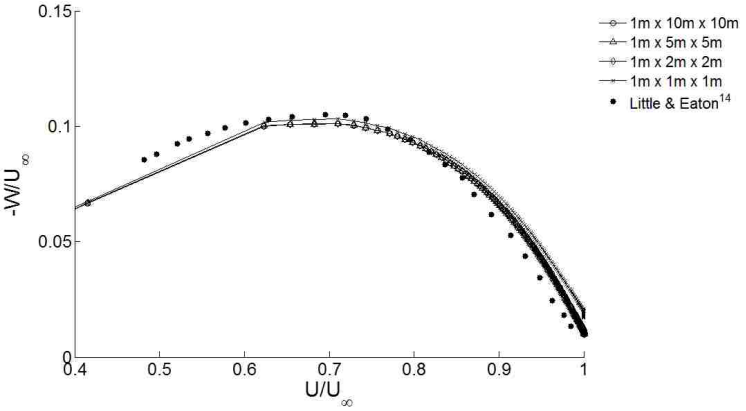

Figure 107. Polar plot of mean velocity profiles. *Comparison plot of the standard k-ω turbulence model for grids with varying computational domain sizes in the radial and tangential directions.*

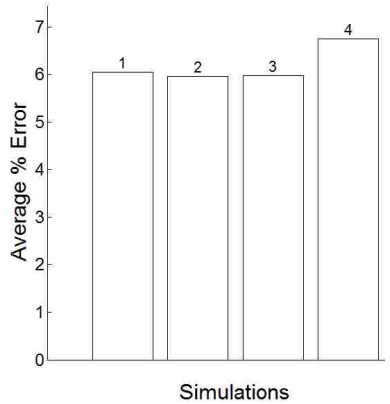

Figure 108. Error of polar mean velocity profiles. *1: 1x10x10m, 2: 1x5x5m, 3: 1x2x2m, 4: 1x1x1m*

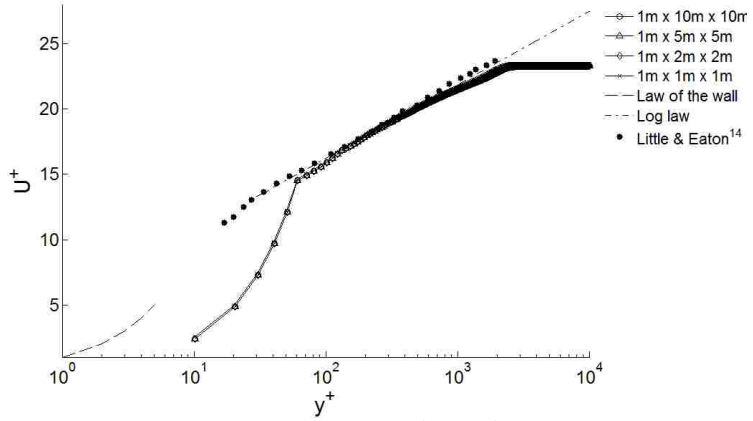

Figure 109. Tangential velocity in rotating reference frame. *Comparison plot of the standard k-ω turbulence model for grids with varying computational domain sizes in the radial and tangential directions.*

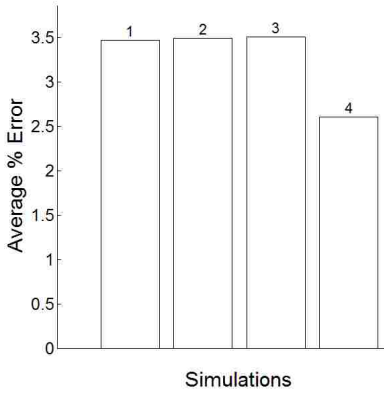

Figure 110. Error of tangential velocity. *1: 1x10x10m, 2: 1x5x5m, 3: 1x2x2m, 4: 1x1x1m*

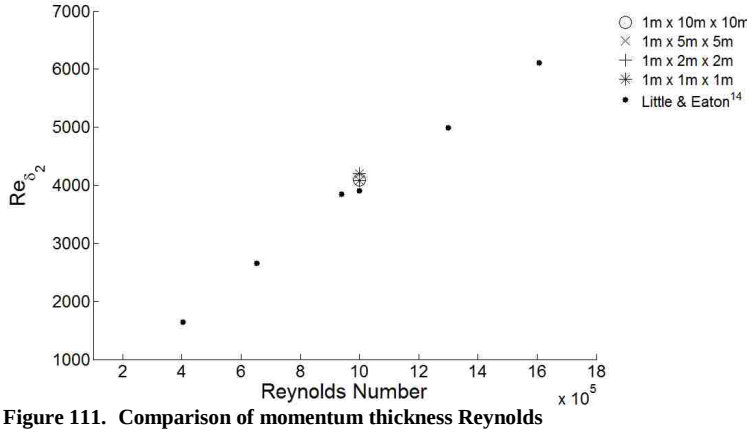

Figure 111. Comparison of momentum thickness Reynolds number. *Comparison plot of the standard k-ω turbulence model for grids with varying computational domain sizes in the radial and tangential directions.*

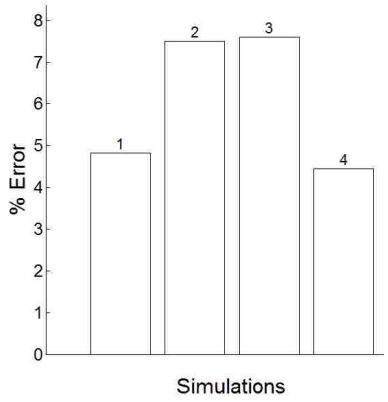

Figure 112. Error of momentum thickness Reynolds number. *1: 1x10x10m, 2: 1x5x5m, 3: 1x2x2m, 4: 1x1x1m*

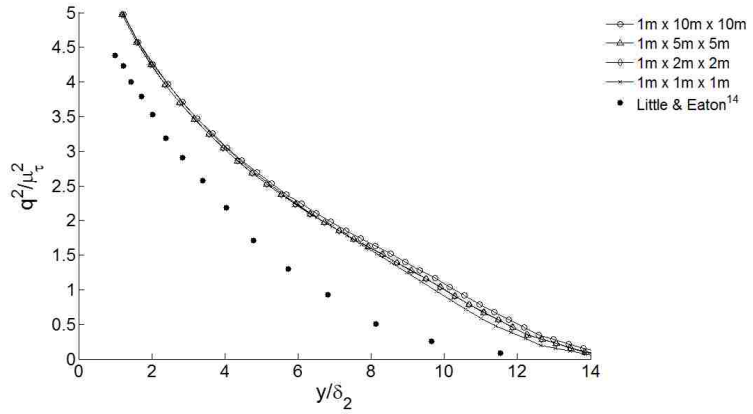

Figure 113. Twice the turbulence kinetic energy. *Comparison plot of the standard k-ω turbulence model for grids with varying computational domain sizes in the radial and tangential directions.*

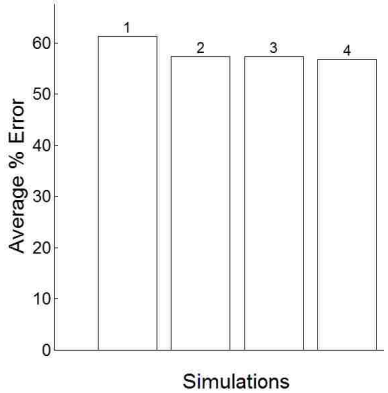

Figure 114. Error of twice the turbulence kinetic energy. *1: 1x10x10m, 2: 1x5x5m, 3: 1x2x2m, 4: 1x1x1m*

Step 5:

The grids used for the axial wall proximity sensitivity study had the following properties:

Wall cell's centroid located at $y^+ = 30$

Computational domain size in radial and tangential direction of 2x2 meters

Radial and tangential grid resolution of 26x26 nodes (uniform grid spacing of = 0.08 *m*)

Stretch ratio 1.1 in axial direction

This sensitivity study will adjust the position of the velocity inlet boundary above the disk's surface. Steps 1-4 positioned the velocity inlet 1 meter above the disk's surface and prescribed an inlet velocity of 1 *m/s*. Here, the inlet velocity of 1 *m/s* was prescribed on the largest domain of 5x2x2 meters (axial, radial, tangential) and the axial velocity was sampled at locations 2.5, 1.0, 0.5, 0.25 and 0.1 meters above the disk's surface at $r = 0.421$ *m*. The measured axial velocities were prescribed at the velocity inlet for each respective simulation. The domain sizes and inlet velocity prescribed for the simulations in this sensitivity study are as follows:

5 x 2 x 2 meters (axial, radial, tangential), velocity prescribed at inlet = 1 *m/s*

2.5 x 2 x 2 meters, velocity prescribed at inlet = 0.996 *m/s*

1 x 2 x 2 meters, velocity prescribed at inlet = 0.889 *m/s*

0.5 x 2 x 2 meters, velocity prescribed at inlet = 0.688 *m/s*

0.25 x 2 x 2 meters, velocity prescribed at inlet = 0.499 *m/s*

0.1 x 2 x 2 meters, velocity prescribed at inlet = 0.349 *m/s*

The mean flow vector magnitude (Figs. 115 and 116), the profile of tangential velocity in the rotating reference frame (Figs. 121 and 122) and the turbulent kinetic energy profile (Figs. 125 and 126) all show a lack of sensitivity to the velocity inlet's position, as all of the simulation profiles are in close agreement.

The crossflow profile (Fig. 117), the polar plot of mean velocity profiles (Fig. 119) and the momentum thickness Reynolds number (Fig. 123) all show a high sensitivity to the velocity inlet's position. The 5 and 2.5 meter axial domains' simulation profiles are in close agreement, while all the other simulation profiles differ from one another. This is clearly seen in the error graphs (Figs. 118,120 and 124), where the two largest domain simulation results have nearly

identical average error values. The average error differs increasingly, from that of the 5x2x2 and 2.5x2x2 meter domain simulations, as the computational domain size decreases.

The computational domain size of 2.5x2x2 meters is the smallest domain size whose simulation results do not stray from simulation results obtained from the largest computational domain. Thus it was chosen as the most suitable grid size for these simulations using the standard k-ω turbulence model with the High y^+ Wall Treatment.

The computation time for the simulation using this grid was 4 minutes and 50 seconds, computed on the desktop computer, out to 1500 iterations. Comparing this time to the 5 hours and 32 minutes it took to compute the simulation on the Nano Linux cluster with the initial y^+ = 30 grid in Step 1 illustrates the benefit of having an efficiently sized grid.

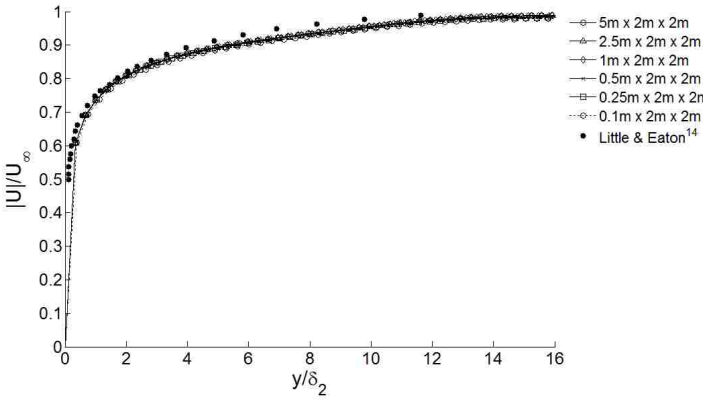

Figure 115. Turbulent mean flow vector magnitude in the rotating reference frame. *Comparison plot of the standard k-ω turbulence model for grids with varying computational domain sizes in the axial direction.*

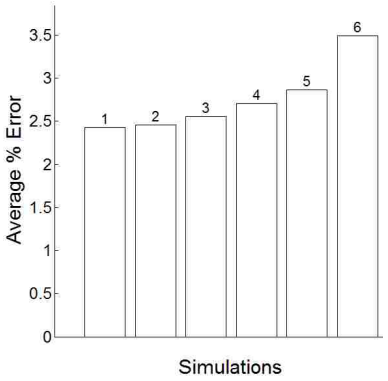

Figure 116. Error of turbulent mean flow vector magnitude. *1: 5x2x2m, 2: 2.5x2x2m, 3: 1x2x2m, 4: 0.5x2x2m, 5: 0.25x2x2m, 6: 0.1x2x2m*

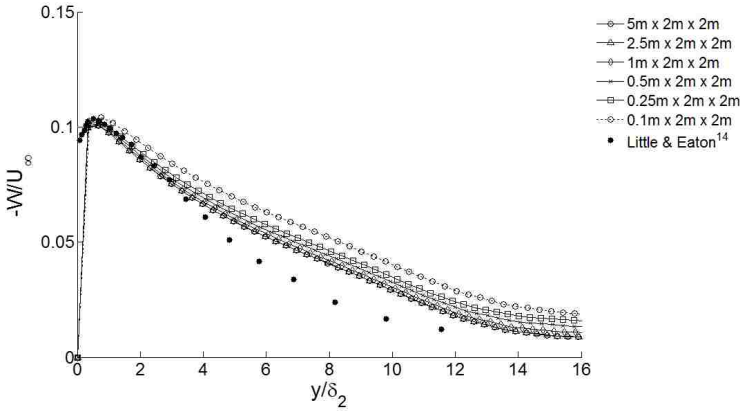

Figure 117. Crossflow profile. *Comparison plot of the standard k-ω turbulence model for grids with varying computational domain sizes in the axial direction.*

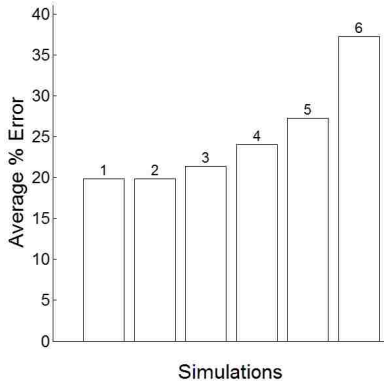

Figure 118. Error of crossflow profile. *1: 5x2x2m, 2: 2.5x2x2m, 3: 1x2x2m, 4: 0.5x2x2m, 5: 0.25x2x2m, 6: 0.1x2x2m*

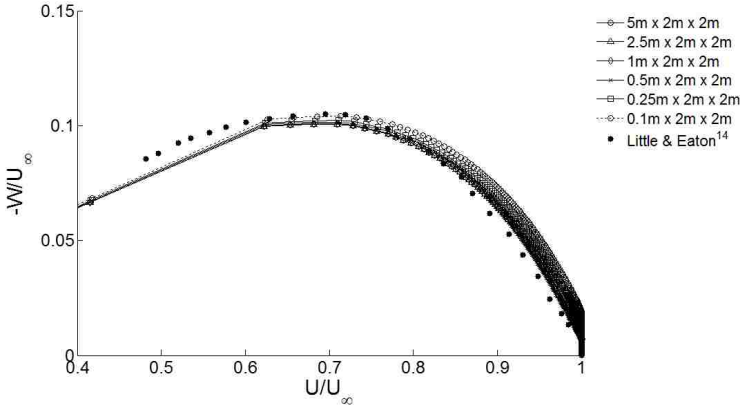

Figure 119. Polar plot of mean velocity profiles. *Comparison plot of the standard k-ω turbulence model for grids with varying computational domain sizes in the axial direction.*

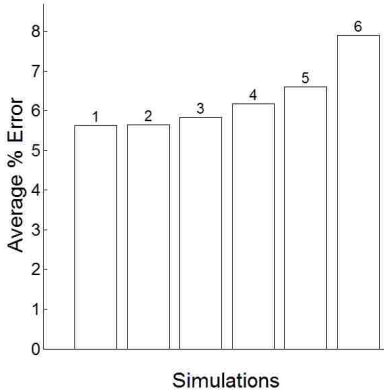

Figure 120. Error of polar mean velocity profiles. *1: 5x2x2m, 2: 2.5x2x2m, 3: 1x2x2m, 4: 0.5x2x2m, 5: 0.25x2x2m, 6: 0.1x2x2m*

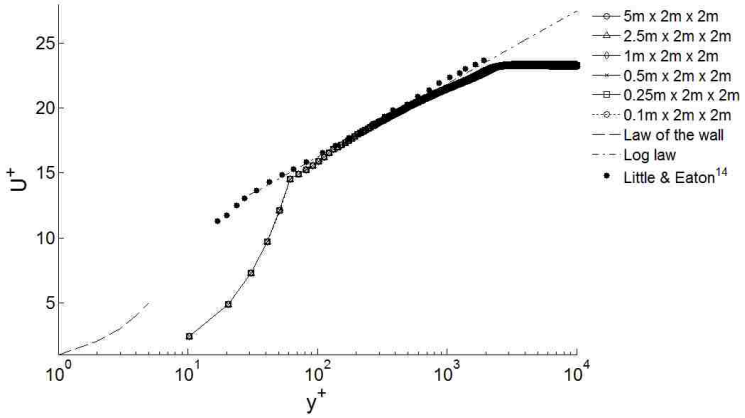

Figure 121. Tangential velocity in rotating reference frame. *Comparison plot of the standard k-ω turbulence model for grids with varying computational domain sizes in the axial direction.*

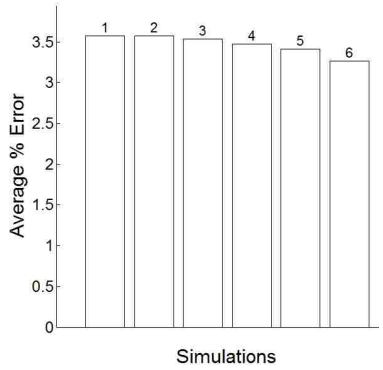

Figure 122. Error of tangential velocity. *1: 5x2x2m, 2: 2.5x2x2m, 3: 1x2x2m, 4: 0.5x2x2m, 5: 0.25x2x2m, 6: 0.1x2x2m*

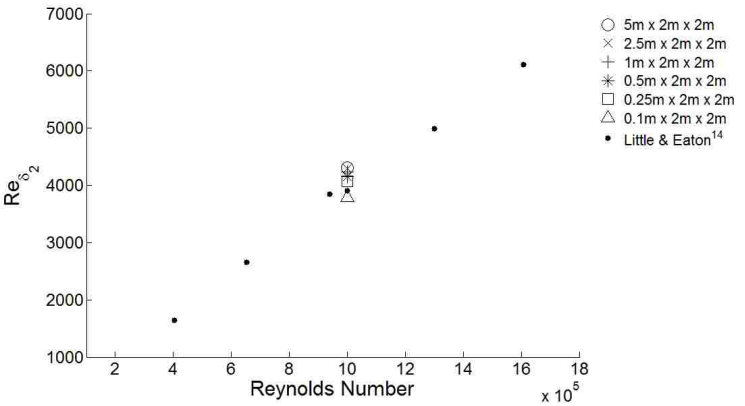

Figure 123. Comparison of momentum thickness Reynolds number. *Comparison plot of the standard k-ω turbulence model for grids with varying computational domain sizes in the axial direction.*

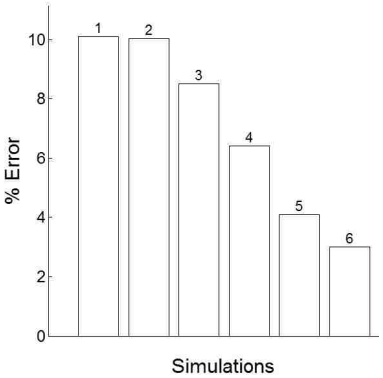

Figure 124. Error of momentum thickness Reynolds number. *1: 5x2x2m, 2: 2.5x2x2m, 3: 1x2x2m, 4: 0.5x2x2m, 5: 0.25x2x2m, 6: 0.1x2x2m*

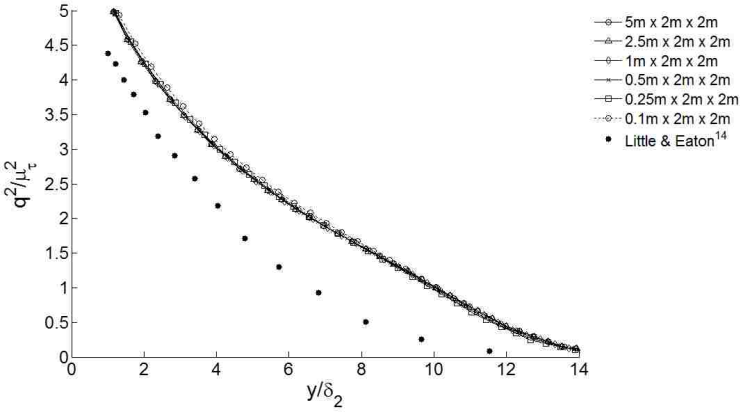

Figure 125. Twice the turbulence kinetic energy. *Comparison plot of the standard k-ω turbulence model for grids with varying computational domain sizes in the axial direction.*

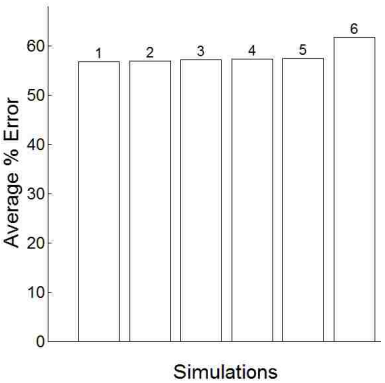

Figure 126. Error of twice the turbulence kinetic energy. *1: 5x2x2m, 2: 2.5x2x2m, 3: 1x2x2m, 4: 0.5x2x2m, 5: 0.25x2x2m, 6: 0.1x2x2m*

3. SST model

Step 1:

The grids used for the y^+ sensitivity study had the following properties:

Computational domain size of 1x5x5 meters (axial x radial x tangential)

Stretch ratio of 1.2 in the axial direction

Uniform radial and tangential resolution of 508x508 nodes

Grids with the following initial cell's centroid y^+ values were included in this sensitivity study:

y^+ = 5 (42 x 508 x 508 nodes)

y^+ = 10 (39 x 508 x 508 nodes)

y^+ = 20 (36 x 508 x 508 nodes)

y^+ = 30 (33 x 508 x 508 nodes)

y^+ = 40 (32 x 508 x 508 nodes)

y^+ = 50 (31 x 508 x 508 nodes)

y^+ = 75 (28 x 508 x 508 nodes)

y^+ = 100 (27 x 508 x 508 nodes)

y^+ = 200 (23 x 508 x 508 nodes)

Since the High y^+ Wall Treatment was used, it was not necessary to go below y^+ = 5 as the simulation results will show. The turbulent mean flow vector magnitude in the rotating reference frame is shown in Fig. 127. The distance above the disk's surface is normalized by the momentum thickness boundary layer, δ_2. All of the simulation results agree very well except near the disk's surface. This disagreement is again due to the refinement differences near the wall. Figure 128 shows the errors of the simulation results. The larger error of the simulations with high y^+ values is mostly due to the data obtained near the disk's surface.

The crossflow profile (Figs. 129 and 130) demonstrates a high sensitivity to different y^+ values near the disk's surface. The y^+ = 20, 30, 40, 50, 75 and 100 simulation profiles agree very well past the near wall discrepancies. The simulations with y^+ = 5 and 10 give results that overshoot the amount of the crossflow near the disk's surface while the simulation with a y^+ = 200 value has a profile that undershoots the amount of the crossflow near the disk's surface.

Figure 131 is the polar plot of mean velocity profiles. The data obtained from the $y^+ = 20$ simulation are in close agreement with the experimental data[14]. This plot demonstrates the inadequacy of the High y^+ Wall Treatment near the disks surface.

Figure 133 is a semi-logarithmic plot of U^+ vs. y^+. All of the simulation profiles are very similar far from the disk's surface and follow the log law and experimental data[14] very closely with the exception of the $y^+ = 5$ and 10 simulations, which show disagreement with the experimental data[14] throughout the computational domain. This is reflected in the error graph of Fig. 134.

Figure 135 shows the momentum thickness Reynolds number for each simulation compared to the experimental value[14], $Re = 10^6$. Figure 136 shows the error of each simulation. The data of simulations with $y^+ = 5$ and 200 have the greatest disagreement from the $y^+ = 10$, 20, 40 and 50 grid simulation results.

Figure 137 plots the normalized turbulent kinetic energy. The results of simulations with $y^+ = 20$, 30, 40 and 50 are in close agreement with each other. Other results vary from this group. Figure 138 shows the average errors of each simulation with respect to the experimental data[14].

Results of the simulations with the $y^+ = 30$ grid demonstrated unexpected discrepancies, as seen in Figs. 134 and 136. These discrepancies may be due to the initial cell's centroid falling in a "gray area" where the segregation between the k-ε and k-ω turbulence models has an effect on the simulations' solution.

Based on the results of the y^+-sensitivity study of the SST turbulence model with the High y^+ Wall Treatment, the grid with $y^+ = 20$ resulted in simulation data that agreed very well with the experimental data[14] and was chosen as the y^+ value for the grids in the next sensitivity study of this turbulence model.

Computational expenses of these simulations were very large because of the fine grids. The computational time of the $y^+ = 20$ grid's simulation was 7 hours 27 minutes. This computation was done on 4 nodes of the Nano Linux cluster, with 1500 iterations.

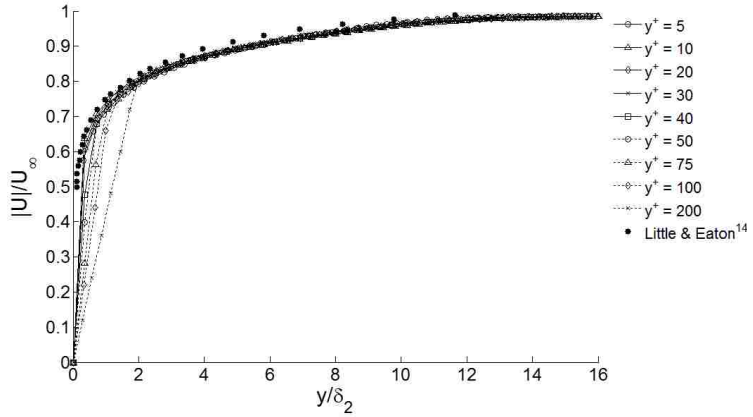

Figure 127. Turbulent mean flow vector magnitude in the rotating reference frame. *Comparison plot of the SST turbulence model for grids with varying y^+ wall cell centroid values.*

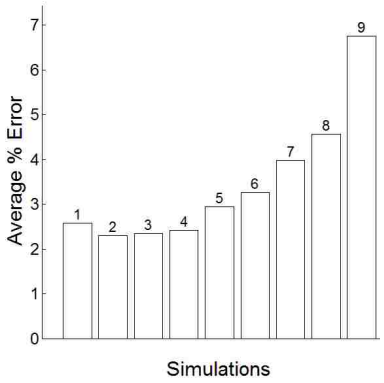

Figure 128. Error of turbulent mean flow vector magnitude. *1: y^+=5, 2: y^+=10, 3: y^+=20, 4: y^+=30, 5: y^+=40, 6: y^+=50, 7: y^+=75, 8: y^+=100, 9: y^+=200*

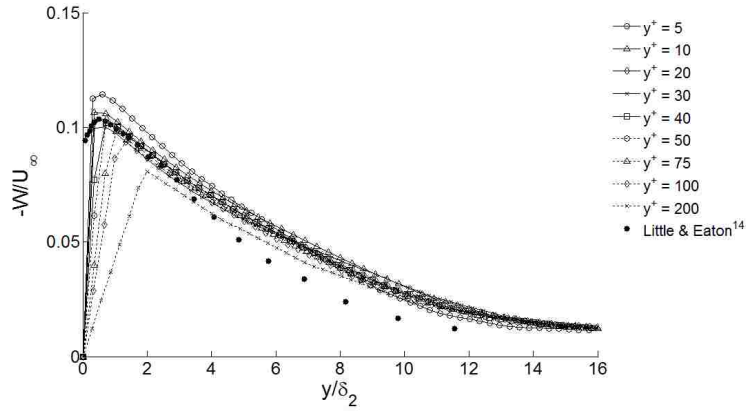

Figure 129. Crossflow profile. *Comparison plot of the SST turbulence model for grids with varying y^+ wall cell centroid values.*

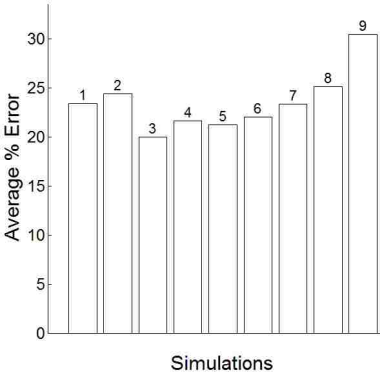

Figure 130. Error of crossflow profile. *1: y^+=5, 2: y^+=10, 3: y^+=20, 4: y^+=30, 5: y^+=40, 6: y^+=50, 7: y^+=75, 8: y^+=100, 9: y^+=200*

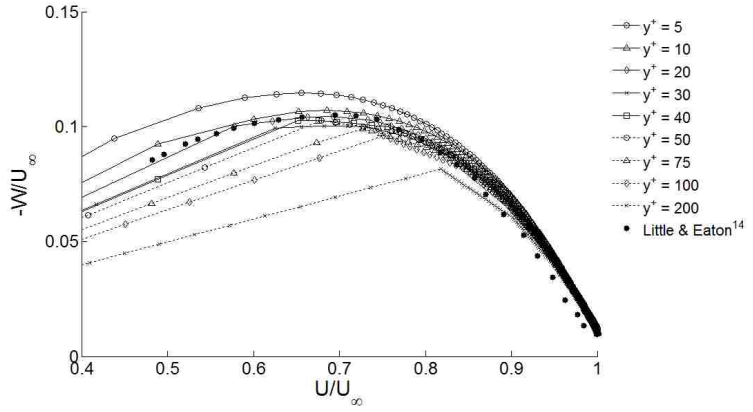

Figure 131. Polar plot of mean velocity profiles. *Comparison plot of the SST turbulence model for grids with varying y^+ wall cell centroid values.*

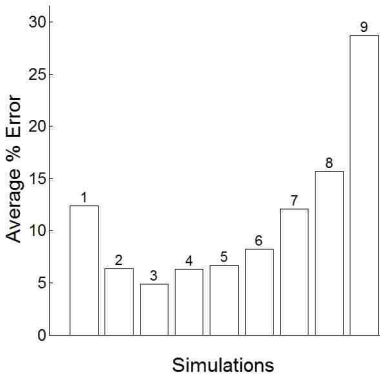

Figure 132. Error of polar mean velocity profiles. *1: y^+=5, 2: y^+=10, 3: y^+=20, 4: y^+=30, 5: y^+=40, 6: y^+=50, 7: y^+=75, 8: y^+=100, 9: y^+=200*

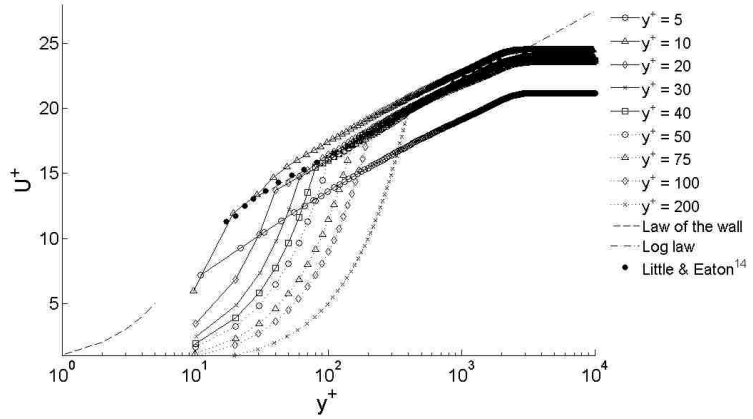

Figure 133. Tangential velocity in rotating reference frame. *Comparison plot of the SST turbulence model for grids with varying y^+ wall cell centroid values.*

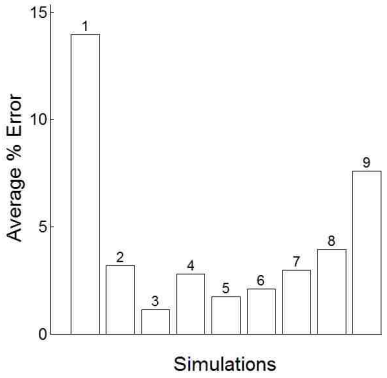

Figure 134. Error of tangential velocity. *1: y^+=5, 2: y^+=10, 3: y^+=20, 4: y^+=30, 5: y^+=40, 6: y^+=50, 7: y^+=75, 8: y^+=100, 9: y^+=200*

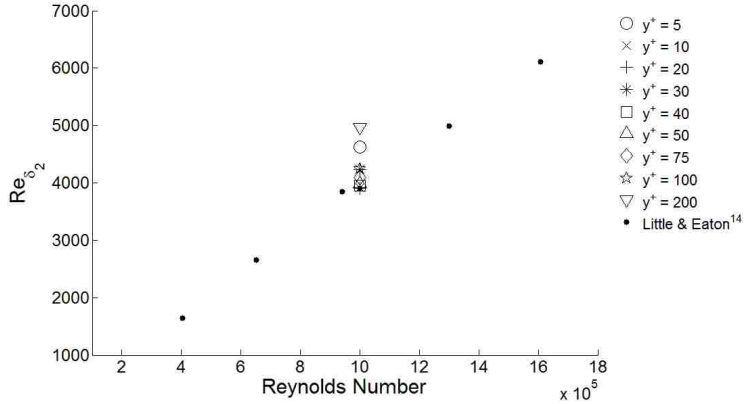

Figure 135. Comparison of momentum thickness Reynolds number. *Comparison plot of the SST turbulence model for grids with varying y^+ wall cell centroid values.*

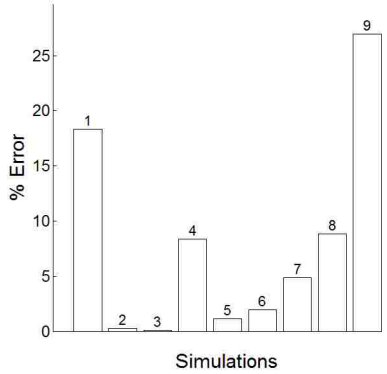

Figure 136. Error of momentum thickness Reynolds number. *1: y^+=5, 2: y^+=10, 3: y^+=20, 4: y^+=30, 5: y^+=40, 6: y^+=50, 7: y^+=75, 8: y^+=100, 9: y^+=200*

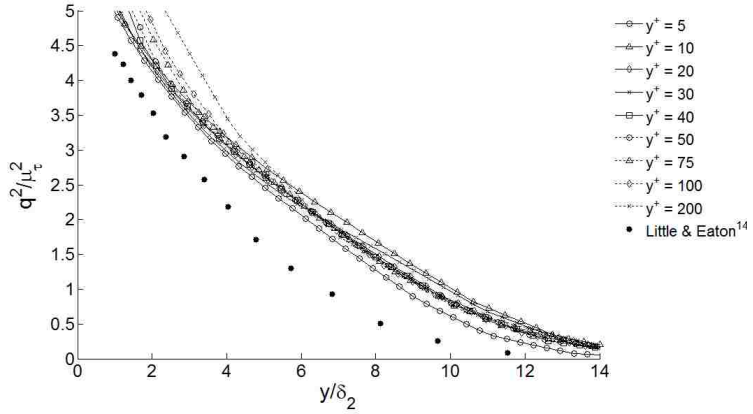

Figure 137. Twice the turbulence kinetic energy. *Comparison plot of the SST turbulence model for grids with varying y^+ wall cell centroid values.*

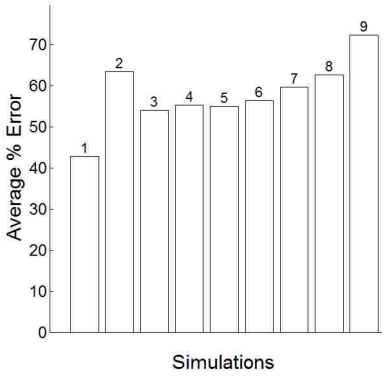

Figure 138. Error of twice the turbulence kinetic energy. *1: y^+=5, 2: y^+=10, 3: y^+=20, 4: y^+=30, 5: y^+=40, 6: y^+=50, 7: y^+=75, 8: y^+=100, 9: y^+=200*

Step 2:

The grids used for the radial and tangential grid resolution sensitivity study had the following properties:

Wall cell's centroid located at $y^+ = 20$

Computational domain size of 1x5x5 meters (axial x radial x tangential)

Stretch ratio of 1.2 in the axial direction

The following grid nodal resolutions were used in this sensitivity study (axial x radial x tangential):

36 x 508 x 508 (uniform radial and tangential grid spacing of $\approx 0.01\ m$)

36 x 254 x 254 (uniform radial and tangential grid spacing of $\approx 0.02\ m$)

36 x 127 x 127 (uniform radial and tangential grid spacing of $\approx 0.04\ m$)

36 x 64 x 64 (uniform radial and tangential grid spacing of $\approx 0.08\ m$)

36 x 32 x 32 (uniform radial and tangential grid spacing of $\approx 0.16\ m$)

The grid in Step 1 is very fine, which results in a simulation that is computationally expensive. In an effort to determine the SST turbulence model's sensitivity to grid refinement in the radial and tangential direction the grid was altered. The grid's radial and tangential grid spacing is doubled in each coarser grid. This results in each grid having four times fewer cells in the domain than the previous grid, which drastically reduces the computational time for each simulation. The coarsest grid that can reproduce the results of the finer grids is sought after.

The turbulent mean flow vector magnitude in the rotating reference frame is shown in Fig. 139. The distance above the disk's surface is normalized by the momentum thickness boundary layer δ_2. Figure 139 shows close agreement among all simulation data. Figure 140 shows the average error of each simulation. All the simulation errors are very similar.

The crossflow profile (Figs. 141 and 142) and the profile of the tangential velocity in the rotating reference frame (Figs. 145 and 146) show the 36x32x32 grid's profiles deviate from the profiles of the other simulations.

The polar plot of mean velocity profiles, seen in Figs. 143 and 144, show all data are in close agreement.

The momentum thickness Reynolds number (Figs. 147 and 148) and the turbulent kinetic energy (Figs. 149 and 150) demonstrate the poor agreement of the 36x32x32 grid's simulation results with the other simulation data.

Based on these results, we infer that the SST turbulence model with the High y^+ Wall Treatment can be as coarse as 36x64x64 nodes in a 1x5x5 meter domain without a substantial loss in the simulation result's accuracy. This equates to an initial wall cell aspect ratio of 99:1.

The grid of $y^+ = 20$ and radial and tangential resolution of 64x64 nodes will be held constant as the sensitivity of the cell stretch ratio in the axial direction is studied in Step 3.

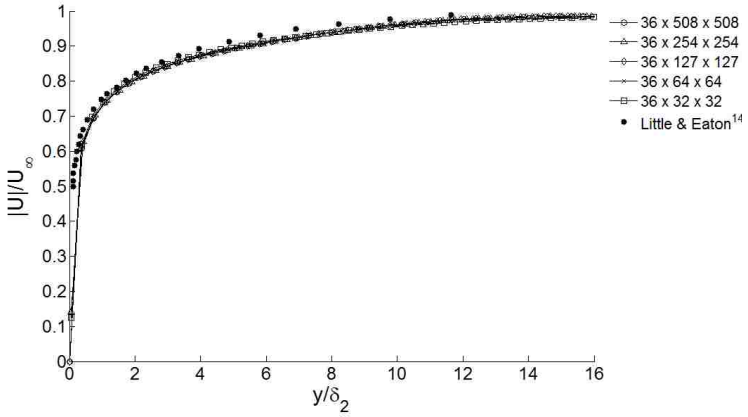

Figure 139. Turbulent mean flow vector magnitude in the rotating reference frame. *Comparison plot of the SST turbulence model for grids with varying grid resolutions in the radial and tangential directions.*

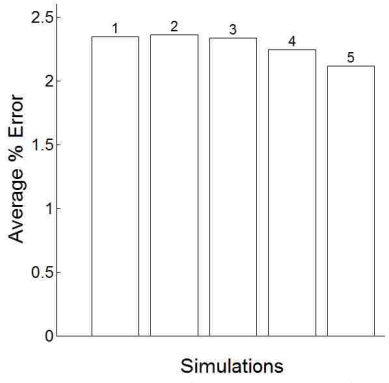

Figure 140. Error of turbulent mean flow vector magnitude. *1: 36x508x508, 2: 36x254x254, 3: 36x127x127, 4: 36x64x64, 5: 36x32x32*

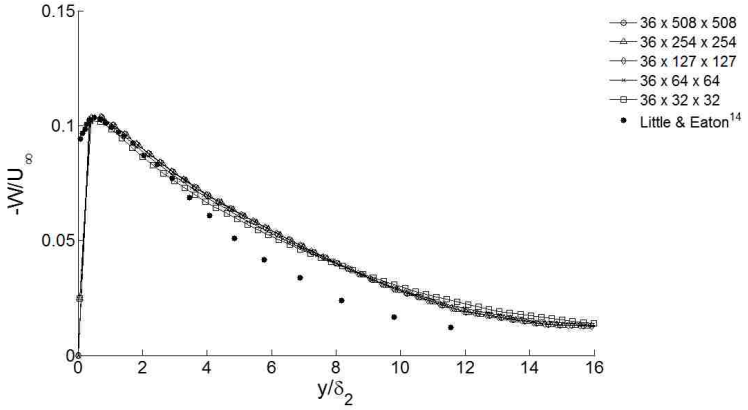

Figure 141. Crossflow profile. *Comparison plot of the SST turbulence model for grids with varying grid resolutions in the radial and tangential directions.*

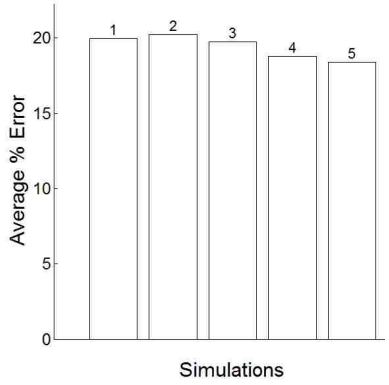

Figure 142. Error of crossflow profile. *1: 36x508x508, 2: 36x254x254, 3: 36x127x127, 4: 36x64x64, 5: 36x32x32*

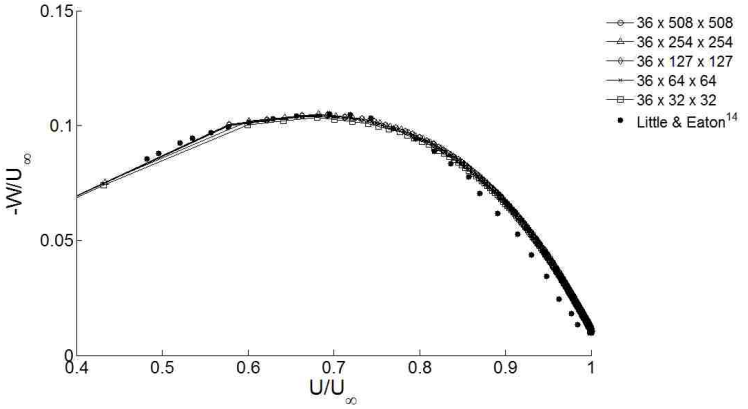

Figure 143. Polar plot of mean velocity profiles. *Comparison plot of the SST turbulence model for grids with varying grid resolutions in the radial and tangential directions.*

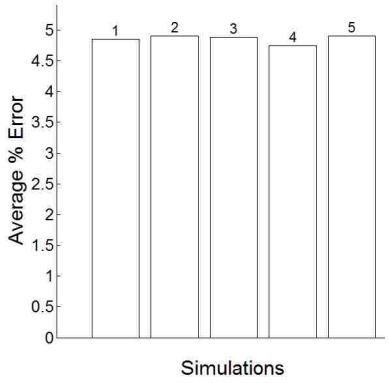

Figure 144. Error of polar mean velocity profiles. *1: 36x508x508, 2: 36x254x254, 3: 36x127x127, 4: 36x64x64, 5: 36x32x32*

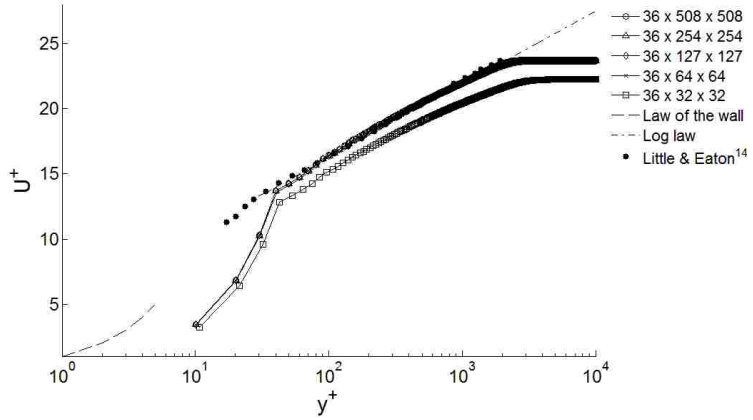

Figure 145. Tangential velocity in rotating reference frame. *Comparison plot of the SST turbulence model for grids with varying grid resolutions in the radial and tangential directions.*

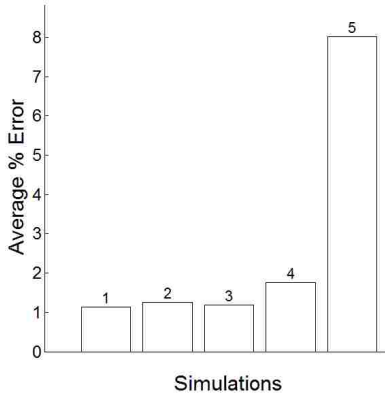

Figure 146. Error of tangential velocity. *1: 36x508x508, 2: 36x254x254, 3: 36x127x127, 4: 36x64x64, 5: 36x32x32*

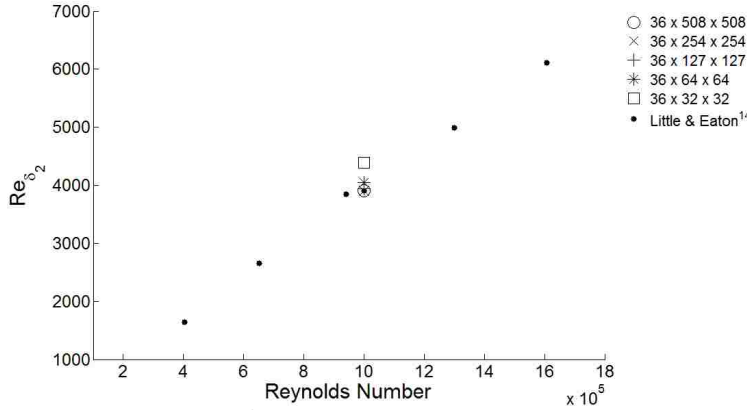

Figure 147. Comparison of momentum thickness Reynolds number. *Comparison plot of the SST turbulence model for grids with varying grid resolutions in the radial and tangential directions.*

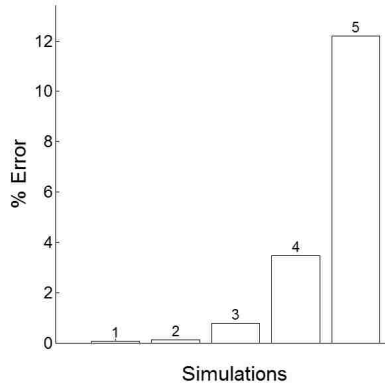

Figure 148. Error of momentum thickness Reynolds number. *1: 36x508x508, 2: 36x254x254, 3: 36x127x127, 4: 36x64x64, 5: 36x32x32*

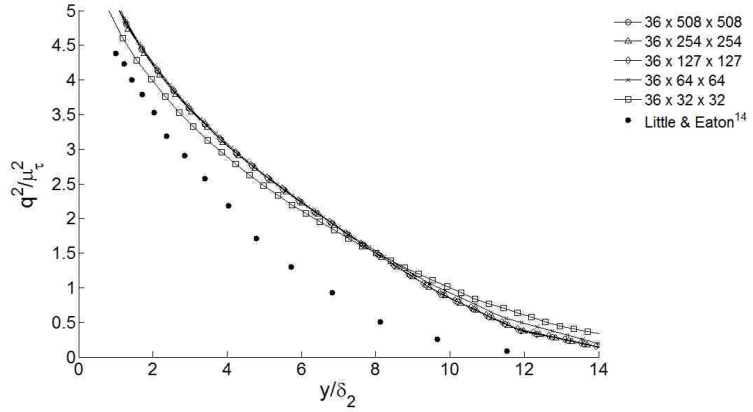

Figure 149. Twice the turbulence kinetic energy. *Comparison plot of the SST turbulence model for grids with varying grid resolutions in the radial and tangential directions.*

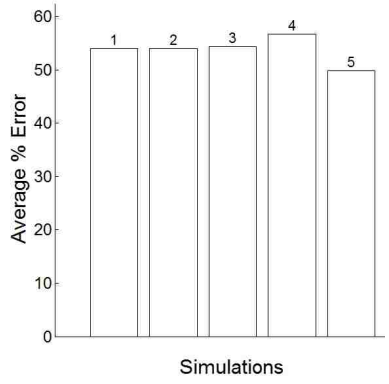

Figure 150. Error of twice the turbulence kinetic energy. *1: 36x508x508, 2: 36x254x254, 3: 36x127x127, 4: 36x64x64, 5: 36x32x32*

Step 3:

The grids used for the axial direction stretch ratio sensitivity study had the following properties:

Wall cell's centroid located at $y^+ = 20$

Computational domain size of 1x5x5 meters (axial x radial x tangential)

Radial and tangential grid resolution of 64x64 nodes (uniform grid spacing of $\approx 0.08\ m$)

In Steps 1 and 2 the grids had a stretch ratio of 1.2. In this study the stretch ratio was changed in each simulation, thus each grid has a different number of nodes in the axial direction. The following stretch ratios were used in this sensitivity study:

1.1 (59 x 64 x 64 nodes)

1.2 (36 x 64 x 64 nodes)

1.3 (27 x 64 x 64 nodes)

1.5 (19 x 64 x 64 nodes)

2.0 (13 x 64 x 64 nodes)

The goal of this sensitivity study is to find the grid with the largest stretch ratio whose simulation profile does not differ significantly from the simulation profiles obtained from smaller stretch ratios.

The turbulent mean flow vector magnitude (Fig. 151) shows close agreement among all data. The profile of the 2.0 stretch ratio simulation slightly disagrees with the profiles of the all other simulations. The error graph in Fig. 152 shows that as the stretch ratio increases, the data are closer to the experimental data[14].

For the crossflow profile (Fig. 153 and 154), the stretch ratio 1.5 and 2.0 simulation results differ from the others.

In the polar plot of mean velocity profiles (Figs. 155 and 156) and the tangential velocity plot (Figs. 157 and 158), all the simulations are in very close agreement with one another.

All of the simulations' turbulent velocity profiles agree very well, with less than a 2% deviation from the experimental data[14].

The momentum thickness Reynolds number (Figs. 159 and 160) shows a high sensitivity to the axial stretch ratio. The momentum thickness Reynolds number of the 2.0 stretch ratio simulation is much larger than the other simulation data.

The turbulent kinetic energy (Figs. 161 and 162) also shows a high sensitivity to varying stretch ratios. All of the simulation profiles vary from one another. The stretch ratio 1.1 and 1.2 simulation profiles are in the closest agreement.

Based on the results of the sensitivity study it is seen that the SST turbulence model with the High y^+ Wall Treatment is very good at replicating results among the 1.1, 1.2 and 1.3 stretch ratio simulations. The sensitivity of the simulation results to the stretch ratio in the turbulent kinetic energy profile was the reason for the selection of a stretch ratio of 1.2 to be used as this sensitivity study goes onto Step 4.

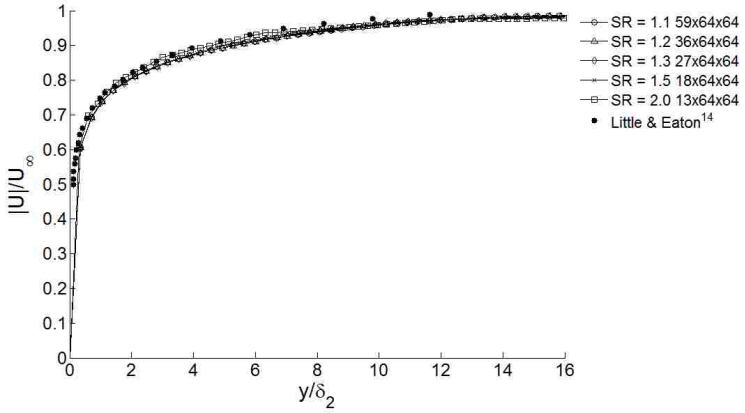

Figure 151. Turbulent mean flow vector magnitude in the rotating reference frame. *Comparison plot of the SST turbulence model for grids with varying cell stretch ratios in the axial direction.*

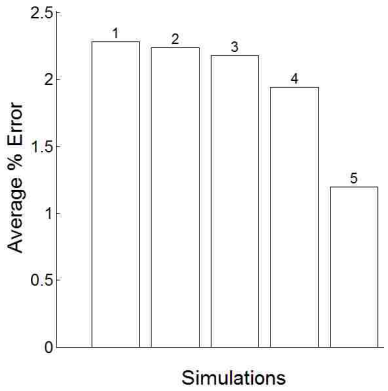

Figure 152. Error of turbulent mean flow vector magnitude. *1: SR=1.1, 2: SR=1.2, 3: SR=1.3, 4: SR=1.5, 5: SR=2.0*

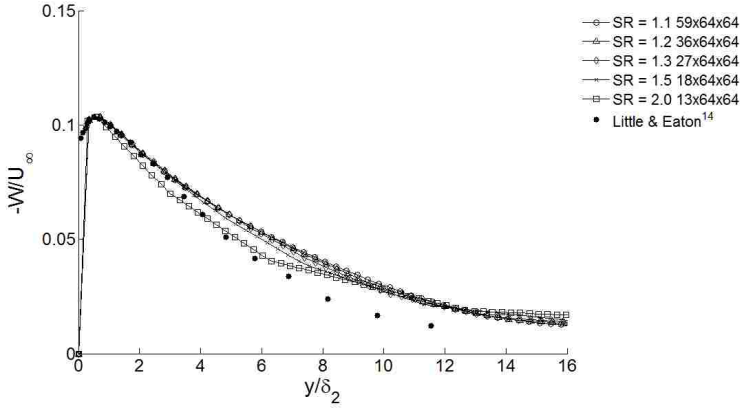

Figure 153. Crossflow profile. *Comparison plot of the SST turbulence model for grids with varying cell stretch ratios in the axial direction.*

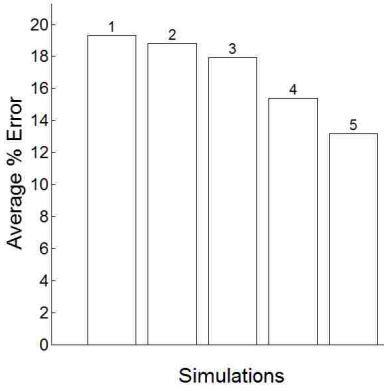

Figure 154. Error of crossflow profile. *1: SR=1.1, 2: SR=1.2, 3: SR=1.3, 4: SR=1.5, 5: SR=2.0*

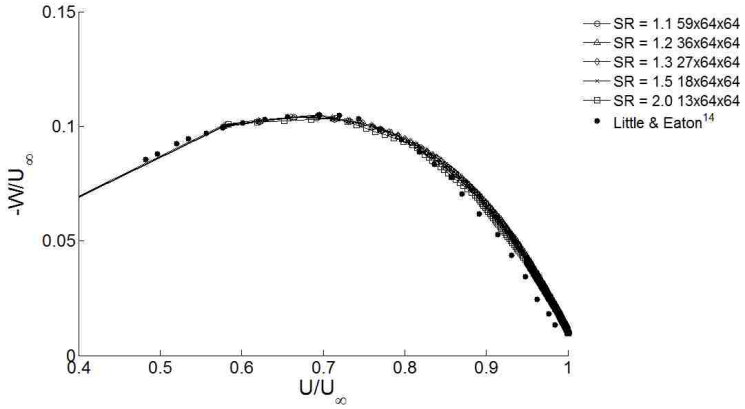

Figure 155. Polar plot of mean velocity profiles. *Comparison plot of the SST turbulence model for grids with varying cell stretch ratios in the axial direction.*

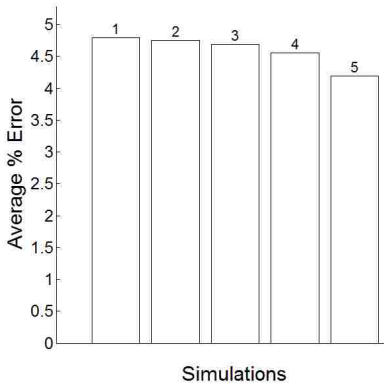

Figure 156. Error of polar mean velocity profiles. *1: SR=1.1, 2: SR=1.2, 3: SR=1.3, 4: SR=1.5, 5: SR=2.0*

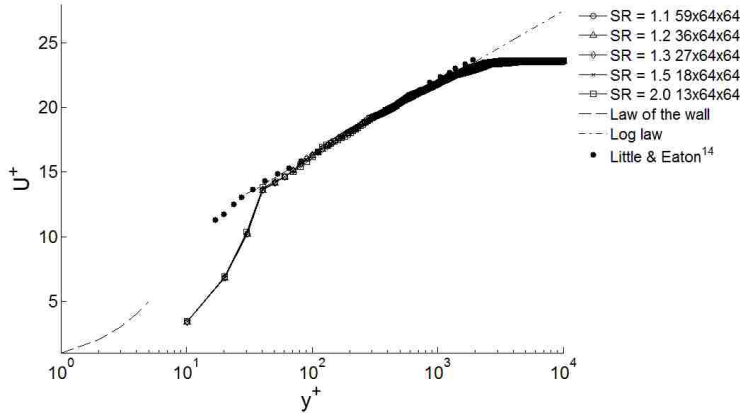

Figure 157. Tangential velocity in rotating reference frame. *Comparison plot of the SST turbulence model for grids with varying cell stretch ratios in the axial direction.*

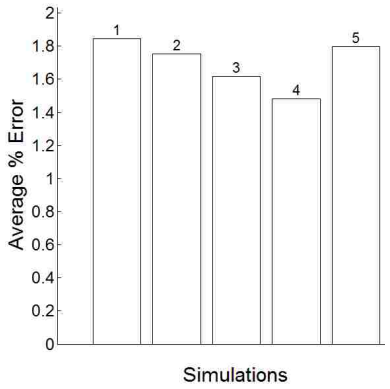

Figure 158. Error of tangential velocity. *1: SR=1.1, 2: SR=1.2, 3: SR=1.3, 4: SR=1.5, 5: SR=2.0*

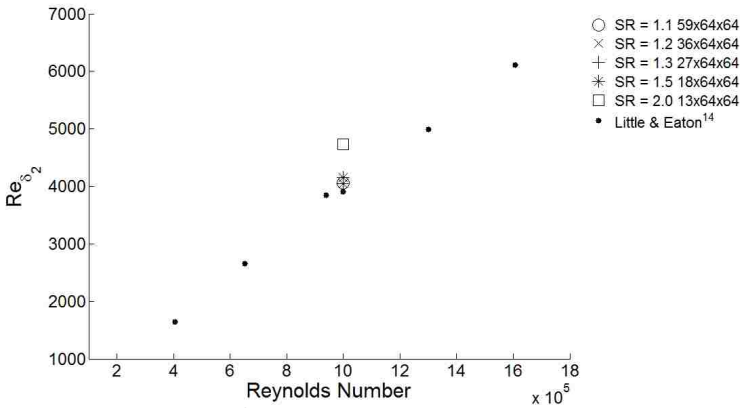

Figure 159. Comparison of momentum thickness Reynolds number. *Comparison plot of the SST turbulence model for grids with varying cell stretch ratios in the axial direction.*

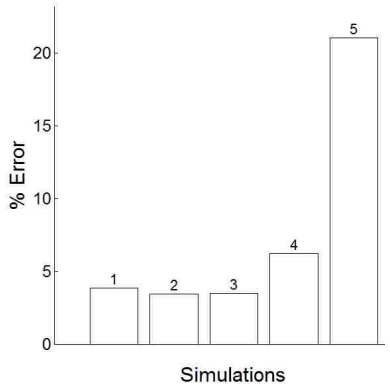

Figure 160. Error of momentum thickness Reynolds number. *1: SR=1.1, 2: SR=1.2, 3: SR=1.3, 4: SR=1.5, 5: SR=2.0*

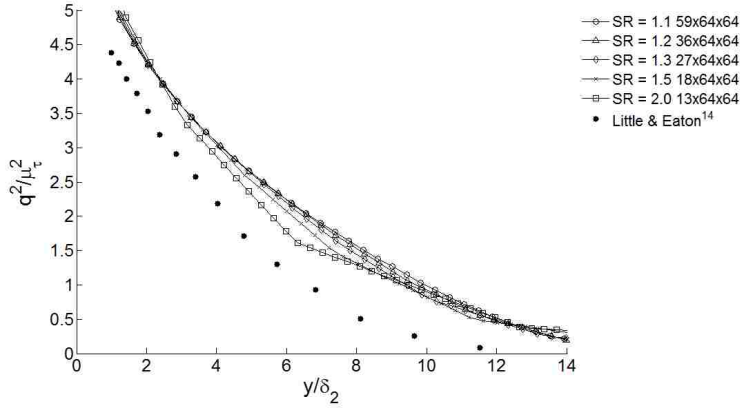

Figure 161. Twice the turbulence kinetic energy. *Comparison plot of the SST turbulence model for grids with varying cell stretch ratios in the axial direction.*

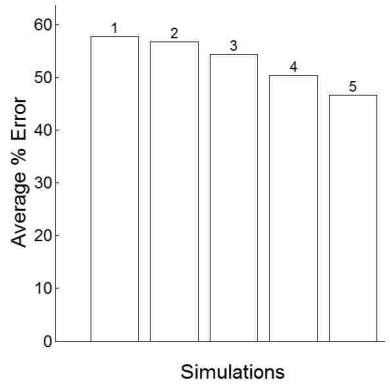

Figure 162. Error of twice the turbulence kinetic energy. *1: SR=1.1, 2: SR=1.2, 3: SR=1.3, 4: SR=1.5, 5: SR=2.0*

Step 4:

The grids used for the radial and tangential wall proximity sensitivity study had the following properties:

Wall cell's centroid located at $y^+ = 20$

Uniform radial and tangential grid spacing of $\approx 0.08\ m$

Stretch ratio of 1.2 in the axial direction

Computational domain size of 1 meter in the axial direction

This sensitivity study will adjust the position of the pressure outlet boundaries. In the previous simulations the computational domain size was 1x5x5 meters in the axial, radial and tangential directions respectively. The line probe at which data is being sampled is at a radius of 0.421 meters from the axis of rotation and extends above the disk's surface 0.1 meters. In Steps 1, 2 and 3 the distance between the line probe and the nearest pressure outlet was 2.079 meters. In this sensitivity study the computational domain was varied in the radial and tangential directions. The domain sizes in this study are:

1 x 10 x 10 meters, 36 x 128 x 128 nodes (axial, radial, tangential)

1 x 5 x 5 meters, 36 x 64 x 64 nodes

1 x 2 x 2 meters, 36 x 26 x 26 nodes

1 x 1 x 1 meters, 36 x 13 x 13 nodes

The goal of this sensitivity study is to find the smallest computational domain whose simulation profile does not vary significantly from the simulation profiles of the larger domains. The smallest computational domain puts the pressure outlets as close as 0.5 meters from the axis of rotation, which is only 0.079 meters from the data sampling locations. The largest domain puts the nearest pressure outlet 4.579 meters away from the data sampling locations.

Figures 163 and 164 show that there is negligible difference between all the profiles of the turbulent mean flow in the rotating reference frame.

The crossflow profile (Figs. 165 and 166) and the polar plot of the mean velocity profile (Figs. 167 and 168) illustrate sensitivity to the pressure outlets' location. The 1x1x1 meter computational domain simulation profile is unable to replicate the simulation profiles of the other domain sizes.

The tangential velocity in the rotating reference frame (Figs. 169 and 170) is nearly unaffected by the proximity of the pressure outlet. All of the simulation profiles are in close agreement with one another and with the experimental data[14].

In Figure 171, the momentum thickness Reynolds number is shown. The 1x1x1 meter domain simulation's momentum thickness Reynolds number is slightly less than that of the other simulations and nearly matches the experimental data[14].

The turbulent kinetic energy profile of the 1x1x1 meter domain's simulation slightly varies from the simulation profiles obtained from the other simulations (Figs. 173 and 174).

The data of this sensitivity study indicate that the domain size can be 1x2x2 meters without significant errors induced onto Star-CCM+'s[8] solution for the SST turbulence model with the High y^+ Wall Treatment.

The last sensitivity study of this turbulence model uses the radial and tangential domain size of 2x2 meters while the axial domain size is varied.

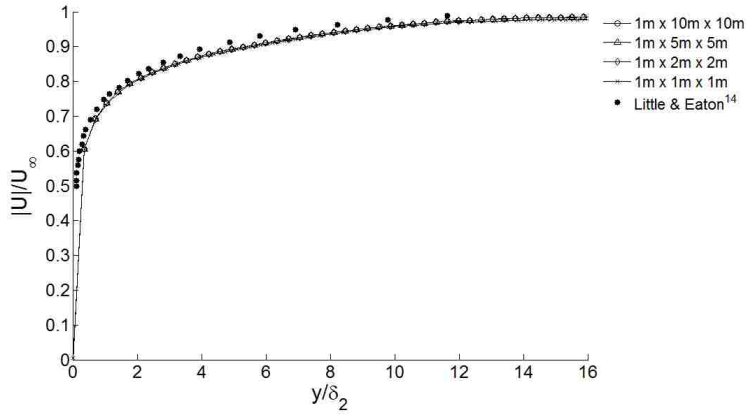

Figure 163. Turbulent mean flow vector magnitude in the rotating reference frame. *Comparison plot of the SST turbulence model for grids with varying computational domain sizes in the radial and tangential directions.*

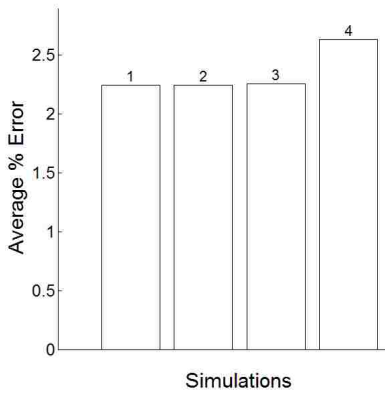

Figure 164. Error of turbulent mean flow vector magnitude. *1: 1x10x10m, 2: 1x5x5m, 3: 1x2x2m, 4: 1x1x1m*

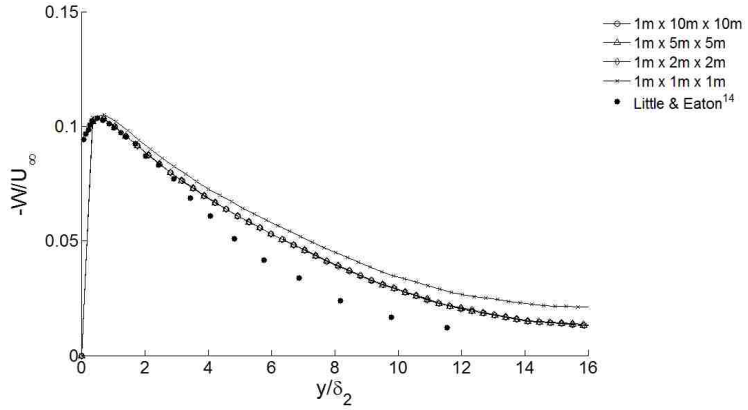

Figure 165. Crossflow profile. *Comparison plot of the SST turbulence model for grids with varying computational domain sizes in the radial and tangential directions.*

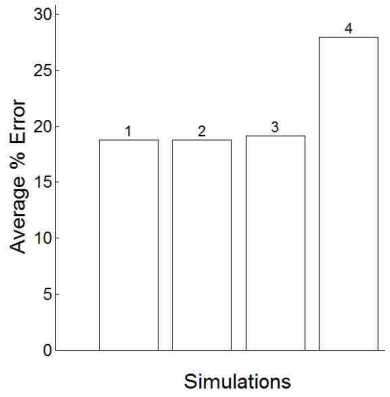

Figure 166. Error of crossflow profile. *1: 1x10x10m, 2: 1x5x5m, 3: 1x2x2m, 4: 1x1x1m*

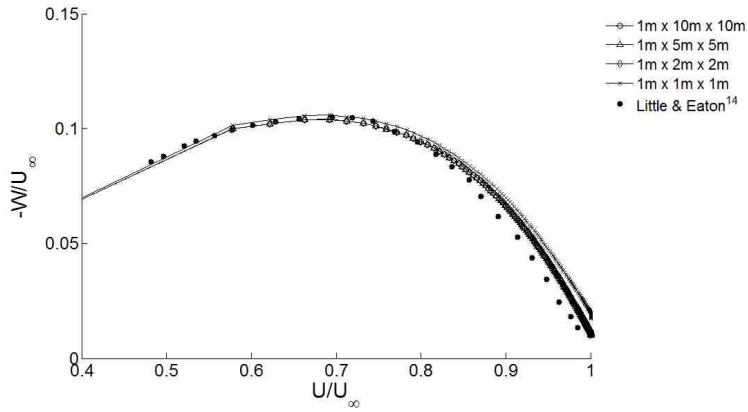

Figure 167. Polar plot of mean velocity profiles. *Comparison plot of the SST turbulence model for grids with varying computational domain sizes in the radial and tangential directions.*

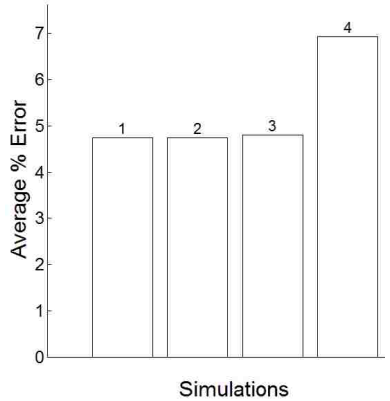

Figure 168. Error of polar mean velocity profiles. *1: 1x10x10m, 2: 1x5x5m, 3: 1x2x2m, 4: 1x1x1m*

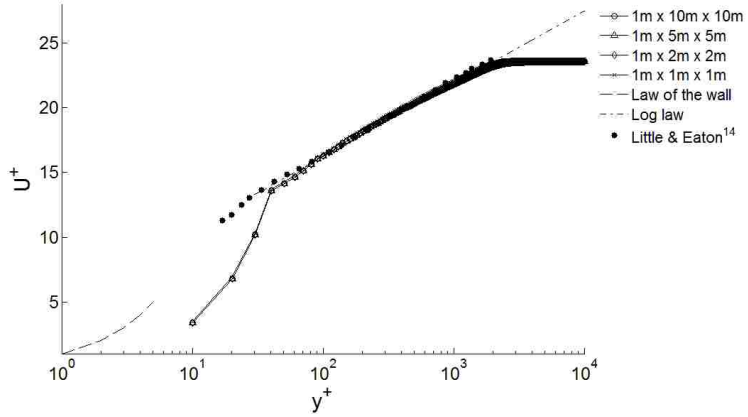

Figure 169. Tangential velocity in rotating reference frame. *Comparison plot of the SST turbulence model for grids with varying computational domain sizes in the radial and tangential directions.*

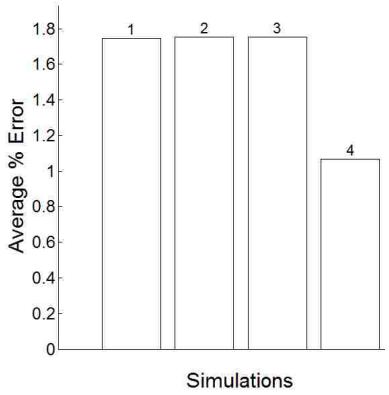

Figure 170. Error of tangential velocity. *1: 1x10x10m, 2: 1x5x5m, 3: 1x2x2m, 4: 1x1x1m*

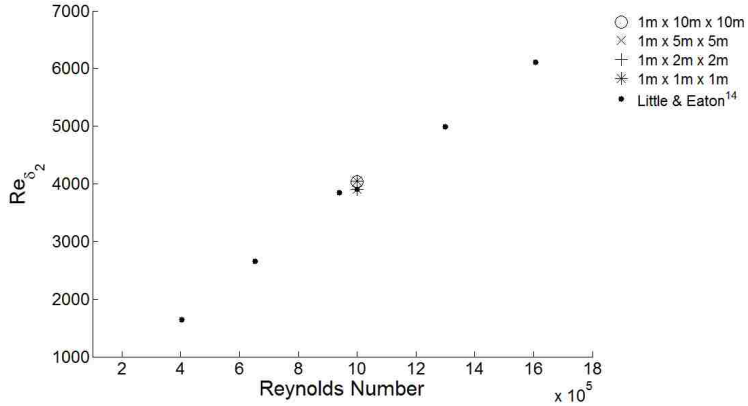

Figure 171. Comparison of momentum thickness Reynolds number. *Comparison plot of the SST turbulence model for grids with varying computational domain sizes in the radial and tangential directions.*

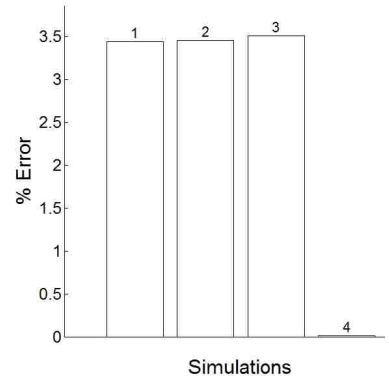

Figure 172. Error of momentum thickness Reynolds number. *1: 1x10x10m, 2: 1x5x5m, 3: 1x2x2m, 4: 1x1x1m*

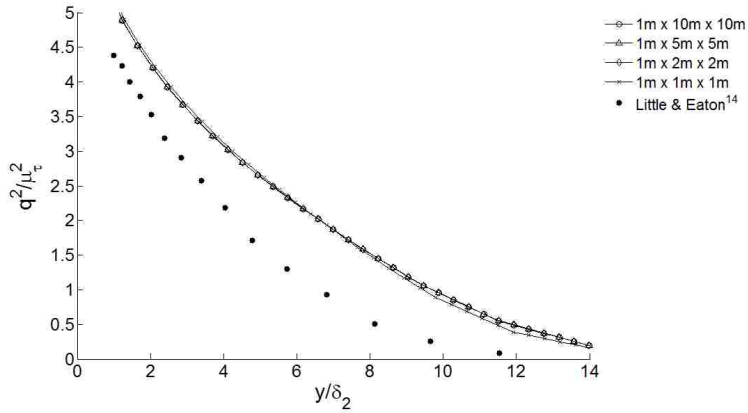

Figure 173. Twice the turbulence kinetic energy. *Comparison plot of the SST turbulence model for grids with varying computational domain sizes in the radial and tangential directions.*

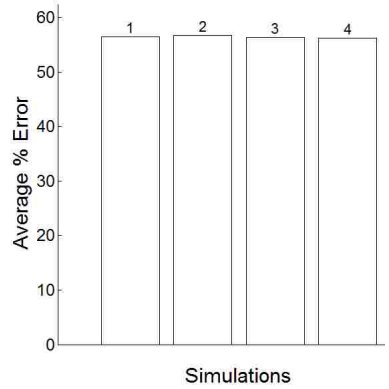

Figure 174. Error of twice the turbulence kinetic energy. *1: 1x10x10m, 2: 1x5x5m, 3: 1x2x2m, 4: 1x1x1m*

Step 5:

The grids used in the axial wall proximity sensitivity study had the following properties:

Wall cell's centroid located at $y^+ = 20$

Computational domain size in the radial and tangential direction of 2x2 meters

Radial and tangential grid resolution of 26x26 nodes (uniform grid spacing of = 0.08 *m*)

Stretch ratio of 1.2 in the axial direction

This sensitivity study will adjust the position of the velocity inlet boundary above the disk's surface. Steps 1-4 positioned the velocity inlet 1 meter above the disk's surface and prescribed an inlet velocity of 1 *m/s*. Here, the inlet velocity of 1 *m/s* was prescribed on the largest domain of 5x2x2 meters (axial, radial, tangential) and the axial velocity was sampled at locations 2.5, 1.0, 0.5, 0.25 and 0.1 meters above the disk's surface at $r = 0.421$ *m*. The measured axial velocities were prescribed at the velocity inlet for each respective simulation. The domain sizes and inlet velocity prescribed for the simulations in this sensitivity study are as follows:

5 x 2 x 2 meters (axial, radial, tangential), velocity prescribed at inlet = 1 *m/s*

2.5 x 2 x 2 meters, velocity prescribed at inlet = 0.996 *m/s*

1 x 2 x 2 meters, velocity prescribed at inlet = 0.887 *m/s*

0.5 x 2 x 2 meters, velocity prescribed at inlet = 0.684 *m/s*

0.25 x 2 x 2 meters, velocity prescribed at inlet = 0.494 *m/s*

0.1 x 2 x 2 meters, velocity prescribed at inlet = 0.344 *m/s*

The mean flow vector magnitude (Figs. 175 and 176), the profile of tangential velocity in the rotating reference frame (Figs. 181 and 182) and the turbulent kinetic energy profile (Figs. 185 and 186) all show a lack of sensitivity to the velocity inlet's position, as all of the simulation profiles are in close agreement.

The crossflow profile (Fig. 177), the polar plot of the mean velocity profiles (Fig. 179) and the momentum thickness Reynolds number (Fig. 183) all show a high sensitivity to the velocity inlet's position. The 5 and 2.5 meter axial domain simulation profiles are in close agreement, while all the other simulation profiles differ from one another. This is clearly seen in the error graphs (Figs. 178, 180 and 184), where the two largest domain simulation results have nearly

identical average error values. The average error differs increasingly, from that of the 5x2x2 and 2.5x2x2 meter domain simulations, as the computational domain size decreases.

The computational domain size of 2.5x2x2 meters is the smallest domain size whose simulation results do not stray from the simulation results obtained in the 5x2x2 meter computational domain. Thus it was chosen as the grid size suitable for the simulations using the SST turbulence model with the High y^+ Wall Treatment.

The computation time for the simulation using this grid was 4 minutes and 19 seconds, computed on the desktop computer, out to 1500 iterations. Comparing this time to the 7 hours and 27 minutes it took to compute the simulation on the Nano Linux cluster, for the initial y^+ = 20 grid in Step 1, illustrates the benefit to having an efficiently sized grid.

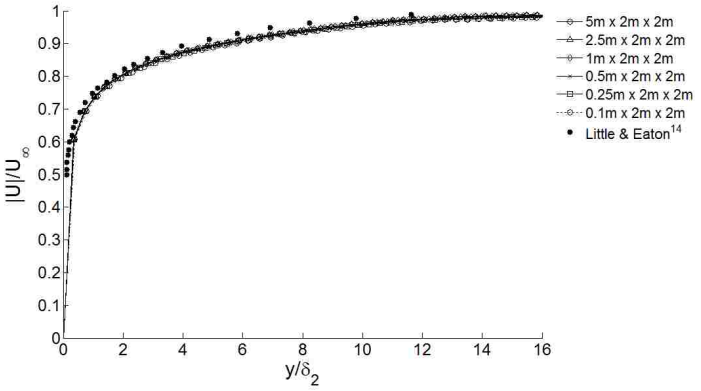

Figure 175. Turbulent mean flow vector magnitude in the rotating reference frame. *Comparison plot of the SST turbulence model for grids with varying computational domain sizes in the axial direction.*

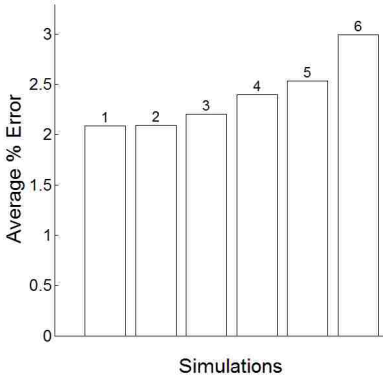

Figure 176. Error of turbulent mean flow vector magnitude. *1: 5x2x2m, 2: 2.5x2x2m, 3: 1x2x2m, 4: 0.5x2x2m, 5: 0.25x2x2m, 6: 0.1x2x2m*

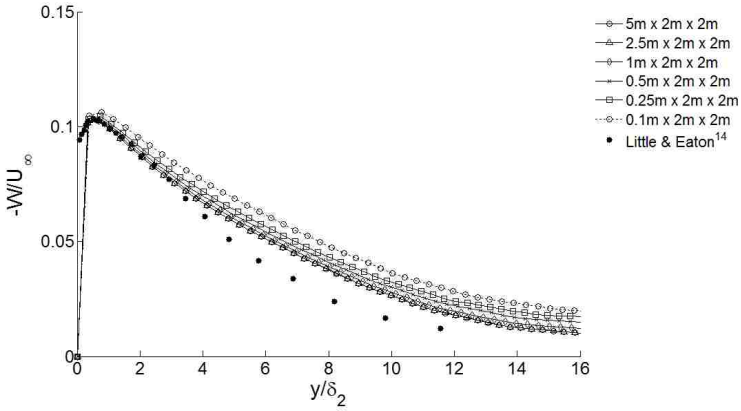

Figure 177. Crossflow profile. *Comparison plot of the SST turbulence model for grids with varying computational domain sizes in the axial direction.*

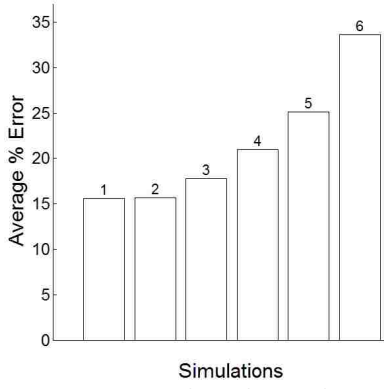

Figure 178. Error of crossflow profile. *1: 5x2x2m, 2: 2.5x2x2m, 3: 1x2x2m, 4: 0.5x2x2m, 5: 0.25x2x2m, 6: 0.1x2x2m*

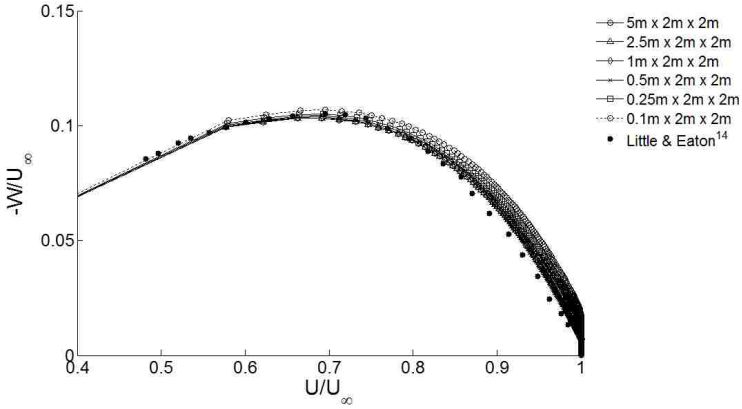

Figure 179. Polar plot of mean velocity profiles. *Comparison plot of the SST turbulence model for grids with varying computational domain sizes in the axial direction.*

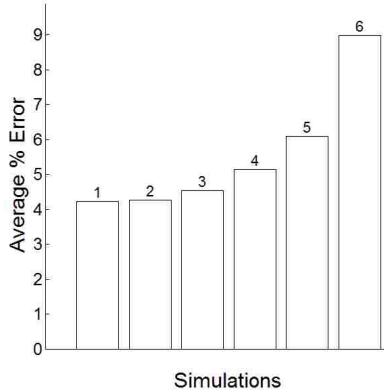

Figure 180. Error of polar mean velocity profiles. *1: 5x2x2m, 2: 2.5x2x2m, 3: 1x2x2m, 4: 0.5x2x2m, 5: 0.25x2x2m, 6: 0.1x2x2m*

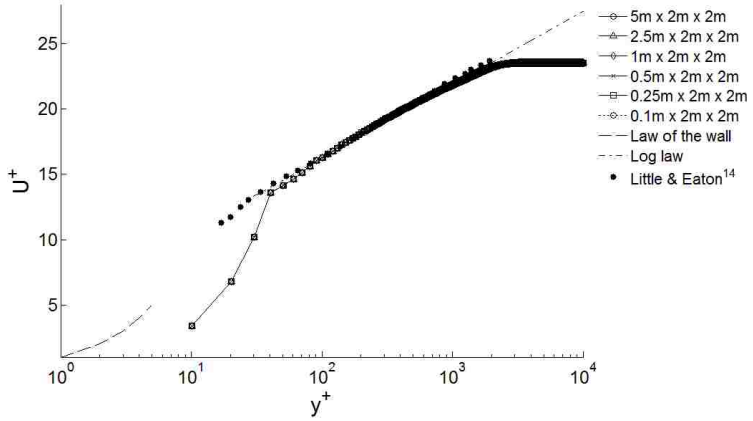

Figure 181. Tangential velocity in rotating reference frame. *Comparison plot of the SST turbulence model for grids with varying computational domain sizes in the axial direction.*

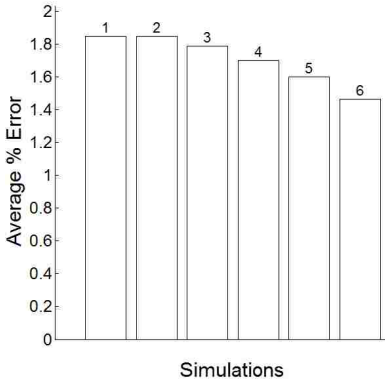

Figure 182. Error of tangential velocity. *1: 5x2x2m, 2: 2.5x2x2m, 3: 1x2x2m, 4: 0.5x2x2m, 5: 0.25x2x2m, 6: 0.1x2x2m*

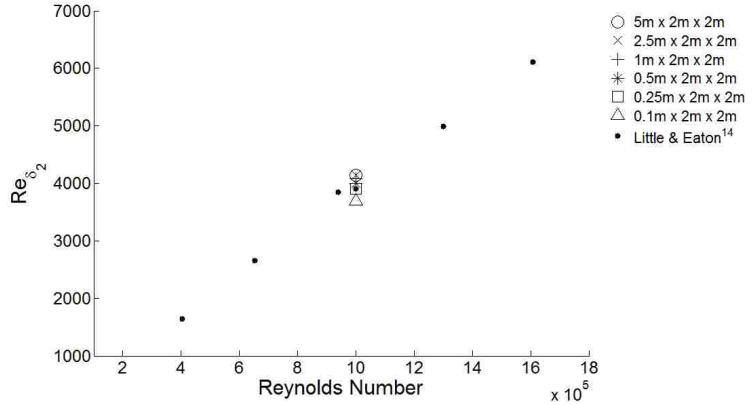

Figure 183. Comparison of momentum thickness Reynolds number. *Comparison plot of the SST turbulence model for grids with varying computational domain sizes in the axial direction.*

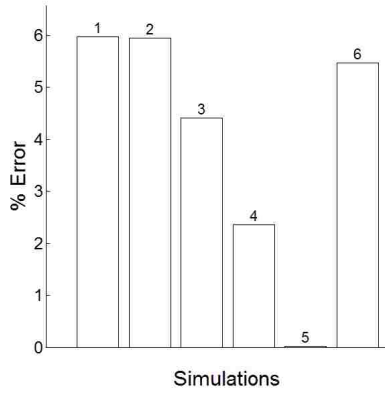

Figure 184. Error of momentum thickness Reynolds number. *1: 5x2x2m, 2: 2.5x2x2m, 3: 1x2x2m, 4: 0.5x2x2m, 5: 0.25x2x2m, 6: 0.1x2x2m*

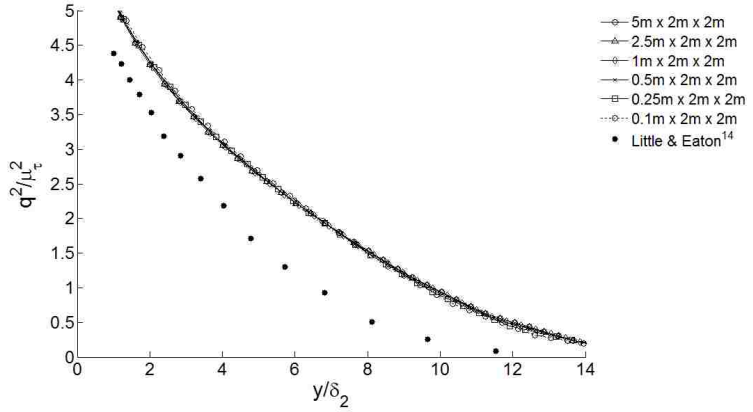

Figure 185. Twice the turbulence kinetic energy. *Comparison plot of the SST turbulence model for grids with varying computational domain sizes in the axial direction.*

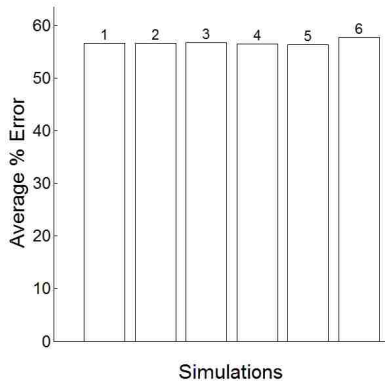

Figure 186. Error of twice the turbulence kinetic energy. *1: 5x2x2m, 2: 2.5x2x2m, 3: 1x2x2m, 4: 0.5x2x2m, 5: 0.25x2x2m, 6: 0.1x2x2m*

4. High-Reynolds Number Spalart-Allmaras model

Step 1:

The grids used for the y^+ sensitivity study had the following properties:

Computational domain size of 1x5x5 meters (axial x radial x tangential)

Stretch ratio of 1.2 in the axial direction

Uniform radial and tangential resolution of 508x508 nodes

Grids with the following initial cell's centroid y^+ values were included in this sensitivity study:

y^+ = 5 (42 x 508 x 508 nodes)

y^+ = 10 (39 x 508 x 508 nodes)

y^+ = 20 (36 x 508 x 508 nodes)

y^+ = 30 (33 x 508 x 508 nodes)

y^+ = 40 (32 x 508 x 508 nodes)

y^+ = 50 (31 x 508 x 508 nodes)

y^+ = 75 (28 x 508 x 508 nodes)

y^+ = 100 (27 x 508 x 508 nodes)

y^+ = 200 (23 x 508 x 508 nodes)

The mean flow vector magnitude in the rotating reference frame is shown in Fig. 187. The distance above the disk's surface is normalized by the momentum thickness boundary layer, δ_2. The y^+ = 10, 20, 30, 40, 50, 75 and 100 simulation profiles are in close agreement past the near wall discrepancies. The y^+ = 5 and 200 simulation profiles have inaccuracies that extend past the region near the disk's surface. Figure 188 shows the errors of the simulations. The high y^+ grids larger error are mostly due to the data near the disk's surface.

In Fig. 189 the crossflow profile demonstrates a very high sensitivity to the size of the initial wall cell. It is clear that disagreements in the results of different simulations extend past the near wall region. The y^+ = 20 and 30 simulation profiles agree with the experimental data[14] very well near the disk's surface. The radial velocity, *W*, is too large near the disk's surface in the y^+ = 5 and 10 simulations. As the y^+ value grows, the value of the radial velocity near the disk's surface

reduces. The high velocity gradient that exists at the surface is not captured by the high y^+ grid simulations.

Figure 191 is the polar plot of the mean velocity profiles. There is a large influence on the velocity profiles near the wall. All straight lines on the left side of the graph are the data interpolations across the initial wall cell. The simulations all follow a similar trend on the right side of the graph, where the data sampling location is furthest from the disk's surface. Although the data follows the same trend far from the disk's surface, the initial wall-cell's size has a large effect as the data being sampled approach the disk's surface. This plot demonstrates the inadequacy of the High y^+ Wall Treatment near the disk's surface. The $y^+ = 200$ simulation's initial cell is so large that the data smoothing over the cell accounts for the data in the approximate range $0 \leq U/U_\infty \leq 0.9$. This is why the high y^+ simulation profiles fall off the experimental data[14] trend so abruptly. This same data fall off is visible down to the resolution of $y^+ = 20$. The $y^+ = 20$ simulation profile is in best agreement with the experimental data[14].

Figure 193 is a semi-logarithmic plot of U^+ vs. y^+. The Star-CCM+[8] simulation data start at the first data point on the line probe that is above the disk's surface, which is located at $y^+ \approx 10$. The results of the simulations are quite interesting. The High-Reynolds Number Spalart-Allmaras turbulence model with the High y^+ Wall Treatment is extremely sensitive to the initial wall cell's size. This affects the model's capability of calculating the distance from the disk's surface in the non-dimensional y^+ units and the non-dimensional velocity, U^+. This models extreme sensitivity in evaluating y^+ values is easily seen by noticing the initial data point is at different y^+ values (Fig. 193) in each simulation although all data are being sampled at the same physical locations above the disk's surface. The sensitivity in evaluating the non-dimensional velocity U^+ is seen by the $y^+ = 30$, 40, 50, 75, 100 and 200 profiles exiting the graph boundaries. None of the simulation profiles are in close agreement with the experimental data[14]. Only results obtained with the $y^+ = 10$ and 20 agree with one another. The error of the simulation results are seen in Fig. 194.

Figure 195 shows the momentum thickness Reynolds number for each simulation compared to the experimental value[14] $Re = 10^6$. Again, the $y^+ = 20$ simulation matches the experimental data[14] best.

The High-Reynolds Number Spalart-Allmaras turbulence model with the High y^+ Wall Treatment showed a high sensitivity to different grids in this sensitivity study. There was not a

single grid that agreed well with other data. Based on the best agreement with the experimental data[14], an initial cell centroid of $y^+ = 20$ was chosen to be held as a constant for the grids on the next sensitivity study of this turbulence model.

Computational expenses of theses simulations were also very large. The computational time of the $y^+ = 20$ grid's simulation was 5 hours 28 minutes. This computation was done on 4 nodes of the Nano Linux Cluster, out to 1500 iterations.

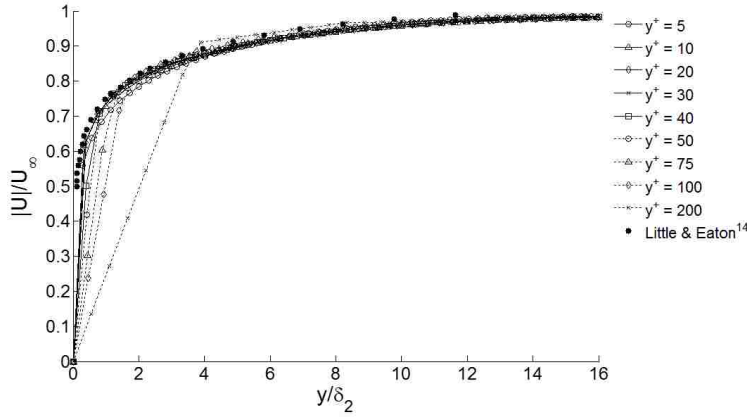

Figure 187. Turbulent mean flow vector magnitude in the rotating reference frame. *Comparison plot of the High-Reynolds Number Spalart-Allmaras turbulence model for grids with varying y^+ wall cell centroid values.*

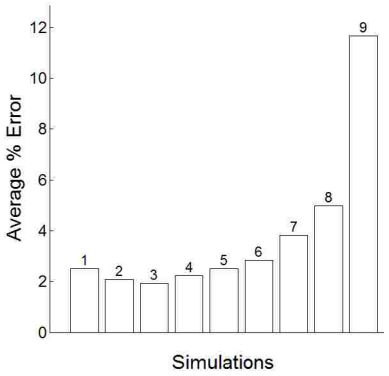

Figure 188. Error of turbulent mean flow vector magnitude. *1: y^+=5, 2: y^+=10, 3: y^+=20, 4: y^+=30, 5: y^+=40, 6: y^+=50, 7: y^+=75, 8: y^+=100, 9: y^+=200*

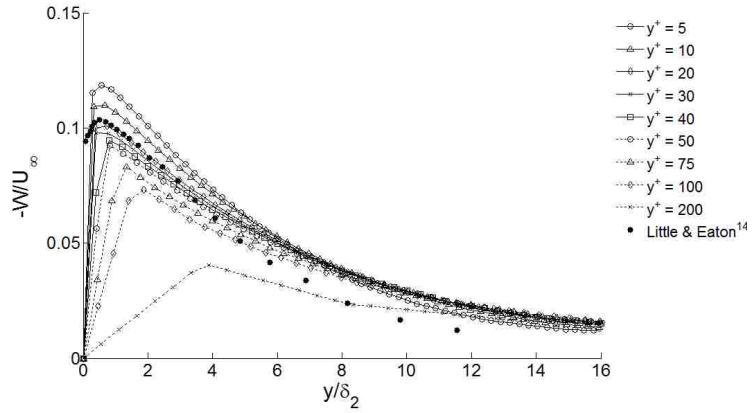

Figure 189. Crossflow profile. *Comparison plot of the High-Reynolds Number Spalart-Allmaras turbulence model for grids with varying y^+ wall cell centroid values.*

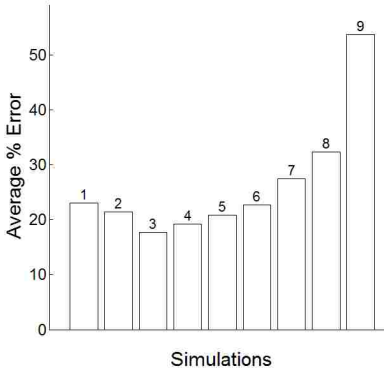

Figure 190. Error of crossflow profile. *1: y^+=5, 2: y^+=10, 3: y^+=20, 4: y^+=30, 5: y^+=40, 6: y^+=50, 7: y^+=75, 8: y^+=100, 9: y^+=200*

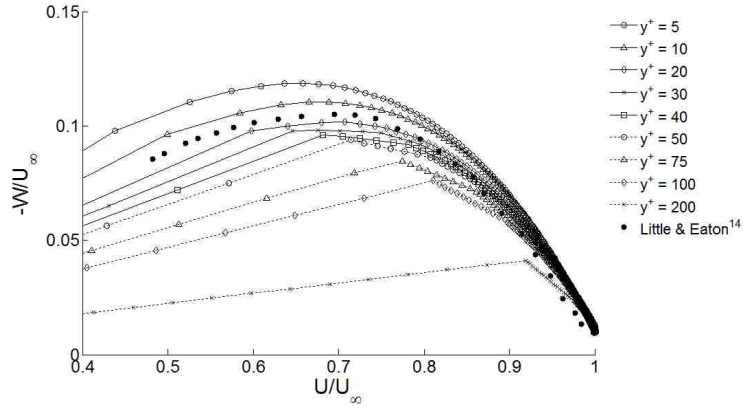

Figure 191. Polar plot of mean velocity profiles. *Comparison plot of the High-Reynolds Number Spalart-Allmaras turbulence model for grids with varying y^+ wall cell centroid values.*

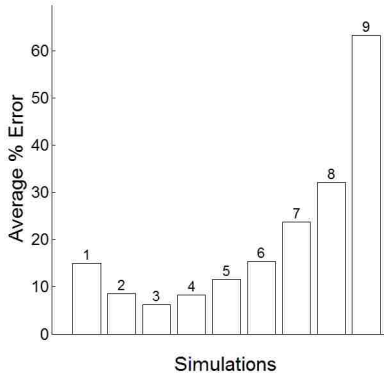

Figure 192. Error of polar mean velocity profiles. *1: y^+=5, 2: y^+=10, 3: y^+=20, 4: y^+=30, 5: y^+=40, 6: y^+=50, 7: y^+=75, 8: y^+=100, 9: y^+=200*

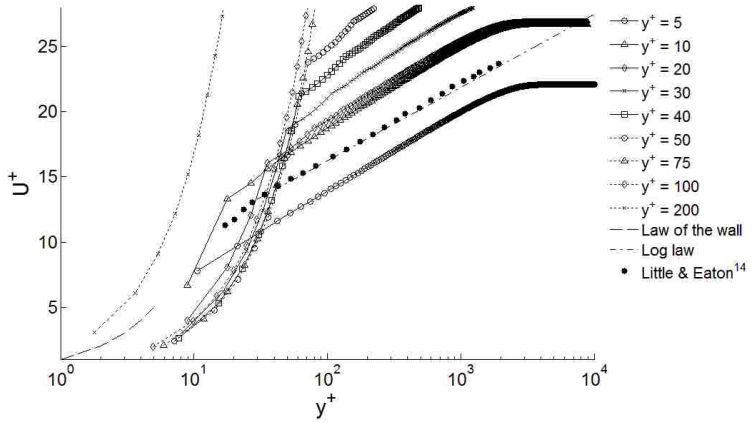

Figure 193. Tangential velocity in rotating reference frame. *Comparison plot of the High-Reynolds Number Spalart-Allmaras turbulence model for grids with varying y^+ wall cell centroid values.*

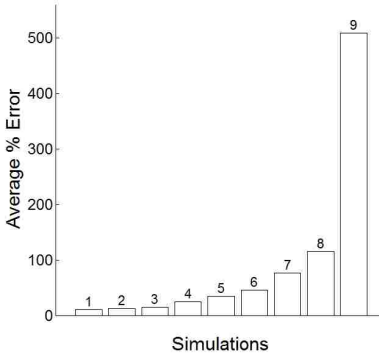

Figure 194. Error of tangential velocity. *1: y^+=5, 2: y^+=10, 3: y^+=20, 4: y^+=30, 5: y^+=40, 6: y^+=50, 7: y^+=75, 8: y^+=100, 9: y^+=200*

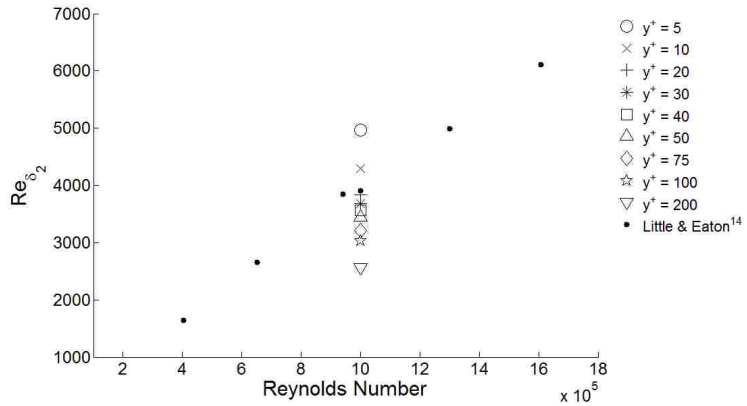

Figure 195. Comparison of momentum thickness Reynolds number. *Comparison plot of the High-Reynolds Number Spalart-Allmaras turbulence model for grids with varying y^+ wall cell centroid values.*

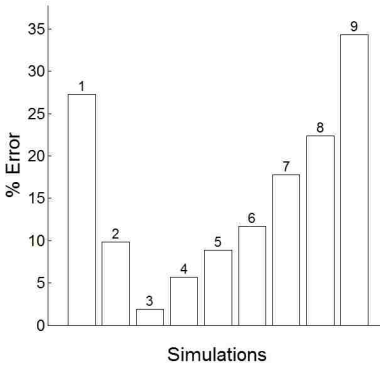

Figure 196. Error of momentum thickness Reynolds number. *1: y^+=5, 2: y^+=10, 3: y^+=20, 4: y^+=30, 5: y^+=40, 6: y^+=50, 7: y^+=75, 8: y^+=100, 9: y^+=200*

Step 2:

The grids used for the radial and tangential grid resolution sensitivity study had the following properties:

Wall cell's centroid located at $y^+ = 20$

Computational domain size of 1x5x5 meters (axial x radial x tangential)

Stretch ratio of 1.2 in the axial direction

The following grid nodal resolutions were used in this sensitivity study (axial x radial x tangential):

36 x 508 x 508 (uniform radial and tangential grid spacing of $\approx 0.01\ m$)

36 x 254 x 254 (uniform radial and tangential grid spacing of $\approx 0.02\ m$)

36 x 127 x 127 (uniform radial and tangential grid spacing of $\approx 0.04\ m$)

36 x 64 x 64 (uniform radial and tangential grid spacing of $\approx 0.08\ m$)

36 x 32 x 32 (uniform radial and tangential grid spacing of $\approx 0.16\ m$)

The grid in Step 1 is very fine, which results in a simulation that is computationally expensive. In an effort to determine the High-Reynolds Number Spalart-Allmaras turbulence model's sensitivity to grid refinement in the radial and tangential direction the grid was coarsened. The grid's radial and tangential grid spacing is doubled in each coarser grid. This results in each grid having four times fewer cells in the domain than the previous grid, which drastically reduces the computational time for each simulation. The simulation with the coarsest grid that can reproduce the simulation profiles of the finer grids is sought after.

The turbulent mean flow vector magnitude in the rotating reference frame is shown in Fig. 197. The distance above the disk's surface is normalized by the momentum thickness boundary layer, δ_2. All of the simulation profiles are in close agreement.

The crossflow profiles (Figs. 199 and 200) and the polar plot of the mean velocity profiles (Figs. 201 and 202) are in close agreement for all simulations.

The simulation profiles of the tangential velocity in the rotating reference frame (Figs. 203 and 204) and the momentum thickness Reynolds number (Figs. 205 and 206) demonstrate a higher sensitivity to the grid refinement. The simulation results obtained on the 36x32x32 grid are in disagreement with the simulation results of the finer grids. Although the 36x64x64 grid's

simulation results are in better agreement with the finest grid's simulation results than the 36x32x32 simulation results, there is a disagreement visible in the error graphs (Figs. 204 and 206).

Based on these results the High-Reynolds Number Spalart-Allmaras turbulence model can be as coarse as 36x127x127 on a 1x5x5 meter domain without the simulation profiles differing from the data of finer grids. This equates to an initial wall cell aspect ratio of 49:1.

The grid with the wall cell's centroid located at $y^+ = 20$ and the radial and tangential resolution of 127x127 nodes will be held constant as the sensitivity of the cell stretch ratio in the axial direction is studied in Step 3.

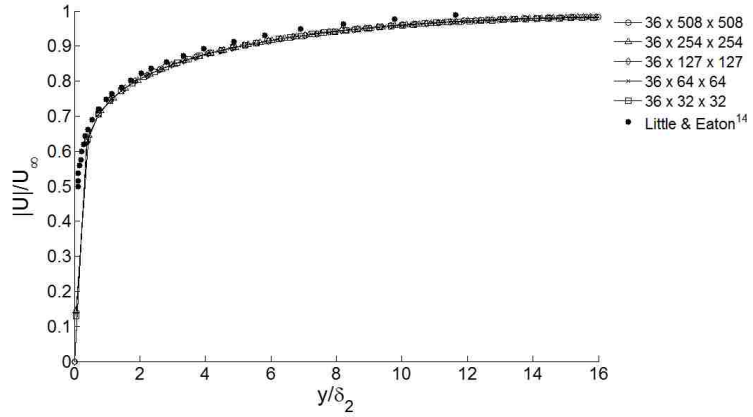

Figure 197. Turbulent mean flow vector magnitude in the rotating reference frame. *Comparison plot of the High-Reynolds Number Spalart-Allmaras turbulence model for grids with varying grid resolutions in the radial and tangential directions.*

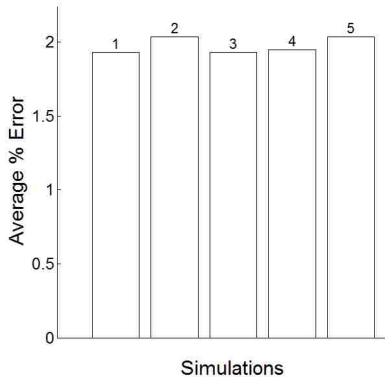

Figure 198. Error of turbulent mean flow vector magnitude. *1: 36x508x508, 2: 36x254x254, 3: 36x127x127, 4: 36x64x64, 5: 36x32x32*

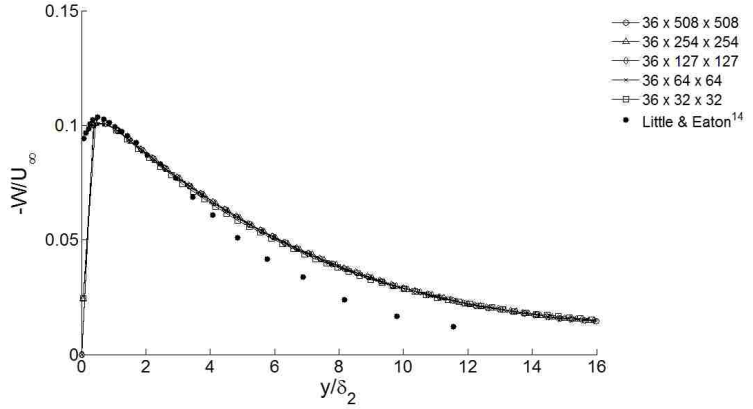

Figure 199. Crossflow profile. *Comparison plot of the High-Reynolds Number Spalart-Allmaras turbulence model for grids with varying grid resolutions in the radial and tangential directions.*

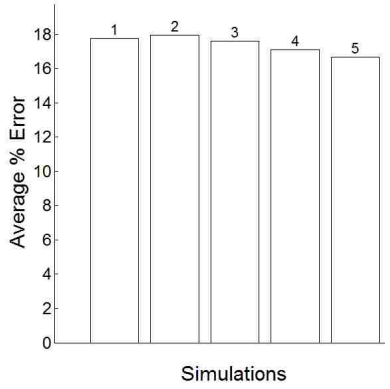

Figure 200. Error of crossflow profile. *1: 36x508x508, 2: 36x254x254, 3: 36x127x127, 4: 36x64x64, 5: 36x32x32*

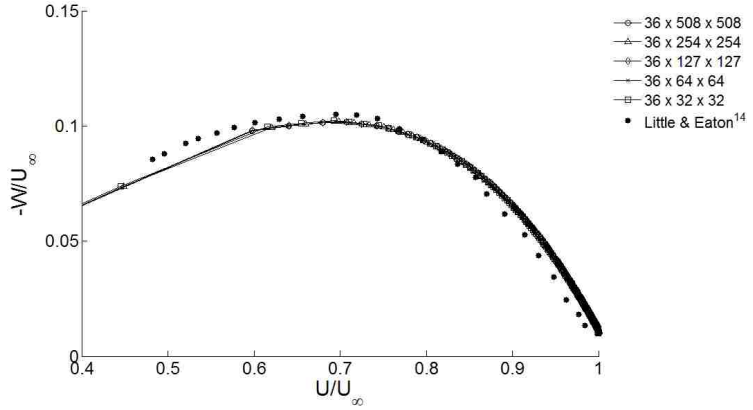

Figure 201. Polar plot of mean velocity profiles. *Comparison plot of the High-Reynolds Number Spalart-Allmaras turbulence model for grids with varying grid resolutions in the radial and tangential directions.*

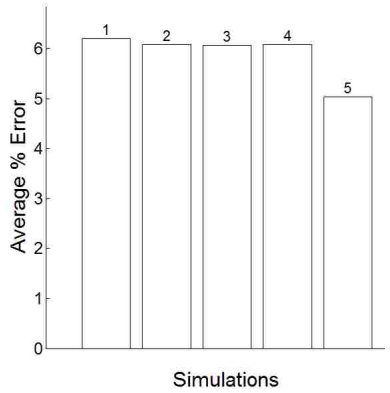

Figure 202. Error of polar mean velocity profiles. *1: 36x508x508, 2: 36x254x254, 3: 36x127x127, 4: 36x64x64, 5: 36x32x32*

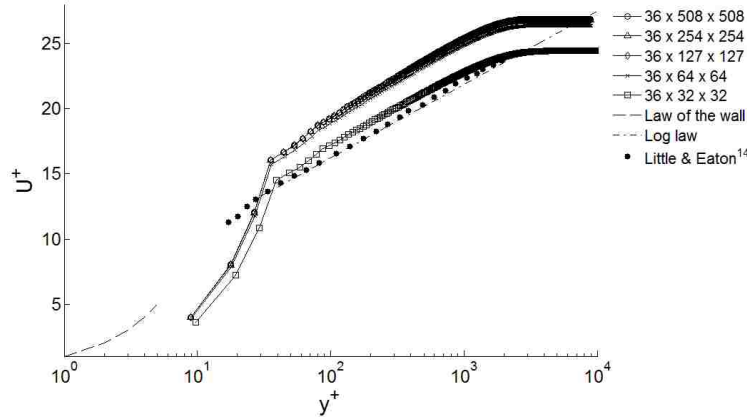

Figure 203. Tangential velocity in rotating reference frame. *Comparison plot of the High-Reynolds Number Spalart-Allmaras turbulence model for grids with varying grid resolutions in the radial and tangential directions.*

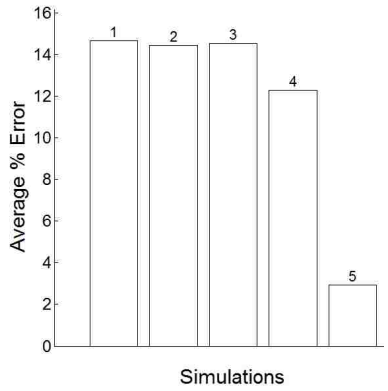

Figure 204. Error of tangential velocity. *1: 36x508x508, 2: 36x254x254, 3: 36x127x127, 4: 36x64x64, 5: 36x32x32*

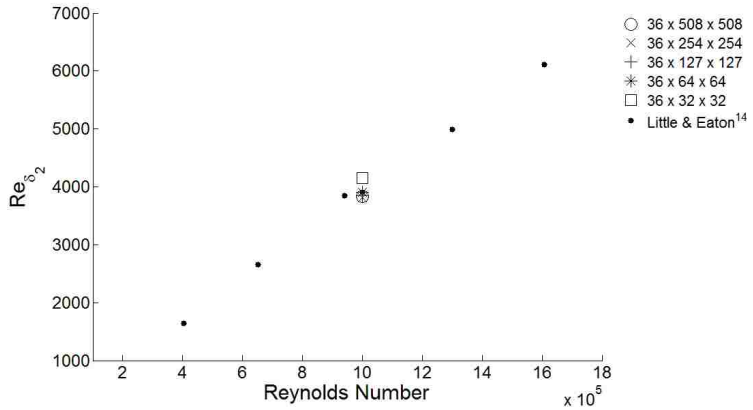

Figure 205. Comparison of momentum thickness Reynolds number. *Comparison plot of the High-Reynolds Number Spalart-Allmaras turbulence model for grids with varying grid resolutions in the radial and tangential directions.*

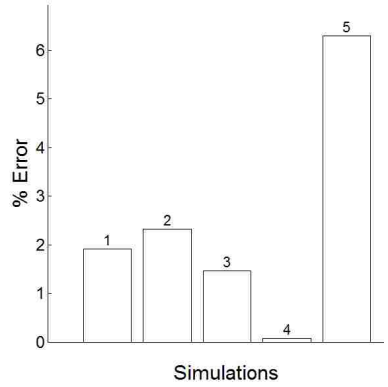

Figure 206. Error of momentum thickness Reynolds number. *1: 36x508x508, 2: 36x254x254, 3: 36x127x127, 4: 36x64x64, 5: 36x32x32*

Step 3:

The grids used in the axial direction stretch ratio sensitivity study had the following properties:

Wall cell's centroid located at $y^+ = 20$

Computational domain size of 1x5x5 meters (axial x radial x tangential)

Radial and tangential grid resolution, 127x127 nodes (uniform grid spacing of $\approx 0.04\ m$)

In Steps 1 and 2 the grids had a stretch ratio of 1.2. In this study the stretch ratio was changed in each simulation, thus each grid has a different number of nodes in the axial direction. The following stretch ratios were used in this sensitivity study:

1.1 (59 x 64 x 64 nodes)

1.2 (36 x 64 x 64 nodes)

1.3 (27 x 64 x 64 nodes)

1.5 (19 x 64 x 64 nodes)

2.0 (13 x 64 x 64 nodes)

The goal of this sensitivity study is to find the grid with the largest stretch ratio whose simulation profile does not differ significantly from the simulation profiles obtained from smaller stretch ratios.

The turbulent mean flow vector magnitude (Fig. 207) shows close agreement among all the simulation profiles. The 2.0 stretch ratio simulation profile slightly disagrees with the finer grid's simulation profiles. The error graph (Fig. 208) shows that as a simulation's stretch ratio increases the profile is closer to the experimental data[14].

The crossflow profile (Fig. 209) illustrates the 2.0 stretch ratio simulation results straying from the 1.1, 1.2, 1.3 and 1.5 stretch ratio simulation profiles. Figure 210 helps to illustrate the difference among the simulations.

In the polar plot of mean velocity profiles (Fig. 211) and the 1.5 and 2.0 stretch ratio simulation profiles are offset from the data grouping of the 1.1, 1.2 and 1.3 stretch ratio simulation profiles.

The simulation profiles of the tangential velocity plot in the rotating reference frame (Fig. 213) show a large sensitivity to the grid's stretch ratio. All the simulation profiles differ from

one another. The 1.1, 1.2 and 1.3 stretch ratio simulation results are relatively close to one another while the 1.5 and 2.0 stretch ratio simulation results are in poor agreement. The tangential velocity profile is poorly replicated by this turbulence model.

The momentum thickness Reynolds number is quite different in the 2.0 and 1.5 stretch ratio simulations than it is in the 1.1, 1.2, 1.3 stretch ratio simulations, as seen in Figs. 215 and 216.

From the results of the sensitivity study, we can infer that there is no stretch ratio at which simulation profiles replicate the results of simulations with the lower stretch ratios or the experimental data[14]. In the interest of reducing the computational time and due to the overall acceptable simulation results, the grid with a stretch ratio of 1.3 was chosen for the study in Step 4 for the High-Reynolds Number Spalart-Allmaras turbulence model with the High y^+ Wall Treatment.

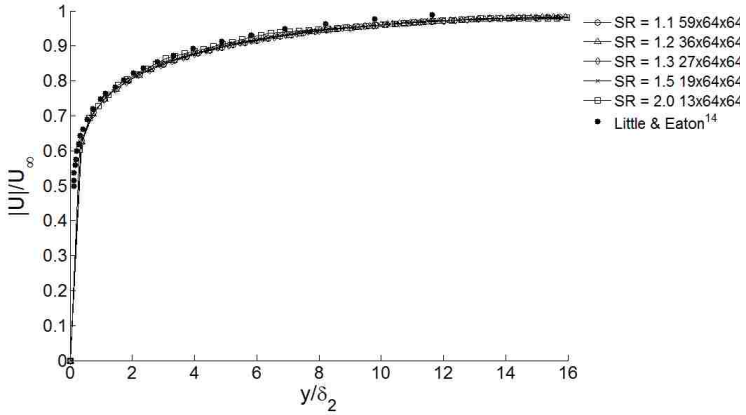

Figure 207. Turbulent mean flow vector magnitude in the rotating reference frame. *Comparison plot of the High-Reynolds Number Spalart-Allmaras turbulence model for grids with varying cell stretch ratios in the axial direction.*

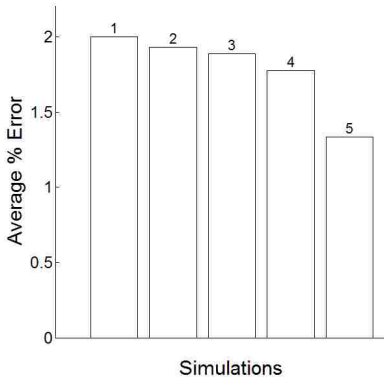

Figure 208. Error of turbulent mean flow vector magnitude. *1: SR=1.1, 2: SR=1.2, 3: SR=1.3, 4: SR=1.5, 5: SR=2.0*

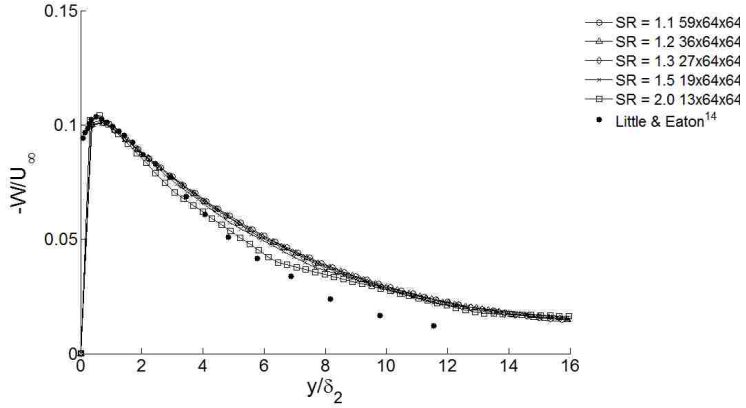

Figure 209. Crossflow profile. *Comparison plot of the High-Reynolds Number Spalart-Allmaras turbulence model for grids with varying cell stretch ratios in the axial direction.*

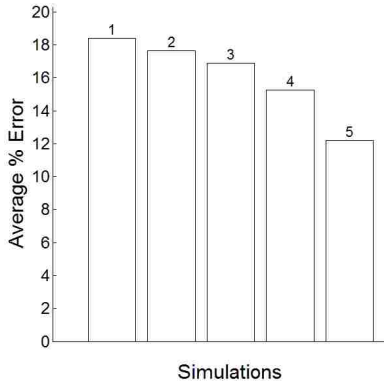

Figure 210. Error of crossflow profile. *1: SR=1.1, 2: SR=1.2, 3: SR=1.3, 4: SR=1.5, 5: SR=2.0*

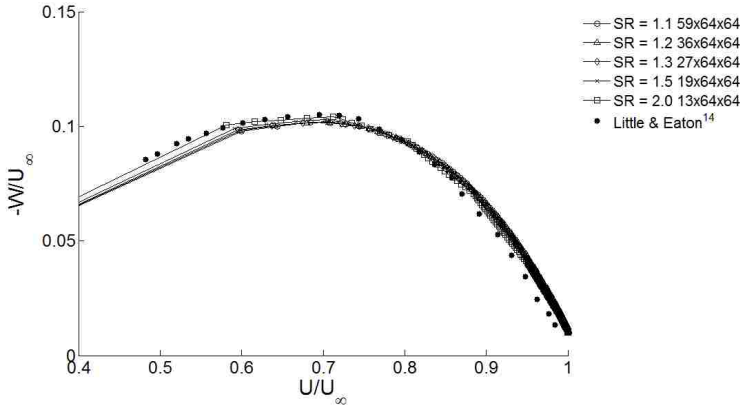

Figure 211. Polar plot of mean velocity profiles. *Comparison plot of the High-Reynolds Number Spalart-Allmaras turbulence model for grids with varying cell stretch ratios in the axial direction.*

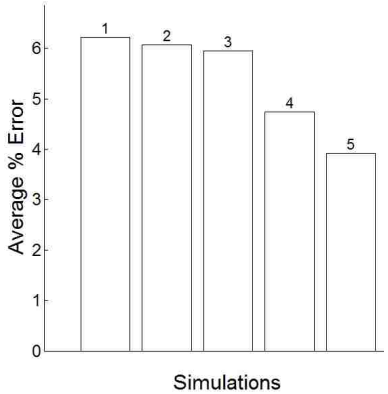

Figure 212. Error of polar mean velocity profiles. *1: SR=1.1, 2: SR=1.2, 3: SR=1.3, 4: SR=1.5, 5: SR=2.0*

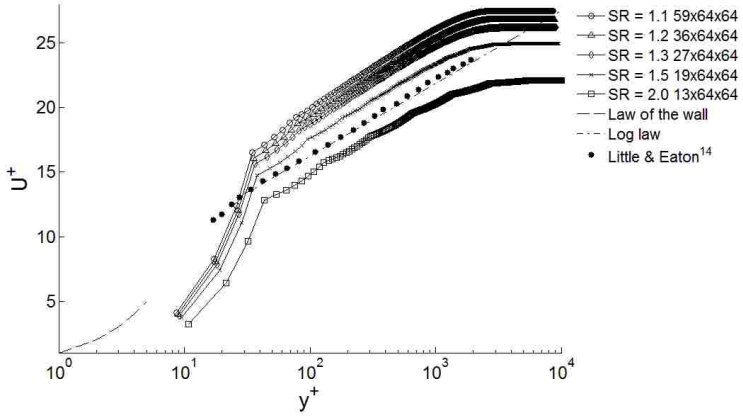

Figure 213. Tangential velocity in rotating reference frame. *Comparison plot of the High-Reynolds Number Spalart-Allmaras turbulence model for grids with varying cell stretch ratios in the axial direction.*

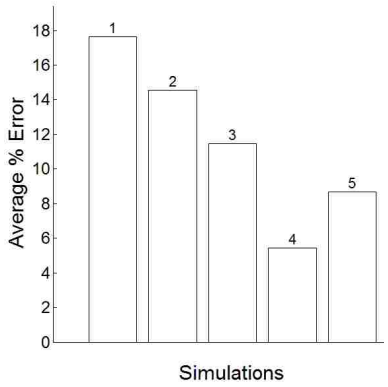

Figure 214. Error of tangential velocity. *1: SR=1.1, 2: SR=1.2, 3: SR=1.3, 4: SR=1.5, 5: SR=2.0*

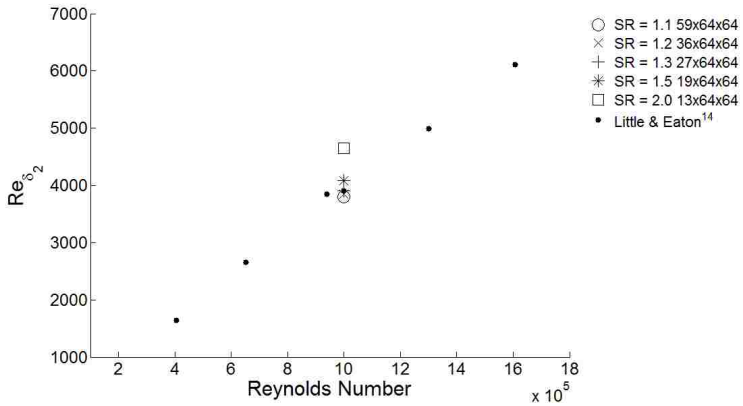

Figure 215. Comparison of momentum thickness Reynolds number. *Comparison plot of the High-Reynolds Number Spalart-Allmaras turbulence model for grids with varying cell stretch ratios in the axial direction.*

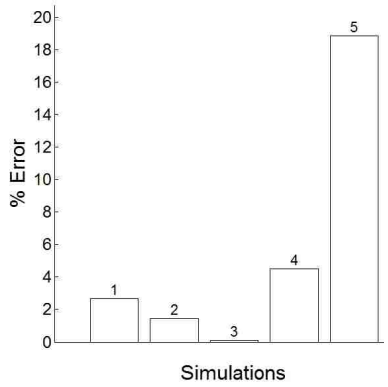

Figure 216. Error of momentum thickness Reynolds number. *1: SR=1.1, 2: SR=1.2, 3: SR=1.3, 4: SR=1.5, 5: SR=2.0*

Step 4:

The grids used for the radial and tangential wall proximity sensitivity study had the following properties:

Wall cell's centroid located at $y^+ = 20$

Uniform radial and tangential grid spacing of $\approx 0.04\ m$

Stretch ratio of 1.3 in the axial direction

Computational domain size of 1 meter in the axial direction

This sensitivity study will adjust the position of the pressure outlet boundaries. In the previous simulations the computational domain size was 1x5x5 meters in the axial, radial and tangential directions respectively. The line probe at which data is being sampled is at a radius of 0.421 meters from the axis of rotation and extends above the disk's surface 0.1 meters. In Steps 1, 2 and 3 the distance between the line probe and the nearest pressure outlet was 2.079 meters. In this sensitivity study the computational domain was varied in the radial and tangential directions. The domain sizes in this study are:

1 x 10 x 10 meters, 27 x 254 x 254 nodes (axial, radial, tangential)

1 x 5 x 5 meters, 27 x 127 x 127 nodes

1 x 2 x 2 meters, 27 x 51 x 51 nodes

1 x 1 x 1 meters, 27 x 26 x 26 nodes

The goal of this sensitivity study is to find the smallest computational domain whose simulation profile does not vary significantly from the simulation profiles of the larger domains. The smallest computational domain puts the pressure outlets as close as 0.5 meters from the axis of rotation, which is only 0.079 meters from the data sampling locations. The largest domain puts the nearest pressure outlet 4.579 meters away from the data sampling locations.

Figures 217 and 218 show that there is a negligible difference among all of the profiles of the turbulent mean flow in the rotating reference frame. Only the smallest domain's simulation profile slightly deviates from others.

The crossflow profile (Figs. 219 and 220) and the polar plot of the mean velocity profile (Figs. 221 and 222) illustrate sensitivity to the pressure outlets' location. The 1x1x1 meter

computational domain simulation profile is unable to replicate the simulation profiles of the other domain sizes.

The tangential velocity in the rotating reference frame (Figs. 223 and 224) is nearly unaffected by the proximity of the pressure outlet. All of the simulation profiles are in close agreement with one another.

In Figure 225 the momentum thickness Reynolds number is shown. The value of the momentum thickness Reynolds number obtained in the 1x1x1 meter domain's simulation is slightly less than that obtained in other simulations.

The data of this sensitivity study indicate that the domain size can be 1x2x2 meters without significant errors induced onto Star-CCM+'s[8] solution for the High-Reynolds Number Spalart-Allmaras turbulence model with the High y^+ Wall Treatment.

The last sensitivity study of this turbulence model uses the radial and tangential domain size of 2x2 meters while the axial domain size is varied.

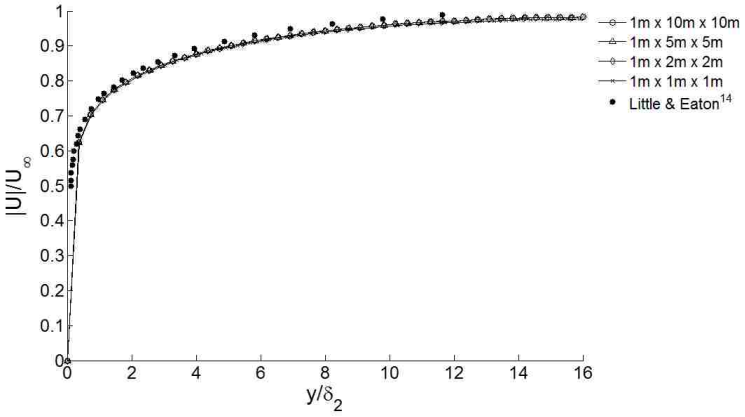

Figure 217. Turbulent mean flow vector magnitude in the rotating reference frame. *Comparison plot of the High-Reynolds Number Spalart-Allmaras turbulence model for grids with varying computational domain sizes in the radial and tangential directions.*

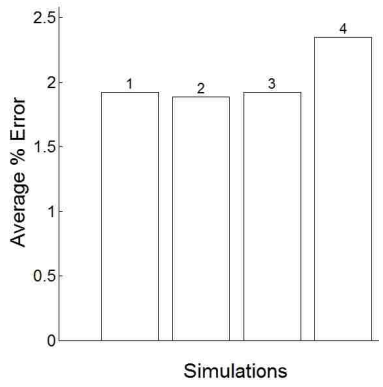

Figure 218. Error of turbulent mean flow vector magnitude. *1: 1x10x10m, 2: 1x5x5m, 3: 1x2x2m, 4: 1x1x1m*

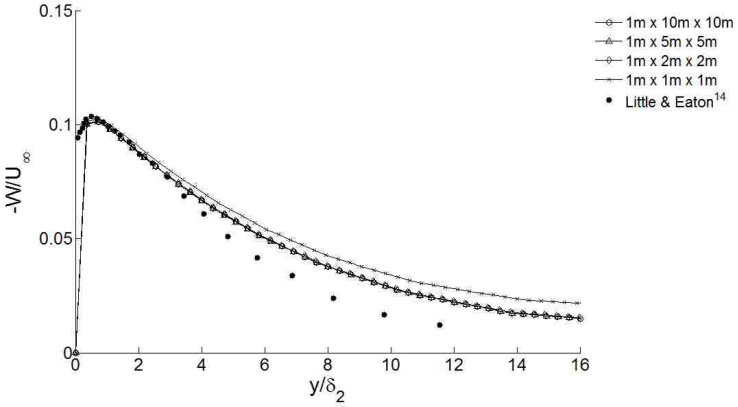

Figure 219. Crossflow profile. *Comparison plot of the High-Reynolds Number Spalart-Allmaras turbulence model for grids with varying computational domain sizes in the radial and tangential directions.*

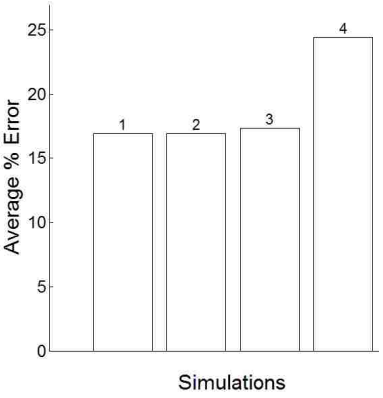

Figure 220. Error of crossflow profile. *1: 1x10x10m, 2: 1x5x5m, 3: 1x2x2m, 4: 1x1x1m*

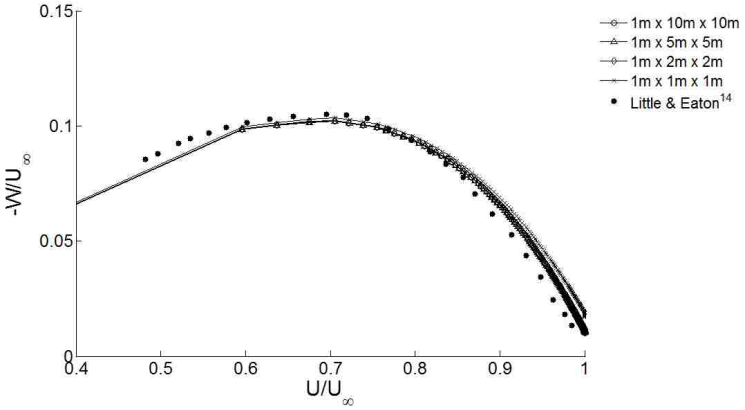

Figure 221. Polar plot of mean velocity profiles. *Comparison plot of the High-Reynolds Number Spalart-Allmaras turbulence model for grids with varying computational domain sizes in the radial and tangential directions.*

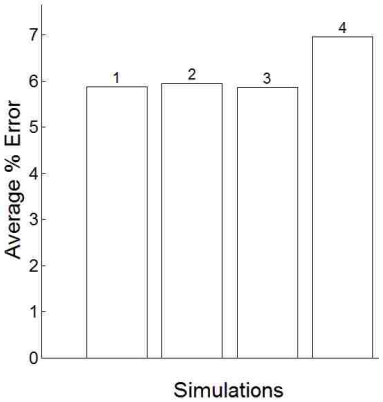

Figure 222. Error of polar mean velocity profiles. *1: 1x10x10m, 2: 1x5x5m, 3: 1x2x2m, 4: 1x1x1m*

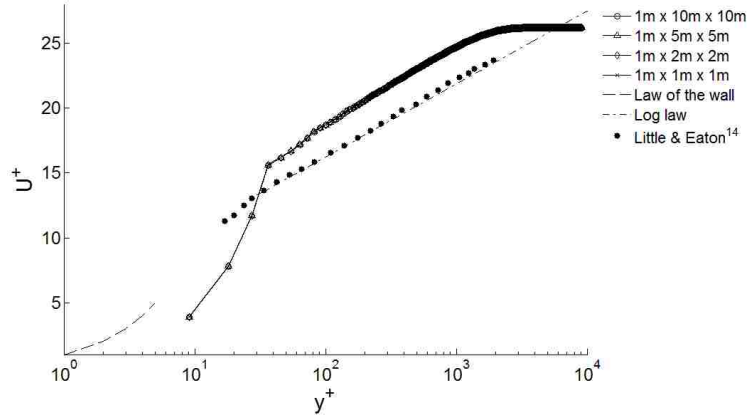

Figure 223. Tangential velocity in rotating reference frame. *Comparison plot of the High-Reynolds Number Spalart-Allmaras turbulence model for grids with varying computational domain sizes in the radial and tangential directions.*

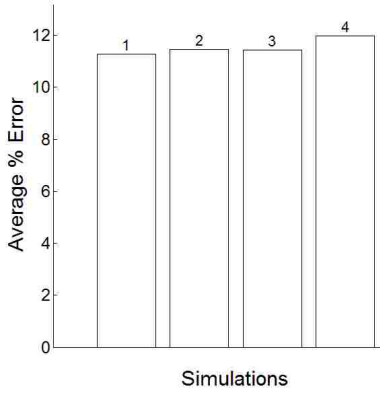

Figure 224. Error of tangential velocity. *1: 1x10x10m, 2: 1x5x5m, 3: 1x2x2m, 4: 1x1x1m*

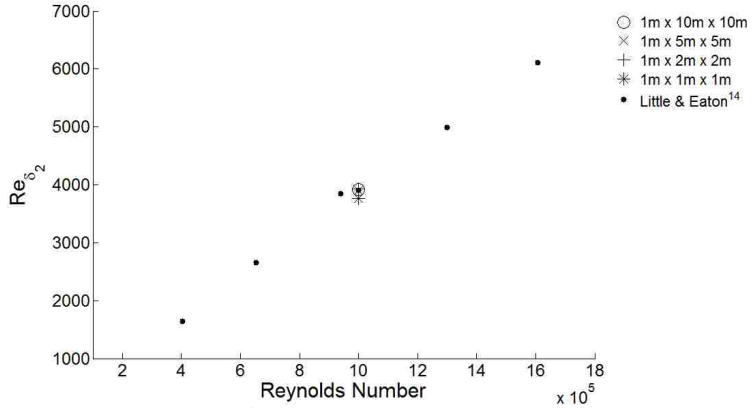

Figure 225. Comparison of momentum thickness Reynolds number. *Comparison plot of the High-Reynolds Number Spalart-Allmaras turbulence model for grids with varying computational domain sizes in the radial and tangential directions.*

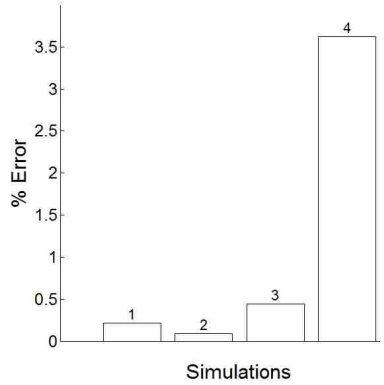

Figure 226. Error of momentum thickness Reynolds number. *1: 1x10x10m, 2: 1x5x5m, 3: 1x2x2m, 4: 1x1x1m*

Step 5:

The grids used in the axial wall proximity sensitivity study had the following properties:

Wall cell's centroid located at $y^+ = 20$

Computational domain size in the radial and tangential direction of 2x2 meters

Radial and tangential grid resolution of 51x51 nodes (uniform grid spacing of = 0.04 *m*)

Stretch ratio of 1.3 in the axial direction

This sensitivity study will adjust the position of the velocity inlet boundary above the disk's surface. Steps 1-4 positioned the velocity inlet 1 meter above the disk's surface and prescribed an inlet velocity of 1 *m/s*. Here, the inlet velocity of 1 *m/s* was prescribed on the largest domain of 5x2x2 meters (axial, radial, tangential) and the axial velocity was sampled at locations 2.5, 1.0, 0.5, 0.25 and 0.1 meters above the disk's surface at $r = 0.421$ *m*. The measured axial velocities were prescribed at the velocity inlet for each respective simulation. The domain sizes and inlet velocity prescribed for the simulations in this sensitivity study are as follows:

5 x 2 x 2 meters (axial, radial, tangential), velocity prescribed at inlet = 1 *m/s*

2.5 x 2 x 2 meters, velocity prescribed at inlet = 0.994 *m/s*

1 x 2 x 2 meters, velocity prescribed at inlet = 0.881 *m/s*

0.5 x 2 x 2 meters, velocity prescribed at inlet = 0.681 *m/s*

0.25 x 2 x 2 meters, velocity prescribed at inlet = 0.492 *m/s*

0.1 x 2 x 2 meters, velocity prescribed at inlet = 0.338 *m/s*

The mean flow vector magnitude (Figs. 227 and 228) and the profile of tangential velocity in the rotating reference frame (Figs. 233 and 234) show a lack of sensitivity to the velocity inlet's position, as all of the simulation profiles are in close agreement with one another.

The crossflow profile (Fig. 229), the polar plot of the mean velocity profiles (Fig. 231) and the momentum thickness Reynolds number (Fig. 235) all show a high sensitivity to the velocity inlet's position. The 5 and 2.5 meter axial domain simulation profiles are in close agreement, while all other simulation profiles differ from one another. This is clearly seen in the error graphs (Figs. 230, 232 and 236), where the two largest domain simulation results have nearly

identical average error values. The average error differs increasingly, from that of the 5x2x2 and 2.5x2x2 meter domain simulations, as the computational domain size decreases.

The computational domain size of 2.5x2x2 meters is the smallest domain size whose simulation results do not stray from simulation results obtained in the largest computational domain. Thus it was chosen as the grid size suitable for these simulations with the High-Reynolds Number Spalart-Allmaras turbulence model with the High y^+ Wall Treatment.

The computation time for this grid size was 6 minutes and 14 seconds, computed on the desktop computer, out to 1500 iterations. Comparing this time to the 5 hours and 28 minutes it took to compute this simulation on the Nano Linux cluster, for the initial $y^+ = 20$ grid in Step 1, illustrates the benefit to having an efficiently sized grid.

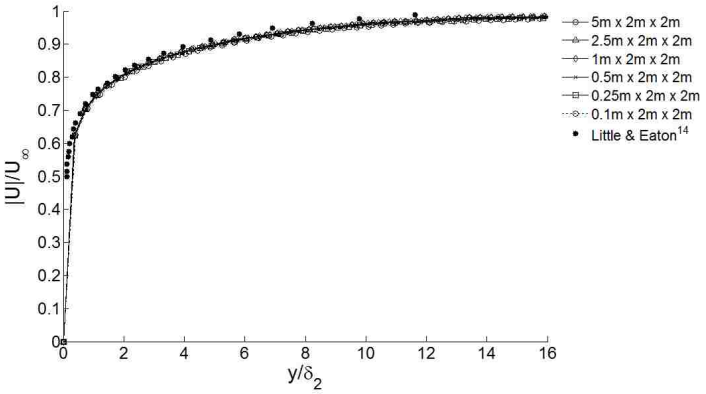

Figure 227. Turbulent mean flow vector magnitude in the rotating reference frame. *Comparison plot of the High-Reynolds Number Spalart-Allmaras turbulence model for grids with varying computational domain sizes in the axial direction.*

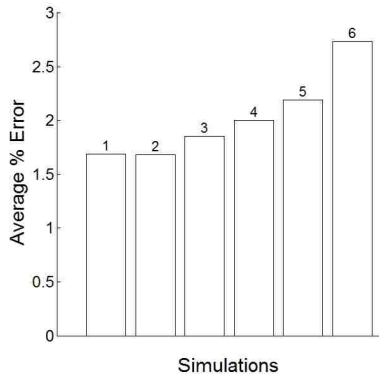

Figure 228. Error of turbulent mean flow vector magnitude. *1: 5x2x2m, 2: 2.5x2x2m, 3: 1x2x2m, 4: 0.5x2x2m, 5: 0.25x2x2m, 6: 0.1x2x2m*

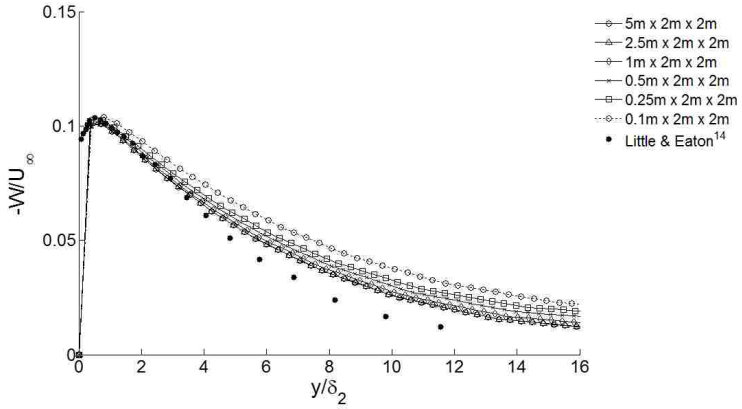

Figure 229. Crossflow profile. *Comparison plot of the High-Reynolds Number Spalart-Allmaras turbulence model for grids with varying computational domain sizes in the axial direction.*

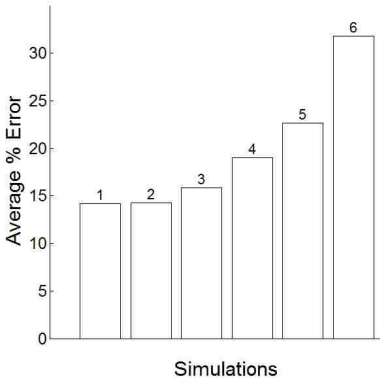

Figure 230. Error of crossflow profile. *1: 5x2x2m, 2: 2.5x2x2m, 3: 1x2x2m, 4: 0.5x2x2m, 5: 0.25x2x2m, 6: 0.1x2x2m*

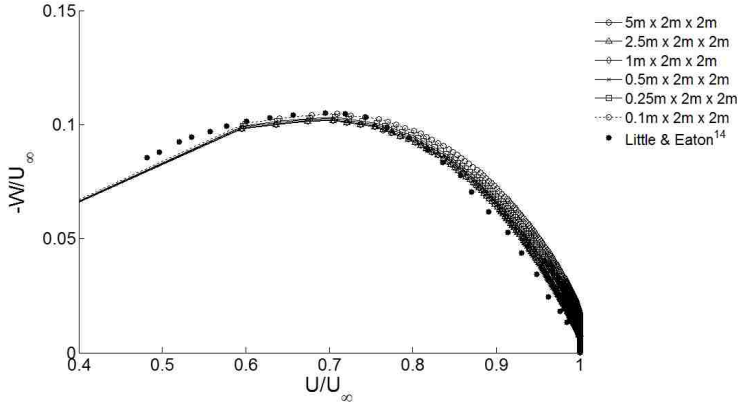

Figure 231. Polar plot of mean velocity profiles. *Comparison plot of the High-Reynolds Number Spalart-Allmaras turbulence model for grids with varying computational domain sizes in the axial direction.*

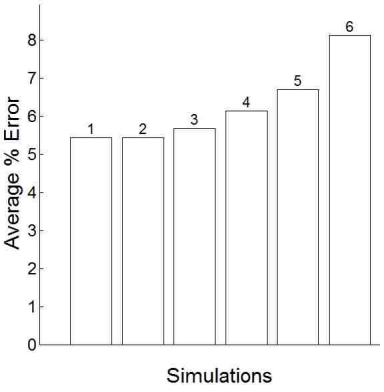

Figure 232. Error of polar mean velocity profiles. *1: 5x2x2m, 2: 2.5x2x2m, 3: 1x2x2m, 4: 0.5x2x2m, 5: 0.25x2x2m, 6: 0.1x2x2m*

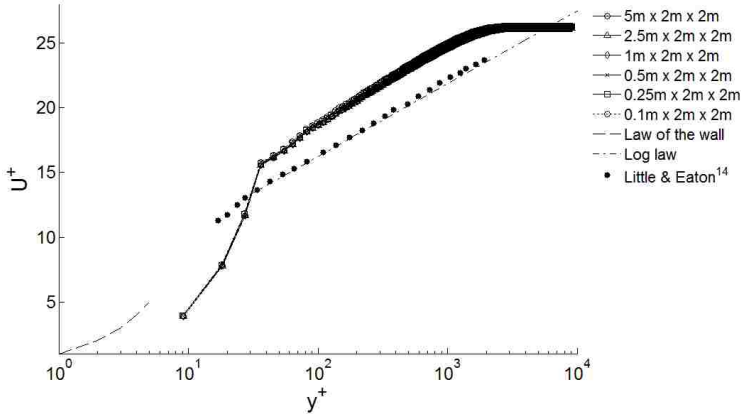

Figure 233. Tangential velocity in rotating reference frame. *Comparison plot of the High-Reynolds Number Spalart-Allmaras turbulence model for grids with varying computational domain sizes in the axial direction.*

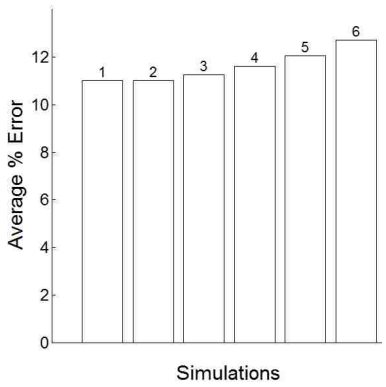

Figure 234. Error of tangential velocity. *1: 5x2x2m, 2: 2.5x2x2m, 3: 1x2x2m, 4: 0.5x2x2m, 5: 0.25x2x2m, 6: 0.1x2x2m*

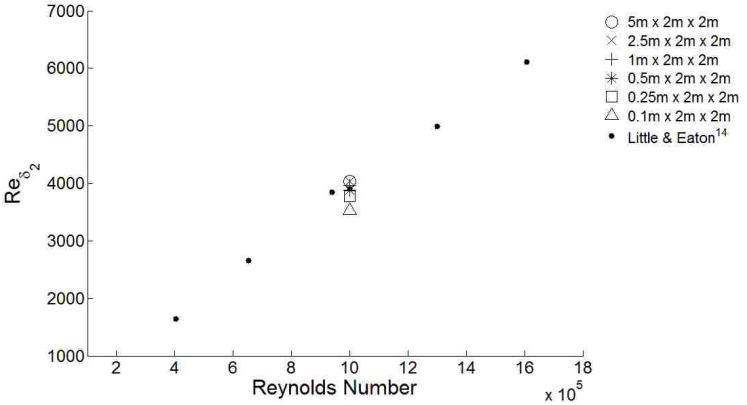

Figure 235. Comparison of momentum thickness Reynolds number. *Comparison plot of the High-Reynolds Number Spalart-Allmaras turbulence model for grids with varying computational domain sizes in the axial direction.*

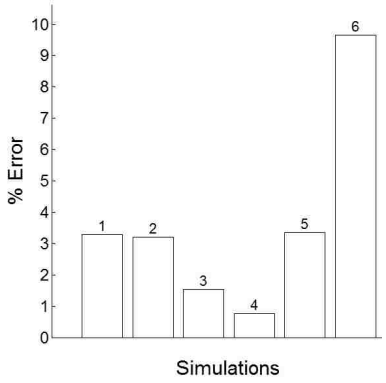

Figure 236. Error of momentum thickness Reynolds number. *1: 5x2x2m, 2: 2.5x2x2m, 3: 1x2x2m, 4: 0.5x2x2m, 5: 0.25x2x2m, 6: 0.1x2x2m*

5. Reynolds Stress Transport model

Step 1:

The grids used for the y^+ sensitivity study had the following properties:

Computational domain size of 1x5x5 meters (axial x radial x tangential)

Stretch ratio of 1.2 in the axial direction

Uniform radial and tangential resolution of 508x508 nodes

Grids with the following initial cell's centroid y^+ values were included in this sensitivity study:

y^+ = 5 (42 x 508 x 508 nodes)

y^+ = 10 (39 x 508 x 508 nodes)

y^+ = 20 (36 x 508 x 508 nodes)

y^+ = 30 (33 x 508 x 508 nodes)

y^+ = 40 (32 x 508 x 508 nodes)

y^+ = 50 (31 x 508 x 508 nodes)

y^+ = 75 (28 x 508 x 508 nodes)

y^+ = 100 (27 x 508 x 508 nodes)

y^+ = 200 (23 x 508 x 508 nodes)

The turbulent mean flow vector magnitude in the rotating reference frame is shown in Fig. 237. The distance above the disk's surface is normalized by the momentum thickness boundary layer, δ_2. All of the y^+ values agree very well except near the disk's surface. As in the previous cases, this disagreement is due to the refinement differences near the wall. Figure 238 shows the errors of the simulation results. The larger errors of the simulations with high y^+ values are mostly due to the data near the disk's surface.

The crossflow profile (Figs. 239 and 240) demonstrates a high sensitivity to different y^+ values near the disk's surface. The y^+ = 20, 30, 40, 50, 75 and 100 simulation profiles agree very well past the near wall discrepancies. The simulations with y^+ = 5 and 10 produce results that overshoot the amount of crossflow near the disk's surface while the simulation with the y^+ = 200 value gives a profile that undershoots the amount of crossflow near the disk surface.

Figure 241 is the polar plot of the mean velocity profiles. The results obtained from the y^+ = 20, 30, 40, and 50 simulations are in close agreement (see also Fig. 242). This plot demonstrates the inadequacy of the High y^+ Wall Treatment near the disks surface. The y^+ = 200 simulation's initial cell is so large that the data smoothing over the cell accounts for the data in the approximate range $0 \leq U/U_\infty \leq 0.8$. This is why the high y^+ simulation profiles fall off the experimental data[14] trend so abruptly. This same data fall off is visible down to the resolution of $y^+ = 10$.

Figure 243 is a semi-logarithmic plot of U^+ vs. y^+. All of the simulation profiles are very similar far from the disk's surface and follow the log law and experimental data[14] very closely with the exception of the y^+ = 5 and 10 simulations' profiles, which show disagreement with the experimental data[14] throughout the computational domain. The errors of the simulation profiles obtained with y^+ = 20, 30, 40 and 50 are very similar (Fig. 244).

Figures 245 and 246 show the momentum thickness Reynolds number and the error for each simulation compared to the Little and Eaton[14] experiment conducted at $Re = 10^6$. The momentum thickness Reynolds number of the y^+ = 200 simulation deviates the most from other data.

Figure 247 plots the normalized turbulent kinetic energy. Again the results of simulations with y^+ = 20, 30, 40 and 50 are in close agreement with one another. Other results vary from this group. Figure 248 shows the average errors for each simulation with respect to the experimental data[14].

The Reynolds stresses and the average errors in their computing are plotted in Figs. 249-254. As one can see, the simulation profiles of y^+ = 20, 30, 40 and 50 again are in close agreement with one another.

Based on the results of the y^+ sensitivity study of the Reynolds Stress Transport Model with the High y^+ Wall Treatment, the grids with y^+ = 20, 30, 40 and 50 all resulted in data that agreed with one another very well. The only significant difference between these simulations was observed near the wall.

Star-CCM+[8] recommends to use y^+ = 30 for simulations with the High y^+ Wall Treatment. The overall close agreement of the results of the simulation with y^+ = 30 with experimental data[14] as also observed in the current study. Therefore, it was chosen as the y^+ value for the grids in the next sensitivity study of this turbulence model.

Computational expenses of the simulations with this model were the largest: the computational time of the y^+ = 30 grid's simulation was 9 hours 42 minutes. This computation was done on 4 nodes of the Nano Linux cluster, with 1500 iterations.

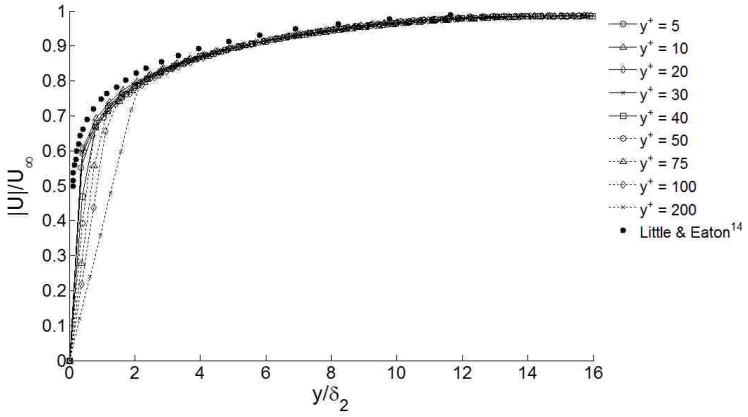

Figure 237. Turbulent mean flow vector magnitude in the rotating reference frame. *Comparison plot of the Reynolds Stress Transport Model for grids with varying y^+ wall cell centroid values.*

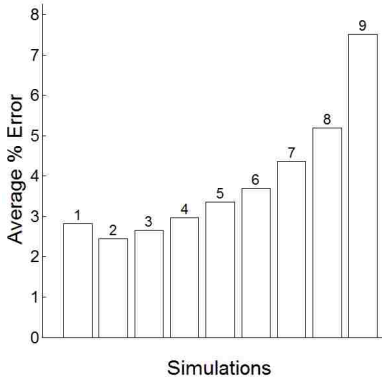

Figure 238. Error of turbulent mean flow vector magnitude. *1: y^+=5, 2: y^+=10, 3: y^+=20, 4: y^+=30, 5: y^+=40, 6: y^+=50, 7: y^+=75, 8: y^+=100, 9: y^+=200*

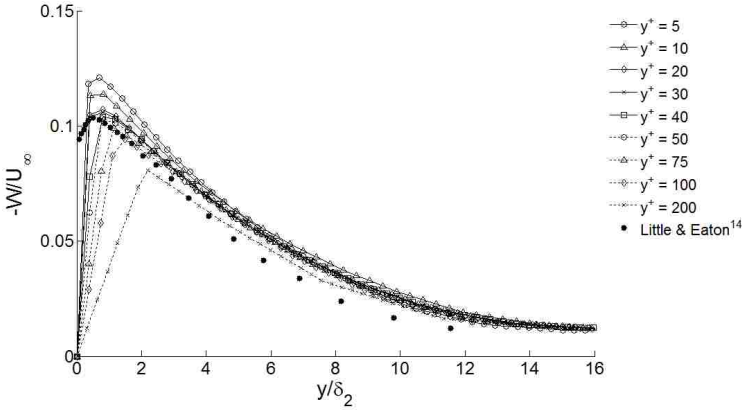

Figure 239. Crossflow profile. *Comparison plot of the Reynolds Stress Transport Model for grids with varying y^+ wall cell centroid values.*

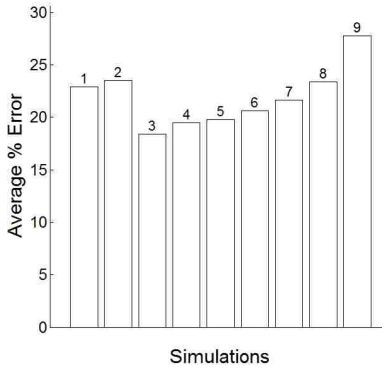

Figure 240. Error of crossflow profile. *1: y^+=5, 2: y^+=10, 3: y^+=20, 4: y^+=30, 5: y^+=40, 6: y^+=50, 7: y^+=75, 8: y^+=100, 9: y^+=200*

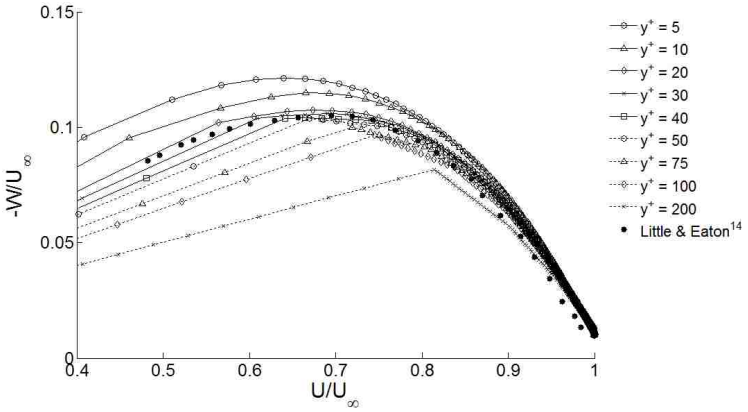

Figure 241. Polar plot of mean velocity profiles. *Comparison plot of the Reynolds Stress Transport Model for grids with varying y^+ wall cell centroid values.*

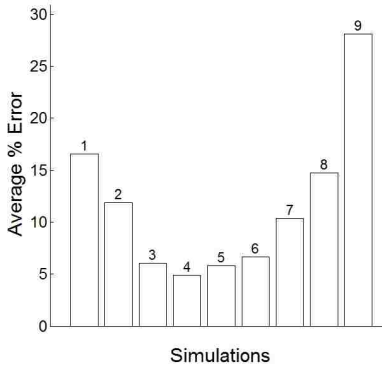

Figure 242. Error of polar mean velocity profiles. *1: y^+=5, 2: y^+=10, 3: y^+=20, 4: y^+=30, 5: y^+=40, 6: y^+=50, 7: y^+=75, 8: y^+=100, 9: y^+=200*

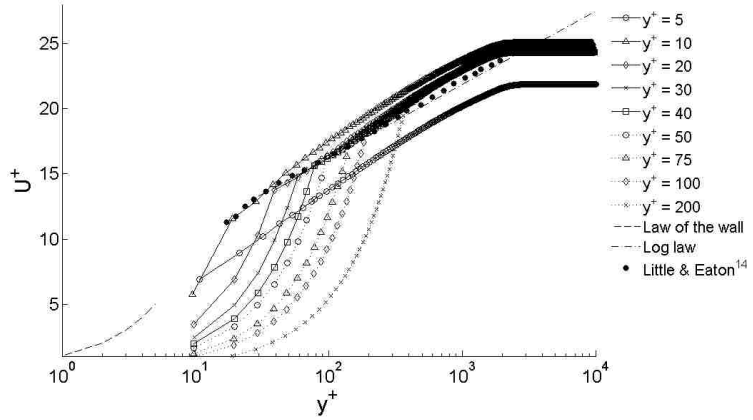

Figure 243. Tangential velocity in rotating reference frame. *Comparison plot of the Reynolds Stress Transport Model for grids with varying y^+ wall cell centroid values.*

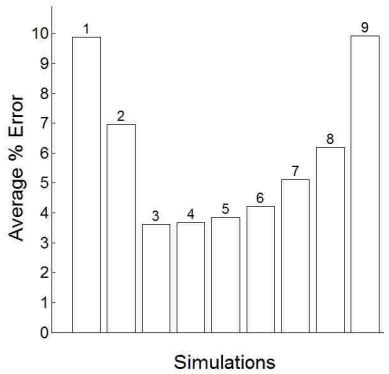

Figure 244. Error of tangential velocity. *1: y^+=5, 2: y^+=10, 3: y^+=20, 4: y^+=30, 5: y^+=40, 6: y^+=50, 7: y^+=75, 8: y^+=100, 9: y^+=200*

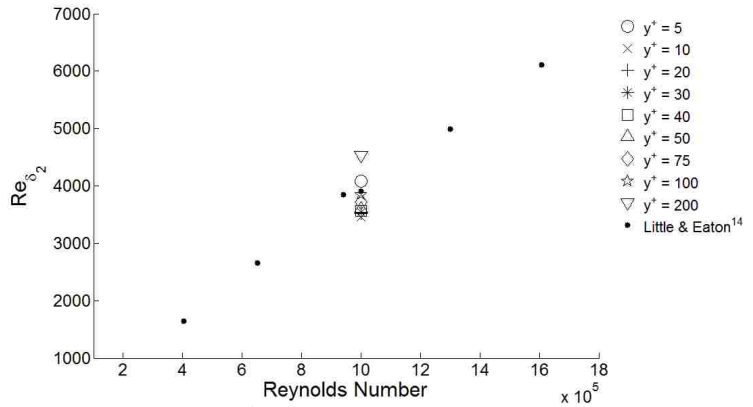

Figure 245. Comparison of momentum thickness Reynolds number. *Comparison plot of the Reynolds Stress Transport Model for grids with varying y^+ wall cell centroid values.*

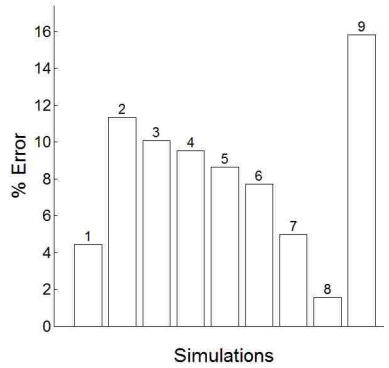

Figure 246. Error of momentum thickness Reynolds number. *1: y^+=5, 2: y^+=10, 3: y^+=20, 4: y^+=30, 5: y^+=40, 6: y^+=50, 7: y^+=75, 8: y^+=100, 9: y^+=200*

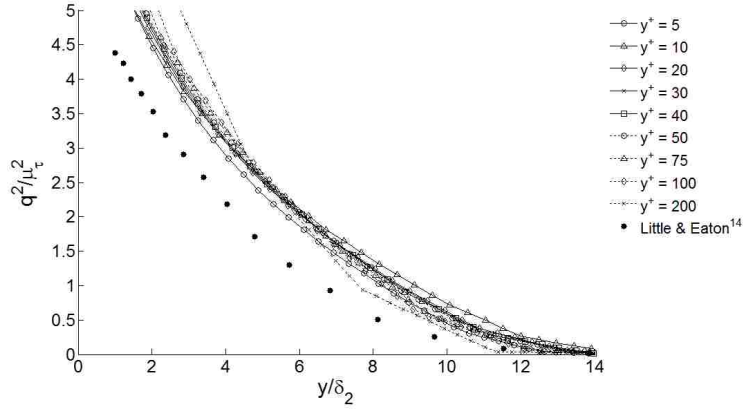

Figure 247. Twice the turbulence kinetic energy. *Comparison plot of the Reynolds Stress Transport Model for grids with varying y^+ wall cell centroid values.*

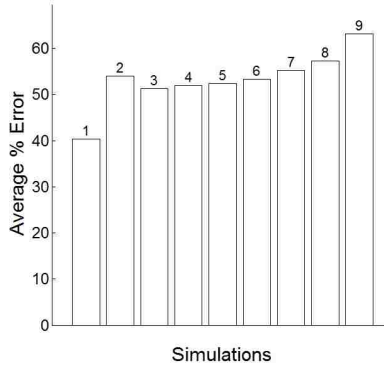

Figure 248. Error of twice the turbulence kinetic energy. *1: y^+=5, 2: y^+=10, 3: y^+=20, 4: y^+=30, 5: y^+=40, 6: y^+=50, 7: y^+=75, 8: y^+=100, 9: y^+=200*

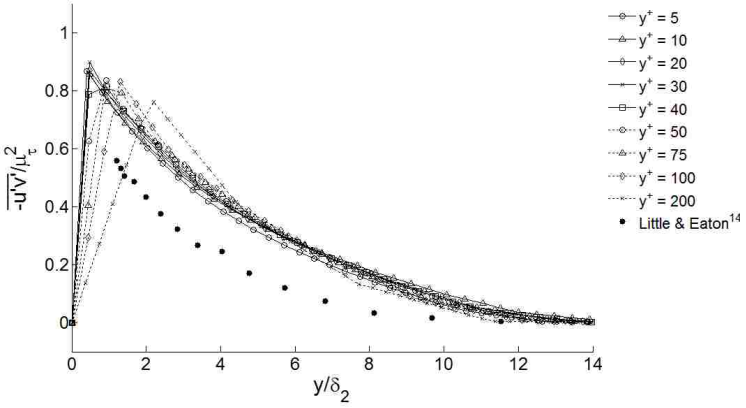

Figure 249. Normalized Reynolds stress, $-\overline{u'v'}$. *Comparison plot of the Reynolds Stress Transport Model for grids with varying y^+ wall cell centroid values.*

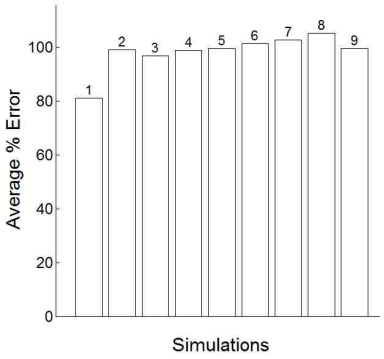

Figure 250. Error of normalized Reynolds stress, $-\boldsymbol{u'v'}$.
1: y^+=5, 2: y^+=10, 3: y^+=20, 4: y^+=30, 5: y^+=40, 6: y^+=50, 7: y^+=75, 8: y^+=100, 9: y^+=200

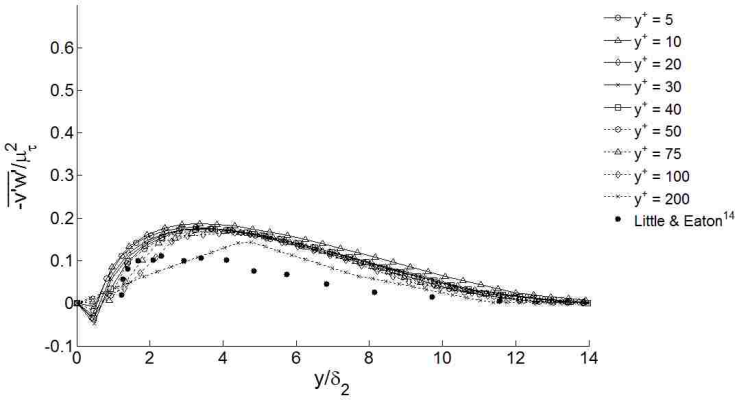

Figure 251. Normalized Reynolds stress, $-\overline{v'w'}$. *Comparison plot of the Reynolds Stress Transport Model for grids with varying y^+ wall cell centroid values.*

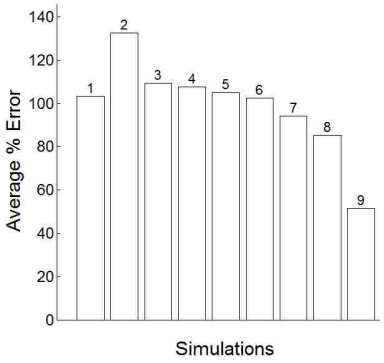

Figure 252. Error of normalized Reynolds stress, $-\boldsymbol{v'w'}$.
1: y^+=5, 2: y^+=10, 3: y^+=20, 4: y^+=30, 5: y^+=40, 6: y^+=50, 7: y^+=75, 8: y^+=100, 9: y^+=200

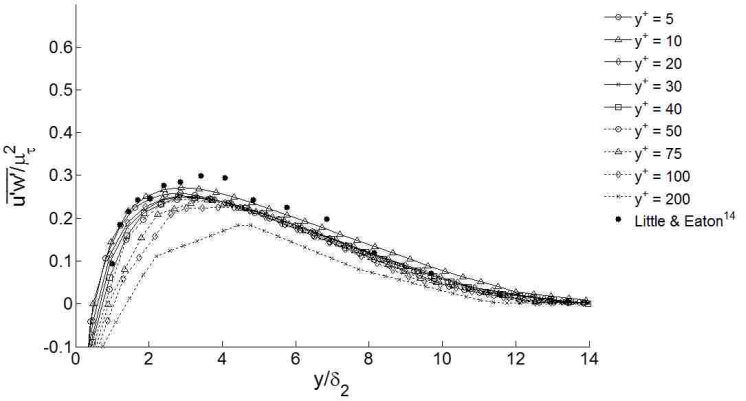

Figure 253. Normalized Reynolds stress, $\overline{u'w'}$. *Comparison plot of the Reynolds Stress Transport Model for grids with varying y^+ wall cell centroid values.*

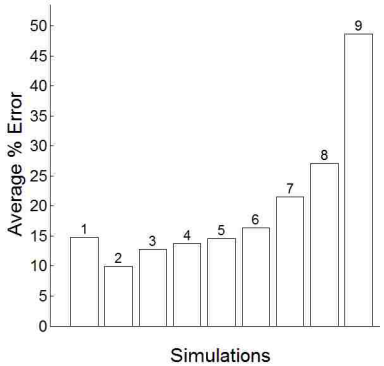

Figure 254. Error of normalized Reynolds stress, $\boldsymbol{u'w'}$.
1: y^+=5, 2: y^+=10, 3: y^+=20, 4: y^+=30, 5: y^+=40, 6: y^+=50, 7: y^+=75, 8: y^+=100, 9: y^+=200

Step 2:

The grids used for the radial and tangential grid resolution sensitivity study had the following properties:

Wall cell's centroid located at $y^+ = 30$

Computational domain size of 1x5x5 meters (axial x radial x tangential)

Stretch ratio of 1.2 in the axial direction

The following grid nodal resolutions were used in this sensitivity study (axial x radial x tangential):

33 x 508 x 508 (uniform radial and tangential grid spacing of $\approx 0.01\ m$)

33 x 254 x 254 (uniform radial and tangential grid spacing of $\approx 0.02\ m$)

33 x 127 x 127 (uniform radial and tangential grid spacing of $\approx 0.04\ m$)

33 x 64 x 64 (uniform radial and tangential grid spacing of $\approx 0.08\ m$)

33 x 32 x 32 (uniform radial and tangential grid spacing of $\approx 0.16\ m$)

In an effort to determine the Reynolds Stress Transport Model's sensitivity to grid refinement in the radial and tangential direction, the grid was coarsened. The grid's radial and tangential grid spacing is doubled in each coarser grid. This results in each grid having four times fewer cells in the domain than the previous grid, which drastically reduces the computational time for each simulation. The simulation with the coarsest grid that can reproduce the simulation profiles of the finer grids is sought after.

The turbulent mean flow vector magnitude in the rotating reference frame is shown in Fig. 255. The distance above the disk's surface is normalized by the momentum thickness boundary layer, δ_2. Figure 251 shows close agreement between the simulation results on all grids. Figure 256 shows the average errors of the simulation results. All of the simulation errors are extremely similar.

All of the simulation results of the crossflow profile (Figs. 257 and 258) and the polar plot of mean velocity profiles (Figs. 259 and 260) are in close agreement with one another.

The tangential velocity in the rotating reference frame (Figs. 261 and 262), the momentum thickness Reynolds number (Figs. 263 and 264) and the turbulent kinetic energy (Figs. 265 and

266) all demonstrate sensitivity to the grid resolution of different simulations. The simulation profile of the 33x32x32 grid is in disagreement with all other simulation profiles.

The Reynolds stresses are plotted in Figs. 267, 269 and 271. Again, the 33x32x32 grid simulation profile differs from the profiles of the other simulations. The average errors of these profiles are given in Figs. 268, 270 and 272 respectively.

Based on these results, the Reynolds Stress Transport Model with the High Wall Treatment can be as coarse as 33x64x64 in a 1x5x5 meter domain. This equates to an initial wall cell aspect ratio of 66:1. The grid of $y^+ = 30$ and radial and tangential resolution of 64x64 nodes will be held constant as the sensitivity of the cell stretch ratio in the axial direction is studied in Step 3.

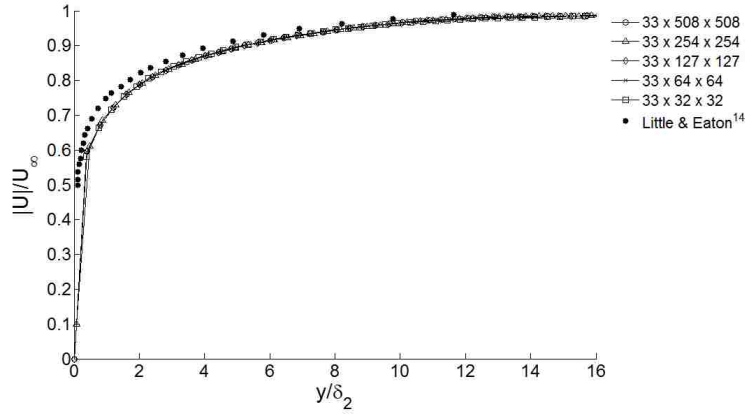

Figure 255. Turbulent mean flow vector magnitude in the rotating reference frame. *Comparison plot of the Reynolds Stress Transport Model for grids with varying grid resolutions in the radial and tangential directions.*

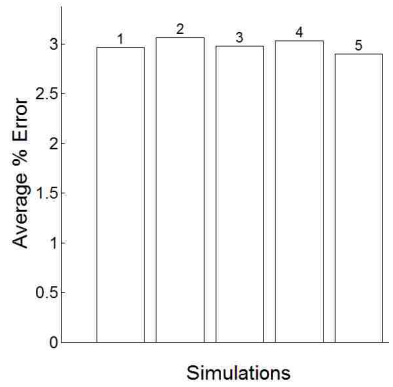

Figure 256. Error of turbulent mean flow vector magnitude. *1: 33x508x508, 2: 33x254x254, 3: 33x127x127, 4: 33x64x64, 5: 33x32x32*

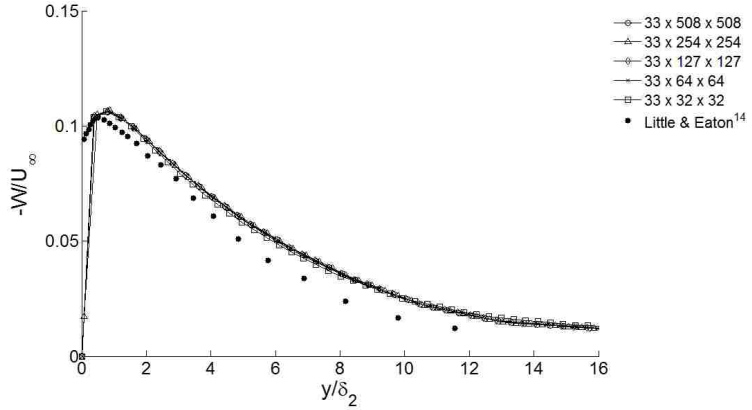

Figure 257. Crossflow profile. *Comparison plot of the Reynolds Stress Transport Model for grids with varying grid resolutions in the radial and tangential directions.*

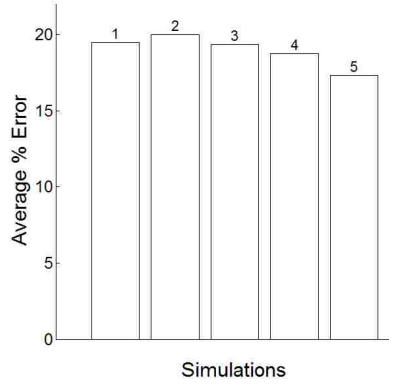

Figure 258. Error of crossflow profile. *1: 33x508x508, 2: 33x254x254, 3: 33x127x127, 4: 33x64x64, 5: 33x32x32*

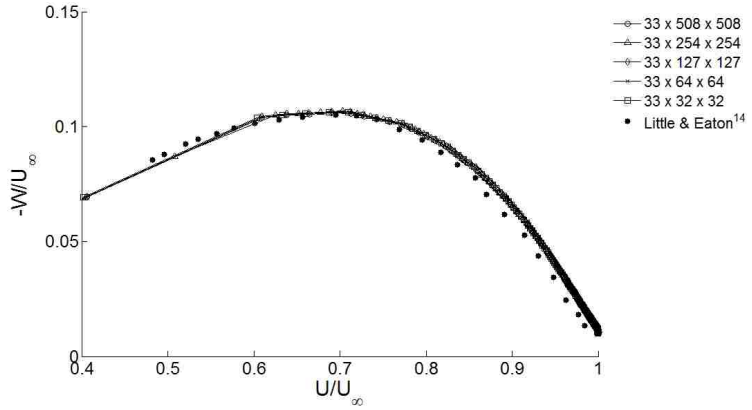

Figure 259. Polar plot of mean velocity profiles. *Comparison plot of the Reynolds Stress Transport Model for grids with varying grid resolutions in the radial and tangential directions.*

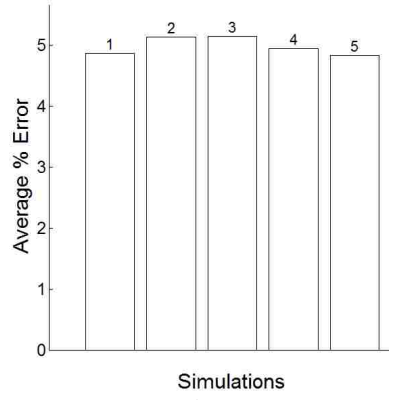

Figure 260. Error of polar mean velocity profiles. *1: 33x508x508, 2: 33x254x254, 3: 33x127x127, 4: 33x64x64, 5: 33x32x32*

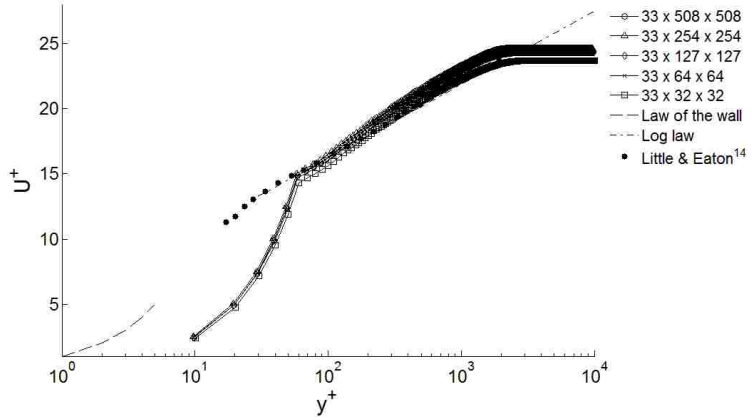

Figure 261. Tangential velocity in rotating reference frame. *Comparison plot of the Reynolds Stress Transport Model for grids with varying grid resolutions in the radial and tangential directions.*

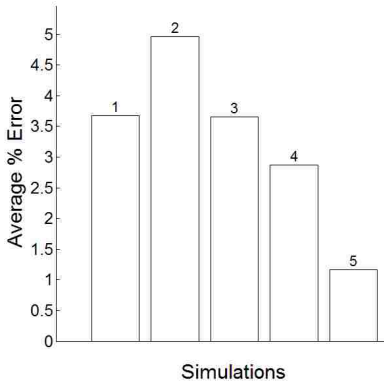

Figure 262. Error of tangential velocity. *1: 33x508x508, 2: 33x254x254, 3: 33x127x127, 4: 33x64x64, 5: 33x32x32*

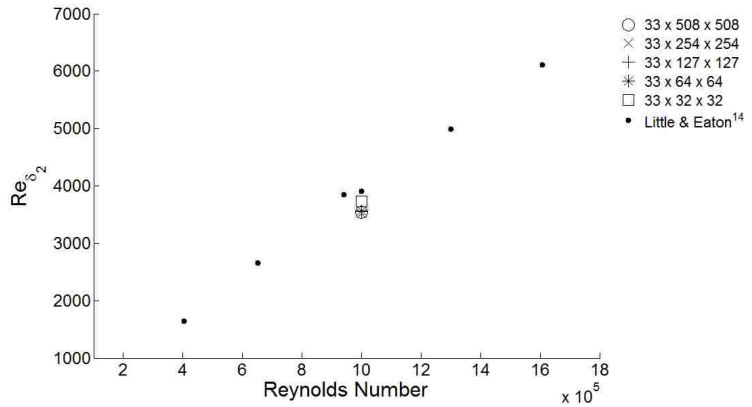

Figure 263. Comparison of momentum thickness Reynolds number. *Comparison plot of the Reynolds Stress Transport Model for grids with varying grid resolutions in the radial and tangential directions.*

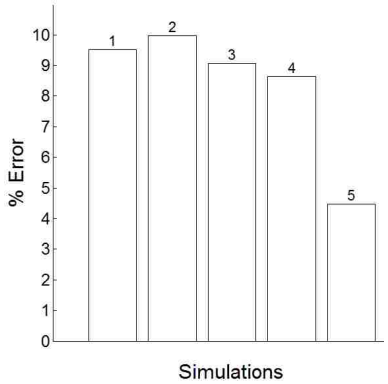

Figure 264. Error of momentum thickness Reynolds number. *1: 33x508x508, 2: 33x254x254, 3: 33x127x127, 4: 33x64x64, 5: 33x32x32*

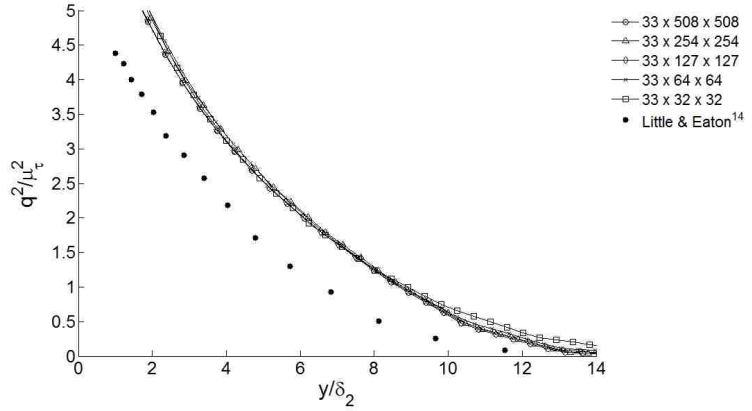

Figure 265. Twice the turbulence kinetic energy. *Comparison plot of the Reynolds Stress Transport Model for grids with varying grid resolutions in the radial and tangential directions.*

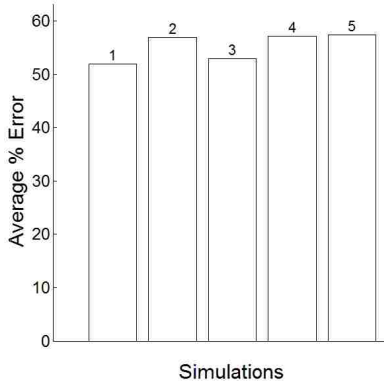

Figure 266. Error of twice the turbulence kinetic energy. *1: 33x508x508, 2: 33x254x254, 3: 33x127x127, 4: 33x64x64, 5: 33x32x32*

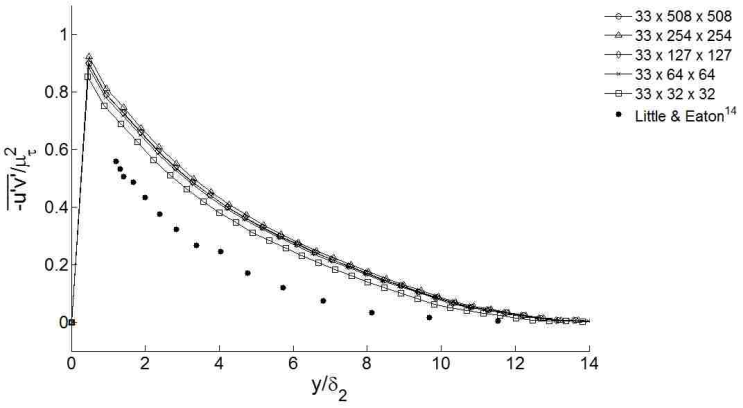

Figure 267. Normalized Reynolds stress, $-\overline{u'v'}$. *Comparison plot of the Reynolds Stress Transport Model for grids with varying y^+ wall cell centroid values.*

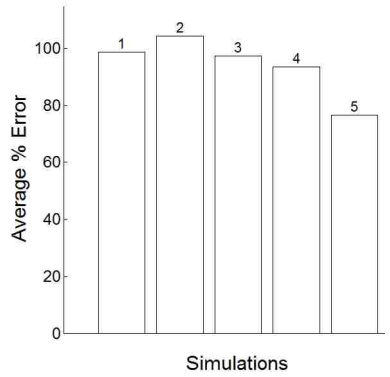

Figure 268. Error of normalized Reynolds stress, $-u'v'$.
1: 33x508x508, 2: 33x254x254, 3: 33x127x127, 4: 33x64x64, 5: 33x32x32

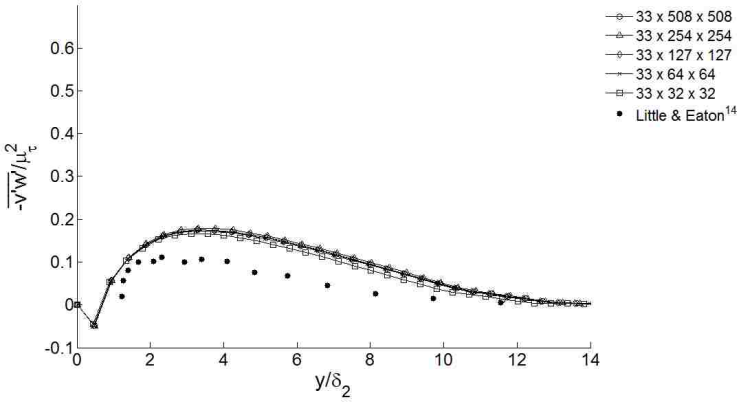

Figure 269. Normalized Reynolds stress, $-\overline{v'w'}$. *Comparison plot of the Reynolds Stress Transport Model for grids with varying y^+ wall cell centroid values.*

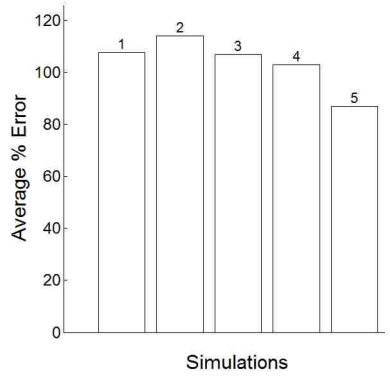

Figure 270. Error of normalized Reynolds stress, $-v'w'$.
1: 33x508x508, 2: 33x254x254, 3: 33x127x127, 4: 33x64x64, 5: 33x32x32

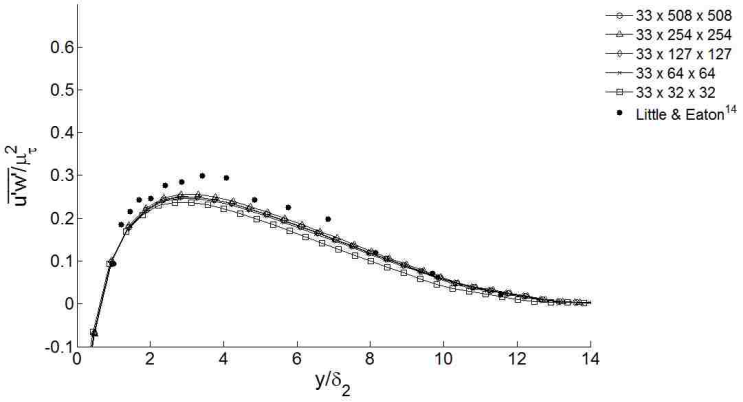

Figure 271. Normalized Reynolds stress, $\overline{u'w'}$. *Comparison plot of the Reynolds Stress Transport Model for grids with varying y^+ wall cell centroid values.*

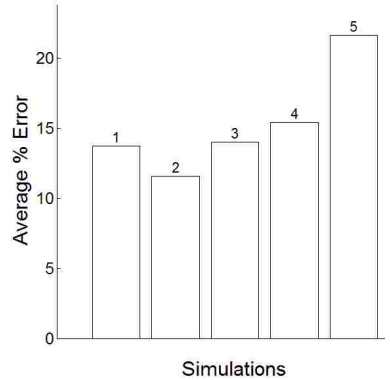

Figure 272. Error of normalized Reynolds stress, $u'w'$.
1: 33x508x508, 2: 33x254x254, 3: 33x127x127, 4: 33x64x64, 5: 33x32x32

Step 3:

The grids used in the axial direction stretch ratio sensitivity study had the following properties:

Wall cell's centroid located at $y^+ = 30$

Computational domain size of 1x5x5 meters (axial x radial x tangential)

Radial and tangential grid resolution of 64x64 nodes (uniform grid spacing of $\approx 0.08\ m$)

In Steps 1 and 2 the grids had a stretch ratio of 1.2. In this study the stretch ratio was changed in each simulation, thus each grid has a different number of nodes in the axial direction. The following stretch ratios were used in this sensitivity study:

1.1 (55 x 64 x 64 nodes)

1.2 (33 x 64 x 64 nodes)

1.3 (25 x 64 x 64 nodes)

1.5 (18 x 64 x 64 nodes)

2.0 (12 x 64 x 64 nodes)

The goal of this sensitivity study is to find the grid with the largest stretch ratio whose simulation profile does not differ significantly from the simulation profiles obtained on grids with smaller stretch ratios.

The turbulent mean flow vector magnitude (Fig. 273) shows close agreement among all simulation profiles, with slight variance observed in the 2.0 stretch ratio simulation profile. The error graph in Fig. 274 shows that the errors of the 1.1, 1.2 and 1.3 stretch ratio grid simulations results are nearly identical.

The crossflow profile (Fig. 275) of the 2.0 stretch ratio simulation disagrees with the other simulation profiles. Figure 276 helps to illustrate subtle differences between all the simulation results.

In the polar plot of the mean velocity profiles (Figs. 277 and 278) the 1.1, 1.2, 1.3 and 1.5 stretch ratio simulation profiles are in close agreement with one another.

The tangential velocity plot (Figs. 279 and 280) shows that all simulation profiles are in close agreement.

The momentum thickness Reynolds number varies in all the simulations, with the largest variances in the 1.5 and 2.0 stretch ratio simulation results, as seen in Fig. 281.

The turbulent kinetic energy (Figs. 283 and 284) shows a high sensitivity to varying axial stretch ratios. All of the simulations disagree with one another, with the largest discrepancies occurring in the 1.3, 1.5 and 2.0 stretch ratio simulation results.

The Reynolds stresses are plotted in Figs. 285, 287 and 289 (the average errors of the simulations are in Figs. 286, 288 and 290 respectively). The simulation profiles obtained on the grids with stretch ratios 2.0 and 1.5 deviate from those obtained on grids with smaller stretch ratios.

The results of the sensitivity study illustrate that the Reynolds Stress Transport Model with the High y^+ Wall Treatment loses a substantial amount of accuracy in its simulation results once the axial stretch ratio exceeds 1.3. The simulation profiles of the 1.1, 1.2 and 1.3 stretch ratio grids are in close agreement throughout most of the comparisons, but due to the better results obtained in the turbulent kinetic energy plot, the 1.2 stretch ratio was chosen for the future grids as this study proceeds to Step 4.

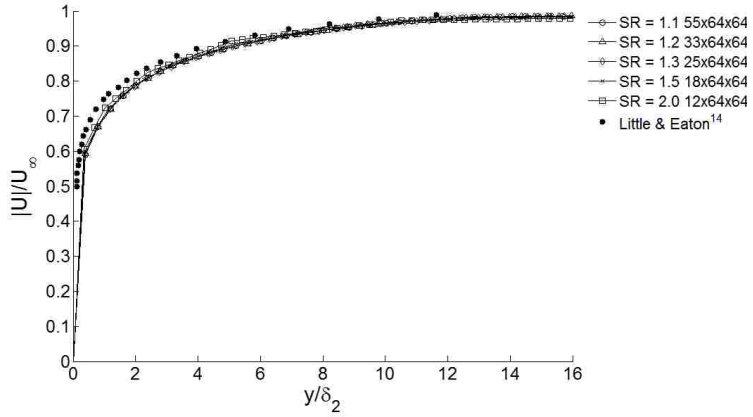

Figure 273. Turbulent mean flow vector magnitude in the rotating reference frame. *Comparison plot of the Reynolds Stress Transport Model for grids with varying cell stretch ratios in the axial direction.*

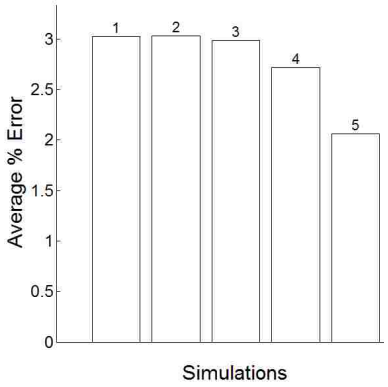

Figure 274. Error of turbulent mean flow vector magnitude. *1: SR=1.1, 2: SR=1.2, 3: SR=1.3, 4: SR=1.5, 5: SR=2.0*

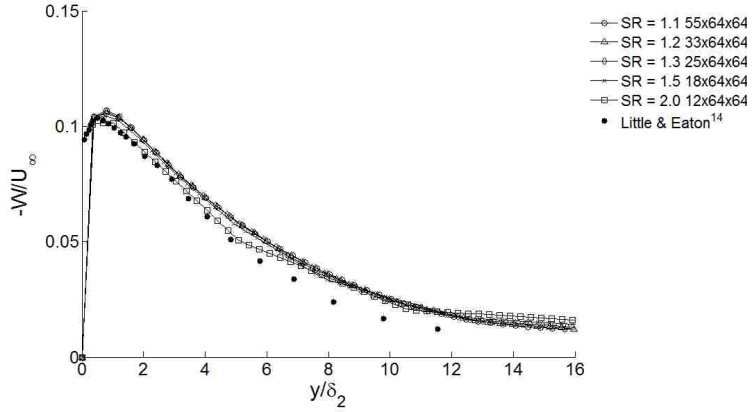

Figure 275. Crossflow profile. *Comparison plot of the Reynolds Stress Transport Model for grids with varying cell stretch ratios in the axial direction.*

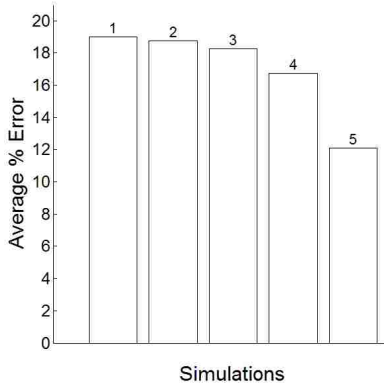

Figure 276. Error of crossflow profile. *1: SR=1.1, 2: SR=1.2, 3: SR=1.3, 4: SR=1.5, 5: SR=2.0*

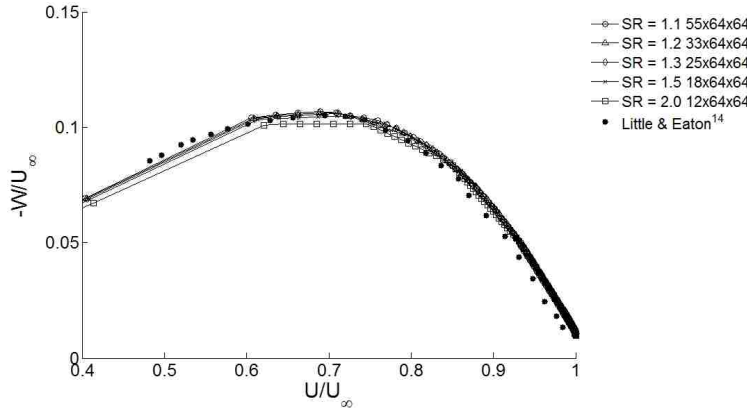

Figure 277. Polar plot of mean velocity profiles. *Comparison plot of the Reynolds Stress Transport Model for grids with varying cell stretch ratios in the axial direction.*

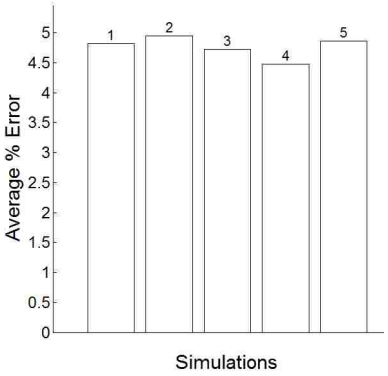

Figure 278. Error of polar mean velocity profiles. *1: SR=1.1, 2: SR=1.2, 3: SR=1.3, 4: SR=1.5, 5: SR=2.0*

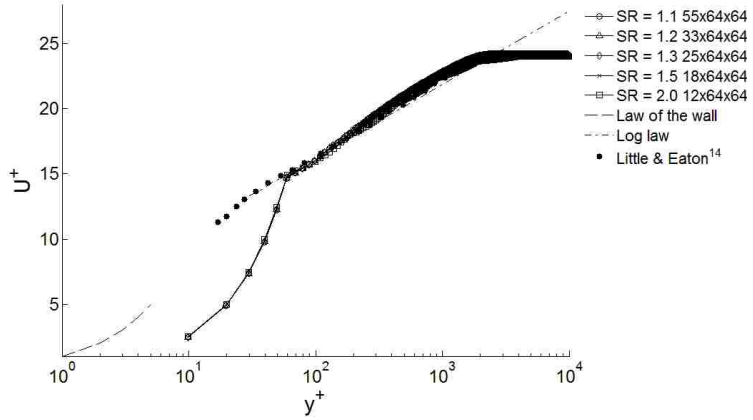

Figure 279. Tangential velocity in rotating reference frame. *Comparison plot of the Reynolds Stress Transport Model for grids with varying cell stretch ratios in the axial direction.*

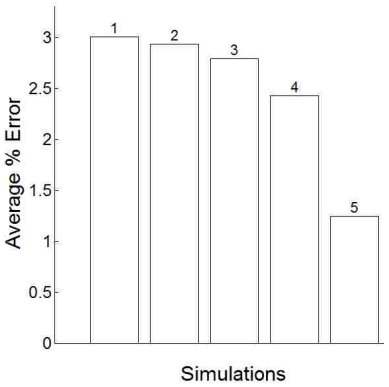

Figure 280. Error of tangential velocity. *1: SR=1.1, 2: SR=1.2, 3: SR=1.3, 4: SR=1.5, 5: SR=2.0*

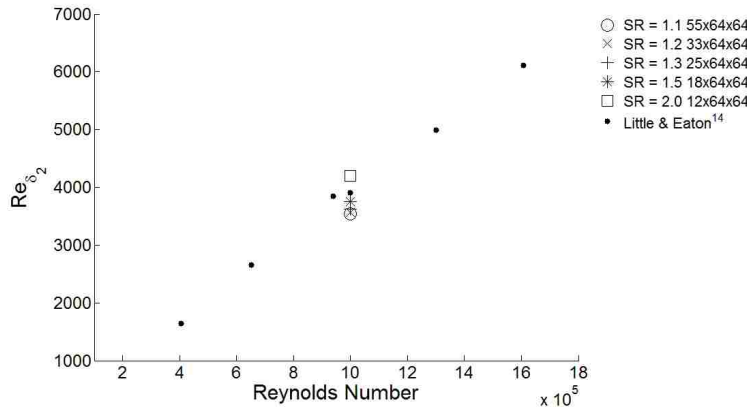

Figure 281. Comparison of momentum thickness Reynolds number. *Comparison plot of the Reynolds Stress Transport Model for grids with varying cell stretch ratios in the axial direction.*

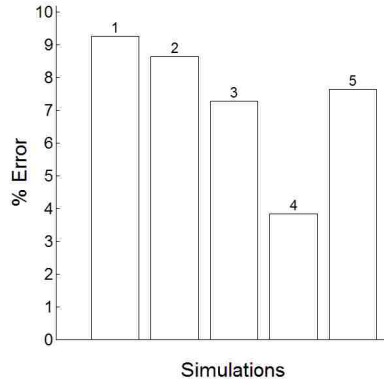

Figure 282. Error of momentum thickness Reynolds number. *1: SR=1.1, 2: SR=1.2, 3: SR=1.3, 4: SR=1.5, 5: SR=2.0*

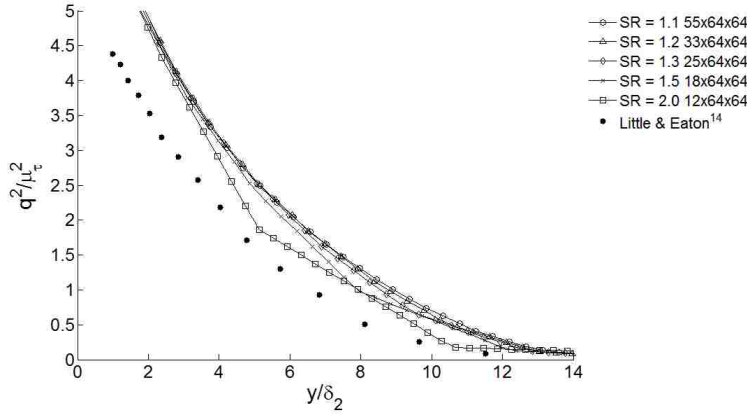

Figure 283. Twice the turbulence kinetic energy. *Comparison plot of the Reynolds Stress Transport Model for grids with varying cell stretch ratios in the axial direction.*

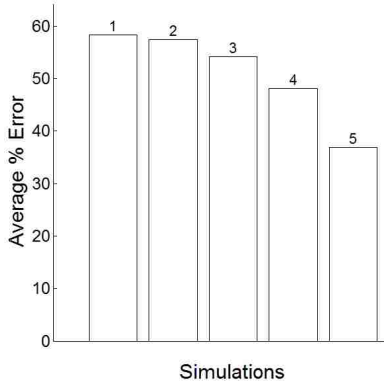

Figure 284. Error of twice the turbulence kinetic energy. *1: SR=1.1, 2: SR=1.2, 3: SR=1.3, 4: SR=1.5, 5: SR=2.0*

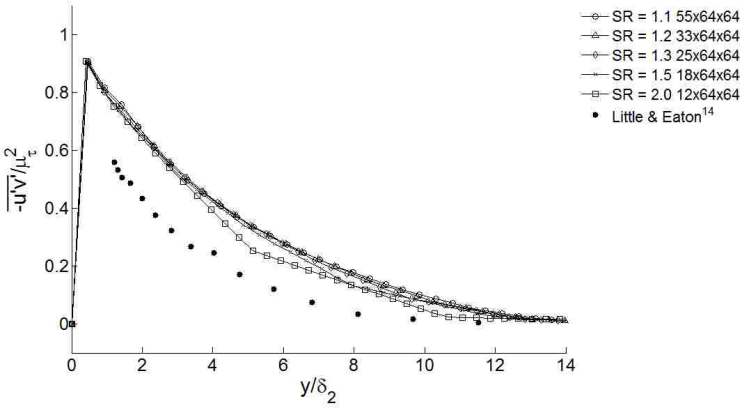

Figure 285. Normalized Reynolds stress, $-\overline{u'v'}$. *Comparison plot of the Reynolds Stress Transport Model for grids with varying y^+ wall cell centroid values.*

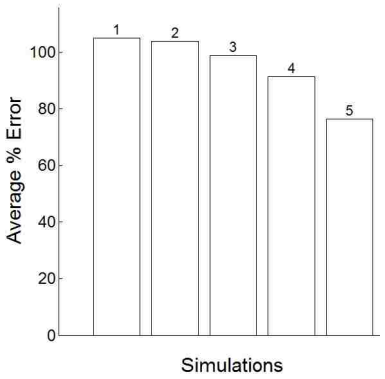

Figure 286. Error of normalized Reynolds stress, $-\boldsymbol{u'v'}$.
1: SR=1.1, 2: SR=1.2, 3: SR=1.3, 4: SR=1.5, 5: SR=2.0

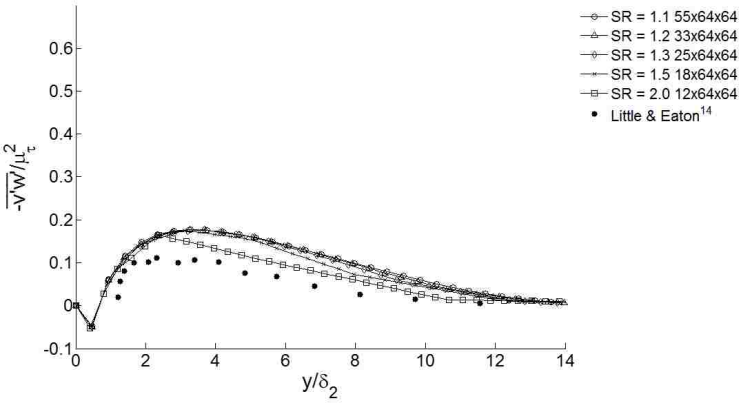

Figure 287. Normalized Reynolds stress, $-\overline{v'w'}$. *Comparison plot of the Reynolds Stress Transport Model for grids with varying y^+ wall cell centroid values.*

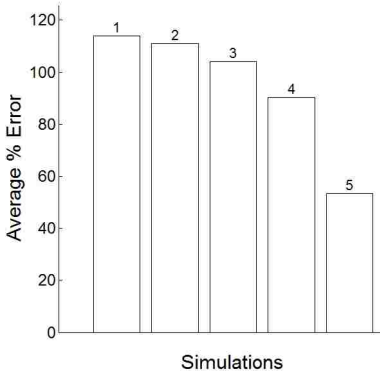

Figure 288. Error of normalized Reynolds stress, $-\boldsymbol{v'w'}$.
1: SR=1.1, 2: SR=1.2, 3: SR=1.3, 4: SR=1.5, 5: SR=2.0

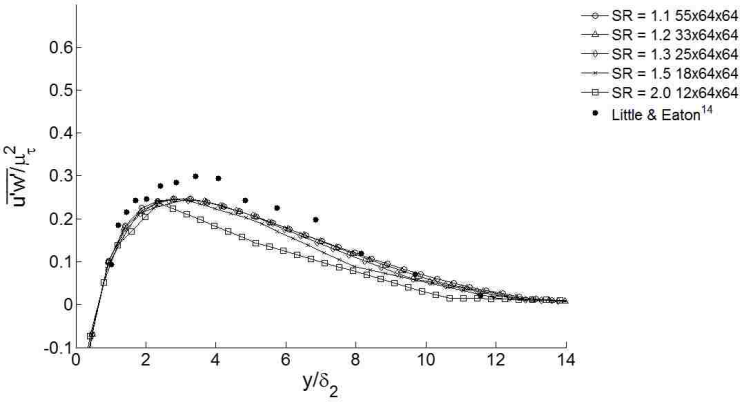

Figure 289. Normalized Reynolds stress, $\overline{u'w'}$. *Comparison plot of the Reynolds Stress Transport Model for grids with varying y^+ wall cell centroid values.*

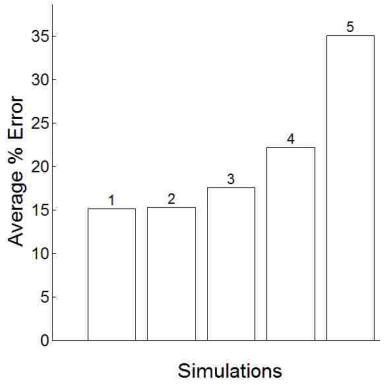

Figure 290. Error of normalized Reynolds stress, $\boldsymbol{u'w'}$.
1: SR=1.1, 2: SR=1.2, 3: SR=1.3, 4: SR=1.5, 5: SR=2.0

Step 4:

The grids used for the radial and tangential wall proximity sensitivity study had the following properties:

Wall cell's centroid located at $y^+ = 30$

Uniform radial and tangential grid spacing of $\approx 0.08\ m$

Stretch ratio of 1.2 in the axial direction

Computational domain size of 1 meter in the axial direction

This sensitivity study will adjust the position of the pressure outlet boundaries. In the previous simulations the computational domain size was 1x5x5 meters in the axial, radial and tangential directions respectively. In Steps 1, 2 and 3 the distance between the line probe and the nearest pressure outlet was 2.079 meters. In this sensitivity study the computational domain was varied in the radial and tangential directions. The domain sizes in this study are:

1 x 10 x 10 meters, 33 x 128 x 128 nodes (axial, radial, tangential)

1 x 5 x 5 meters, 33 x 64 x 64 nodes

1 x 2 x 2 meters, 33 x 26 x 26 nodes

1 x 1 x 1 meters, 33 x 13 x 13 nodes

The goal of this sensitivity study is to find the smallest computational domain whose simulation profile does not vary significantly from the simulation profiles of the larger domains. The smallest computational domain puts the pressure outlets as close as 0.5 meters from the axis of rotation, which is only 0.079 meters from the data sampling locations. The largest domain puts the nearest pressure outlet 4.579 meters away from the data sampling locations.

Figures 291 and 292 show that there is negligible difference between all the profiles of the turbulent mean flow vector magnitude in the rotating reference frame. Only the smallest domain's simulation profile differs slightly far from the disk's surface.

The crossflow profile (Figs. 293 and 294) and the polar plot of the mean velocity profile (Figs. 295 and 296) illustrate sensitivity to the pressure outlets' location. The 1x1x1 meter computational domain simulation profile is unable to replicate the simulation profiles of the other domain sizes.

The tangential velocity in the rotating reference frame (Figs. 297 and 298) is nearly unaffected by the proximity of the pressure outlet. All of the simulation profiles are in close agreement.

In Figures 299 and 300 the momentum thickness Reynolds number and the average errors of the simulations are shown. The momentum thickness Reynolds number obtained in the 1x1x1 meter domain is slightly less than the other data.

The turbulent kinetic energy (Figs. 301 and 302) simulation profiles are in close agreement with one another.

The Reynolds stresses in Figs. 303, 305 and 307 show close agreement among all the simulation profiles with only slight differences in the 1x1x1 meter domain's profile. This difference is so small it is only easily seen in the error graphs (Figs. 304, 306 and 308).

It is clear from these data that the domain size can be 1x2x2 meters for these simulations with this turbulence model.

The last sensitivity study of the Reynolds Stress Transport model with the High y^+ Wall Treatment uses the radial and tangential domain size of 2x2 meters while the axial domain size is varied.

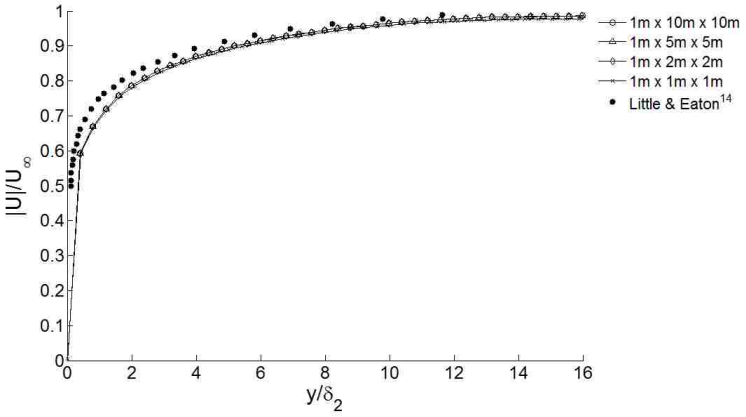

Figure 291. Turbulent mean flow vector magnitude in the rotating reference frame. *Comparison plot of the Reynolds Stress Transport Model for grids with varying computational domain sizes in the radial and tangential directions.*

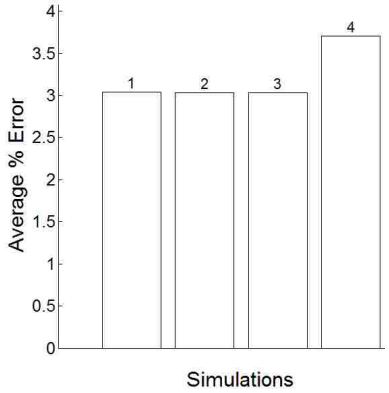

Figure 292. Error of turbulent mean flow vector magnitude. *1: 1x10x10m, 2: 1x5x5m, 3: 1x2x2m, 4: 1x1x1m*

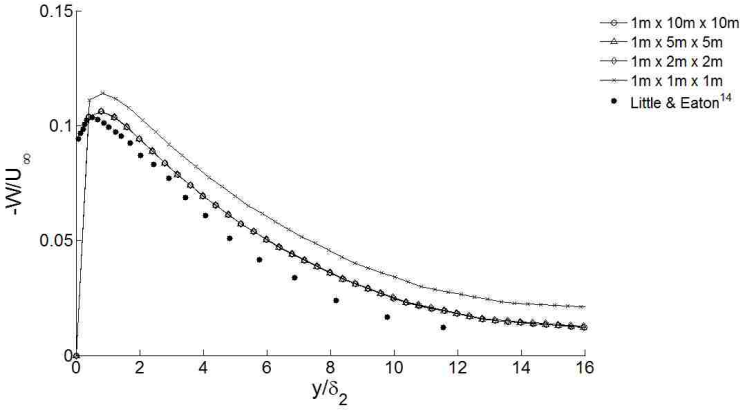

Figure 293. Crossflow profile. *Comparison plot of the Reynolds Stress Transport Model for grids with varying computational domain sizes in the radial and tangential directions.*

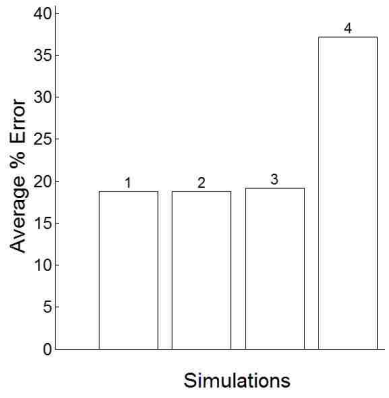

Figure 294. Error of crossflow profile. *1: 1x10x10m, 2: 1x5x5m, 3: 1x2x2m, 4: 1x1x1m*

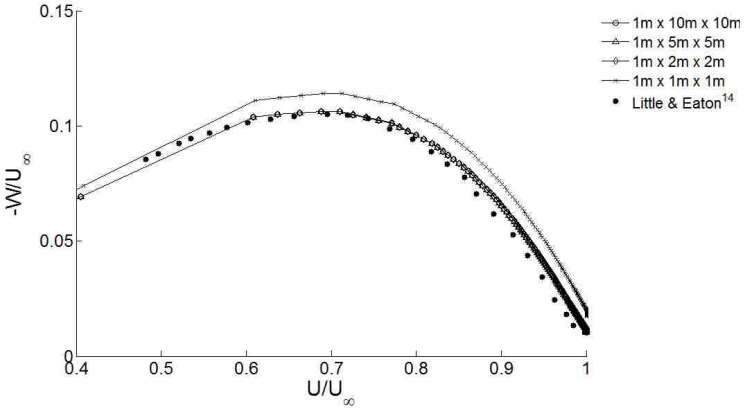

Figure 295. Polar plot of mean velocity profiles. *Comparison plot of the Reynolds Stress Transport Model for grids with varying computational domain sizes in the radial and tangential directions.*

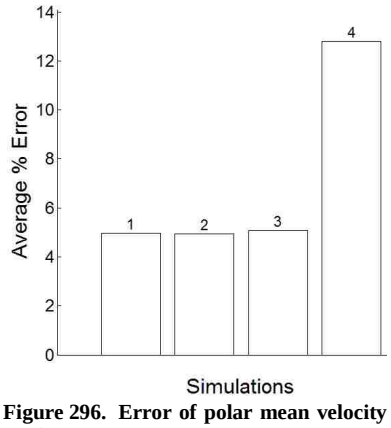

Figure 296. Error of polar mean velocity profiles. *1: 1x10x10m, 2: 1x5x5m, 3: 1x2x2m, 4: 1x1x1m*

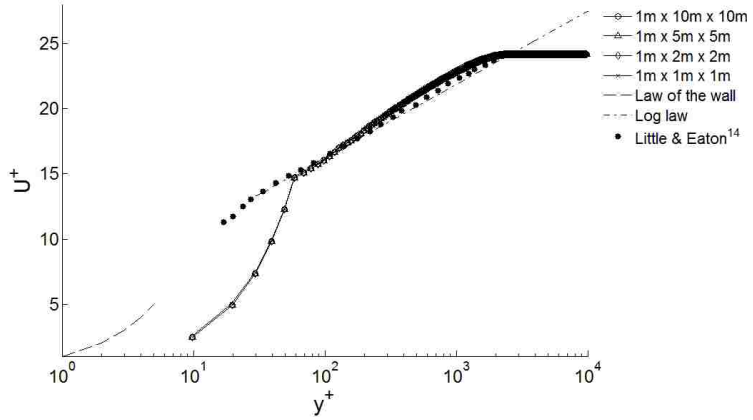

Figure 297. Tangential velocity in rotating reference frame. *Comparison plot of the Reynolds Stress Transport Model for grids with varying computational domain sizes in the radial and tangential directions.*

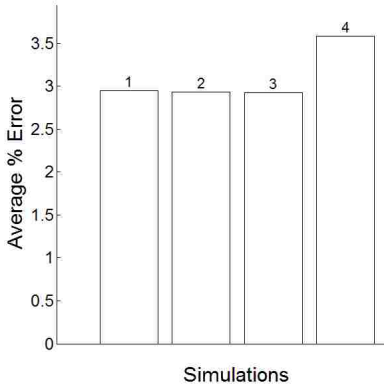

Figure 298. Error of tangential velocity. *1: 1x10x10m, 2: 1x5x5m, 3: 1x2x2m, 4: 1x1x1m*

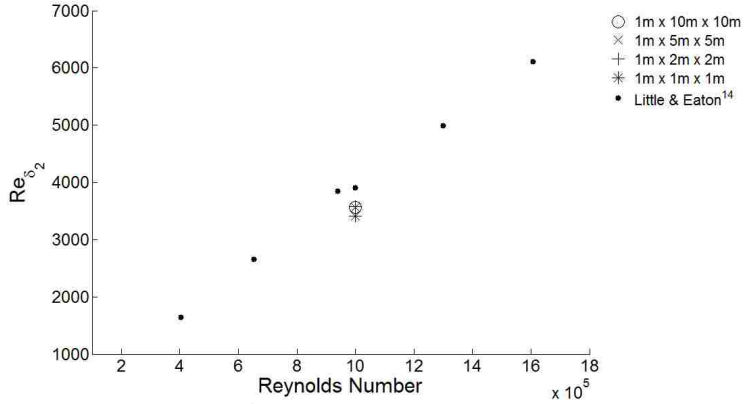

Figure 299. Comparison of momentum thickness Reynolds number. *Comparison plot of the Reynolds Stress Transport Model for grids with varying computational domain sizes in the radial and tangential directions.*

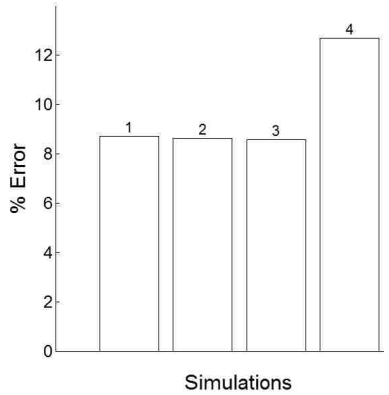

Figure 300. Error of momentum thickness Reynolds number. *1: 1x10x10m, 2: 1x5x5m, 3: 1x2x2m, 4: 1x1x1m*

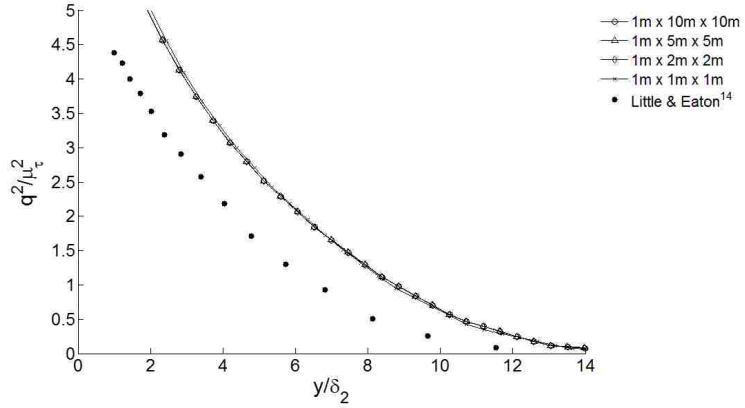

Figure 301. Twice the turbulence kinetic energy. *Comparison plot of the Reynolds Stress Transport Model for grids with varying computational domain sizes in the radial and tangential directions.*

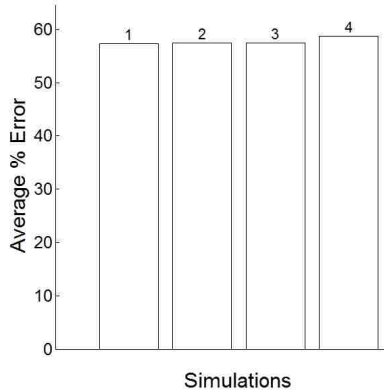

Figure 302. Error of twice the turbulence kinetic energy. *1: 1x10x10m, 2: 1x5x5m, 3: 1x2x2m, 4: 1x1x1m*

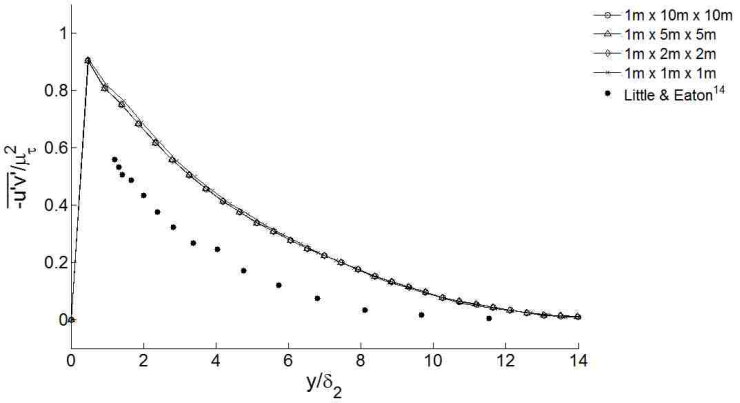

Figure 303. Normalized Reynolds stress, $-\overline{u'v'}$. *Comparison plot of the Reynolds Stress Transport Model for grids with varying y^+ wall cell centroid values.*

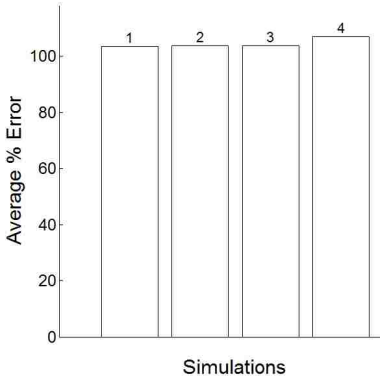

Figure 304. Error of normalized Reynolds stress, $-u'v'$.
1: 1x10x10m, 2: 1x5x5m, 3: 1x2x2m, 4: 1x1x1m

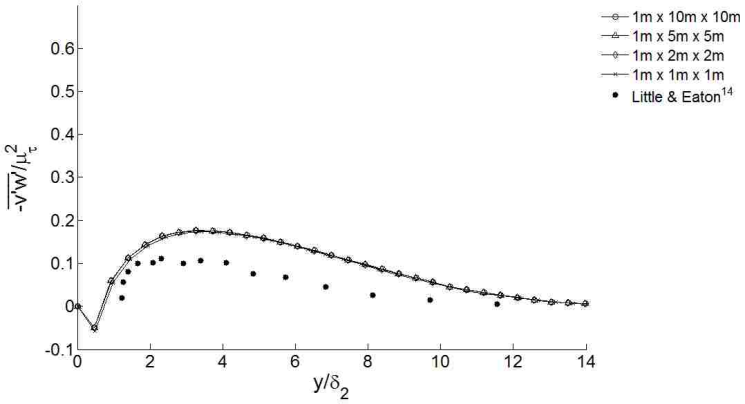

Figure 305. Normalized Reynolds stress, $-\overline{v'w'}$. *Comparison plot of the Reynolds Stress Transport Model for grids with varying y^+ wall cell centroid values.*

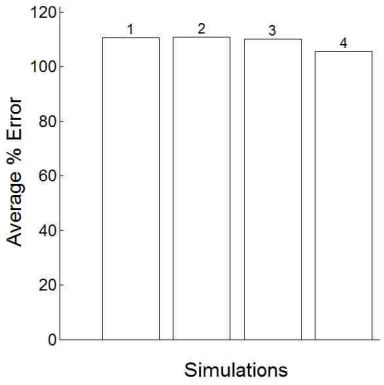

Figure 306. Error of normalized Reynolds stress, $-v'w'$.
1: 1x10x10m, 2: 1x5x5m, 3: 1x2x2m, 4: 1x1x1m

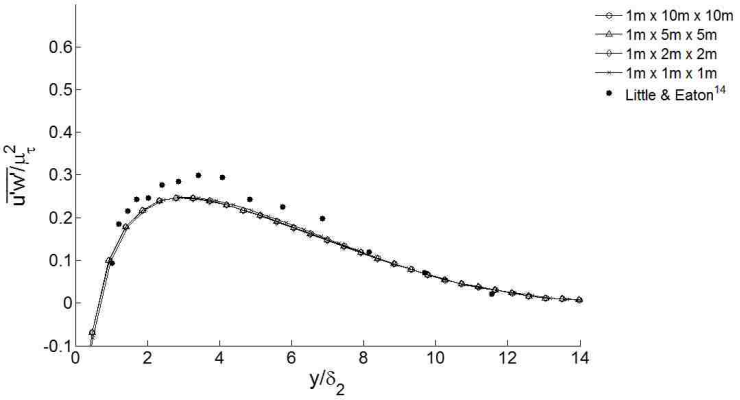

Figure 307. Normalized Reynolds stress, $\overline{u'w'}$. *Comparison plot of the Reynolds Stress Transport Model for grids with varying y^+ wall cell centroid values.*

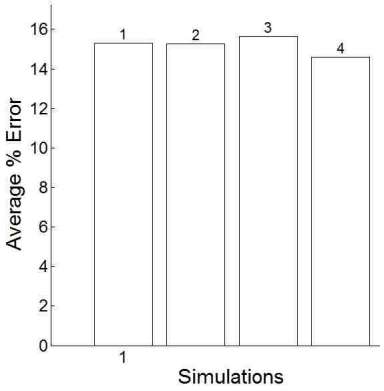

Figure 308. Error of normalized Reynolds stress, $u'w'$.
1: 1x10x10m, 2: 1x5x5m, 3: 1x2x2m, 4: 1x1x1m

Step 5:

The grids used in the axial wall proximity sensitivity study had the following properties:

Wall cell's centroid located at $y^+ = 30$

Computational domain size in the radial and tangential direction of 2x2 meters

Radial and tangential grid resolution of 26x26 nodes (uniform grid spacing of = 0.08 *m*)

Stretch ratio of 1.2 in the axial direction

This sensitivity study will adjust the position of the velocity inlet boundary above the disk's surface. Steps 1-4 positioned the velocity inlet 1 meter above the disk's surface and prescribed an inlet velocity of 1 *m/s*. Here, the inlet velocity of 1 *m/s* was prescribed on the largest domain of 5x2x2 meters (axial, radial, tangential) and the axial velocity was sampled at locations 2.5, 1.0, 0.5, 0.25 and 0.1 meters above the disk's surface at $r = 0.421$ *m*. The measured axial velocities were prescribed at the velocity inlet for each respective simulation. The domain sizes and inlet velocity prescribed for the simulations in this sensitivity study are as follows:

5 x 2 x 2 meters (axial, radial, tangential), velocity prescribed at inlet = 1 *m/s*

2.5 x 2 x 2 meters, velocity prescribed at inlet = 0.995 *m/s*

1 x 2 x 2 meters, velocity prescribed at inlet = 0.880 *m/s*

0.5 x 2 x 2 meters, velocity prescribed at inlet = 0.670 *m/s*

0.25 x 2 x 2 meters, velocity prescribed at inlet = 0.471 *m/s*

0.1 x 2 x 2 meters, velocity prescribed at inlet = 0.313 *m/s*

The mean flow vector magnitude (Figs. 309 and 310) and the profile of tangential velocity in the rotating reference frame (Figs. 315 and 316) show a lack of sensitivity to the velocity inlet's position, as all of the simulation profiles are in close agreement.

The crossflow profile (Figs. 311 and 312), the polar plot of mean velocity profiles (Figs. 313 and 314), the momentum thickness Reynolds number (Figs. 317 and 318) and the turbulent kinetic energy profile (Figs. 319 and 320) all show sensitivity to the velocity inlet's position. All the simulation profiles differ from one another.

The Reynolds stresses are plotted in Figs. 321, 323 and 325. The stress profiles illustrate this model's sensitivity to the location of the velocity inlet. The average errors of these profiles are given in Figs. 322, 324 and 326 respectively. The average error differs in each simulation.

This is the only turbulence model that was not able to replicate the simulation profiles of the 5.0 meter axial domain simulation results with a smaller domain's simulation results. Thus the 5x2x2 meter computational domain was chosen as the suitable grid size for these simulations using the Reynolds Stress Transport model with the High y^+ Wall Treatment.

The computation time for this grid size was 6 minutes and 15 seconds, computed on the desktop computer, out to 1500 iterations. Comparing this time to the 9 hours and 42 minutes it took to compute the simulation on the Nano Linux cluster, for the initial $y^+ = 30$ grid in Step 1, illustrates the benefit of having an efficiently sized grid.

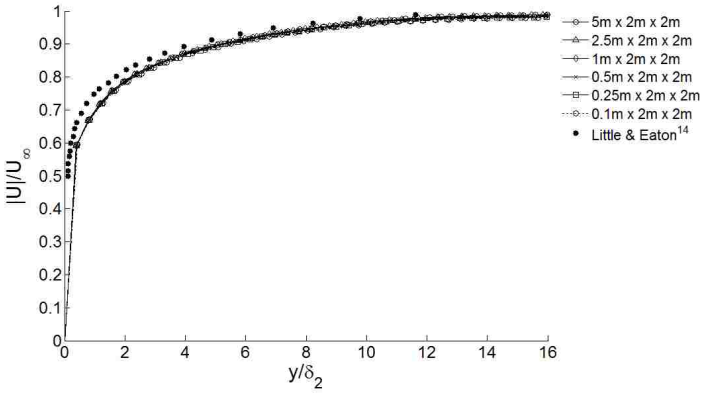

Figure 309. Turbulent mean flow vector magnitude in the rotating reference frame. *Comparison plot of the Reynolds Stress Transport Model for grids with varying computational domain sizes in the axial direction.*

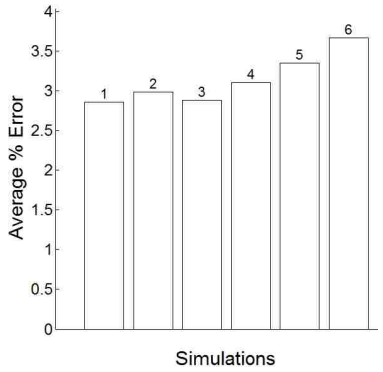

Figure 310. Error of turbulent mean flow vector magnitude. *1: 5x2x2m, 2: 2.5x2x2m, 3: 1x2x2m, 4: 0.5x2x2m, 5: 0.25x2x2m, 6: 0.1x2x2m*

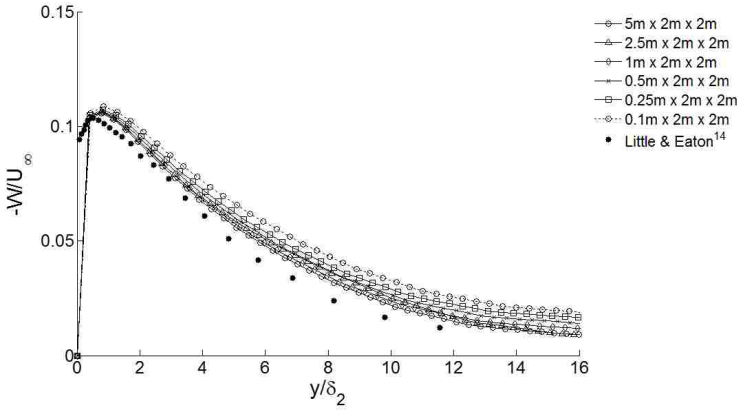

Figure 311. Crossflow profile. *Comparison plot of the Reynolds Stress Transport Model for grids with varying computational domain sizes in the axial direction.*

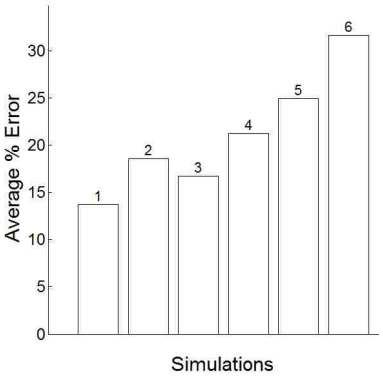

Figure 312. Error of crossflow profile. *1: 5x2x2m, 2: 2.5x2x2m, 3: 1x2x2m, 4: 0.5x2x2m, 5: 0.25x2x2m, 6: 0.1x2x2m*

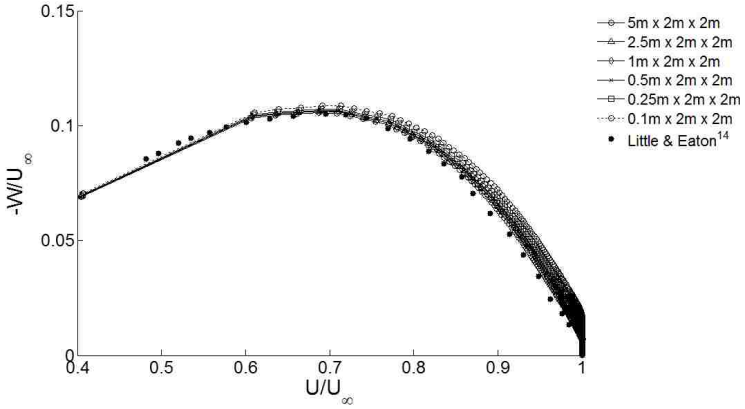

Figure 313. Polar plot of mean velocity profiles. *Comparison plot of the Reynolds Stress Transport Model for grids with varying computational domain sizes in the axial direction.*

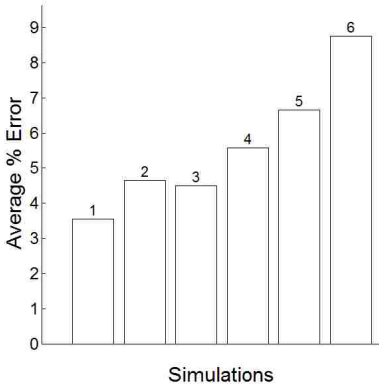

Figure 314. Error of polar mean velocity profiles. *1: 5x2x2m, 2: 2.5x2x2m, 3: 1x2x2m, 4: 0.5x2x2m, 5: 0.25x2x2m, 6: 0.1x2x2m*

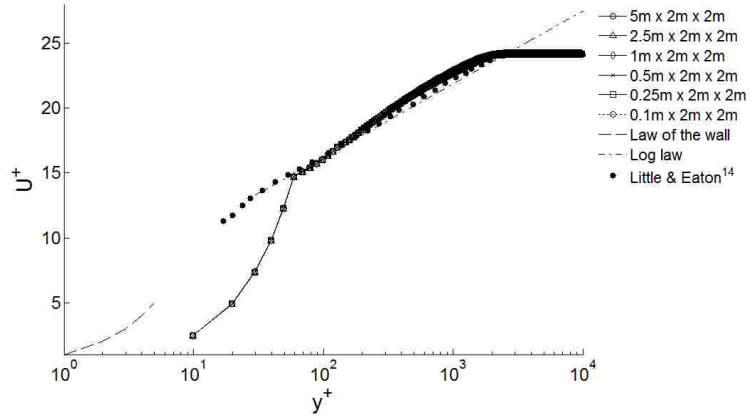

Figure 315. Tangential velocity in rotating reference frame. *Comparison plot of the Reynolds Stress Transport Model for grids with varying computational domain sizes in the axial direction.*

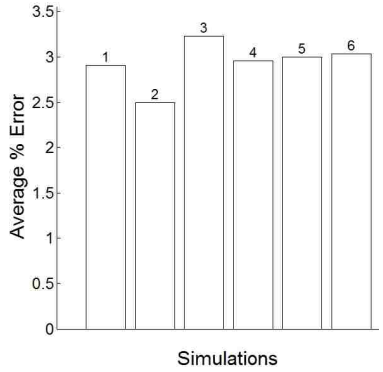

Figure 316. Error of tangential velocity. *1: 5x2x2m, 2: 2.5x2x2m, 3: 1x2x2m, 4: 0.5x2x2m, 5: 0.25x2x2m, 6: 0.1x2x2m*

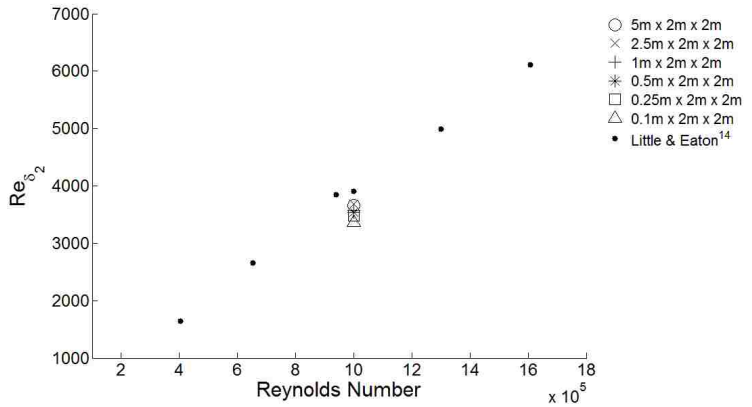

Figure 317. Comparison of momentum thickness Reynolds number. *Comparison plot of the Reynolds Stress Transport Model for grids with varying computational domain sizes in the axial direction.*

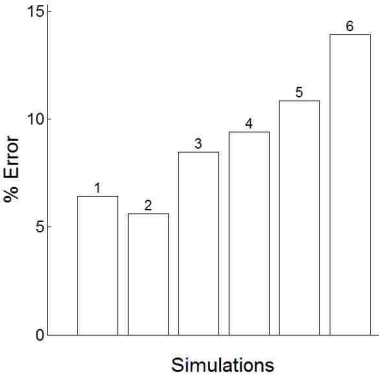

Figure 318. Error of momentum thickness Reynolds number. *1: 5x2x2m, 2: 2.5x2x2m, 3: 1x2x2m, 4: 0.5x2x2m, 5: 0.25x2x2m, 6: 0.1x2x2m*

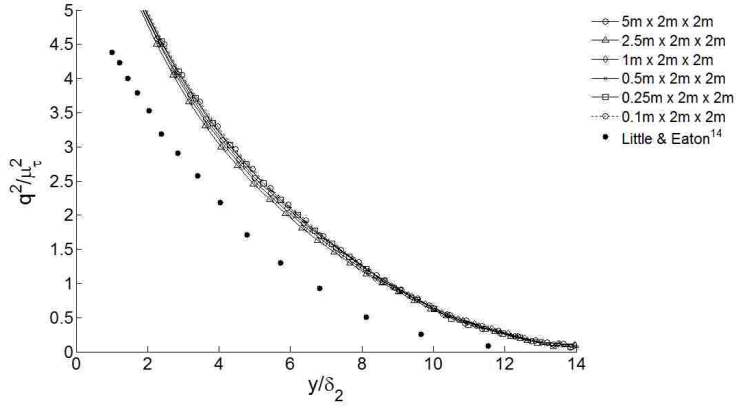

Figure 319. Twice the turbulence kinetic energy. *Comparison plot of the Reynolds Stress Transport Model for grids with varying computational domain sizes in the axial direction.*

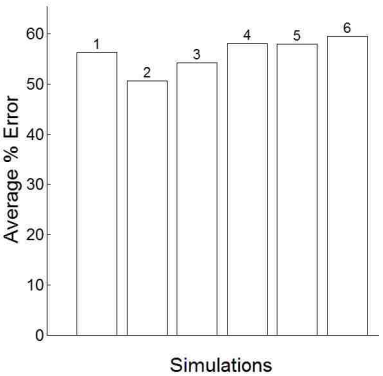

Figure 320. Error of twice the turbulence kinetic energy. *1: 5x2x2m, 2: 2.5x2x2m 3: 1x2x2m, 4: 0.5x2x2m, 5: 0.25x2x2m, 6: 0.1x2x2m*

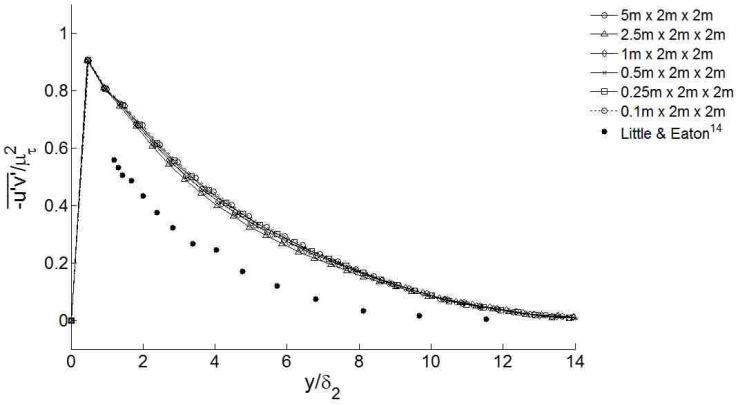

Figure 321. Normalized Reynolds stress, $-\overline{u'v'}$. *Comparison plot of the Reynolds Stress Transport Model for grids with varying y^+ wall cell centroid values.*

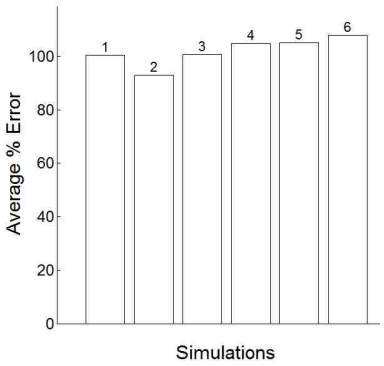

Figure 322. Error of normalized Reynolds stress, $-u'v'$.
1: 5x2x2m, 2: 2.5x2x2m, 3: 1x2x2m, 4: 0.5x2x2m, 5: 0.25x2x2m, 6: 0.1x2x2m

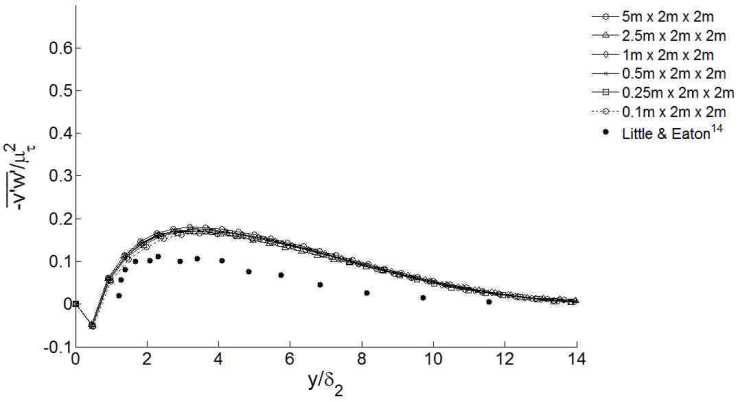

Figure 323. Normalized Reynolds stress, $-\overline{v'w'}$. *Comparison plot of the Reynolds Stress Transport Model for grids with varying y^+ wall cell centroid values.*

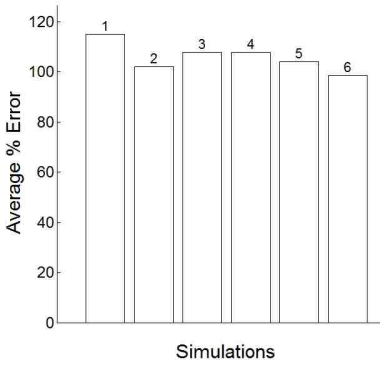

Figure 324. Error of normalized Reynolds stress, $-v'w'$.
1: 5x2x2m, 2: 2.5x2x2m, 3: 1x2x2m, 4: 0.5x2x2m, 5: 0.25x2x2m, 6: 0.1x2x2m

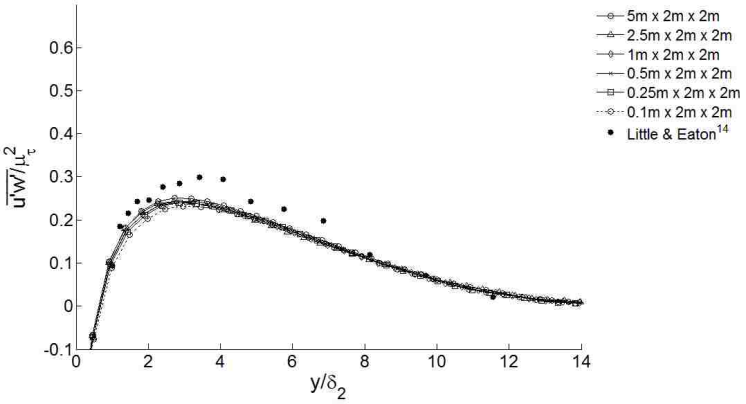

Figure 325. Normalized Reynolds stress, $\overline{u'w'}$. *Comparison plot of the Reynolds Stress Transport Model for grids with varying y^+ wall cell centroid values.*

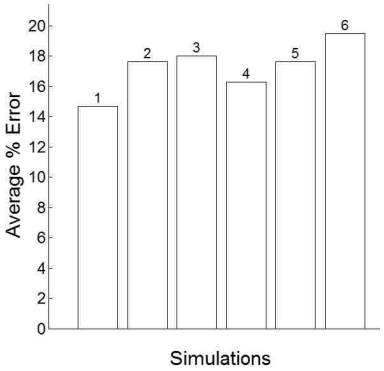

Figure 326. Error of normalized Reynolds stress, $u'w'$.
1: 5x2x2m, 2: 2.5x2x2m, 3: 1x2x2m, 4: 0.5x2x2m, 5: 0.25x2x2m, 6: 0.1x2x2m

6. Turbulence Model Comparison

The five turbulence models are compared in this section. Each turbulence model's simulation in Star-CCM+[8] was computed on the most suitable grid found through the sensitivity studies in the previous sections. The most suitable grid was chosen based on minimized computational cost while maintaining accurate results. The *k-ε*, *k-ω*, SST, and High-Reynolds Number Spalart-Allmaras turbulence models all resulted in computational domains with axial lengths of 2.5 meters that matched the simulation profiles obtained in the 5-meter axial domain. The Reynolds Stress Transport Model was the only turbulence model that had varying results between the simulation profiles obtained in the computational domains with 2.5 and 5-meter axial lengths. Therefore, to achieve consistent comparisons between turbulence models, all of the grids in this sensitivity study have an axial length of 5 meters and the prescribed flow velocity of 1 *m/s* at the inlet. Below, details on the grids used and the computational time required to conduct the simulations with each turbulence model are presented.

Standard *k-ε* with High y^+ Wall Treatment

Initial cell centroid located at $y^+ = 30$

Uniform radial and tangential grid size = 0.08 meters

Axial stretch ratio = 1.3

Computational domain size = 5 x 2 x 2 meters (axial, radial, tangential)

Grid resolution = 31 x 26 x 26 nodes

Computational time = 3 minutes 30 seconds

Number of iterations = 1500

Computed on the desktop computer

Standard k-ω with High y^+ Wall Treatment

Initial cell centroid located at $y^+ = 30$

Uniform radial and tangential grid size = 0.08 meters

Axial stretch ratio = 1.1

Computational domain size = 5 x 2 x 2 meters

Grid resolution = 72 x 26 x 26 nodes

Computational time = 4 minutes 15 seconds

Number of iterations = 1500

Computed on the desktop computer

SST with High y^+ Wall Treatment

Initial cell centroid located at $y^+ = 20$

Uniform radial and tangential grid size = 0.08 meters

Axial stretch ratio = 1.2

Computational domain size = 5 x 2 x 2 meters

Grid resolution = 44 x 26 x 26 nodes

Computational time = 4 minutes 18 seconds

Number of iterations = 1500

Computed on the desktop computer

High-Reynolds Number Spalart-Allmaras with High y^+ Wall Treatment

Initial cell centroid located at $y^+ = 20$

Uniform radial and tangential grid size = 0.04 meters

Axial stretch ratio = 1.3

Computational domain size = 5 x 2 x 2 meters

Grid resolution = 33 x 51 x 51 nodes

Computational time = 6 minutes 16 seconds

Number of iterations = 1500

Computed on the desktop computer

RSTM with High y^+ Wall Treatment

Initial cell centroid located at $y^+ = 30$

Uniform radial and tangential grid size = 0.08 meters

Axial stretch ratio = 1.2

Computational domain size = 5 x 2 x 2 meters

Grid resolution = 42 x 26 x 26 nodes

Computational time = 6 minutes 15 seconds

Number of iterations = 1500

Computed on the desktop computer

All the models are plotted in each graph with the exception of turbulent kinetic energy graphs (Figs. 337 and 338), where the High-Reynolds Number Spalart-Allmaras turbulence model with the High y^+ Wall Treatment is not present because Star-CCM+[8] does not solve for the turbulent kinetic energy in this turbulence model.

The turbulent mean flow vector magnitude (Figs. 327 and 328) shows close agreement among all the turbulence models and the experimental data[14]. The simulation profiles obtained with the RSTM and standard k-ε models slightly undershoot the velocity magnitude near the surface of the disk.

The crossflow profile (Figs. 329 and 330) of the RSTM and standard k-ε model simulations do not match the other simulation profiles near the disk's surface. The simulation profiles of the standard k-ω, SST and High-Reynolds Number Spalart-Allmaras models are in close agreement near the disk's surface, but the profiles begin to stray from one another far from the disk.

The polar plot of the mean velocities (Figs. 331 and 332) shows close agreement among the simulation profiles far from the disk (far right of graph), but as the data sampling location becomes closer to the disk's surface (left side of graph) the turbulence models' simulation profiles differ from one another.

Figure 333 shows the turbulent mean tangential flow in its non dimensional form U^+ vs. y^+. The simulation profile of the High-Reynolds Number Spalart-Allmaras model does a poor job of replicating the experimental data[14] and the other models' simulation profiles. Considering that the High-Reynolds Number Spalart-Allmaras model's simulation profiles of the mean flow vector magnitude and the crossflow profile are in close agreement with the other turbulence

models' simulation profiles (Figs. 327 and 329) it can be inferred that the lack of accuracy in Fig. 331 arises from the High-Reynolds Number Spalart-Allmaras turbulence model's inability to accurately convert the physical values of velocity and position to the non-dimensional values U^+ and y^+. Equations 1 and 9 show that the inaccurate calculation of the friction velocity, μ_τ, is responsible for the large variance of the High-Reynolds Number Spalart-Allmaras model's simulation profile that is present in Fig. 331. The simulation profiles of the other turbulence models are in close agreement with one another near the disk's surface. The data do not agree at the disk's surface because there are different initial cell y^+ values in the simulations.

The momentum thickness Reynolds number (Figs. 335 and 336) and the turbulent kinetic energy (Figs. 337 and 338) show a lack of agreement among the data obtained with different turbulence models.

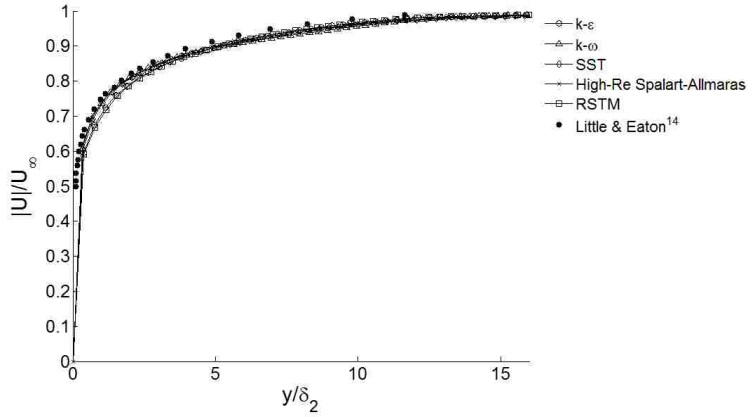

Figure 327. Turbulent mean flow vector magnitude in the rotating reference frame.

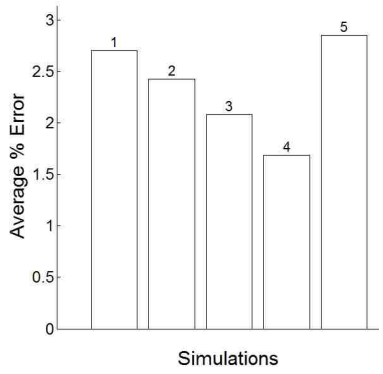

Figure 328. Error of turbulent mean flow vector magnitude. *1: k-ε, 2: k-ω, 3: SST, 4: High-Re Spalart-Allmaras, 5: RSTM*

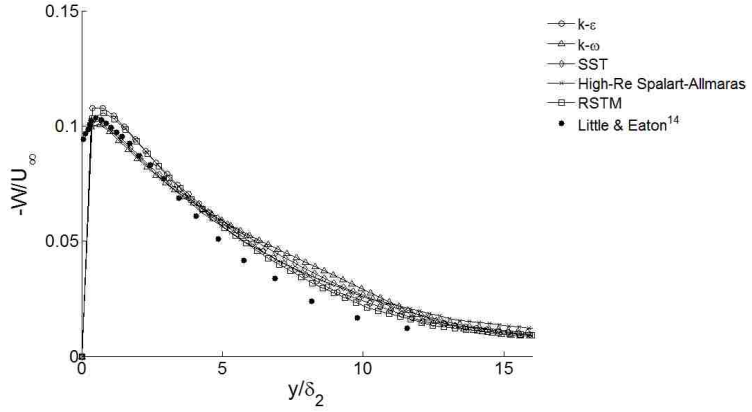

Figure 329. Crossflow profile.

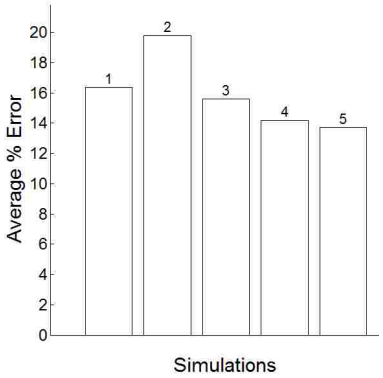

Figure 330. Error of crossflow profile. *1: k-ε, 2: k-ω, 3: SST, 4: High-Re Spalart-Allmaras, 5: RSTM*

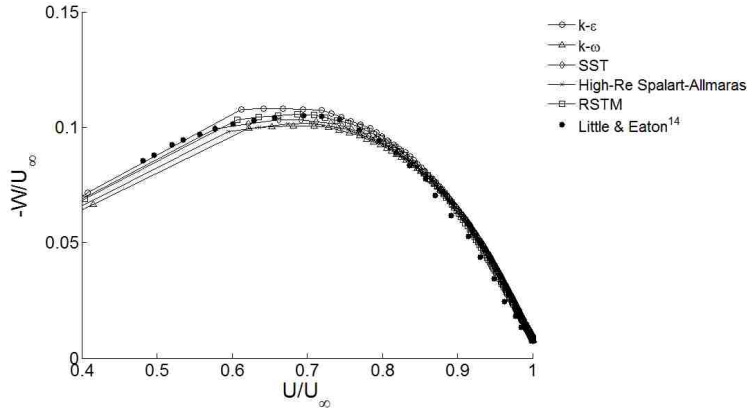

Figure 331. Polar plot of mean velocity profiles.

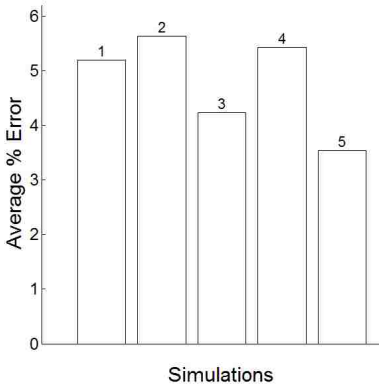

Figure 332. Error of polar mean velocity profiles. *1: k-ε, 2: k-ω, 3: SST, 4: High-Re Spalart-Allmaras, 5: RSTM*

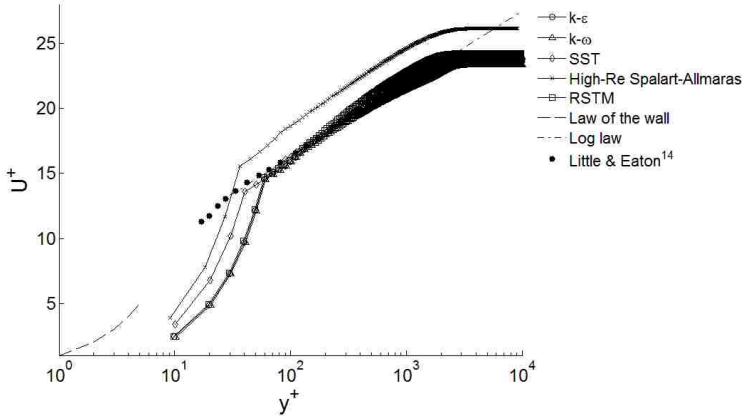

Figure 333. Tangential velocity in rotating reference frame.

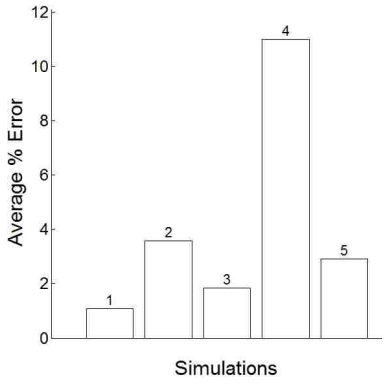

Figure 334. Error of tangential velocity. *1: k-ε, 2: k-ω, 3: SST, 4: High-Re Spalart-Allmaras, 5: RSTM*

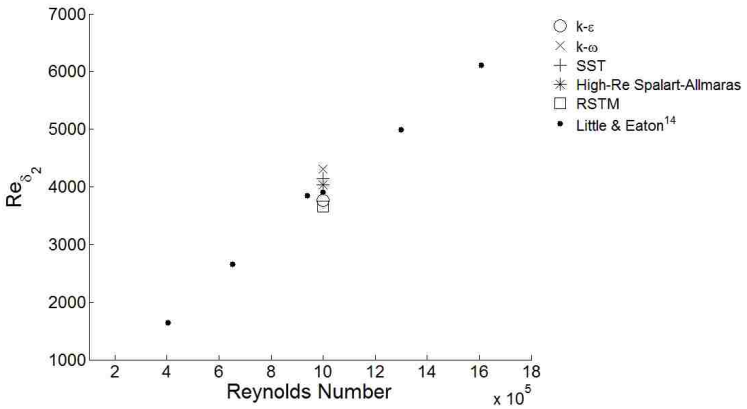

Figure 335. Comparison of momentum thickness Reynolds number.

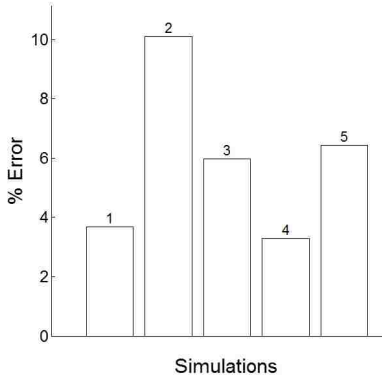

Figure 336. Error of momentum thickness Reynolds number. *1: k-ε, 2: k-ω, 3: SST, 4: High-Re Spalart-Allmaras, 5: RSTM*

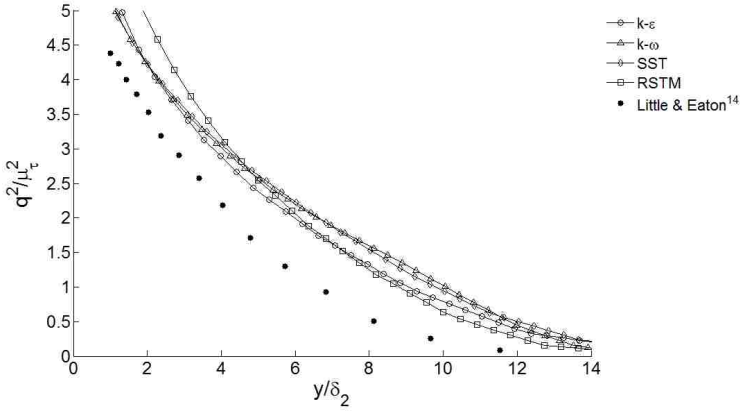

Figure 337. Twice the turbulence kinetic energy.

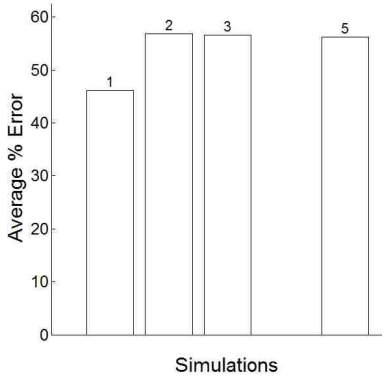

Figure 338. Error of twice the turbulence kinetic energy. *1: k-ε, 2: k-ω, 3: SST, 5: RSTM*

7. Wall Treatment

Using wall treatments (also referred to as wall functions) saves computational time which is extremely useful for analysts who do not have access to high performance computing. The desire to get quick results on a desktop computer provides motivation to speed up computations. The question is posed: How much accuracy is one losing when utilizing a simulation with wall treatments versus a simulation without wall treatments? In this section simulations were conducted with the standard k-ε turbulence model with the High y^+ Wall Treatment and the Low y^+ Wall Treatment. The Low y^+ Wall Treatment is Star-CCM+'s[8] option for no wall treatment. The simulation with the High y^+ Wall Treatment was computed on a desktop computer while the simulation with no wall treatment (Low y^+ Wall Treatment) was computed on the high performace Nano Linux cluster. The following are the grids and computation time for each simulation.

Standard k-ε with High y^+ Wall Treatment

Initial cell centroid located at $y^+ = 30$

Uniform radial and tangential grid size = 0.08 meters

Axial stretch ratio = 1.3

Computational domain size = 2.5 x 2 x 2 meters (axial, radial, tangential)

Grid resolution = 29 x 26 x 26 nodes

Initial wall cell aspect ratio ≈ 66:1

Computational time ≈ 3 minutes

Number of iterations = 1500

Computed on the desktop computer

Standard *k*-ε with no wall treatment (Low y^+ Wall Treatment)

Initial cell centroid located at $y^+ = 1$

Uniform radial and tangential grid size = 0.004 meters

Axial stretch ratio = 1.3

Computational domain size = 2.5 x 2 x 2 meters (axial, radial, tangential)

Grid resolution = 42 x 501 x 501 nodes

Initial wall cell aspect ratio ≈ 99:1

Computational time ≈ 7 hours 44 minutes

Number of iterations = 1500

Computed on the Nano Linux cluster: 4 nodes

The radial and tangential grid resolution is very fine in the simulation of the standard *k*-ε turbulence model without wall treatment because the aspect ratio of the initial wall cell must not be too large. The limiting of the cell aspect ratio prevents the simulation from having an error in Star-CCM+[8].

The mean velocity vector magnitude (Figs. 339 and 340) and the crossflow profile (Figs. 341 and 342) show very close agreement among the simulation results.

The polar plot of the mean velocity profiles (Figs. 343 and 344) exhibits close agreement except near the disk's surface.

Figure 345 shows the tangential velocity of the two models. To better illustrate the difference among the turbulence models near the disk's surface, a more refined data sampling region was added near the disk's surface. The data is sampled down to a value of $y^+ = 1$. The standard *k*-ε turbulence model with no wall treatment has close agreement with both the analytical solutions and the experimental data[14]. The standard *k*-ε turbulence model with the High y^+ Wall Treatment is unable to replicate the results of the analytical solutions near the disk's surface, but as the data sampling falls outside the initial wall cell ($y^+ \geq 60$) the profile is in close agreement with the log law and experimental data[14] (see also the average error graph in Fig. 346).

The momentum thickness Reynolds number (Figs. 347 and 348) of each simulation is close to the experimental data[14].

The turbulent kinetic energy displays another interesting difference between the two models. Although both models show close agreement throughout the domain, the standard *k*-ε turbulence

model with no wall treatment is able to capture the boundary condition of zero turbulent kinetic energy at the disk's surface while the standard k-ε turbulence model with the High y^+ Wall Treatment is unable to.

These results illustrate the High y^+ Wall Treatment's inability to capture the flow physics near the disk's surface, but there is very close agreement among the models' simulation profiles past the near-wall discrepancies.

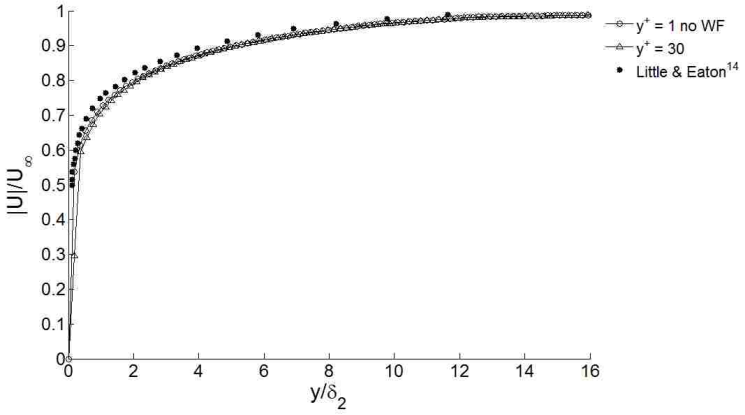

Figure 339. Turbulent mean flow vector magnitude in the rotating reference frame. *Comparison plot of the standard k-ε turbulence model with and without wall functions.*

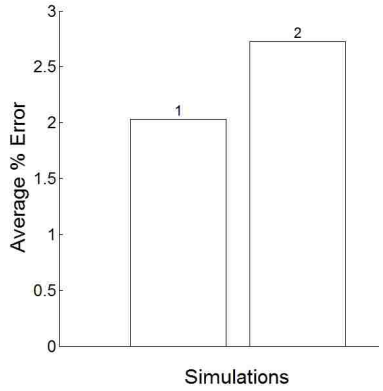

Figure 340. Error of turbulent mean flow vector magnitude.
1: y^+=1 without wall functions,
2: y^+=30 with wall functions

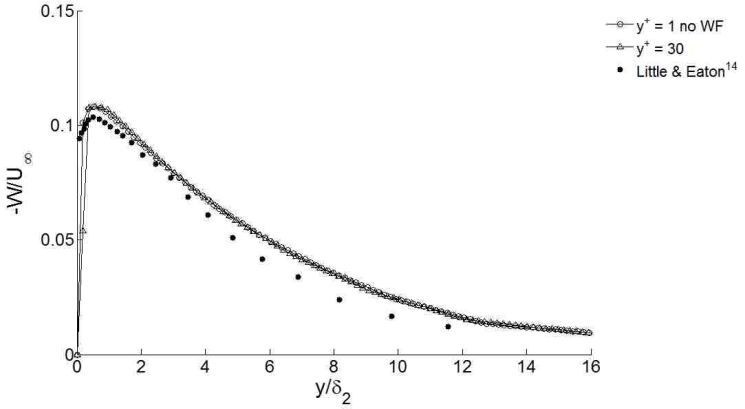

Figure 341. Crossflow profile. *Comparison plot of the standard k-ε turbulence model with and without wall functions.*

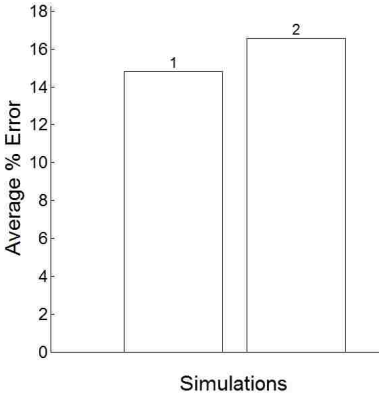

Figure 342. Error of crossflow profile.
1: y^+=1 without wall functions,
2: y^+=30 with wall functions

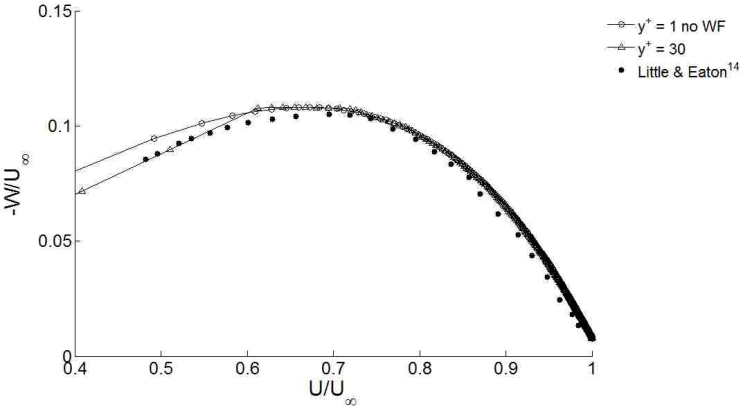

Figure 343. Polar plot of mean velocity profiles. *Comparison plot of the standard k-ε turbulence model with and without wall functions.*

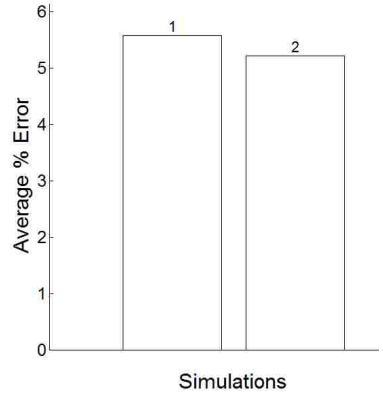

Figure 344. Error of polar mean velocity profiles.
1: y^+=1 without wall functions,
2: y^+=30 with wall functions

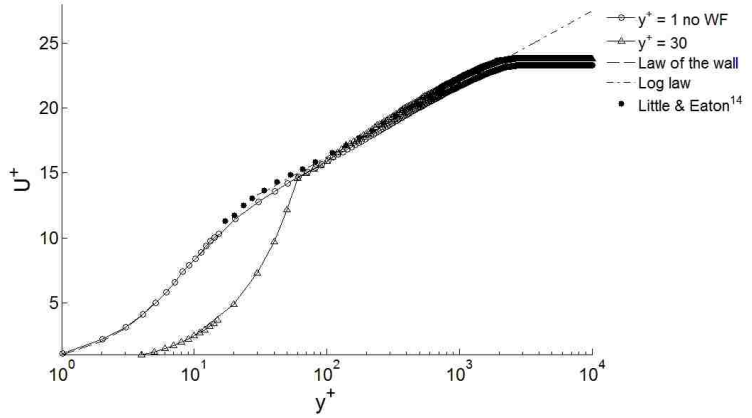

Figure 345. Tangential velocity in rotating reference frame. *Comparison plot of the standard k-ε turbulence model with and without wall functions.*

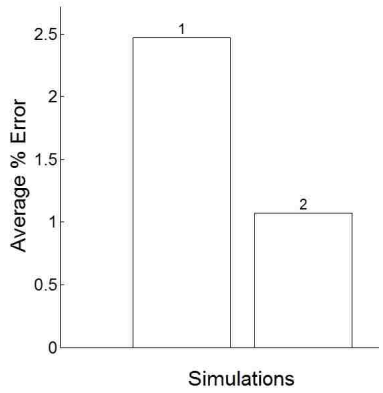

Figure 346. Error of tangential velocity.
1: y^+=1 without wall functions,
2: y^+=30 with wall functions

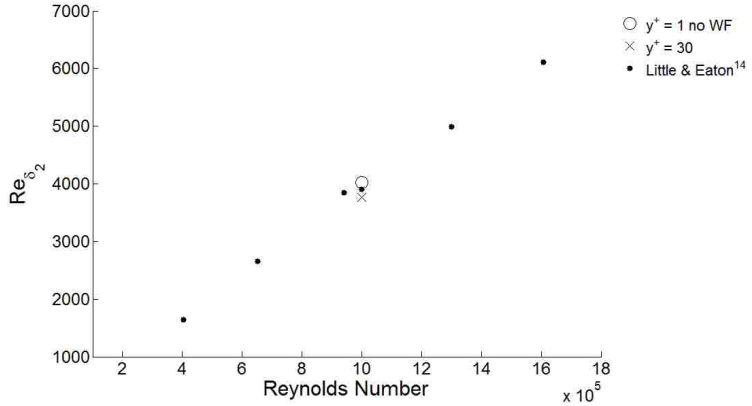

Figure 347. Comparison of momentum thickness Reynolds number. *Comparison plot of the standard k-ε turbulence model with and without wall functions.*

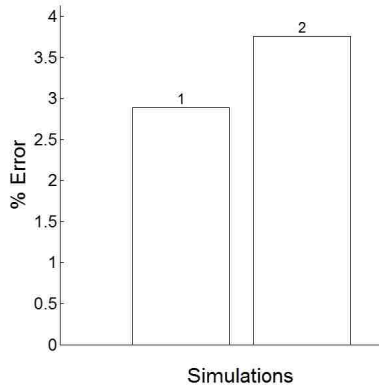

Figure 348. Error of momentum thickness Reynolds number.
1: y^+=1 without wall functions,
2: y^+=30 with wall functions

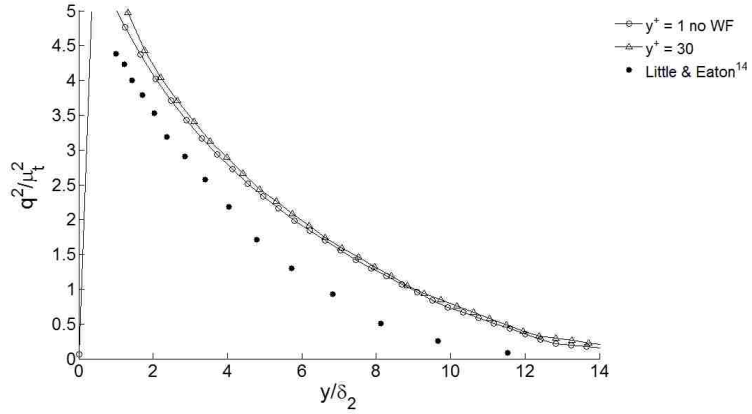

Figure 349. Twice the turbulence kinetic energy. *Comparison plot of the standard k-ε turbulence model with and without wall functions.*

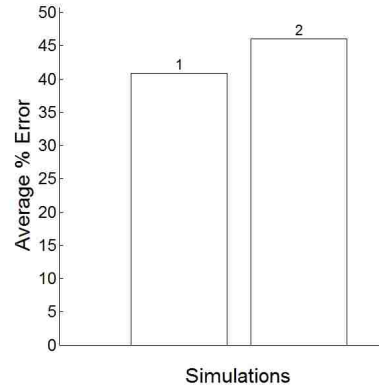

Figure 350. Error of twice the turbulence kinetic energy.
1: y^+=1 without wall functions,
2: y^+=30 with wall functions

VI. Conclusions

As shown, the computational time to conduct simulations with high-refinement grids can take hours on a high performance computer. This option may not be available or affordable for design purposes in industry. Yet, it is desirable that computations realistically reproduce the flow features.

The current study demonstrates that a reasonable compromise between these requirements can be found if a sensitivity study is conducted for flow geometry and flow parameters of interest at the initial design stage. The goal of such analysis is to determine i) the grid parameters most suitable for the problem and ii) possibly a turbulence model that is less sensitive to variations in the simulation parameters.

In regard to a grid, what was sought in the current study was the coarsest grid that allows one to replicate simulation results obtained with a given turbulence model on more fine grids. It was found that by coarsening the grid in certain ways the time required to complete the simulations can be reduced from hours on high-performance computing facilities to minutes on a local desktop computer.

In regard to a turbulence model, it is important to emphasize that the purpose of this sensitivity study is not to identify a model that produces the most accurate simulation results in comparison with experimental data, but one that is able to replicate results of simulations obtained with finer grids on a coarser grid and is more robust to changes in gird parameters.

It was found that the High-Reynolds Number Spalart-Allmaras model is the most sensitive to changes in the grid's initial wall-cell length and requires fine grids to obtain results that were still not as accurate as those obtained with other models. This model, along with the RSTM, required the longest computational time to generate an adequate solution.

The standard k-ω model demonstrated the highest sensitivity to changes of the axial stretch ratio. Sensitivity to the other grid parameters was not so pronounced.

The SST model showed a unique sensitivity to the initial wall-cell length. When the near-wall centroid was located at $y^+ = 30$ the simulation results deviated from the results obtained with neighboring y^+ values ($y^+ = 20$ and 40). The computational time of the SST model was approximately the same as the standard k-ω model.

Simulations with the Reynolds Stress Transport model showed sensitivity to the position of the inlet velocity boundary that was not observed in simulations with other models.

Both the RSTM and k-ε turbulence models showed high sensitivity to grids containing cells with high aspect ratios ($\geq$ 1000:1) at the disk's surface. These turbulence model simulations were unable to obtain a converged solution. The residuals computed at each iteration increased until Star-CCM+[8] had an error that terminated the simulation. This error did not occur on the other turbulence models when running simulations on grids that contained cells with high aspect ratios.

With the k-ε turbulence model, the results of simulations of finer grids were reproduced with very coarse grids. This resulted in this model having the fastest computation time required for conducting simulations.

Utilizing the High y^+ Wall Treatment model allows one to accelerate simulations enormously. The difference in the results obtained using the k-ε model with and without wall treatment was only significant in the region near the disk's surface. Thus, if a general picture of the flow structure is of interest rather than the near-wall regions, simulations with the High y^+ Wall Treatment model are a far less computationally demanding alternative.

Based on the results of this study, the standard k-ε turbulence model with the High y^+ Wall Treatment is recommended as the turbulence model choice in Star-CCM+[8] for simulations of a flow over a rotating disk.

It is the desire of this author that this research be utilized as a reference for the sensitivity analysis of simulations of a flow around a wind turbine with respect to simulation parameters.

References

[1]IBISWorld. "Wind Power Generation in the US - Industry Market Research Report" IBISWorld.TM-90401, 2011, http://www.evwind.es/noticias.php?id_not=11708.

[2]BTM Consultants. "International Wind Energy Development – World Update 2010."BTM Consultants DK-6950, 2011, http://www.windtoday.net/info/articles_email.html?ID=106940.

[3]Spalart, P. R., and Allmaras, S. R., "A One-Equation Turbulence Model for Aerodynamic Flows," AIAA-92-0439, 1992.

[4]Jones, W. P., and Launder, B. E., "The Calculation of Low-Reynolds Number Phenomena with a Two-Equation Model of Turbulence," *Int. J. of Heat and Mass Transfer*, Vol. 16, 1973, pp. 1119-1130.

[5]Wilcox, D. C., "Reassessment of the Scale-Determining Equation for advanced Turbulence Models," *AIAA Journal*, Vol. 26, No. 11, 1988, pp. 1299-1310.

[6]Menter, F. R., and Rumsey, C. L., "Assessment of Two-Equation Turbulence Models for Transonic Flows," AIAA-94-2343, 1994.

[7] Gibson, M. M., and Launder, B. E., "Ground effects on pressure fluctuations in the atmospheric boundary layer," *J. Fluid Mech.*, Vol. 86, 1978, pp. 491-511.

[8]Star-CCM+. Computational fluid dynamics solver, Software Package, Ver. 6.02.007, CD-adapco.

[9]ANSYS ICEM CFD. Fluid and structural meshing program, Software Package, Ver. 13.0, ANSYS.

[10]Von Karman, T., "Uber Laminare und Turbulente Reibung," *Z. Angew. Math Mech*, Vol. 1, 1921, pp. 233-252.

[11]Cochran, W., "The Flow due to a Rotating Disk," *Proceedings of the Cambridge Philosophical Society*, Vol. 30, 1934, pp. 365-375.

[12]White, F., *Viscous Fluid Flow*, 2nd ed., McGraw-Hill, 1991, pp. 154-161.

[13]Xiaohua, W., and Squires, K. D., "Prediction and investigation of the turbulent flow over a rotating disk," *J. Fluid Mech.*, Vol. 418, 2000, pp. 231-264.

[14]Little, H. S., and Eaton, J. K., "Turbulence characteristics of the boundary layer on a rotating disk," *J. Fluid Mech.*, Vol. 266, 1994, pp.175-207.

[15]Kobayashi, R., Kohama, Y., and Takamadate, Ch., "Spiral Vortices in Boundary Layer Transition Regime on a Rotating Disk," *Acta Mechanica*, Vol. 35, 1980, pp. 71-82.

[16]Lien, F. S., and Leschziner, M. A., "Assessment of turbulence-transport models including non-linear RNG eddy-viscosity formulation and second-moment closure for flow over a backward-facing step," *Computers Fluids*, Vol. 23, 1994, pp. 983-1004.

[17] Nichols, R. H., and Buning, P. G., "User's Manual for OVERFLOW 2.1," University of Alabama and NASA Langley Research Center, 2008.